Bio-Adhesion

And

Cleanliness in Bio-Processing

Jonathan Raymond Palmer

A dissertation submitted to Imperial College London for the degree of

Doctor of Philosophy

April 2017

Surface and Particle Engineering Lab, Department of Chemical Engineering

Imperial College London

Acknowledgments

I am deeply indebted to my supervisor Dr Daryl Williams, for all of his support and for his taking a chance on bringing me on board with this project. I would like to thank my new friends dotted all over Imperial College for their good conversation and support (you know who you are). I am indebted to the engineers within the mechanical work shop facility within the Chemical Engineering Department specifically Tony Meredith, Bob (Richard Brace), and Richard Wallington for helping me with the practical engineering aspects of the work. I would also like to acknowledge Dr Huw Williams for allowing me carry out some of the biology work in his lab.

My colleagues at Procter and Gamble specifically; Dr Kevin Wright, and Gareth Davies, for allowing access to their facility, and their support and guidance.

I would like to thank Thomas Young (deceased) for his pioneering efforts in the fields of surface interfacial science, specifically surface energy characterisation, and interferometry, both of which have been instrumental in this project.

Lastly, and not least to my wife Julie Palmer for supporting me at home, being kind, supportive and forgiving my absences, and to my two children Isabel and Thomas, for being good.

Copyright

Declaration

All work referred to in this thesis was carried out at the Department of Chemical Engineering, Imperial College London, and at Procter and Gamble, Egham, UK between March 2013 and March 2017. Except where acknowledged, all content is original work of the author and no part of the thesis has been submitted for a degree at any other institution.

Table of Contents

10

Abbreviations

AFM	Atomic Force Microscopy
AU	Airy Unit
BEA	Brass Einlehner Abrasion value
BSA	Bovine Serum Albumin
CA	Contact Angle
CCD	Charge-Coupled Device
ConA	Concanavalin A
CF	Cystic Fibrosis
CFU	Colony Forming Unit
CNC	Computer Numeric Control
DIM	Diiodomethane
2D	2 Dimensional
3D	3 Dimensional
EHEDG	European Hygienic Engineering and Design Group
EPS	Extracellular Polymorphic (or Polysaccharides) Substances
FRET	Fluorescence Resonance Energy Transfer
FPLC	Fast Protein Liquid Chromatography
FS-TSB	Full Strength Tryptic Soya Broth
GFP	Green Fluorescent Protein
ISS	International Space Station

LHS	Left Hand Side
OTC	Over The Counter
PBS	Phosphate Buffered Saline
P&G	Procter and Gamble
PC	Polycarbonate
PDMS	Poly(dimethylsiloxane)
PE	Polyethylene
PMMA	Polymethylmethacrylate
PP	Polypropylene
PSI	Phase-Shifting Interferometry
PSM	Phenol Soluble Modulin (small excreted protein)
PTFE	Polytetrafluoroethylene
QCM	Quartz Crystal Microbalance
RBCs	Red Blood Cells
RC	Rough Coupon
RHS	Right Hand Side
RI	Refractive Index
RSCV	Rugose Small-Colony Variants
RT	Room Temperature
SC	Smooth Coupon
SDS	Sodium Dodecyl Sulfate
SDS-PAGE	Sodium Dodecyl Sulfate Poly-Acrylamide Gel Electrophoresis

SEM	Scanning Electron Microscopy
SLM	Standard Light Microscopy
SPR	Surface Plasmon Resonance
SRS	Stanford Research Systems
SS	Stainless Steel
T	Threshold
TB	*Mycobacterium tuberculosis*
TSA	Tryptic Soya Agar
TSB	Tryptic Soya Broth
TSP	Tris Sodium Phosphate
UDHR	Ultra Dawn Hand Renewal
UV	Ultra-Violet
VSI	Vertical scanning Interferometry
WLI	White Light Interferometry
WT	Wild Type (native/unmodified reference material)

Abstract

Biofilms are a significant problem for many industries including medical devices, the oil and gas industry, consumer product manufacturers and water distribution systems. Biofilms are communities of microbes that attach and grow on almost any surface. Biofilms are able to establish quickly in a matter of hours and can be very difficult to remove.

This thesis was focused on increasing the understanding of biofilm interaction with different substratum materials, for both the initial surface colonisation and for mature biofilm lifecycle stages using a *Pseudomonas aeruginosa* (*PA)* model. The surface energy and the surface roughness, for a number of substratums were investigated in this thesis. The effects of a number of proprietary and non-proprietary surface coatings which primarily changed surface energies and or topography were investigated.

This work has confirmed that surface energy is important in *Pseudomonas* bio-adhesion, with correlations observed in both the initial attachment of microbes, but also in high shear cleaning experiments for mature biofilms. Biofilm-substratum interfacial adhesion remains an important region even in mature biofilms, suggesting that surfaces that exhibit lower colonisation rates may also be easier to clean. Initial attachment studies confirm 1/3 less microbe attachment to polymer surfaces compared to metal surfaces; roughness was not a significant parameter.

PTFE-AF coatings on 316 stainless steel showed 88 percent decrease in initial microbe attachment coupled with enhanced cleanability. Industries currently using stainless steel in microbe applications could from benefit this coating; limiting future biofilm colonisation rates and improved cleanability.

It is demonstrated that *Pseudomonas* naturally colonises at low levels on selected transparent polycarbonate surfaces and given its good chemical compatibility and low cost would be an alternative to stainless steel.

A range of commercial surface coatings, which are meant to reduce microbial adhesion, were also tested in this thesis; this study could not affirm such claimed performance.

CHAPTER 1   General Introduction

1.1   Introduction to Microbes and the Biofilm Phenotype

Bacteria are a unicellular (exist as single cells) and prokaryotic (lack an membrane bound internal cellular machinery) form of life, that have inhabited this planet for some 3.5 billion years (Solomon et al., 1999) and perhaps even earlier, since 3.7 billion years (Nutman et al., 2016). Their total biomass likely exceeds that of both animals and plants together on the planet. Bacteria are found thriving in every environment on Earth, from the driest desserts and highest mountains to the bottom of the sea at temperatures exceeding hundreds of degrees to living within solid rock miles below the surface (Baker et al., 2016). They are persistent, and given time, adaptive to almost any environment; man-made or natural.

Bacteria predominantly exist in either a planktonic state, which is where they are found in suspension or in either a biofilm (sessile state), where they are immobilised on a surface in contact with water (Davies, 2000). It is thought that some 99 percent of bacteria exist as a biofilm at some point during their life cycle (Garrett et al., 2008, de Kievit, 2011). They grow as highly organised multi-cellular, multi-species communities, that involve sensing and responding to cues, such as bacterial cell density, nutrient availability and the energy resources present in the environment (Moreau-Marquis et al., 2008). The sessile state is now generally considered the predominate mode of microbial life in nature (Otto, 2008), and is thought to be a survival strategy for bacteria, helping to enable them to effectively compete in a world full of multicellular organisms, and numerous other competitors and prey species (DePas et al., 2014).

Not all microbes will form biofilms in all circumstances. For example Prouty found that *Salmonella enterica,* which lives in the gut and is found on gall stones, would only form a biofilm in the presence of bile, and not in a Luria-Bertani broth alone, (Prouty et al., 2002), suggesting an environmental selectivity for the biofilm phenotype that is likely to extend to many microbes which have evolved to exploit a particular niche environment.

Biofilms are thought to be associated with some 65 percent of human infections, including dental problems, ear infections and those arising from medical implants, but they are also responsible for a large amount of corrosion, impedance of heat transfer in chemical plants, and bio-fouling in industry (de Kievit, 2011).

Biofilms have been found to be useful, not only in the digestive tract where they help breakdown food particles, but also in bioremediation. A good example being a recently discovered species

that can break down polyethylene terephthalate (PET), which is the major component of plastic bottles (Yoshida et al., 2016).

With the introduction of antimicrobial agents in the 1940s there were many early successes in the reduction or elimination of pathogenic organisms such as *Mycobacterium tuberculosis* (TB) from some countries. However, more recently there has been a steady rise in the numbers of microbes resistant to these agents and now some organisms such as *Staphylococcus aurerus*, *Enterococcus faecalis* and TB are now resistant to almost all antibiotics (Lewis and Klibanov, 2005, Levy and Marshall, 2004). Due to the protective nature that biofilms afford their residents, and the fact that biofilms have been shown to be environments where enhanced horizontal gene transfer is taking place between microbes (Madsen et al., 2012), there has never been a greater need to further understand the formation of these structures and their relationship to the surfaces they attach.

1.2. Evolution of the Biofilm Phenotype

Generally bacteria tend to form biofilms in oligotrophic (poor nutrient) environments. This is because nutrients and cations tend to bind to surfaces, which then become attractive to microbes that, subsequently go on to express extracellular matrix that then further increases nutrient absorption to the surface. Some scientists think that the biofilm state is preferred for growth and exchange of genetic material whilst the planktonic state is adopted mainly for dissemination purposes (Costerton et al., 1995). The exchange of genetic material being far more efficient due to both the proximity of the microbes to one another, and due to lower diffusional coefficients relative to the bulk, allowing high local concentrations of plasmids to occur. Due to the fact the vast majority of microbes are able to form a biofilms, it is thought that this phenotype evolved very early on in their evolution.

1.3. Critical Factors in Biofilm Development

Surface chemistry of the substrate or substratum is a critical factor in biofilm development, principally because certain surface types can either leach organic material or promote the accumulation of organic material on the surface forming a conditioning layer (Dexter et al., 1975). This behaviour in turn may promote microbial binding, and or provide carbon sources to aid growth. In some cases where a surface may not have been properly cleaned, Extracellular Polymorphic (or Polysaccharides) Substances (EPS) may be present from a pre-existing biofilm, and its presence could greatly speedup the colonisation of that area. Different bacteria, as eluded to in the introduction, can have different affinities or environmental requirements for different

17

surfaces, and therefore at least in the initial colonisation steps of biofilm formation, the type and numbers of bacteria entering a system can also affect the rate of biofilm establishment.

Within an industrial manufacturing environment where aqueous based formulations are produced, poor plant design can be an important factor causing increased biofilm prevalence. Areas of manufacturing plant that possess either greatly reduced or no fluid flow are called 'dead legs' and can result in stagnant areas of liquid flow within the plant. Such areas may not facilitate easy access for cleaning agents, and/or can also be areas where a build-up of carbon sources (sludge) can occur, all of which aids biofilm formation. Also, if the manufacturing plant piping has many branching points these can be a source of fluid turbulence. Liquid flow rate and turbulence can be important, as this can shrink the diffusion boundary layer thickness, and aid in the transfer of the bacterium from the bulk to the surface.

Surface pitting and scratching of substrates caused by corrosion or other processes can help in the transfer of bacteria to the surface due to a turbulent flow fields being created proximal to the surface, but can also help provide protection from high shear whilst limiting the diffusion of anti-microbial agents (Simões et al., 2003).

Temperature can also have an effect on the rate of biofilm formation, but in a surprising way. Temperature dependent changes in flagella expression levels in some species were found by Herald and Zottola (Herald and Zottola, 1988) whilst investigating *Listeria monocytogenes* (35°C, 21°C, and 10°C) where the numbers of flagella on the surface of the microbes increased with decreasing with temperature. This behavior could also be true of other species for example *PA*, which reinforces the need to keep temperature constant across experiments. Garret et al (Garrett et al., 2008) discussed the importance of temperature on biofilm formation, stating that optimal physiological temperatures were related to optimal microbial cell division and enzyme activity, both of which will increase the rate of biofilm establishment. High temperatures used to enhance biofilm cleaning has been shown to have the opposite effect, where dried biofilm cake were observed to form at temperatures of between 80-90°C which were more difficult to clean (Marion-Ferey et al., 2003).

The cleaning frequency, and types of chemicals used, can help disrupt newly established or mature biofilms. Mature biofilms often slough off parts of the EPS. This biomaterial travels downstream and can be used by other bacteria to aid further colonisation. Regular cleaning can thus help reduce the occurrence of a biofilm. Cleaning chemicals need to have a broad mode of actions so that they can act on the many different microbial species found in the environment. It

is also important that chemicals are of sufficiently high concentration to kill the bacteria outright, whether in a biofilm or not, as passive exposure off microbes to ineffective levels of chemical agents can result in natural selection and increased resistance to these agents.

1.4. Advantages to Living in a Biofilm

Most bacteria live in biofilm communities because there are many distinct advantages compared to the planktonic existence. One major advantage is that biofilm communities become highly resistant to toxic products, including antibiotics, cleaners, and disinfectants found in the typical household or industrial environment. One example of this behaviour was demonstrated by Peng and colleagues, whereby planktonic cells show a 5 log CFU decrease in cell numbers when exposed to 25ppm hypochlorite, or 100ppm of a quaternary ammonium compound for 15 seconds, whereas little effect was detected even following a 5 minute exposure on sessile communities cultured on stainless steel (Peng et al., 2002). This behaviour can also be seen, following biofilm formation in mammals, where both innate and adaptive immune defence strategies are less potent against mature biofilms (Høiby et al., 2001). This decrease in immune response efficacy is mainly due to the inability of immune system components to penetrate the extracellular matrix and thus access the microbial population (Donlan and Costerton, 2002). Bacteria living within biofilms often adopt many different survival strategies including for example EPS production, expression of multidrug efflux pumps (acrAB) and phenotypic changes in their membrane protein composition (Olofsson et al., 2003).

Summary of benefits for microbes living in biofilms:

- Create their own micro environment
- Inter-species support within nutritional chains, inter-species communication
- Protection against desiccation
- Exchange of genetic material
- Increased availability of nutrients by uptake from liquid passing by increased absorption of nutrients by EPS
- Storage of carbon compounds (sugars) within EPS
- More nutrients found on surfaces relative to bulk in typical natural environments

1.5. What can Trigger Biofilm Formation?

Biofilm formation is triggered by a number of factors which can be either environmental or microbial in origin. Trigger factors that facilitate biofilm formation in one species can facilitate biofilm breakup in another. This is discussed below.

Oxidative stress in some bacteria can lead to biofilm formation as was seen in *S. epidermidis*, where experiments showed with increasing hydrogen peroxide levels up to 50mM lead to increases in biofilm formation (Liu et al., 2013). The same observations were seen in *Azotobacter vinelandii* (Villa et al., 2012).

Interestingly, efforts to combat microbes with the use of biocides can actually trigger biofilm formation as Kolari et al (2003) discovered when studying moderately thermophilic microbes identified from the paper industry. Some 39 strains of 95 identified organisms increased biofilm production by 5-753 percent in the presence of 5ppm methylene bisthiocyanate or 2,2,-dibromo-3-nitrilopropionamide (Kolari et al., 2003).

Temperature changes can also play a role in biofilm formation (Kuczynska-Wisnik et al., 2010), for example in *E. coli* where temperature sensitive proteins hslTS/ibpAB are up-regulated some 30-75 fold in increasing temperatures. These proteins have been implicated in biofilm formation (Chuang et al., 1993).

Ultimately, taking in to account the apparent fact that some 99 percent of all known microbial species form biofilms (Garrett et al., 2008, de Kievit, 2011), and taking into account their abundance in nature and biodiversity, one could surmise that biofilm formation is, in any setting where liquid water is present, inevitable.

1.6. Types of Surface that can be Colonised

Colonisable surfaces can be biological or non-biological in nature. For example *PA* form a biofilm within the lungs of cystic fibrosis (CF) patients, and is a major contributor to the morbidity and mortality of this genetic disease (Moreau-Marquis et al., 2008). Almost any inanimate surface can be colonised including various metals such as stainless steel (Hood and Zottola, 1997) as found in food processing systems, or polymers as found in medical devices such as catheters (Baier, 1972). Indeed, no substratum material has to date been found which can totally prevent colonisation for extended periods. But different substratums have shown a reduced tendency to be colonised. This trend tends to be surface energy linked, with either a positive or negative correlation, and is literature source dependent. This point is discussed at length in Chapter 1.20.1.

Much work has been reported on trying to understand how bacteria bind to different surfaces, and to ultimately design a surface that will prevent or at least retard microbial adhesion. Surfaces tested include various steel grades (Arnold et al., 2004, Verran and Whitehead, 2006, Briandet et al., 1999, Olofsson et al., 2003, Jayaraman et al., 1999), titanium (Verran and Whitehead, 2006), to polystyrene (Loosdrecht et al., 1990, Jones et al., 2003), gold (Chen et al., 2010), silicon (de Kerchove and Elimelech, 2008), quartz (Walker et al., 2005), PTFE, PMMA, (Gottenbos et al., 1999) and glass (Li and Logan, 2004, Otto et al., 1999a, Marcus et al., 2012, Poortinga et al., 2001), including polyamide materials used in membranes (Powell et al., 2017). However, Gottenbos, Li and Hogt (Gottenbos et al., 2000, Li and Logan, 2004, Hogt et al., 1985), found biofilms were able to develop on all substrates tested.

1.7 Biofilm Heterogeneity

It had been assumed for many years that the microbial inhabitants of biofilms were uniformly distributed throughout the structure (de Beer et al., 1994a). However, this hypothesis could not be further from the truth.

The biofilm microbial population can be remarkably heterogeneous, and can in the natural environment consist of many different microbial species, which is in turn, brought about by the heterogeneity of the environment within a biofilm itself. An example of this heterogeneity was found by (van der Mei and Busscher, 2001), where differing microbial zeta potentials were detected in a number tested individual cells from a monoculture. Such data strongly suggests intra-species heterogeneity within a monoculture. Microbes are often unevenly distributed over the surface and there can be large variations in cell density and composition over both time and space (Maukonen et al., 2003). Fazli and colleagues were able to show within the context of chronic wound infection that the distribution of *PA* and *Staphylococcus aureus* was not random at all, but shows some level of spatial organisation, with *PA* always found deep within the wound and *S. aureus* proximal to the wound surface (Fazli et al., 2009). This distribution was related to the potential specialist roles some bacteria can play in preventing wound healing, though this specialisation can probably be applied to most biofilms across nature. Similar observations were also made by Stoodley et al (Stoodley et al., 2012), whereby the apparent composition of the microbial biofilm changes over time, but also noted large voids and interstitial spaces within the biofilm structure, as well as the presence of areas exhibiting multispecies cohabitation. Recent observations have found that mature *Bacillus* biofilms cultured on agar, are able to form a complex organised network of channels that facilitate the flow of nutrient fluids from the margins of the

colony to the interior, powered by the evaporative processes occurring at the centre-surface of the colony (Zhang et al., 2015).

From a biofilm sampling perspective it is noteworthy that simple swabs of a biofilm surface or testing of bacteria sloughing from the biofilm surface may bias conclusions to the population demographic.

In mature biofilms, it is likely that internal nutrients, waste, and oxygen gradients will lead to the establishment of niche environments and allow for colonisation of specialist organisms or the adaptation of the existing populace as noted previously. This species diversity very much contributes to the difficulties encountered when removing biofilms (de Kievit, 2011).
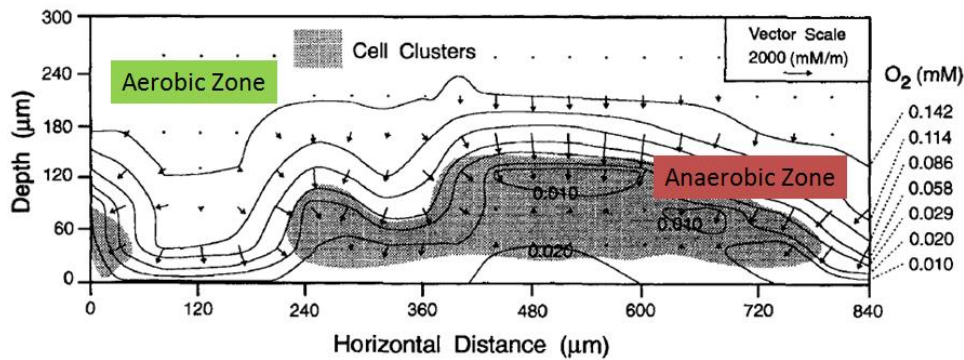
Figure 1.1. Adapted from de Beer et al (de Beer et al., 1994b). Showing the oxygen concentration mM (local concentration), and biofilm depth (approx. 160μm), emphasising the differences in oxygen concentration to changes in biofilm depth but also the uneven distribution of microbes in this biofilm.

L.A. Bjergbaek and colleagues (Bjergbæk et al., 2006) worked on different strains of *E. coli* both laboratory strains (*E. coli* K12) and clinical isolates. They found that the availability of oxygen and media impacted the growth curves of biofilms and affected their architecture, forming tall mushroom-shaped micro colonies in aerobic conditions and thinner less heterogeneous structures in anaerobic conditions. This behaviour was of course highly strain dependent and with variances amongst the clinical isolates.

Lawrence and colleagues, (Lawrence et al., 1991) working with various P*seudomonas* species (*aeruginosa fluroescens*) and *Vibrio parahaemolyicus*, found that the density of the biofilms can differ according to species. For example, it was observed that *Pseudomonas* species biofilms were far denser at the substratum-interface, whereas with *Vibrio parahaemolyicus* the denser

22

regions were observed at the top of the biofilm. It was also found that the biofilms tended to be open structures that were highly hydrated and consisted between 73 to 98 percent open space and extracellular materials (Lawrence et al., 1991).

Another example of the heterogeneity of the biofilm environment came from Wilton's published work (Wilton et al., 2016), who found that the presence of eDNA, can have a spatial expression relationship with other EPS molecules (Ma et al., 2009). eDNA was found to acidify the near surroundings thus creating a local niche environment. The change in acidity has been shown quite convincingly to enhance biofilm tolerance to a number of antibiotics (Wilton et al., 2016).

Taken together, the diversity of these structures conveys many advantages and is likely to be the primary reason they exist in the first instance. With one author commenting that the "sheer varieties of surfaces and environments that have been occupied by biofilms are almost infinite. It follows that combinations of the biofilm structural and temporal heterogeneity are just as numerous" (Garrett et al., 2008).

1.8 Antibiotic Resistance Hypothesis, and General Chemical Resistance.
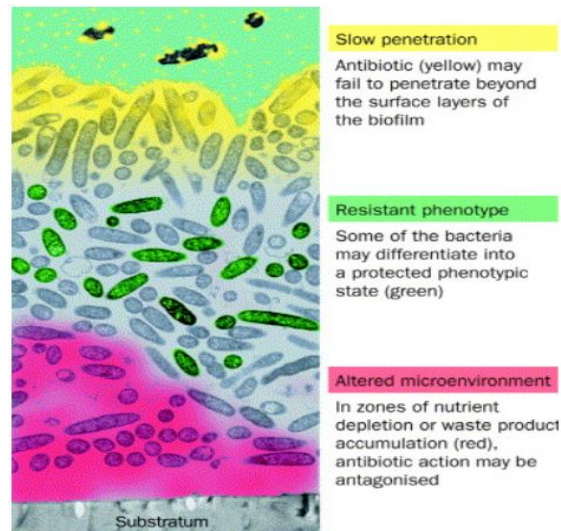
Figure 1.2. Proposed mechanisms for antibiotic resistance within biofilms. (Stewart and William Costerton, 2001).

The above Figure 1.2 details three of the proposed mechanisms for how some microbes may become resistant to antibiotics or indeed other forms of chemical attack, some of which can be attributed to the heterogeneous mature of the biofilm environment as discussed in Chapter 1.7.

The first hypothesis is based on the slow permeation of an agent through the biofilm, which can be by diffusive means or through deactivation of the agent by the microbes themselves. For example, Ampicillin can be broken down in β-lactamase positive *Klebsiella pneumoniae* bacteria at the surface of a biofilm at a greater rate than it can diffuse through the structure and interact with those residents deeper in the biofilm (Anderl et al., 2000).

The second theory is based upon there being microbes existing in different depths within a biofilm that result in them being phenotypically different from the rest of the population. For example in some cases researchers have found with increasing biofilm depth there can be changes in pH (Zhang and Bishop, 1996). This difference in phenotype may render them more resistant to a chemical substance, and allow them to persist, and evolve. Also, the biological activity of an agent may not extend into the pH found at depth within a biofilm, and thus may render it inactive.

The third theory is based on a small proportion of the biofilm population entering a state of suspended animation, developing a phenotype similar to that of a spore. These persister cells which may only make up 1 percent of the population could go on to repopulate a biofilm if the remainder are killed (Stewart and William Costerton, 2001).
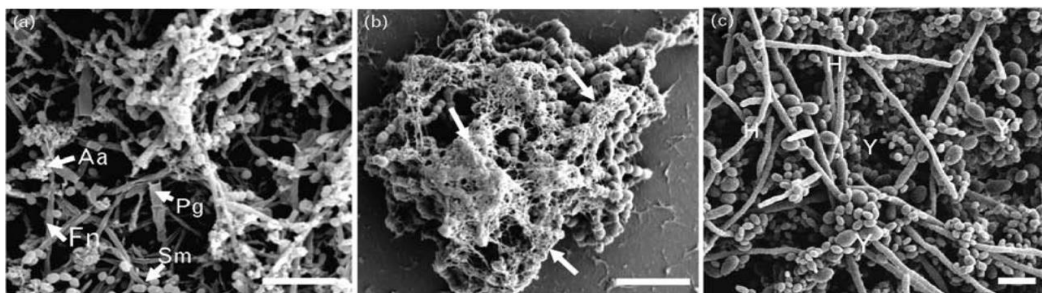
Figure 1.3. SEM micrographs of biofilm from a clinical environment. A. Biofilm consisting of *Streptococcus mitis* (Sm), *Fusobacterium nucleatum* (Fn), *Aggregatibacter actinomycetemcomitams* (Aa) and *Porphyromonas gingivalis* (Pg). B, is *Streptococcus mutans* biofilm EPS indicated (arrow) surrounding cells. C, is *Candida albicans* biofilm, both yeasts (Y) and hyphae (H) shown which form a dense lattice structure. Scale bar is 10µm. Taken from (Ramage et al., 2010)

Figure 1.3 emphasises the complex and heterogeneous nature of a multispecies biofilm as seen with a SEM. Pores can be clearly identified, similar to those observed by Zhang (Zhang et al., 2015), allowing nutrients and waste products out, but also the EPS can also been seen, as well as the many different species that make up this biofilm.

1.9 Biofilm Morphology

The morphology of biofilms is incredibly diverse; it varies from species to species, and even within strains. But one can also imagine a biofilm's morphology changing with time, as they grow, requiring the creation of fluid channels like those recently observed in Bacillus biofilms grown on agar (Zhang et al., 2015). Local surface and bulk fluid condition changes could alter their morphology, for example increases in shear stress in the bulk would potentially enhance film sloughing. Biofilms have been described by one author (Dunne, 2002) as resembling an 'underwater coral reef' complete with 'pyramidal or mushroom-shaped' structures. They can come complete with cavities, channels and other structural elements that allow for the exchange of nutrients and waste products, similar to what is found in social insect nests, (i.e. termites) that are used to manage both airflow and colony temperature.

Gross changes in biofilm morphology are reflected in some emergent properties in multi species biofilms, as were detected by Burmølle et al (2006) whereby the culturing of 4 different species of microbe resulted in an increase in biomass of some >165 percent relative to their equivalent mono species biofilms, as well as a decrease in antimicrobial agent susceptibility (Burmølle et al., 2006). Ergo, one could imagine as a biofilm acquires different species of microbe overtime in the natural environment, its structure and or morphology would also change.

Studies of microbial biofilms using confocal laser scanning microscopy typically find that microbe density increases with biofilm depth, and this observation was found to be true for *Pseudomonas* biofilms (Korber et al., 1997, Korber et al., 1989, Lawrence et al., 1991).

One paper found a clear link between surface hydrophobicity and colony morphology, whilst investigating the bacterium CW5. Whereby bacterial growth on hydrophobic surfaces resulted in a tightly packed morphology, with either single or paired cells, hydrophilic surfaces resulted in linked filamentous structures adhered to the surface via a single 'terminal cell' (Dalton, 1994). The same group also previously reported differing attachment rates according to hydrophobicity, with an approximate 5 fold increase detected on hydrophobic glass beads (Angles et al., 1993).

Research on the science of chaos (Lorenz, 1963), and related topics covered in the popular book Chaos (Gleick, 1998) where the sensitivity of initial conditions are thoroughly discussed pertaining to weather patterns and other natural phenomenon describable by the mathematics of chaos are also important in microbial studies. I believe this way of thinking is also highly relevant in the study of biofilms and their resultant morphology. Particularly because from this viewpoint biofilm growth occurs within a chaotic turbulent flow environment upon non-ideal surfaces, whereby the microbes swim around in the bulk liquid and attaching to the surface and each other at random positions. These sensitive initial conditions seemingly can only have chaotic effects on the final biofilm morphological conformation. This may be why reported studies investigating biofilm morphology are few.

1.10 *Pseudomonas* Colony Morphology

As stated above, generally biofilm morphology on inanimate surfaces by most species consists of the majority of the population of residing proximal to the surface (Lawrence et al., 1991, Korber et al., 1993, Korber et al., 1989).

Pseudomonas colony morphology has been shown to be dependent on the fluid flow conditions about a substratum, for example those grown in high shear and turbulent flow regimes typically

were more strongly adhered to a given surface, and were also found to be more dense and more stable with greater biomass (Pereira et al., 2002, Purevdorj et al., 2002). These biofilm attributes was also related to increased diffusion coefficients (Vieira et al., 1993) from the bulk. Conversely, differences in morphology have also been attributed to the observation of increased *Pseudomonas* anti-microbial resistance to biocides when cultured in turbulent flow regimes verses laminar flow regimes (Simões et al., 2003).

Steinberger and Holden found when *PA* was grown in an unsaturated water environment two distinct growth phases were detected. There was an initial rapid growth, typically involving increasing numbers of colony members, followed by a slower second growth phase where most EPS accumulation was observed (Steinberger and Holden, 2004).

Different colony morphologies have been observed in the literature when grown in flow, namely carpets, and mushroom shaped colonies (Klausen et al., 2003, Lawrence et al., 1991, Pamp and Tolker-Nielsen, 2007, Auerbach et al., 2000)}.

1.11 Biofilm Formation Steps

The growth and establishment of biofilms is ultimately the general sum of the cell attachment, detachment and growth processes. Biofilm establishment is a multistep process involving the establishment of a conditioning surface, microbe adhesion, micro colony formation, population growth, and biofilm maturation involving the establishment of a bacterial produced extracellular matrix, and desorption (sloughing) of some cells.

Biofilms can vary in thickness from monolayers of cells to thick formations such as algal mats (Christensen, 1989), to bodies as large as the Great Barrier Reef.
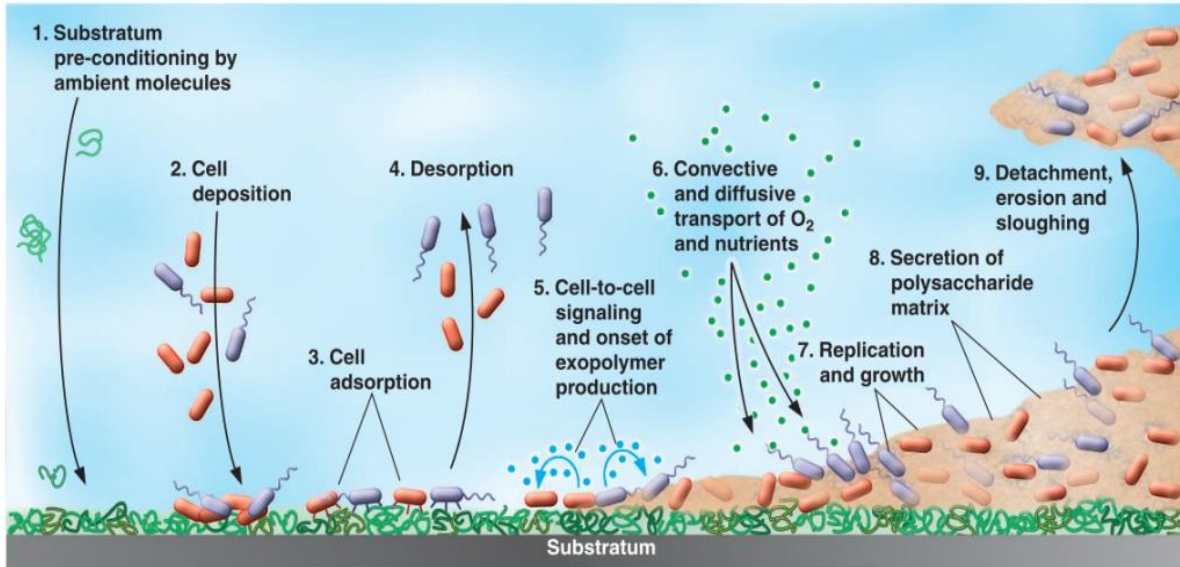
Figure 1.4. Depiction of biofilm development stages. Taken from Bryers and Ratner(Bryers and Ratner, 2004).

1.11.1 The Conditioning Layer

A conditioning layer is a material layer formed from molecules that attach initially to a surface, typically absorbed from the near bulk environment; this attachment can be either permanent or transient in nature. This layer may act to enhance anchorage of microbes and can act as possible carbon sources for the biofilm. These layers could act to make a substratum more favourable for microbial colonisation or not, and potentially have the effects of altering overall biofilm morphology.

The formation of conditioning layers is thought to be very rapid, and consists of the absorption of these materials to the substrate surface. These materials can include fragments of protein, lipid, carbohydrate and charged ions (Chmielewski and Frank, 2003). Both the transport rate to the surface and extent of absorption are important (Characklis, 1981). The conditioning film introduces physical, chemical, and biological heterogeneities at the substrate surface (de Kerchove and Elimelech, 2008, Melo and Bott, 1997). The formation of this layer starts only seconds after placing any surface into the relevant solution i.e. sea water (Compère et al., 2001) or blood (Murga et al., 2001), and is a thermodynamically driven process. In the example of implanted medical devices, proteins from the bodies inflammatory response system absorb onto the device surface which may serve to not only provide a better surface for bacteria to bind, but

also to confuse host immune responses leading to frustrated phagocytosis of macrophages which inhabits wound healing (Bryers and Ratner, 2004), and promotes inflammatory responses. Conditioning films have been shown to be between 30-80nm in thickness (Darren R. Korber et al., 1995), with some reported to be 4.4-13.8 nm thick (Lyman et al., 1968).

Conditioning layer components can also be both expressed by microbes in the near environment such as Alginate (an exo-polysaccharide) or can be made up of naturally occurring inorganic salts for example calcium chloride and magnesium chloride (de Kerchove and Elimelech, 2008) which form a polyelectrolyte surface, all of which play an important role in the adherence of microbes to different surfaces.

Adsorption of material to a surface can impart a number of complex changes in the physical properties of the surface including topography, wetting behaviour, surface change, and mechanical stiffness (Stadler et al., 2003, Carpentier and Cerf, 1993, Dickson and Koohmaraie, 1989), some of which are permanent modifications (Mettler, 1998). These changes to the surface may help create a more favourable surface environment that could enhance bacterial binding and or affinity, as well as creating an increased local nutrient environment compared to that of the bulk medium (Kumar and Anand, 1998).

This spontaneous creation of a thin conditioning film is thought to come about due to a decrease in total free energy of the substratum-bulk fluid system (Dexter, 1979b). This change in the Helmholtz free energy (ΔF), for the absorption of organic matter from the liquid bulk upon a substratum can be written as per Eqn. 1, for keeping constant temperature, pressure, volume, and when neglecting entropy changes:

$$\Delta F = \gamma_{SO} + \gamma_{OW} - \gamma_{SW} \qquad \text{Eqn. 1}$$

where γ_{SW} = surface energy of solid-water interface, γ_{SO} = surface energy of solid-absorbed organic, γ_{OW} = surface energy of organic-water interface.

In order for the above equation to be valid it is proposed that the ΔF for the absorption of the conditioning film is minimised or near zero, as γ_S for both the substratum and the bulk fluid enter equilibrium (Dexter, 1979b).

Changes in microbial cell adhesion and biofilm formation in some gram negative species including *PA* were detected by Murga et al following the establishment of conditioning films consisting of human blood borne components (Murga et al., 2001).

The removal of a conditioning layer can be very difficult as Verran and Whitehead (Verran and Whitehead, 2006) found when trying to remove both BSA and *S. aureus* from high surface energy materials such as a stainless steel surface, using SDS and an high velocity airbrush system. They found that although the bacterium could be removed, subsequent experiments on the stainless steel surface highlighted that the coverage of the BSA only worsened. Indeed even low surface energy surfaces have a propensity to recruit permanent conditioning films, as was detected on PTFE and PE surfaces (Lyman et al., 1968) for albumin, fibrinogen, and immunoglobulin, which could not be removed, even with extreme pHs.

Fletcher worked with *Pseudomonas*, cultured in seawater, and tested the effect of different proteins on *Pseudomonas* adhesion on a polystyrene (Fletcher, 1976). Protein conditioning films tested included BSA, gelatin, fibrinogen, pepsin, protamine and histone. The bacteria were also exposed to these proteins independently before and during adhesion as controls. Following the adhesion of the bacteria, these surfaces were rinsed and any bound cells were then fixed and stained with a gram stain kit. Results showed that proteins that were co-incubated with the bacteria during adhesion, prevented adhesion (Fletcher, 1976). But this result may be due to the conditioning films near instantaneous formation prior to initial bacterial surface interactions, which likely occur over longer time periods. This effect was also observed by Meadows (Meadows, 1971) with albumin and milk proteins (Parkar et al., 2001), and in testing multiple proteins with many microbial species on stainless steel (Barnes et al., 1999).

However, conditioning layers containing casein and gelatin were observed enhancing microbe attachment (Fletcher, 1976). The basic proteins tested had no effect on bacterial adhesion in these experiments. It was thought that the inhibition of bacterial attachment observed was likely due to steric exclusion (Fletcher, 1976). *In-vitro* testing of numerous microbe species also found that conditioning films formed by human blood also enhanced biofilm formation (Murga et al., 2001).

Parker investigated the effect of the removal of some cell surface components in combination with the addition of skim milk as a surface conditioning agent on stainless steel using numerous *Bacillus stearothermophilus* strains (Parkar et al, 2001). His group found that the more hydrophobic spores were more readily bound to the surface, and that the presence of a skim milk

conditioning film reduced adhesion of both the bacterium in both vegetative and spore states. However the effect was not concentration dependent within the 1% and 10% v/w skimmed milk powder concentrations tested (Parkar et al., 2001). This observation is contradictory to that discussed above where casein was observed enhancing microbe adhesion, the main difference between the two studies being different microbes were used, highlighting the importance of studying multiple bacterial species models.

It is noteworthy that some authors (Kim et al., 2006) have attributed changes in levels of nutrient availability in the bulk for the lack of biofilm formation on a given surface when using different complex biological bulk media formulations (often of biological origin such as plant, animal, fungi). However, in such experiments it would be impossible to show whether the establishment of a conditioning film may be also be a contributory factor, as has been observed and discussed above.

One author performed simple adhesive experiments by testing the interfacial strength of glass substratums-biofilm interface with and without the presence of a conditioning (saliva) film (Busscher and van Der Mei, 1995). They found that the biofilms were more easily removed when the conditioning film was present. The author concluded that the failure of the conditioning film was cohesive, ie. within the film itself, which is an interesting idea indeed.

Conditioning films are thus a vital variable, as I believe that microbes actually see very little of the actual substratum. However, it is the nature of the conditioning surface that perhaps plays a greater role in microbial recruitment to the surface. The nature of the substratum maybe only important in the recruitment of conditioning molecules.

This area is likely to be one of the areas of study I will undertake as part of this research project, as this appears to be a largely neglected area of biofilm research and perhaps one of the most important steps in early biofilm establishment.

1.11.2   Active Bacterial Transport

Active bacterial transport is influenced by the presence of flagella on the bacteria cell surface. These flagella rotate rapidly powered by electrochemical potentials and electrostatic interactions across the cell membrane (de Kerchove and Elimelech, 2008). Flagella are discussed later in this Chapter.

The first bacteria that interact and bind to the substratum are arguably the most important, as they provide the foundation for the whole colony, linking colony and EPS to the substratum/conditioning surface. This potential interface has been shown to be potentially important in cleaning studies using high shear (Busscher and van Der Mei, 1995) .

1.11.3   Cell Adhesion

Adhesion of microbes to a surface can be either active or passive. Passive attachment is driven by diffusion, gravity (sedimentation) due to differences in specific gravity between the bacteria and the bulk fluid, as well as fluid dynamics such as Brownian motion and convective mass transport (Palmer et al., 2007). Long range nonspecific interactions between the substratum and the bacterium can occur over distances of approximately 50nm, and are typically a function of both distance and free energy. Short range interactions which are more specific become more effective when the bacterium is less than 3nm from the surface (An and Friedman, 1998, Kim et al., 2012).

Active adhesion is attachment that is facilitated by the bacterium themselves, which includes the use of motor appendages, pili and flagella, but also the expression of adhesion proteins. Attachment typically occurs within 5 to 30 seconds (Amano et al., 1999, Chmielewski and Frank, 2003) and occurs in two stages; reversible followed by irreversible adhesion. The former process typically being associated with passive attachment, and the latter with active attachment which can take between 20 minutes and 4 hours. Active attachment requires the expression of adhesive molecules (adhesins) which help strengthen adhesion, the expression of which can be depend on the type of surface presented to the bacterium and its genomic repertoire.

The fundamental adhesion forces involved in these above process include van der Walls forces, electrostatic forces, hydrogen bonding, and dipole-dipole interactions (Amano et al., 1999, An and Friedman, 1998, Chmielewski and Frank, 2003). Surface roughness and micro-topography are also thought to be very important factors in adhesion (Palmer et al., 2007), but this analysis is disputed (Barnes et al., 1999). Most bacteria present a negatively charged surface to the environment, coupled with numerous hydrophobic cell surface proteins or components (Donlan, 2002). The time taken for irreversible cell-surface adhesion has been shown to vary, with some species such as *Streptococcus* taking 30 seconds (Flint et al., 1997), and others (*Staphylococcus*, *Acinetobacter* and *Streptococcus*) up to 10 minutes (Meinders et al., 1995), with no difference being observed after an incubation time of up to 24 hours.

Christersson et al concluded after performing flow experiments, that the initial attachment and detachment phase, were non-specific in nature and that only specific adhesion interactions would likely follow an initial nonspecific contact with a substratum (Christersson et al., 1988).
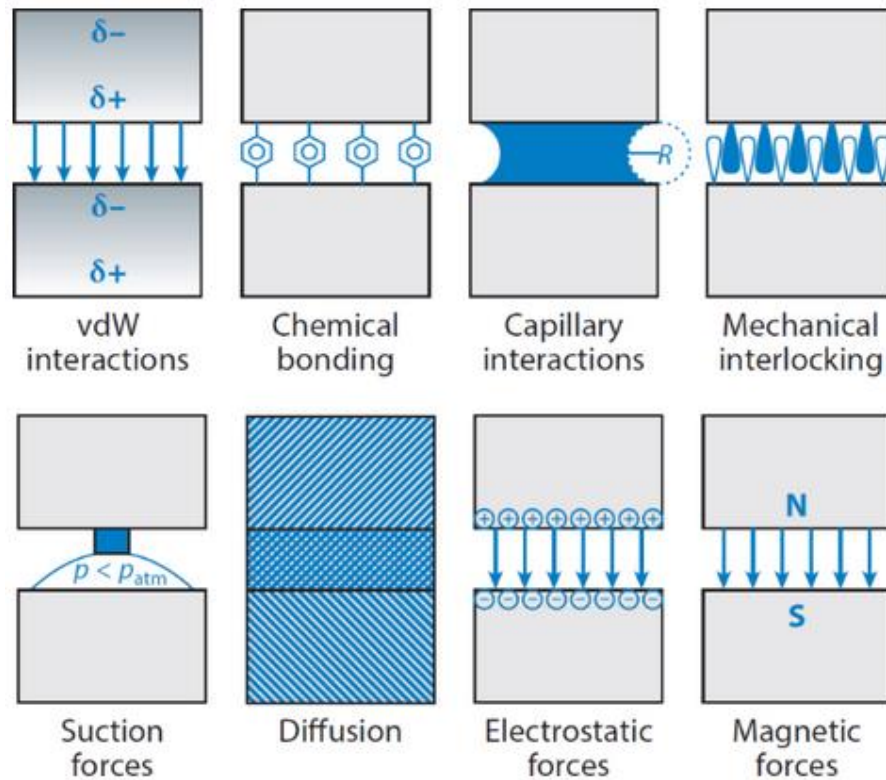
Figure 1.5. Diagram showing different models for adhesion. Taken from (Gorb, 2014)

It is important to remember that the propensity for adhesion relies on the forces contributed by both the microbe and the surface, and thus an understanding of the hydrophobicity and electrostatic properties (i.e. zeta potential) of both the microbe and the surface under study can be useful. Dickson and Koohmaraie made an important observation that the relative degree of bacterial cell surface hydrophobicity can vary greatly depending on the measurement method employed (Dickson and Koohmaraie, 1989), and this observation is likely true for any type of surface property measurement.

Properties of the substratum	Properties of the bulk fluid	Properties of the cell
Roughness	Flow rate and velocity	Cell surface hydrophobicity
Hydrophobicity	pH	Fimbriae
Presence of conditioning film	Temperature	Flagella
Surface energy	Cations- concentration and type	Extracellular Polymeric Substances (EPS)
Surface charge	Presence of antimicrobial agents	Surface charge

Table 1.1. Summary of important variables in cell attachment to surfaces adapted from Dunne, An and Freidman(Dunne, 2002, An and Friedman, 1998).

Strength of cell adhesion can be very time dependent as Vadillo- Rodríguez et al showed using AFM. The strength of adhesion of the microbe *Streptococcus* thermophiles increased some 100-1000 fold within 1 minute (Vadillo-Rodríguez et al., 2004). This may have been due to an increase in surface area contact of the bacterial cell wall or other cell surface components with the substratum following an initial contact phase, thus increasing its affinity.

Divalent cations have also been shown to play an important role in adhesion events. de-Kerchove and Elimelech, using *PA* investigated the effects of calcium and magnesium chloride and found that with increasing concentrations (0 to 30mM), there was a decrease in microbe electrophoretic mobility, and thus a net decrease in surface charge, which increased bacterial deposition rates (de Kerchove and Elimelech, 2008). This reduction in negative charge reduced the large repulsive forces of similarly charged surfaces predicted by DVLO theory. This finding was corroborated by work performed on *Pseudomonas putida* KT2442 by Abu-lail and Camesano (Abu-Lail and Camesano, 2003a).

Interestingly, research comparing the effect of monovalent (KCl) and divalent (CaCl$_2$) salts on adhesion using *Cryptosporidium parvum* oocytes by Kunar and Elimelech (Kuznar and Elimelech, 2004) found using optical microscopy that increasing CaCl$_2$ concentration increased adhesion on quartz surfaces, however this behaviour was not the case for the monovalent salt, even though DVLO theory predicts the absence of the electrostatic energy barrier for both salts. This difference was thought to be due to electrostatic repulsion, where the electrostatic component arises from charged functional groups and/or polyelectrolytes, the repulsion arises from the compression of

the surface polymers in contact with the surface (Kuznar and Elimelech, 2004). Thus, the differences between the presence of mono and divalent salts is the ability of Ca^{2+} to associate with the glyco-protein's amino acid side chains found on the *C. parvum* surface, neutralising their charge which then facilitates their collapse, thus reducing their steric repulsive force. $CaCl_2$ is thought to have a two pronged effect thorough both surface protein conformational changes along with a reduction in surface electrostatic interactions on microbial adhesion (Kuznar and Elimelech, 2004).

Loosdrecht et al. working with a range of bacteria including *Pseudomonas* and *E.coli*, found that cell surface hydrophobicity plays an important role in enhancing adhesion of microbes, in this case to negatively charged polystyrene with a water contact angle of 70° (van Loosdrecht et al., 1987).

In addition the role of LPS in bacterial adhesion using *E.coli* JM109 cells was evaluated using AFM by Abu-Lail and Camesano (Abu-Lail and Camesano, 2003b). The LPS was removed (approximately 80 percent) using 100mM ethylenediaminetetraacetic acid (EDTA). Their work revealed on average adhesion between the *E. coli* and the silicon nitride tip of the AFM to be far lower, dropping from -2.1nN±1.8 to -0.4nN ±0.36.

The growth phase of microbes can have quite large effects on their propensity to bind to surfaces, and this effect can be species specific. For example Bruinsma (Bruinsma et al., 2001), found that *PA* adhered better to both hydrophobic and hydrophilic (silicone rubber and glass respectively) surfaces when in mid-exponential growth phase. In contrast Walker (Walker et al., 2005) found that stationary phase cells were much more adhesive than mid-exponential phase cells when working with *Escherichia coli* on quartz surfaces. Marcus and co-workers (Marcus et al., 2012) found similar artefacts, whereby *PA* that was in exponential phase was hydrophilic (water contact angle 22°±3%) and when in stationary phase was hydrophobic (contact angle 80° ±3%). Interestingly they also showed using QCM-D that the hydrophobic *PA* species formed an elastic contact for both hydrophilic and hydrophobic surfaces (silica (SiO_2 water 48°±2) and polyvinylidene fluoride (PVDF water 90°±4) respectively. They also showed that the hydrophilic cells were exhibiting elastic properties on hydrophobic surfaces, but more viscoelastic at higher overtones, with hydrophilic cells on a hydrophilic surfaces the connection was always viscoelastic at all overtones. This may have been due to the viscoelastic deformation of the microbial cells at higher overtones.

The expression of bacteria cell surface fimbriae is dependent on levels of gene expression, and thus bacteria can shift from a fimbriae phenotype to a non-fimbriae phenotype. This allows bacteria to present a different surface with different binding characteristics to the environment (Otto et al., 1999b).

Metal oxides on the surface have also been shown to increase the adhesion of negatively changed bacteria principally due to their positive charge, but also due to their hydrophobicity (Li and Logan, 2004).

Dickson and Koohmaraie found a linear correlation between both cell surface charge and hydrophobicity of the microbes themselves and initial attachment to biological surfaces (lean meat muscle and fat), with increases in cell surface hydrophobicity correlating well with that of the substratum hydrophobicity, i.e. fat content (Dickson and Koohmaraie, 1989).

Other important environmental consideration is temperature and bulk nutrient concentration. One study found that *Enterobacter sakazakii* biofilm formation was inhibited at a temperature of 12°C, but restored at 25°C, and that in nutrient deficient medias (Kim et al., 2006) biofilm formation was also absent. The temperature sensitivity observation is most likely relevant to other species. Other important temperature ranges were noted by Dickson when evaluating *Salmonella* adhesion to biological surfaces (Dickson, 1991). The observed correlation between bulk nutrient deficiency and biofilm formation may be due to the establishment of an inhibitory conditioning film, or due to the reported lack of nutrients in the bulk. Both observations are however important.

Increases in inoculum concentration have also been shown to be important in the initial binding of microbes. The age of the culture has also been shown to be vital, where younger (16-24hr) cultures (in log/stationary phase) bound more readily than older cultures (66hr) (Dickson, 1991). This behaviour is likely due to changes in their cell surface structures, as the microbes are stressed, and emphasises the importance of keeping initial binding methods standardised. Interestingly, Meadows found that not only did dead bacteria bind to surfaces, but that the manner in which they were slain affected their ability to adhere. With those killed by UV light were able to bind to the same extent as those that were viable, however those killed with heat or formalin exposure bound far less readily (Meadows, 1971). It is important to remember that, as discussed by Van der Mei and Busscher, mixed within any population of microbes, multispecies or mono

species will be cells of different surface charge and hydrophobicity, thus some cells will always adhere to any given surface (van der Mei and Busscher, 2001).

In addition to the general observations noted above, it is important to recognise that for a global cell surface or substratum, free energy considerations whilst always present and important, maybe superseded by other factors. Specific cell surface-conditioning film, or substratum interactions will trump any global view (Busscher et al., 2008). An example taking data from two authors (Petersen et al., 2002) and (Xu et al., 2007), shows with some clarity the effect of specific cell surface receptor-conditioning recognition, and how this can cause deviations from what one would expect/predict from cell surface global variables generally (see Table 1.2).

Streptococcus mutans Strain	Water contact angle (θ)	Zeta potential (mV)	Adhesion (10^6 cm^{-2})	
			Glass	Glass with Saliva conditioning film
LT11 (with type I/II antigen	29°	-20	12.1	9.6
IB03987 (without type I/II antigen	33°	-25	11.8	2.5

Table 1.2. Adapted from (Busscher et al., 2008), showing data from Petersen (Petersen et al., 2002) and Xu (Xu et al., 2007), emphasising the similarities in cell surface change and hydrophobicity and substratum interaction. But showing greater surface affinity with saliva conditioning film, due to specific molecular recognition due to presence of type I/II antigen, versus no saliva conditioning film.

Table 1.2 relates a microbe that is found in the oral cavity, with the presence of a conditioning film (saliva) found in its niche environment. This example is also very likely relevant to microbes that have evolved to exist on inanimate surfaces in industrial or other settings with naturally/ human made occurring conditioning films found locally, and thus it is important to be aware of this complex and potentially unpredictable phenomena.

1.11.4   Twitching and Micro Colony Formation

Micro colony formation is the process where single or small groups (50 or less) of microbes coalesce into larger collections which form the basis of an early stage biofilm (Zhao et al., 2013).

Twitching describes the jerking movements of cells as they move on a surface and is thought to be enacted through the extension and contraction of type IV pili (Darzins and Russell, 1997, Whitchurch et al., 1991). How individual surface attached bacteria organise themselves is not currently known (Zhao et al., 2013). However, Zhao and colleagues found that *PA* deposits a trail of polysaccharides (Psl), on the surface as they twitch, which is built upon by other cells once encountered in a positive feedback manner. This suggests a mechanism whereby the micro colonies self-organise on a surface, interestingly a similar system exists within many corporative insect species eg snails and ants. However, additional studies using mutants have shown that Psl as well as Pel and Alginate knockout mutants still stably form biofilms readily (Cole et al., 2014). Other interesting research has found that eDNA plays a vital role in *Pseudomonas* biofilms where self-organising cellular communities create columns, following eDNA paths, during colony expansion at the margins ensuring efficient migration of microbes from the interior to the envelope (Gloag et al., 2013). Merz and colleagues (Merz et al., 2000) did some fascinating work, with *Neisseria gonorrhoea* and were able to see type IV pili at work in promoting twitching motility.
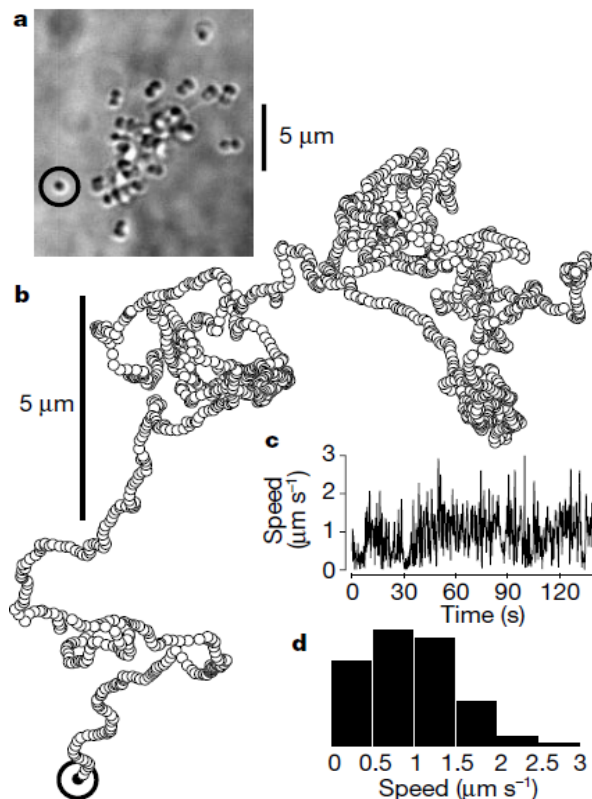
Figure 1.6. The twitching motility of *N. gonorrhoeae* on a glass cover slip. **a**, image of cell on glass cover slip, tracked diplo-coccus is circled. **b**, is track for the N. gonorrhoeae took over a 3 minute period. **c** and **d**, show the speed of travel in µms[-1](Merz et al., 2000).

It is twitching motility that ultimately promotes the formation of micro colonies (first signs of increased microbe community order), from the initially surface dispersed monolayers of cells following initial surface attachment which is somewhat disordered. It can be thought of as the process which is equivalent to allowing the grouping of people (walking) following uncontrolled parachuting down to Earth from 50 miles high in a category 5 hurricane (i.e. a turbulent flow).

1.11.5   Biofilm Maturation

Biofilm maturation is characterised by the production of EPS, increased bacterial cell density and increased colony complexity. It is at this advanced stage that the overall superstructure of a biofilm is built, whether that is flattened or mushroom shaped. Growth during and following this stage is mainly reliant on the nutrients in the bulk, the perfusion of those nutrients into the biofilm to the colony members, and subsequent waste removal. Another important biofilm limiting consideration is the amount of turbulence about the substratum, and depth of boundary layer (Dunne, 2002).

1.11.6   Biofilm Dispersion

Biofilm dispersal is an important part of the life cycle of a biofilm, and helps facilitate the spread of the colony onto virgin surfaces. Dispersal is accomplished is a number of ways; detaching of progeny cells, deliberate detachment in response to environmental cues (changes in nutrients), quorum sensing or by shearing caused by the effects of flow (Donlan, 2002). Indeed micro-colonies have been detected rolling across a surface in the presence of fluid shear (Rupp et al., 2005), similar to the dispersion mechanisms utilised by some plants eg. Tumble weed.

1.12 What are Fimbriae (Pili) or Fibrillae and Flagella

Fimbriae, Pili and Flagella are different types proteinaceous filaments that extent out from the cell surface that fulfil different functions, from motility to cell adhesion.

Both Fimbriae and Pili are used by bacteria to attach to both surfaces and to each other (adhesion and cohesion respectively). One form of Pili called 'sex pili' is used during conjugation where by a 'male bacteria' transfers plasmid DNA to a recipient 'female bacteria' (Slonczewski and Foster, 2011), however bacteria are of course hermaphrodites. This mode, which could be considered one of the mechanisms used by microbes to engage in horizontal gene transfer, of course greatly benefits from the close proximately of microbes found within biofilm structures.

Fimbriae are rigid, filamentous structures on the cell surface that are typically no more than 4 to 7nm diameter and from 0.2 up to 20µm in length (An and Friedman, 1998), and thus extend a considerable distance from the bacterial cell surface. Bacterial Fimbriae are polymers consisting of many identical repeating monomers called Pilin (An and Friedman, 1998, Slonczewski and Foster, 2011). There can be between 100 and 1000 Fimbriae on a single bacterium and these can be distributed evenly over the cell or may be localised (Singleton, 1999). Fimbriae subunits are typically rich in non-polar amino acids and thus are mostly hydrophobic. Fimbriae are typically found on gram-negative bacteria and are bound to the outer membrane of the bacteria and it is on these structures that adhesion molecules are commonly located (Singleton, 1999).

One type of Fimbriae/Pili of note is type 4 (IV), which occurs in some gram negative bacteria for example *E. coli*. They are located on one pole of the cell and are associated with twitching motility and adhesion. This type is also called bundle forming Pili (Singleton, 1999).

Flagella are external cell structures, which tend to be ridged helical structures that can rotate rapidly. They are mainly used for locomotion, they are important as they allow bacteria to overcome the viscous nature of their aqueous environments, and allow travel through the medium as opposed to travelling with it. These can be found at just one pole of a bacterium, both poles or at various points on the bacterium; this can be very species specific. Korber and colleagues (Korber et al., 1989) carried out experiments using *P. fluorescens* and observed that mutants that were immobile attached to surfaces at a slower rate than those that were mobile, highlighting the importance of in-fluid motility in biofilm establishment. In other experiments using *Listeria monocytogenes* (Vatanyoopaisarn et al., 2000), showed that flagella were helping to facilitate adhesion to stainless steel surfaces, as well as locomotion.

1.13 Adhesin Molecules

Adhesin molecules as the name suggests are molecules that promote the adhesion of a microbe to a surface. They are often expressed when required, and can promote specificity in binding as well as increasing the affinity of adhesion events. This has been shown often within the context of bacterial-host interactions, and as such are important pathogenic determinates (Klemm and Schembri, 2000), or when binding to saliva conditioning films on glass (Busscher and van Der Mei, 1995). Adhesins can either be proteinaceous and or have a sugar component to them, and can either be affiliated with the termini of a pili or fimbriae but also occur on the microbial cell surface. The principle binding peptide type presented by many microbes upon their surface for

nonspecific binding is thought by at least one author to be lipoteichoic acid (a polyglycerol phosphate polymer) in nature (Baier, 2015).

1.14 The Extracellular Polymorphic/Polysaccharide Substance (EPS) or Extracellular Polymorphic/Polysaccharide Matrix (EPM)

Interestingly, EPS is expressed by large numbers of cell types, from eukaryotic to prokaryotic cell types. Examples from eukaryotes includes bone, cartilage, and connective tissue (Becker et al., 2000) all of which play a key role in maintaining the superstructure of their multi-cellular communities (our bodies for example). In eukaryotes the EPS serves to aid attachment of cells, and helps form local structures to allow fluid flow such as in bones (collagen), and even to attract and hold water (proteoglycans) (Becker et al., 2000), with similar observations also being made in prokaryotic biofilms (Zhang et al., 2015). In eukaryotes the ECM can be anchored to cells via proteoglycan linkages, and in some cases the proteoglycans can be imbedded in the plasma membrane of cells, covalently linked to membrane phospholipids or found bound to cell surface receptors (i.e. adhesive glycoproteins (Becker et al., 2000).

EPS is a bacterially produced material that they express into their environment. The material consists mainly of polysaccharides but also proteins and nucleic acids. Other constituents can also associate with the EPS and these can be non-cellular in nature such as mineral deposits or blood components depending on the biofilms environment (Donlan, 2002). EPS in prokaryotes ultimately serves the same purpose in eukaryotes.

The actual surface topology and structure imparted onto a biofilm by the EPS can greatly affect local hydrodynamics, which in itself affects a biofilm through all development stages. This increased surface irregularity enhances convective mass transport proximal to the surface, provides protection to microbes from shear forces, and increases the surface area available for attachment, for resident microbes and those incoming from the bulk. In mature biofilms the rate of cell division can also be affected hydrodynamics through limiting or enhancing metabolite availability (Lewandowski, 2005). Conversely, the growth of a biofilm out from the surface towards the bulk fluid environment, courtesy of the EPS, can enhance biofilm sloughing due to the presence of greater turbulence towards the boundary layer. Interesting, shear can play a role in inducing phenotypic responses resulting in changes in the mechanical properties of the EPS and thus the biofilm as a whole (Stoodley et al., 2002a), suggesting a dynamic relationship between EPS production, mechanical properties, spatial expression and the local bulk flow regimes.
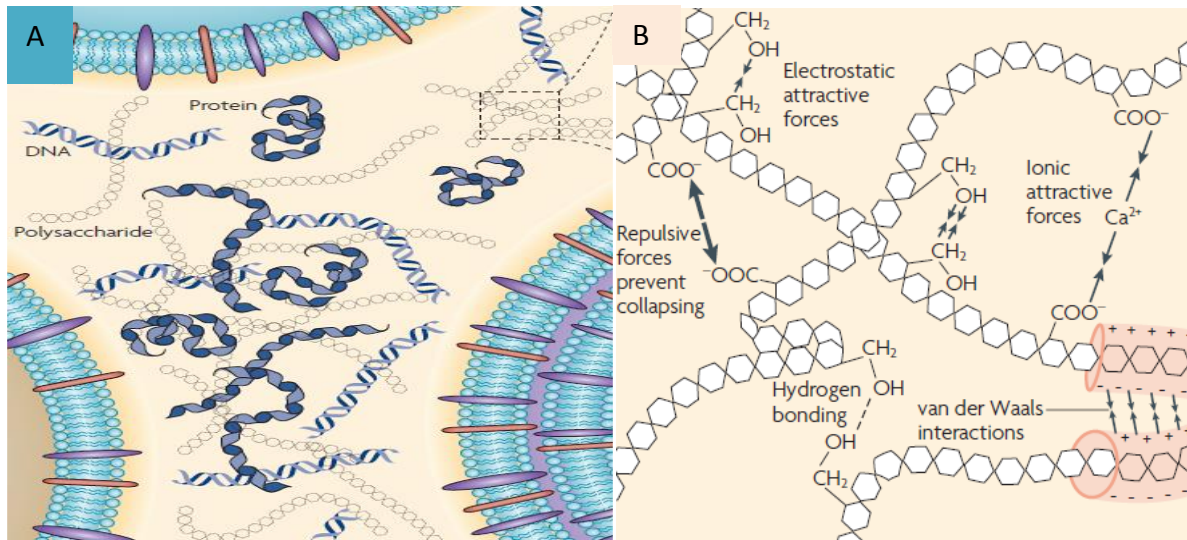
Figure 1.7. A, Idealised diagram of the internal structure of the EPS, showing the major components. B, Schematic of the forces involved in stabilising the EPS structure. Both figures were modified from Flemming and Wingender (Flemming and Wingender, 2010).

The EPS often surrounds the cells within a biofilm and thus represents their most immediate environment. The exo-polysaccharides are the major structural component of a biofilm, and the EPS is the sum of many individual polymeric units, each of which can differ in local concentration, cohesiveness, charge, sorption capacity, specificity for binding cells, resulting in very diverse habitat. However, the ultimate function is to support microbes to live in a multi-species community (Flemming and Wingender, 2010), under conditions that would otherwise be unfavourable, for example during desiccation, or where they maybe susceptible to prolonged attacks from host immune defences.

The polysaccharide components typically take the form of long linear, or branched moieties with a molecular mass of approximately 500-2000kD, and, as with biological systems, the largest component of the matrix is water which supports the structure. Most EPS constituents are hydrophilic conveying net biofilm hydrophilicity, which is of benefit as during desiccation; biofilms tend to hold onto water far longer than the external bulk environment. EPS is typically negatively charged, however does contain positively charged regions (Gordon et al., 1988). There are examples however, of microbes expressing hydrophobic matrixes for example *Rhydococcus* species, which produce polysaccharides rich in methyl and acetyl groups (Neu et al., 1992).

42

The multi-component nature of the biofilm matrix results in its behaving as an amorphous substance, which means often they can behave in a viscoelastic manner, (Flemming and Wingender, 2010). Korstgens and colleagues, (Korstgens et al., 2001) found this when investigating *PA* biofilm under increasing shear stress. The biofilm was initially behaving elastically, and then reached a point at which viscous type deformation became more prevalent. This viscoelastic behaviour was attributed to the complex polymer bundle type arrangement seen in biofilms.

EPS represents a complex and dynamic structural material phenomenon that is subject to dynamic remodelling and has been shown to be both protective on biotic and abiotic surfaces, from host immune responses, or desiccation respectively. It appears to offer most of the principle benefits of being in a biofilm to its residents, and it is immensely complex. The constituents of biofilm are discussed in more detail in relation to *Pseudomonas* biofilms in Chapter 1.25.1.

1.15 Properties of Microbe Cell Surfaces

Bacteria consist of three main components. Firstly there are the appendages, these are made of proteins attached to the surface and take the form of flagella, fimbriae and pili. Secondly there is the cell envelope consisting of the capsule, cell wall and plasma membrane. Thirdly, is a cytoplasmic region containing a cells genome, other nuclear material and protein synthesis hardware.

The bacterial cell surface is the sum of both the appendages and envelope, and it is these that are exposed to, sense and are used by the bacteria to interact directly with their environment.
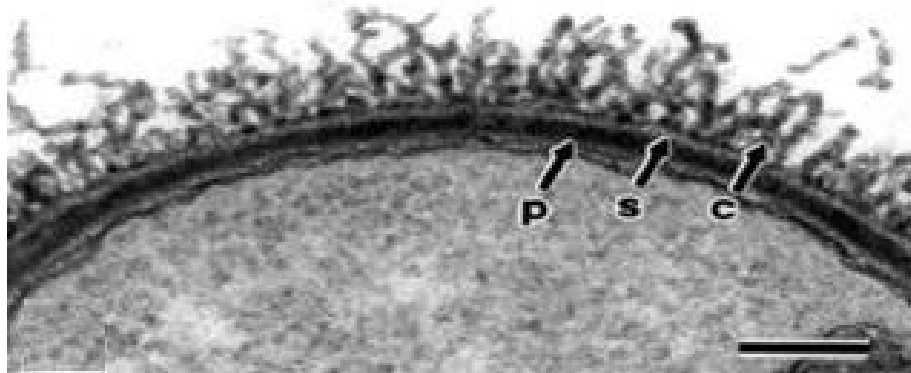
Figure 1.8. Cross section of cell wall of *Bacillus anthracis* using TEM. **P** denotes the peptidoglycan cell wall. **S** refers to the S-layer which consists of two proteins including the major antigen. **C** denotes the poly-D-glutamic acid capsule that is exterior and completely covers **S**-layer proteins. Bar 250nm(Mesnage et al., 1998).

1.15.1   The Glycocalyx, Bacterial Capsule and Slime Layer

Glycocalyx meaning 'sugar coat' is a carbohydrate rich zone that surrounds many types of bacteria, both gram positive and gram negative. These sugars can be constituents of either glycoproteins, or glycolipids, and either have been excreted from the cell and then reabsorbed onto the cell surface or are physically tethered to the cell surface. They are very water soluble, and have a high water content, with the sugar groups facing out into the extracellular environment (Alberts et al., 1983).

Very well ordered and large glycocalyx structures tend to be associated with the bacterial cell surfaces and are known as bacterial capsules. These form distinct margins on the outside of bacteria and can be seen either stained or unstained as a clear region surrounding the cell using standard light microscopy. Some early experiments by Hogt and colleagues in the mid-eighties also highlighted the importance of proteins within the capsule regarding adhesion, whereby following exposure to proteolytic enzymes both hydrophobicity and adhesion were observed to be reduced (An and Friedman, 1998, Hogt et al., 1985).

When the capsules become loosely attached or dissociated from the bacterium they are formed around they (the so called slime layer) they are thought to further aid in the initial biofilm formation process by assisting in the attachment of other microbes. (Alberts et al., 1983, An and Friedman, 1998).

Bacterium	Capsule composition	Structural subunits
Gram-positive Bacteria		
Bacillus anthracis	polypeptide (polyglutamic acid)	D-glutamic acid
Bacillus megaterium	polypeptide and polysaccharide	D-glutamic acid, amino sugars, sugars
Streptococcus pyogenes	polysaccharide (hyaluronic acid)	N-acetyl-glucosamine and glucuronic acid
Gram-negative Bacteria		
Escherichia coli	polysaccharide (colonic acid)	glucose, galactose, fucose glucuronic acid
Pseudomonas aeruginosa	polysaccharide	mannuronic acid
Agrobacterium tumefaciens	polysaccharide	(glucan) glucose

Table 1.3. Different bacterial species and their capsules principle chemical components ((Todar, 2013b).

1.15.2   The Surface Layer or S-Layer

The S layer is typically the outer most part of the cell and it is found overlaying the cell wall. It consists of a repeating pattern of identical monomolecular proteins or glycoprotein subunits, these are arranged in either squares or hexagons (Singleton, 1999, Sára and Sleytr, 2000), see Figure 1.8 and Figure 1.9. S-layers are thought to play an important function role in the bacterial life cycle and possibly adhesion because they are ubiquitous and thus most likely important in nature. Their expression however can be lost when environmental isolates are brought in the laboratory, and used over extended periods (Sleytr, 1996), which can complicate the study of S-layers. In gram negative bacteria the S-layer is thought to be attached to the LPS, and in gram positive bacteria it is thought to be anchored in place by a thin peptidoglycan layer found as part of the cell wall. In either case it is approximately 2-8nm thick, and is thought to be attached non-covalently, with an

amino acid composition high in acidic and hydrophobic amino acids (Sára and Sleytr, 2000), most with isoelectric points (pI) in the acidic pH range (Mesnage et al., 1998). With its hydrophobic components, this layer could possibly charge the surface of a microbe and make it more hydrophobic, all of which are characteristics potentially important in adhesion phenomena.
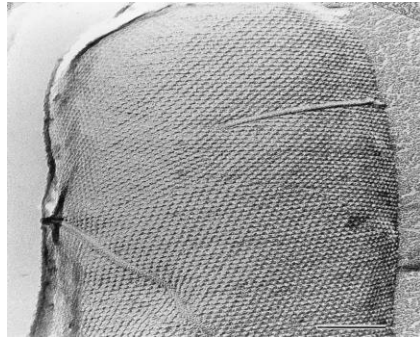
Figure 1.9. SEM micrograph of a S-layer. (Bar is 100nm, (Sára and Sleytr, 2000).

1.16 The Cell Envelope, Membranes and Microbial Cell Walls

The vast majority of microorganisms possess cell membranes with other supporting structures, with the exception to mycoplasmas. Typically the cell wall is accompanied by outer membranes and capsules (Slonczewski and Foster, 2011), which comprises the cell envelope.

Biological membranes are essential to life as currently understood. Cell membranes form barriers between the internal components of cells and their external environment, thus define the cellular boundaries. They are selective semi-permeable structures which allow the flow of nutrients and into and out-of cells. The passage of these molecules can be facilitated by both active and passive transport. The size limit for passive transport is approximately 750-1000 Daltons (Dowhan et al., 2008). Membranes are critical in facilitating cellular interactions and responses with the environment, i.e. detecting environmental or cellular signalling queues.

1.16.1   Properties of Microbe Cell Surfaces

The outer leaflet of the outer membrane of gram-negative bacteria is not a monolayer of phospholipids, but rather consists mainly of lipopolysaccharide (LPS). In some cases such as *E. coli*, the surface can contain as much as 75 percent LPS and 25 percent proteins (Abu-Lail and Camesano, 2003b, Amro et al., 2000). LPS generally consists of lipid A which is responsible for most of the immunological response in mammals, and is attached to both the outer membrane as

well as the inner and outer core of hydrophilic polysaccharides. These polysaccharides are made of heptose, glucose, galactose, and N-acetylglucosamine molecules. The outer most part of the LPS is the O-polysaccharide (O-antigen), whose composition is strain specific (Walker et al., 2005). The O-antigen has been shown to confer hydrophilic properties to gram negative bacteria (Williams and Fletcher, 1996). There are approximately 3.5 million LPS molecules present in the outer membrane of a typical gram positive bacteria (Walker et al., 2004). LPS can extend approximately 30Å above the surface and thus interact freely with the external environment. Interestingly, most outer membrane proteins are β-barrels consisting of either eight or twenty four β-strands (Wiener and Horanyi, 2011).

Gram-negative species tend to have only one layer of peptidoglycan, and possess a far larger periplasm, with some also having an S-layer (Slonczewski and Foster, 2011).
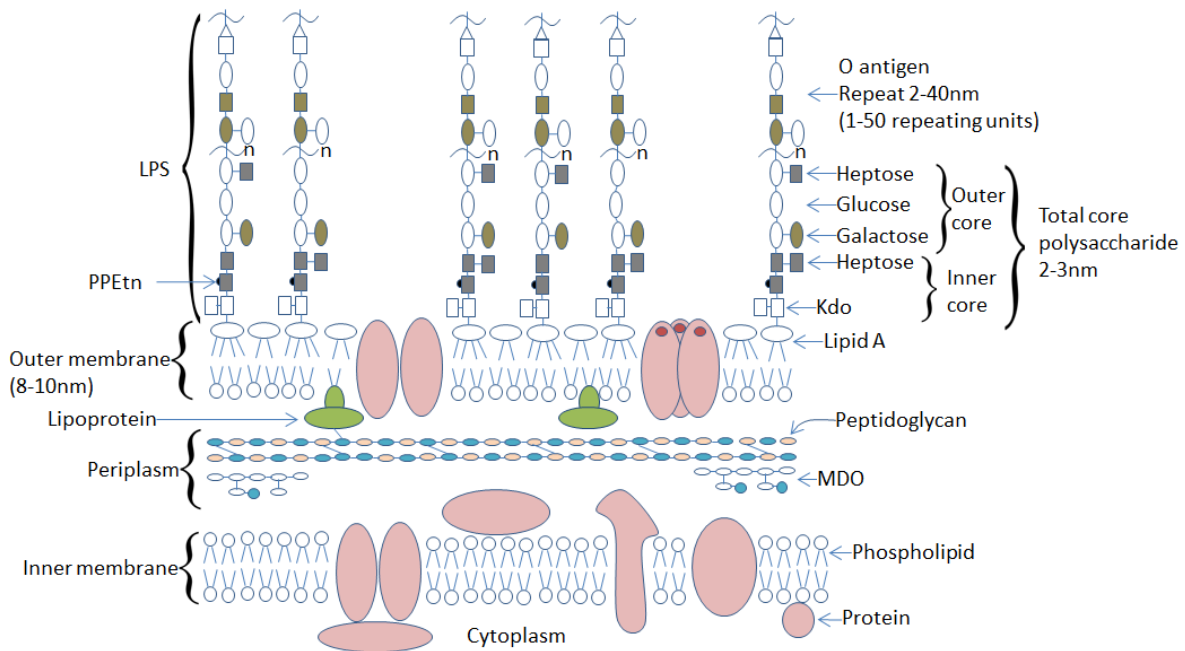
Figure 1.10. Overview of structure of cell envelope of gram negative bacteria. Detailing both inner and outer membranes, periplasmic space and LPS. Kdo is 3-deoxy-D-mannooctulosonic acid. PPEtn is ethanolamine pyrophosphate. MDO is membrane-derived oligosaccharide. Colours are for illustration purposes only. Adapted from various studies (Burks et al., 2003, Dowhan et al., 2008).

Lipids are the fundamental building block of biological membranes. They are amphipathic and so possess both a hydrophilic head and hydrophobic tail (see Figure 1.10). In solution phospholipids readily associate with each other. Phosphatidylethanolamine (PE) is one of the most abundant phospholipids in nature, and can make up as much as 75 percent of the total lipid population in *E. coli* (Dowhan et al., 2008). Lipid makeup is very varied; this in combination with variation within the LPS can give rise to very different membrane characteristics, i.e. surface charge and hydrophobicity variations even within a bacterial species.
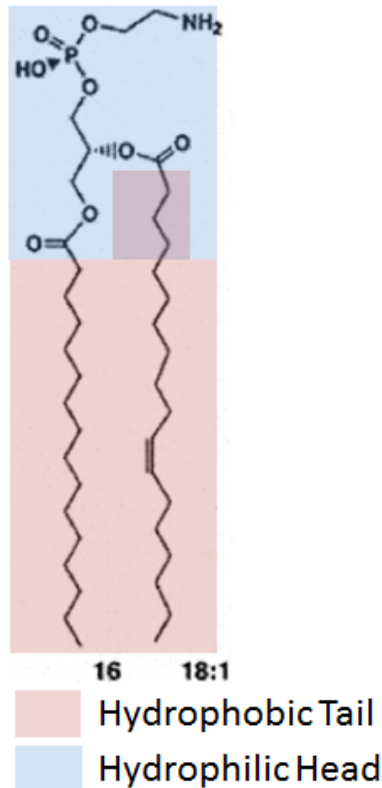
Figure 1.11. Structure of a typical glycerol based phospholipid phosphatidylethanolamine (PE), one of the most abundant lipids. Indicated in pink and blue are the hydrophobic hydrocarbon fatty acid tail and hydrophilic phosphate head with glycerol, respectively. A phosphate group forms a bond between the amine and the oxygen rich hydrophilic component. Adapted from Dowhan et al and Slonczewski and Foster (Dowhan et al., 2008, Slonczewski and Foster, 2011).

Phospholipids are the main constituents of both the inner and outer membranes on gram negative bacteria. In between both the inner and outer membrane is the periplasmic space (Figure 1.9). Here many proteins are found involved in catabolite production, were complex molecules are broken down into simpler sugars prior to transport across the inner membrane into the cytoplasm (Dowhan et al., 2008).

Transport of solutes across the inner membrane requires active transportation, as it is otherwise impermeable to solutes. Pores exist in the outer membrane that allows the passage of molecules up to approximately 600D in mass, with high molecular moieties requiring active transport. However, the outer membrane is permeable to ions which results in the periplasm resident proteins being subject to changing pH and salt concentrations (Slonczewski and Foster, 2011).

Interestingly, the phosphate group that links both the fatty acid and polar head together carries a negative charge at physiological pHs, and it is for this reason most bacteria carry a net negative charge (Slonczewski and Foster, 2011). However, different lipids contain different polar heads. For example PE presents an amine group to the environment, which at physiological pH carries a positive charge, with both Phosphatidylglycerol and Di-phosphatidylglycerol (cardiolipin), a glycerol type molecule is presented to the environment.
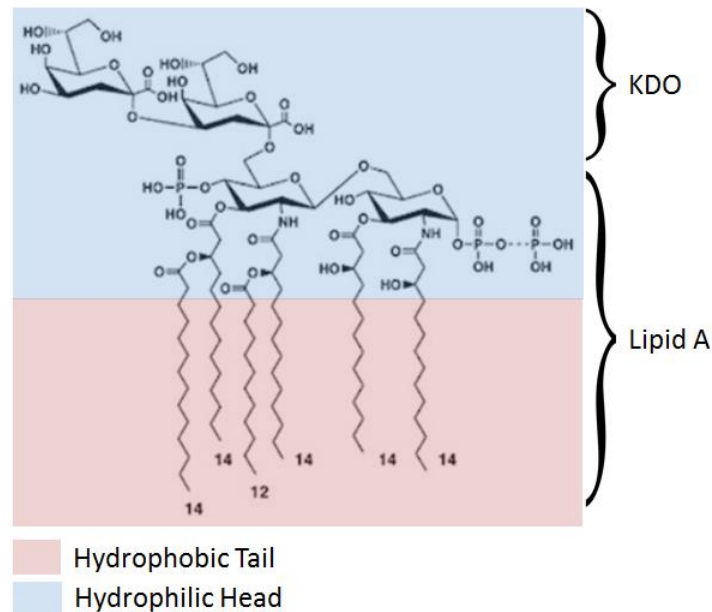
Figure 1.12. Structure of KDO-lipid domain, of gram negative *E. coli*. Lipid-A is a disaccharide (dimer) of glucosamine phosphate, that has multiple ester and amide bonds to fatty acid chains. Numbers 12 and 14 signify the carbon chain length. The KDO-Lipid A structure forms part of LPS, as detailed in Figure 1.9. Adapted from Dowhan et al and Slonczewski and Foster (Dowhan et al., 2008, Slonczewski and Foster, 2011).

Cells express different outer membrane proteins in different environmental conditions. In an environment low in nutrients, cells express pores of a large size to maximise nutrient uptake and vice versa (Slonczewski and Foster, 2011).

The surface properties of bacteria can be very species and strain specific. Li and Logan found that two stains of *E. coli* tested (D21 and JM109) were hydrophilic, but another *E. coli* strain D2 was hydrophobic, but all three were negatively charged (Li and Logan, 2004). These differences are most likely due to membrane property variations explained above.

Peptidoglycan (Murein-Wall)

Peptidoglycan is thought to be unique to bacteria. It is possessed by both gram negative and positive bacteria, but gram positive possess a far thicker peptidoglycan layer. Hence they stain gram positive, following crystal violet staining. Peptidoglycan forms a protective mesh like structure that protects bacteria from physical stresses and osmotic pressure, as well as helping to convey structural rigidity. It also influences cell shape (Slonczewski and Foster, 2011) and is possibly involved in catalysing enzymatic reactions. Peptidoglycan is a polymer of amino-sugars that are cross linked. The sugars consist of repeating disaccharides; N-acetylglucosamine and N-acetylmuramic acid. The amino acid component also consists of repeating tetramer units of; L-alanine, D-glutamic acid, m-diaminopimelic acid (ξ-Lysine derivative), and D-alanine; this can vary in length from four to six residues. Glycosidic linkages form the bonds between both the disaccharides and the disaccharides and tetrameric peptide unit. An amine bond forms the cross link between anti-parallel peptides of the ξ-lycine derivative (m-Diaminopimelic acid) and the C-terminus D-alanine. The formation of the peptide cross link results in the loss of a second D-alanine (Slonczewski and Foster, 2011).
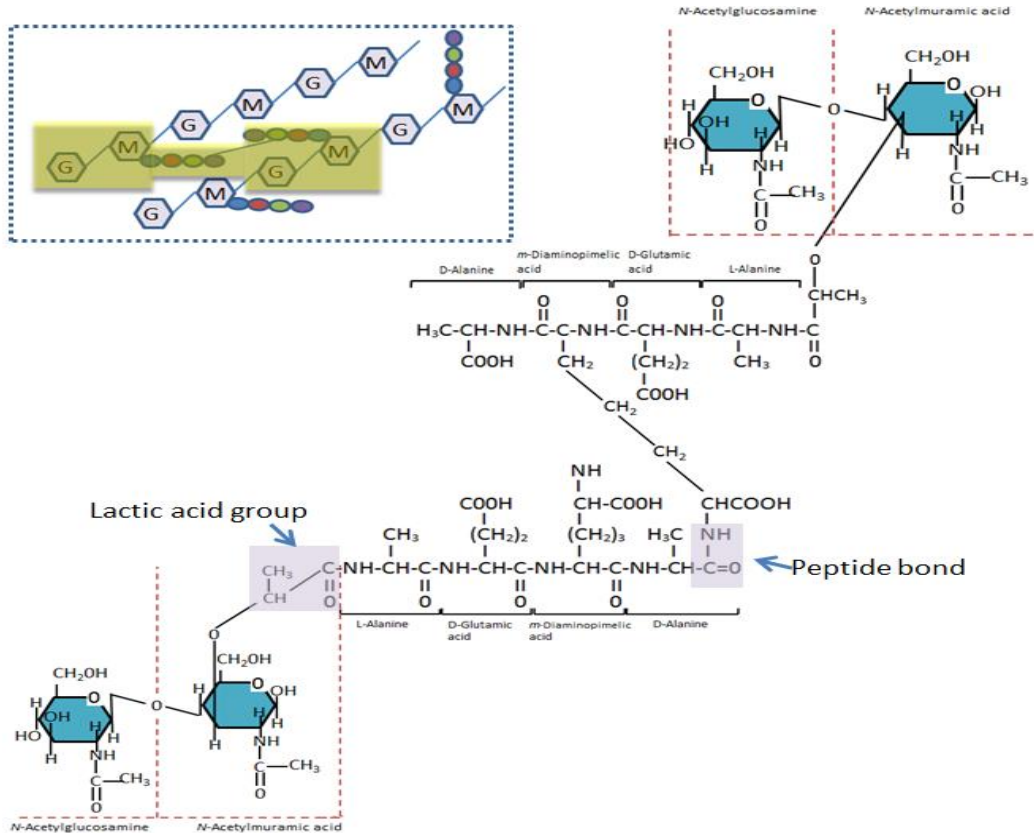
Figure 1.13. Example of peptidoglycan molecular structure found in bacterial cell walls. The glycan disaccharide units of *N*-acetylglycosamine (G) and *N*-aceytlmuramic acid (M) is attached four amino acids (L-ala, glu, lysine (ξ-carboxy derivative) and D-ala. The N terminus on L-ala, is attached to AMA via a lactate group, and the C terminus of D-ala is bound to the carboxyl side chain. Inset: Diagram of disaccharide repeating units in capital letters. G is *N*-acetylglycosamine and M is *N*-aceytlmuramic acid. Highlighted is the polymer section expanded on in the figure. Adapted from Slonczewski and Foster (Slonczewski and Foster, 2011).

1.17 Gram Positive Bacteria

Gram positive bacteria possess a simpler cell wall than gram negative bacteria. They lack the outer membrane, and significantly have a far thicker peptidoglycan layer than the gram negatives, which gives rise to their classification.

Examples of gram negative and gram positive bacteria

Gram negative	Gram positive
Aeromonas	*Bacillus*
Bacteroides	*Clostridium*
Bordetella	*Lactobacillius*
Brucella	*Listeria*
Escherichia	*Propionibacterium*
Haemophilus	*Staphylococcus*
Pseudomonas	*Streptococcus*
Salmonella	*Streptomyces*
Thiobacillus	*Streptoverticillium*

Table 1.4. Examples of gram positive and gram negative species. Adapted from Singleton (Singleton, 1999).

1.18 Quorum Sensing

Quorum sensing is a form of communication that exists between all of the residents of a biofilm. It works via auto-induction queues that are triggered when signal molecules, that are expressed into the near environment, reach a critical concentration, which is in turn correlated to both cell density (Shirtliff et al., 2002) and diffusion coefficients of the signal molecules in the biofilm. Quorum sensing is a communication method that allows a biofilm to make collective decision for the good of the colony; where consensuses are made. One example of this phenomenon was found in *PA* whereby quorum sensing was mediated by acyl homoserine lactone and quinolone which are responsible for augmenting the expression of eDNA (Allesen-Holm et al., 2006) locally within a colony. This is a very important area of biofilm research but is beyond the primary scope of this project.

1.19 Microbe Induced Corrosion (MIC)

The corrosion of surfaces possess a major problem in many industries, and three types of bacteria are implicated in the corrosion of metals. These are the sulfate reducing bacteria, sulphur oxidising bacteria and iron oxidising bacteria (Chemtex, 2013). These bacteria are involved in redox reactions whereby metals on the surface are oxidised as a means of generating ATP, which is a microbe's principle energy currency. However, this process is not the only mechanism by which a surface can be corroded. Geesey et al found that some microbes expressed acidic

polysaccharides into their environment which promoted the deterioration of metallic copper surfaces (Geesey et al., 1988). Some surfaces therefore appear to be under a dual attack, both direct and indirect, where surface sites both proximal and distal from the biofilm can be corroded.

Sulfate reducing bacteria for example *Desulfovibrio* and *Desulfomaculum* species cause corrosion of cast iron, carbon, low alloy steels, stainless steels, and high nickel and high copper alloys (Zuo et al., 2004, Sheng et al., 2007). Sulphur reducing bacteria have been observed damaging carbon steel which include; *Bacillus, Hafnia alvei, Desulfovibrio gigas* (Jack et al., 1992), as well as *Pseudomonas* corroding mild steel (Obuekwe et al., 1987), and *Methanococcus maripaludis* has been observed facilitating accelerated corrosion of iron rich materials (Mori et al., 2010).

Interestingly, some microbe species have been observed conferring resistance to corrosion, for example *Bacillus subtilis* (Örnek et al., 2002, Mansfeld et al., 2002) and *Pseudomonas flava* (Gunasekaran et al., 2004) on aluminium substrata by expressing a protective polyglutamate / polyaspartate and phosphate conditioning film, respectively.

One method used to measure metal corrosion is called polarisation resistance. This method was used by Jayaraman (Jayaraman et al., 1999) to investigate the effect of using microbial peptide inhibitors expressed in bacteria which form a biofilm that were used to compete with and reduce the occurrence of sulphur reducing bacteria biofilms which can cause stainless steel corrosion; this did show some success. This idea is similar to the drinking of probiotic yogurts that allegedly promote the colonisation of 'good' bacteria via competition over 'bad' bacteria in the human gut.

1.20 Surface Topography and Energy Effects on Bio-adhesion, Initial Attachment and Cleaning

Both surface roughness and chemistry formulation can influence initial attachment and the resultant biofilm. Generally, surface energy considerations appear important in the initial attachment, with some studies also indicating surface roughness is important. Many authors also report that the importance of surface roughness is often superseded by that of substrate surface energy. These observations are discussed at length in Chapter sections 1.20.1 and 1.20.2. Nevertheless, surface roughness does appear important in microbe retention, and cleaning (Ortega et al., 2010).

1.20.1 Surface Energy and Microbial Attachment

Surface topography is widely thought to play an important role in microbial initial microbial retention (Whitehead and Verran, 2006). However, most studies attribute increases in free surface energy with increases in initial microbe attachment (Fletcher and Pringle, 1985), with some authors finding maximum microbe retention found at surface energies of 75-105 mJ/ m^2, above which point bacterial attachment decreases again (Fletcher and Pringle, 1985), see Figure 1.13.
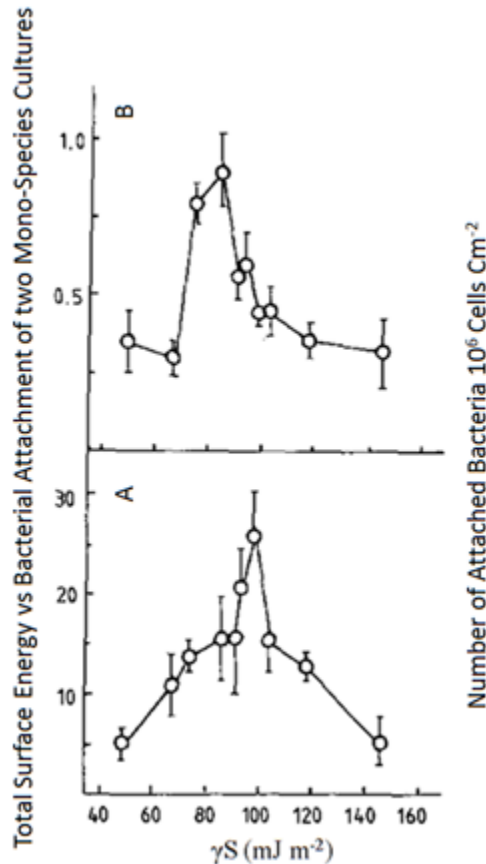
Figure 1.14. Total surface energy (γ_S) versus number of bound bacteria. (A) *Aeromonas hydropholia* H22; (B) *Acinetobacter* sp. H3 (Fletcher and Pringle, 1985)

Another study on different substratum's exposed to a marine environment found that low γ_S of 20-25 mJ/m^{-2} retained fewer microbes when suspended in the sea harbour environment (Dexter et al., 1975), with Teflon[TM] surfaces yielding less microbes per cm^2 over a 500 hour test period. Of course studies like this have entirely neglected all other surface factors including surface roughness. But bearing this limitation in mind, microbe attachment and growth does appear to be

very much dependent on surface energy in these studies, with this conclusions being confirmed by subsequent investigations (Pereni et al., 2006).
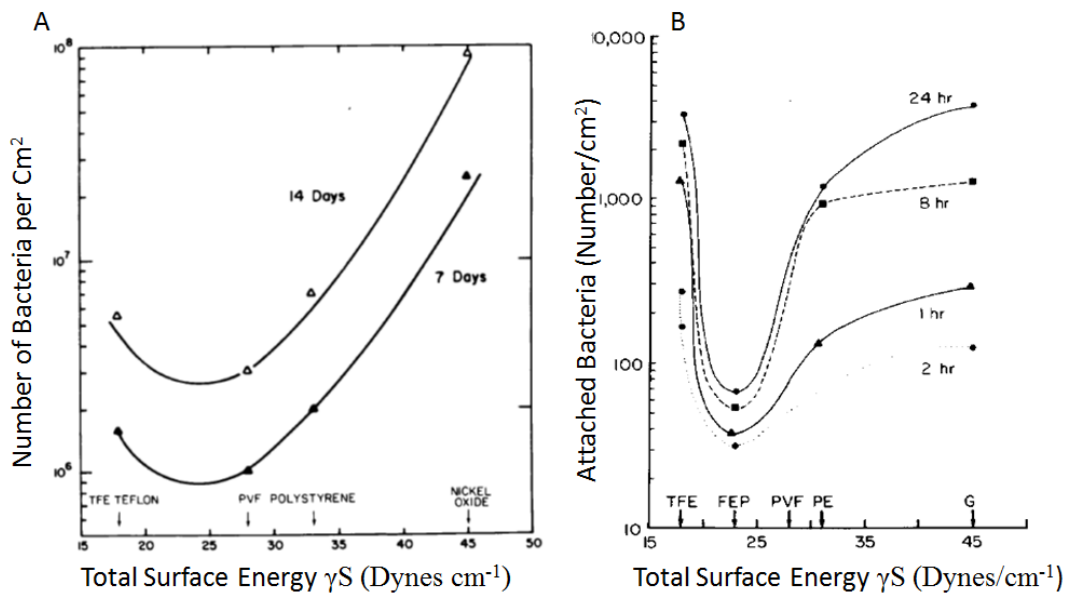
Figure 1.15. (A) Number of marine bacteria adhered to surface versus total surface energy (γ_S), f3ollowing 366-504 hour sample exposure in harbour sea water. (B) Total number of marine bacteria adhered to surface versus total surface energy (γ_S). (Dexter, 1979b).

In the early 1970s a hypothesis was proposed by Baier that bio-adhesion (in this case serum components), was intimately linked to the surface energy of the substratum (Figure 1.16). This general negative correlation proposed in 1972 by Baier (Baier, 1972) whilst investigating the absorption of serum components to material substrates. Baier suggested a zone of minimal bio-adhesion resulting from a predominance of substratum-bulk exposed methyl groups that is likely applicable to all biological matter binding to a given surface. The hypothesis model is based on extended DLVO theory (Zhao et al., 2004). The extended DLVO theory takes into account the hydrophobic/hydrophilic and osmotic interactions (Chang and Chang, 2002, Hermansson, 1999) as well as the standard net electrostatic interactions calculated for a flat surface and idealised homogeneous cells including additive factors; van der Waals interactions (attractive) and the steric/electrostatic interactions of the double layer of the cells and substratum (which is repulsive due to the net negative changes present on most cell surfaces (Hermansson, 1999, Hori and Matsumoto, 2010).

56

$$\Delta G_{slm}(y) = \Delta G_{slm}^{LW}(y) + \Delta G_{slm}^{AB}(y) + \Delta G_{slm}^{EL}(y) \qquad \text{Eqn. 2}$$

Extended DLVO theory $\Delta G_{slm}(y)$ is the total Gibbs energy, $\Delta G_{slm}^{LW}(y)$, $\Delta G_{slm}^{AB}(y)$ and $\Delta G_{slm}^{EL}(y)$ is the Lifshitz-Van der Waal, acid-base interaction term, and electrostatic contribution, respectively. With y being the distance between the interacting cell and the flat substratum surface (Meinders et al., 1995).
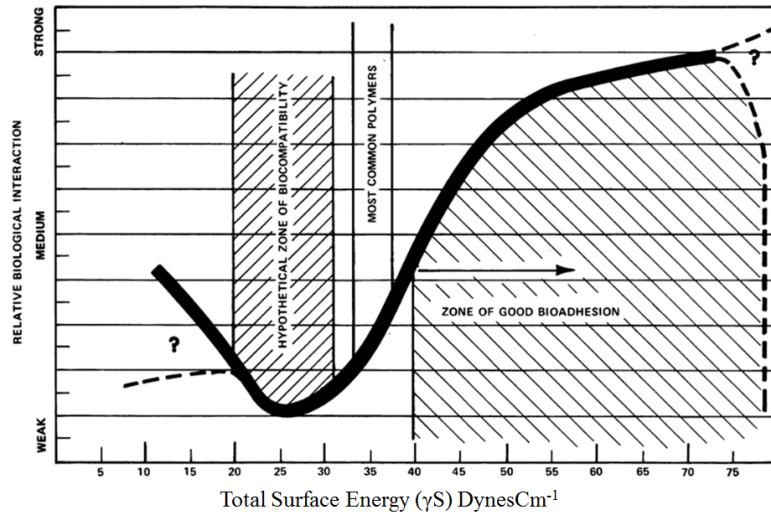
Figure 1.16. Showing the proposed 'Baier curve' for general bio-adhesion versus surface energy relationship (Baier, 1973).

A great deal of research conducted on the initial binding of bacteria appears to support this hypothesis, as well as research to be presented in this thesis. It is however, noteworthy that the bio-adhesion hypothesis proposed by Baier in 1973 was based around the simple but questionable assumption that the surfaces of the microbes would be unchanging, essentially similar fixed colloidal surfaces. Despite this clearly fragile assumption, much data does confirm the overall surface energy-microbe retention relationship proposed by Baier.

Other papers written subsequently corroborate the Baier hypothesis, with correlations similar to that noted above being observed (Baier et al., 1985, Dexter, 1979b, Dexter, 1979a, Hilbert et al., 2003). A proposed mechanism and plausible rationale for this decrease in microbe retention is due to the non-specific binding of proteinacious cellular components of the microbes onto substrates, and their subsequent denaturation, when proximal to 'high' energy surfaces. More recently research has investigated microbial retention on surface with different surface energies (see Figure 1.16).
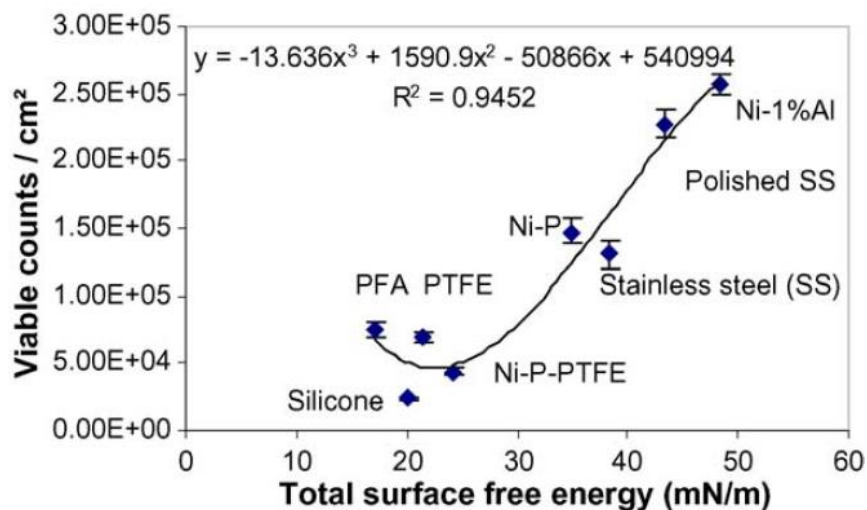
Figure 1.17. *PA* AK1 initial binding after 1 hour on surfaces of differing surface energies (mJ/m^2) (Pereni et al., 2006).

The binding data of *PA* taken from Pereni (Pereni et al., 2006) appears to fit well with the Baier curve, discussed above, and with other literature pertaining to microbe surface energy retention published (Liu and Zhao, 2005). Reductions in bio-adhesion have also been observed in membrane fouling studies, whereby filters with lower total surface energy had decreases in fouling levels (Hamza et al., 1997).

However, this surface energy relationship is not always evident with some deviations also being reported in the literature. Chang and co-workers (Chang et al., 1977) observed that when protein (albumin and fibrinogen) was present in solution the Baier correlation was lost. However, following the removal of these interfering proteins the link was restored. This phenomena was also observed by others (Lyman et al., 1968); (Neumann et al., 1979). Mohandas et al (Mohandas et al., 1974) found when studying the adhesion of RBCs to four different surfaces (glass, siliconised glass, polyethylene and Teflon^{TM}), that the presence of proteins interfered with the substratum-surface energy link with RBC retention. This study also showed that increases in RBC-substratum incubation time increased the strength of adhesion.

The surface energy and in particular the surface hydrophobicity of materials used in transplantation have been shown to be important in implant bio-comparability, thereby the nonspecific substratum binding of the recipient plasma proteins for example fibrinogen, albumin

and IgG are thought to facilitate the partial unfolding of these proteins that precipitate immune responses and enhance implant rejection (Thevenot et al., 2008).

In summation, the surface energy of a substrate is a vital variable in bio adhesion events, with lower γ_S resulting in correlative decreases in biological accumulations. However, proteinaceous thin films have been observed interfering or masking these observations. It is therefore likely that substrate surface energy will only be relevant in low-dilute nutrient environments such as; marine, air conditioning, industrial manufacturing and similar in-home environments. This project will examine this relationship further examining any correlations between substratum surface energy and;

1) Initial attachment of *PA*
2) Net biomass accumulation in mature 4 day old *PA* biofilm
3) Ease of mature biofilm removal using increased shear

1.20.2   Surface Topography - Roughness

In dental research, a threshold of R_a <0.2µm was concluded to be the surface roughness at which decreases in microbial retention plateau (Bollenl et al., 1997), following the review of numerous materials, indicating that roughness appeared to supersede that of surface chemistry considerations. However, other convincing studies examined the binding of *S. aureus, L. monocytogenes*, *S. marcescens. P. fragi* and *E. coli* to two stainless steel roughness variants, R_a=0.412µm and 0.035µm, (2B versus mirror finish, respectively), and found no statistical difference in adhesion (Barnes et al., 1999).

Some research has shown a clear link between surface roughness and hydrodynamics on the effectiveness of the antimicrobial agent TSP (Korber et al., 1997) on *Salmonella enteritidis*. With 48-72 hour old biofilms, the older biofilms showed increased resistance to TSP treatment on all preparations. Korber and colleagues found the inclusion of large surface irregularities (crevice widths of 0.5, 0.3, and 0.15 mm) enhanced the survival of the *Salmonella* microbes at depth, when compared to those that were cultured on 'smooth' unmodified surfaces. That is, they established an inverse relationship detected between cell viability and crevice size.

The effect of surface roughness and cleaning has been linked in previous studies. For example Verran and Whitehead found a build-up of organic matter (BSA) was detected following repeated cycles of biofilm cleaning and BSA exposure. Increases in stainless steel substratum roughness were found to inhibit cleaning of the conditioning film which itself went on to greatly enhance the

retention of cells during cleaning (Whitehead and Verran, 2006). This phenomena was also observed elsewhere (Frank and Chmielewski, 2001) (Blel et al., 2008).

Some studies have suggested that surface roughness is a more important variable in bacterial attachment than surface energy. Quiynen et al (Quirynen et al., 1990, Quirynen et al., 1996) tested rough and smooth variants of polyfluorethylenepropylene and cellulose acetate (γ_S = 20 and 58 mN/m respectively, with both having R_a =0.1 and 2.2µm) in the oral cavity of patents over a 3 and 6 day periods and found increased initial colonisation on the rough variants. However, at 6 days these observed differences were lost, but they found that the lower the γ_S the lower the microbe counts. It is important to remember that the oral cavetti is a chaotic, high shear environment (with a tongue flapping about), and so given this environment; the initial attachment of the microbes is likely to be greatly aided by the protection afforded by the roughened surfaces. Conversely, given enough time for the biofilms to mature, the γ_S of the substratum would become important, with lower surface energy materials increasing the likelihood of major biofilm sloughing (delamination) events, like those reported in this work (Chapter 9.1). Other surface roughness-microbe adhesion and retention correlations have also seen increases in roughness as having positive correlations with microbe adhesion (Whitehead et al., 2005, Medilanski et al., 2002, Allion et al., 2006, Boyd et al., 2002). It is noteworthy that all of these works were performed on metals (stainless steel) only, and did not measure surface energy. Boyd et al observed maximal microbe (*S. aureus*) binding where substratum features were approximately 1µm (Boyd et al., 2002). This was thought to be because the substratum features were on the same scale to that of the microbes, where maximal substratum-microbe contact is thought to be found. To this end the EHEDG recommends for a hygienic surface to have R_a <0.8µm.

Numerous other studies conducted on metals (mainly stainless steel) have found no correlation between surface roughness and microbe binding to stainless steel (Barnes et al., 1999), (Guðbjörnsdóttir, 2005, Hilbert et al., 2003, Mueller et al., 1992, Tide et al., 1999). Because of these discrepancies in these reported datasets, surface roughness is unable to be used to predict microbe attachment.

Differences in surface roughness had little effect on cleaning in experiments conducted by Ortega et al (Ortega et al., 2010), where little difference was observed between R_a of 0.04 and 0.14µm, but greater microbe retention was observed at an R_a of 1.37µm. Herein, no correlations were detected between surface roughness, microbe initial attachment and cleaning.

1.21 Engineered Surfaces for Biofilm Studies

Instead of using substratum's that possess known innate roughness's in biofilm research, which are uncontrolled, some research groups have attempted the fabrication of precise topographical features using a range of starting materials. Some of which are modelled on naturally occurring biosurfaces, with features either on the macro or nano phase scale (<100nm), which have shown some interesting results, in either retarding or enhancing microbial attachments, this is discussed below. Engineered biosurface emulated materials include NILT (NIL. Technology. Corp, 2016) modelled on banana leaves, and Sharklet™ poly(dimethylsiloxane) films modelled on shark skin (Chung et al., 2007), discussed in Chapter 1.27.3, and Chapter 1.27.5, respectively.

Research in this area first occurred in an effort to find new biomaterial implant surfaces and topographies for implant related materials, where enhanced cell adhesion was the required. Popat et al (Popat et al., 2007) found that by introducing nano porous structures to aluminum oxide, cell adhesion was increased by 45 percent versus amorphous control substrates. Another report also found changes in eukaryotic gene expression as a result of different surface topographies (Dalby et al., 2003). Some studies also investigated the effects of small nano surface substratum changes on the expression of cellular appendages (Hsu et al., 2013), and discovered that some microbes do in fact genotypically respond to local topographical differences resulting in cell surface structural differences. This observation possibly helps explain the enhanced microbe binding by Mitik-Dineva et al (Mitik-Dineva et al., 2008), where a threefold increase in microbe attachment was detected on chemically treated glass (Park et al., 2008), coupled with increased metabolism, also observed by Mitik-Dineva et al (Mitik-Dineva et al., 2009) and coupled with increases in EPS. Conversely, reductions in microbial adhesion have also been observed by Diaz et al who found that net reductions of microbes were observed on nano structured substratum's and interestingly the orientations of the substratum's groves affected the spread to the colony frontier, thus retarding colony extension on gold surfaces (Díaz et al., 2009). This retardation of microbial migration was also observed in modified catheter devices utilising novel topographies modeled on shark skin (Reddy et al., 2011). Microbial adhesion reductions were also observed by (Puckett et al., 2010) using on amorphous nano textured surface structures on titanium substratum's.

Taken altogether, the engineering of surface topographies to generically reduce bio-adhesion has been observed with some application dependent successes with interesting observations (Chung et al., 2007). As such they will be investigated in this project in the context of both non-engineered

substratums, but also by testing some commercially available nano engineered materials, as discussed in Chapter 1.27.3 and Chapter 1.27.5.

1.22 Mass Transport and Biofilms

Microbes and conditioning agents are transported to the substratum by convective and diffusive mass transport. An important component relating to the deposition of these molecules is convective mass transport, which is depended upon the fluid hydrodynamics around the attachment site. The liquid flow field over the attachment site will either be laminar or turbulent. Laminar flows are defined as flows with no mixing between the layers and show smooth parallel flow patterns that run parallel with the surface, with turbulent flows defined as chaotic and seemingly random, resulting in a great deal of localised fluid mixing which can result in increased microbe and conditioning agent transport to the surface. The contribution from all of the hydrodynamic forces, for example convection and diffusion, coupled with sedimentation, helps facilitate the transport of the biofilm components to the surface. Importantly, convective mass transport transports material proximal to the surface, but it is often diffusion that facilities contact with the surface.

In either a turbulent or laminar flow scenario, the velocity of the fluid immediately proximal to the surface will be relatively low; this is due to low shear proximal to the surface. The thickness of this liquid layer is called the hydrodynamic boundary layer and is dependent on the velocity of the surrounding fluid relative to the surface (Donlan, 2002). The greater the fluid flow velocity then the thinner this layer with a typical thickness 0.06 x10^{-4}m (Busscher and van der Mei, 2006). It is outside the boundary layer where the laminar or turbulent flow of fluid can be found. In flows that are either laminar or minimally turbulent, the hydrodynamic layer can be thicker and can substantially affect cell-substratum interactions (Donlan, 2002), as the cells have a thicker barrier to penetrate to reach the surface, and vice versa. The latter effect was seen experimentally with increasing bacterial deposition rates Rijnaarts and Zheng (Rijnaarts et al., 1993 and Zheng et al., 1994) coupled with increasing flow rates. Conversely, high flow rates and an increase in turbulence proximal to the surface can also create sufficient shear forces to force the detachment of cells from the surface in mature biofilms, which can be important in cellular dispersion, and large scale biofilm sloughing. Sjollema and colleagues, (Sjollema et al., 1988) observed higher microbial surface deposition rates correlated with increases in fluid flow rates due to higher mass transport.

Typically, more compact and denser biofilms form under increased shear conditions, as is event below (Figure 1.17) (Liu and Tay, 2002), resulting in a more physically stable biofilm.
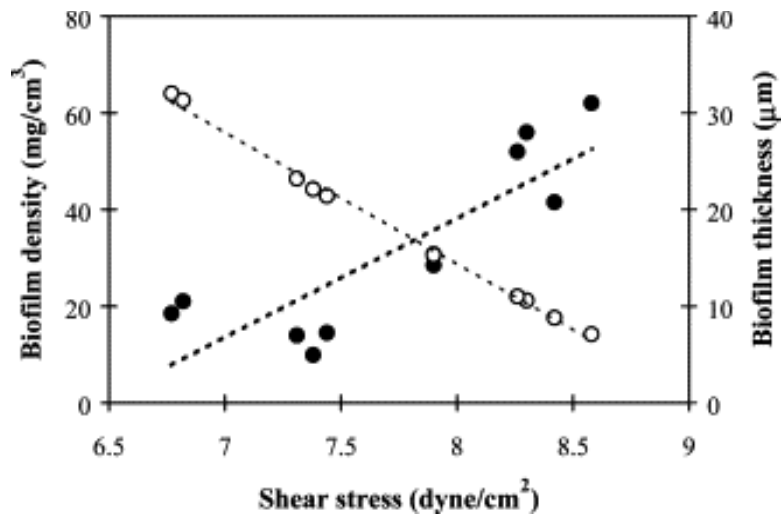
Figure 1.18. Correlation between shear rate, biofilm density and biofilm thickness. Taken from Liu and Tay (Liu and Tay, 2002).

It is important to note that there is a limit at which increasing shear stress will decrease attachment of microbes to a substratum and is where microbe detachment exceeds that of attachment. Mohamed et al found that adhesive events of *S. aureus* increased at shears of between 50 to 300s^{-1} due to favorable mass transport, however decreased when shear was higher than 500s^{-1} (0.5 x10^{-3}nN) (Mohamed et al., 2000). This particular limit, which is dependent on numerous environmental factors for example substratum R_a, R_z, total surface energy and also the microbial species under investigation. It's important to remember that laminar or turbulent flows only are important when there is fluid flow. In stagnant environments, these constraints become less important, and sedimentation and diffusion become more important (Busscher and van der Mei, 2006).
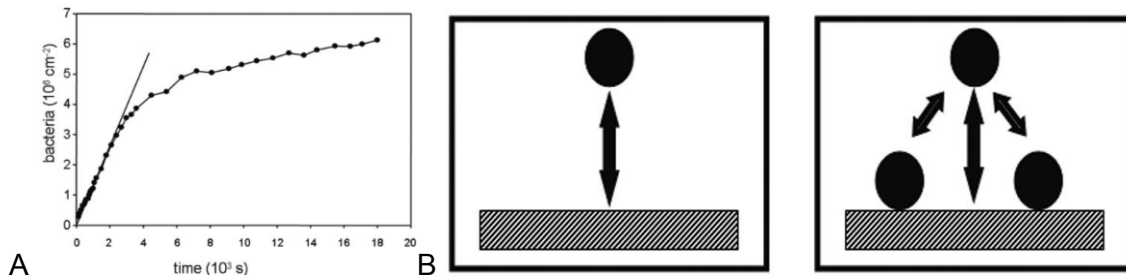
Figure 1.19. **A** Deposition kinetics versus time for *Enterococcus faecalis* OG1X on fluoroethylenepropylene in PBS, pH 7.0. **B** Possible adhesion interactions of microbes with either substratum or combination of microbial cohesion and adhesion giving rise to different binding kinetics (Busscher and van der Mei, 2006).

Figure 1.19A, shows the typical deposition profile in the initial biofilm establishment phase. Two different kinetic rates can be seen. The initial, more rapid kinetics are due to the biofilm's founding members adhering to the substratum/conditioning surface only, and is considered the true microbe-substratum interaction rate. The latter kinetic rate is lower because there are less binding sites available and microbial cohesion is starting to take place (Busscher and van der Mei, 2006), as illustrated in Figure 1.19B.

Increases in liquid flow rates (0.3, 0.6, 1.2, and 1.8 cm s^{-1}) results in increasing shear. Subsequently changes in the fluid Reynolds number was found to increase the efficacy of antimicrobial agent TSP against 3 day old *Salmonella enteritidis* biofilms, when cultured on a roughened surfaces glass surfaces (Korber et al., 1997). This increase was likely due to enhanced penetration of the biofilm superstructure, with TSP being more effectively driven down into the cracks and crevices of the modified glass surface at higher shear rates.

Kober and colleagues found that when monitoring the deposition of *Pseudomonas fluorescens* at increasing flow rates and shear, the microbes that were more likely to reach and attach to a substratum (glass) were the flagellated phenotype, and interestingly those cells that were flagellated also dispersed (twitched) across the surface more rapidly (Korber et al., 1989).

Fluid flow rates and thus fluid dynamics about a substratum or biofilm is thus important from an attachment, growth, sloughing, and biocide treatment perspective. Thus, in both the real world and in biofilm research, such constraints should be kept fixed and be known.

1.23 Reynolds Number Relevance to Microbial Life

The Reynolds number R_e (Eqn. 3) is used to distinguish between laminar and turbulent flow in fluids. It is dimensionless quantity as it's simply a ratio between inertial and viscous forces. In laminar flows viscous forces are dominate (retards motion) over inertial forces where $R_e = <10^3$. Within laminar flows, stream lines (density lines) are organised that result in both little liquid mixing and varying flow rates between density lines.

$$R_e = \frac{\rho VL}{\mu} = \frac{Inertial\ Forces}{Viscous\ Forces}$$
Eqn. 3

L = Length (m) traveled by fluid. V = velocity (m/s) of object relative to fluid). μ = dynamic viscosity of fluid (pa·s or N·s/m^2 or kg/(m.s)). ρ = density of fluid (kg/m^3).

In turbulent flow inertial forces dominate (maintain motion) and Reynolds numbers are typically $>10^4$. The inertial forces cause circular eddies which create turbulence which in turn induces mixing. Such behavior can be very difficult to predict.

Reynolds numbers are used in numerous industries to design different flow systems, and often scale models are used to represent actual flows to aid in plant design. Reynolds number has significance in both models and the real world. Reynolds number is commonly applied to flow within pipes.

$$R_e = \frac{\rho VD_H}{\mu} = \frac{VD_H}{v} = \frac{QD_H}{vA}$$
Eqn. 4

D_H is the hydraulic diameter of the pipe; its characteristic travelled length L (m). Q is the volumetric flow rate (m^3/s). A is the pipe cross-sectional area (m^2). V is the mean velocity of the fluid (m/s). μ is dynamic viscosity of the fluid (pa·s or N·s/m^2 or kg/(m.s)). v is kinematic viscosity ($v = \mu/\rho$)= 10^{-4}m/s =1 stoke.

The Reynolds number is important regarding biofilm development because Reynolds numbers of 10,000 or higher result in bacteria being randomly transferred to the surface of the pipe, which will increase the likelihood of cellular adhesion taking place. This conclusion is due to their relatively small mass and thus inertia of microbes, and as such they are at the mercy of the local fluid currents around them.

Interesting, large forms of life also have to contend with large Reynolds numbers which allow humans for example to freely move in air (a fluid), whereas small organisms and seeds for example operate at low Reynolds numbers (more viscous) and float in the air. Also, interestingly due to the 'stickiness' of water at low Reynolds numbers, bacteria can carry approximately 100 times their mass in water with them, making locomotion at the small scale very costly in energy.

Bacteria need to continually impart energy into locomotion, because they lack any significant inertia to carry them forward, as opposed to whales in water where only occasional effort is required, as their momentum will carry them forward for an extended period.

1.24 Preventing Biofilm Formation

There is currently no substratum material, natural or otherwise, that can totally prevent biofilm formation. As discussed in Chapter 1.20.1 and 1.20.2 there are substratum's that either due to their γ_S or topography respectively, have been shown to reduce the rate of microbe surface adhesion. A small number of thin surface coatings have been developed (De Prijck et al., 2007, Kaper et al., 2003, Majumdar et al., 2008, Li et al., 2013, Zodrow et al., 2012), but these only reduce microbial adhesion rates.

The only way to prevent biofilm formation is to sterilise substratum and completely seal it in a vacuum away from contamination sources and water. Such instances would not be terribly useful in most industrial applications, thus efforts are directed at reducing colonisation and or aiding cleaning and sanitisation processes.

1.25 Pseudomonas aeruginosa

PA is a gram-negative microbe that is ubiquitous in the environment, where it survives in many different environmental conditions. These include colonising plants, animals, insects and living in soil (Hardalo and Edberg, 1997). Pseudomonas has been observed thriving in both nutrient abundant environments such as in the human lung (Hogardt et al., 2000), and can survive for extended periods (100+days) in nutrient deficient environments such as distilled water and deionised water (Favero et al., 1971).

PA has a very large genome of some 6.6 million base pairs (Thomson N.R., 2008), and a larger proportion of transcriptional regulators or environmental sensors than that of other bacterial species (Stover et al., 2000). Such features are perhaps suggestive as to its ability to live and thrive in many environments, exhibiting a large adaptive range. One example of the flexibility of

this organism was observed by J.R. Govan (Govan, 1975), whereby a mucoid phenotype spontaneously reverted to a non-mucoid phenotype when removed from the lung and cultured in-vitro (Darzins A., 1984). Also, recently *PA* cultures were sent into space on board the ISS, (Kim et al., 2013), where novel phenotypes were observed in zero gravity, relative to 'normal' control biofilms grown on earth.

PA are also pleomorphic, and thus are able to as individuals, alter their size and shape in response to changes to their environment, though they lack the ability to produce spores (Development, 2006).

Infection with *PA* in the general populace is rare, and this organism is generally thought of as an opportunistic pathogen, infecting peoples with immune deficiency syndromes, or those who have suffered a severe burn (Molina., 1991, Pollack., 1995).

Interesting Lawrence et al (Lawrence et al., 1991) found that a microbial biofilm can consist of 72 to 99 percent extracellular materials and void space when examining various *Pseudomonas* species.

PA was the microbe model used in all experimentation in this thesis, as culturing conditions are well established (Méchin et al., 1999, Bridier et al., 2011, Pamp and Tolker-Nielsen, 2007, Lawrence et al., 1991), and additionally it forms biofilms readily.
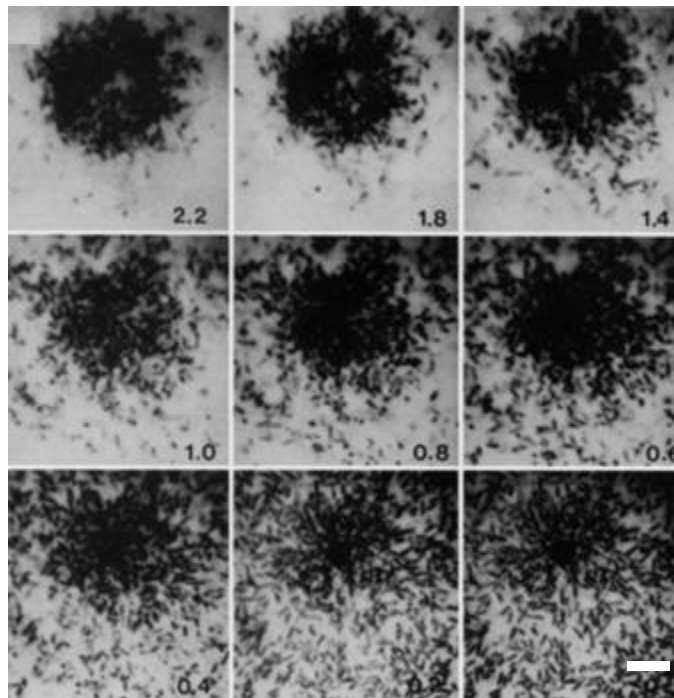
Figure 1.20. Scanning confocal laser images of a *PA* biofilm grown in continuous flow environment, cultured for 24-48 hours at 23±2°C, in minimal medium and stained with 0.1 percent fluorescein. Each image was taken at different heights above the surface as numbered in μm. Bar is 5μm. (Lawrence et al., 1991).

Pseudomonas adhesion to surfaces has been shown to be mediated by flagella motility (Lawrence et al., 1987), and the type IV pili that are critical for the twitching motility (O'Toole and Kolter, 1998a) which is important in micro colony formation and ultimately mature biofilm formation. This observation has been seen in other microbe species for example *Pseudomonas fluorescens* (Korber et al., 1994), and *E. coli* (Pratt and Kolter, 1998).

PA is widely used in biofilm research as it is easy to culture, and forms biofilms readily on many different surfaces (Mikkelsen et al., 2013). *PA* is also found growing within the industrial manufacturing plants on inanimate surfaces (Wright et al., 2013) and on medical equipment (Engelhart et al., 2002). It is also the main pathogenic determinant in some human infections for example Cystic Fibrosis (CF) (Yoon et al., 2002). *Pseudomonas* was also chosen for study in this project because it is thought to be a primary coloniser in a wide range of aqueous systems.

A particular strain of *PA* was used in this project, namely NCTC 12924 (ATCC equivalent strain 9027). This strain was originally isolated in 1943, from the ear of infection of Mr C.P.Hegarty (Mai-Prochnow et al., 2015). *PA* 12924 (ATCC 9027) is best known for its expression of Rhamnolipid, a naturally occurring surfactant used in the environment in bioremediation. Rhamnolipid is a hexose sugar with an attached lipid component (Zhang and Miller, 1992). Its genome is 6,362,326bp in size with a predicted total number of 5772 protein coding genes (Mai-Prochnow et al., 2015). Of potential importance is the lack of gene regulator *MucA* which represses sigma factor AlgU, which is thought to be responsible for the switching from a non-mucoid to a mucoid strain (Martin et al., 1993), potentially resulting in an abundance of alginate being produced by this strain of *PA* (Bragonzi et al., 2006, Mai-Prochnow et al., 2015). Given the complexity of biochemical pathways, especially the alginate biosynthetic pathway, the absence of *MucA* does not necessarily mean that alginate will be the predominant polysaccharide, but that it is likely to be so; see Figure 1.22.

1.25.1 *PA* EPS Composition

PA EPS Polysaccharide Composition
Polysaccharides play a diverse role in biofilms, and in some instances can make up the majority of the biofilm mass in some species and in specific environments. Their roles include food storage, and protection for colony members from antibiotics, desiccation or host immune defenses (Mai et al., 1993, Chang et al., 2007), cell attachment enhancement, and can also help form an important part of biofilm superstructure (Stoodley et al., 2002b). Polysaccharides are also the most important component in the emergence of colony viscoelastic behaviour (Orgad et al., 2011), which is thought to be useful in high shear environments, allowing the dissipation of energy, and so protecting the biofilm inhabitants.

PA is able produce at least three main types of polysaccharides in its EPS which have differing expression levels that appears dependent on the near environment (Daniel J. Wozniak, 2003). These are alginate, Pel and Psl. Each polysaccharide is expressed via its own operon, with some interconnectivity apparent between them (Franklin et al., 2011), and other sugar precursor synthetic pathways, i.e. rhamanose. Interestingly, it appears that *Pseudomonas* biofilms tend to have an overabundance of only one polysaccharide at any one time, but potentially have the ability to produce all three (Franklin et al., 2011). Evidence supporting this view was also provided by Jones et al (Jones et al., 2013) who found an inverse expression relationship between alginate and Psl. Variation between stains have also been observed, eg. PA01 has the ability to make

both Pel and Psl, but PA14 lacks three genes needed to synthesize Psl, thus can only make Pel, (Colvin et al., 2011), and by coincidence the genome of PA14 just happens to be smaller than PA01 (Lee et al., 2006a). One morphological phenotype that was found in the lung of CF patients called the 'rugose small-colony variant' has been shown to produce both Psl and Pel, which is interesting as the predominate phenotype found is typically is the mucoid type which predominately expresses alginate in the CF lung (Govan and Deretic, 1996). Why two phenotypes would potentially coexist is not currently known.

The EPS Polysaccharide Alginate

Alginate was first EPS to be chemically characterised in 1973 (Evans and Linker, 1973) and was found to be a high molecular weight, anionic, acidic polysaccharide, consisting of non-repeating subunits. Over production in *Pseudomonas* is linked to a 'mucoidy' phenotype (Hentzer et al., 2001), that is typically observed in the lungs of CF patients, resulting in a very slimy, and hard to eradicate biofilm that can result in patient death (Govan and Deretic, 1996). It's over expression has also been linked to increases in net biofilm thickness in *Pseudomonas* (Orgad et al., 2011). Alginate does not appear to be in direct contact with colony members, but tends to be expressed in abundance into the bulk of the lung sputum (Franklin et al., 2011). For a long time, it was assumed that due to the abundance of alginate detected in CF patients, and the observed increase in antibiotic resistance, resulting from its expression, that it was also an essential component of the non-mucosal phenotype. This assumption was later contradicted by works carried out in 2003 (Daniel J. Wozniak, 2003) and in 2012 (Colvin et al., 2012), wherein Psl or Pel was found to be the primary matrix polysaccharide on the solid (inanimate) substratums. Wozniak (Daniel J. Wozniak, 2003) also showed through gene mutation studies that alginate was not just absent, but was not required for non-mucosal biofilm formation on solid substratums.
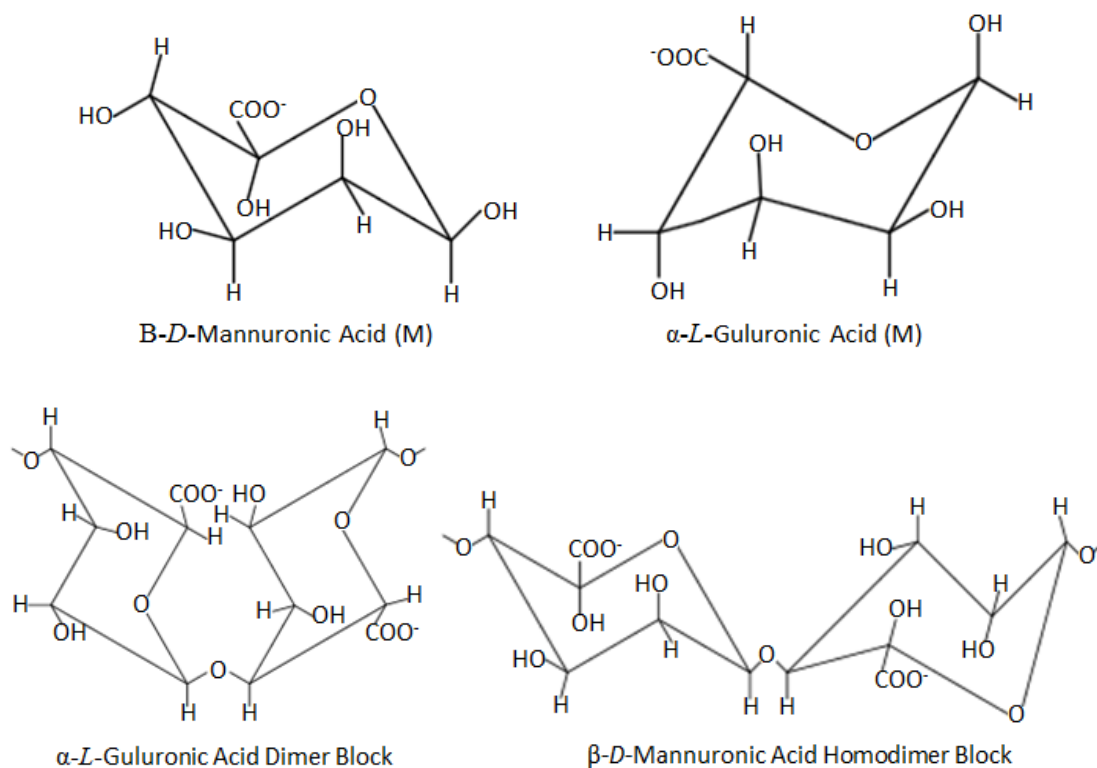
Figure 1.21. Structure of alginate constituent residues mannuronic acid and guluronic acid, and resultant homopolymeric blocks.
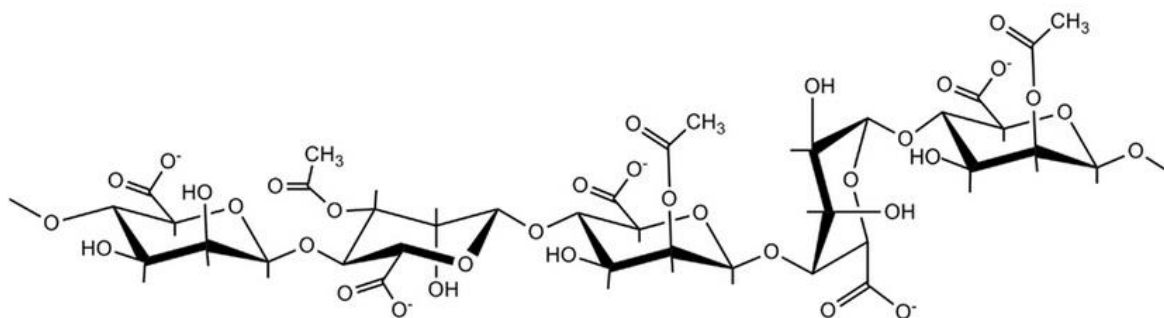
β-D-ManUA-(1->4)-3-O-acetyl-β-D-ManUA-(1->4)-2-O-acetyl-β-D-ManUA-(1->4)-β-L-GulUA-(1->4)-2-O-acetyl-β-D-ManUA

Figure 1.22. Structure of alginate (Franklin et al., 2011).

Since the sequencing of *Pseudomonas* strain 9027, the strain to be used in this project, a notable finding is that *MucA*, a key negative regulator of the alginate biosynthetic pathway, is absent (Mai-

Prochnow et al., 2015). It is highly likely but not guaranteed that alginate is the predominant polysaccharide expressed in the biofilms observed in this project.
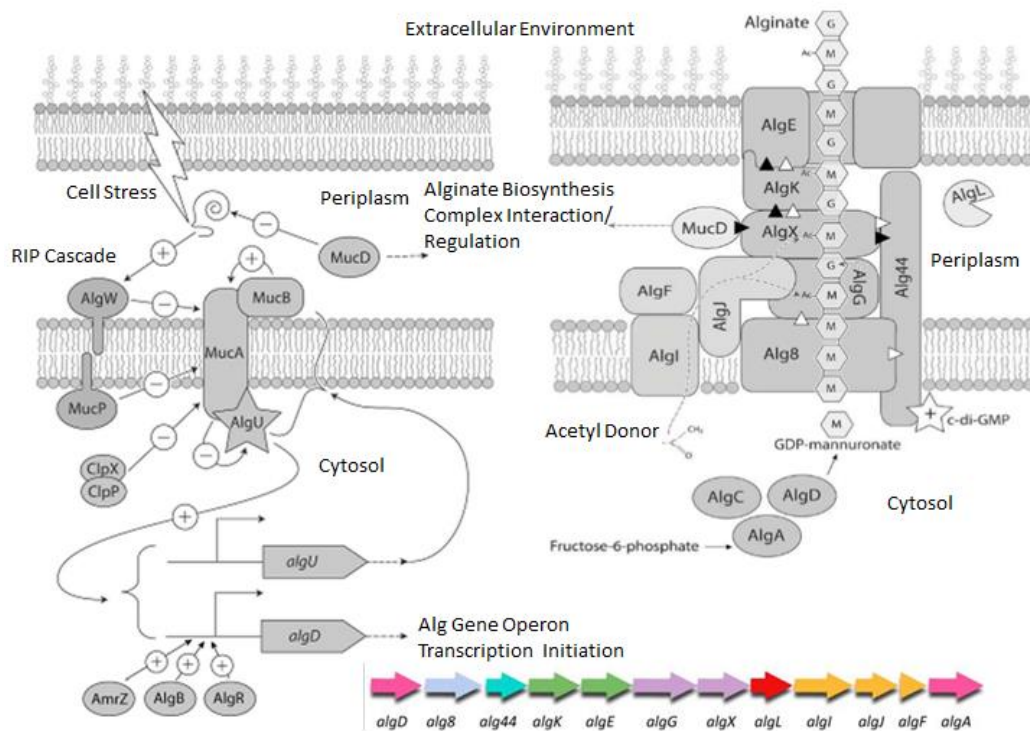
Figure 1.23. Alginate polysaccharide regulation and biosynthetic pathway overview, complete with alginate operon. Adapted from Hay and Franklin (Hay et al., 2013) (Franklin et al., 2011).

The EPS Psl Polysaccharide

Some of the first evidence of the importance of Psl in *Pseudomonas* biofilm formation was put forward by Wozniak in 2003 who found little or no alginate (Daniel J. Wozniak, 2003), but Psl was found in abundance (Jones et al., 2013). In contrast to alginate, Psl is branched and has a neutral charge arising from a repeating pentamer of low molecular weight, of approximately 6500D in size (Byrd et al., 2009, Kocharova et al., 1988). Kocharova et al also thought at the time (Kocharova et al., 1988) that this now named Psl polysaccharide may be cell surface attached, which was later confirmed by Ma et al (Ma et al., 2009). The synthesis of Psl is via a 11 gene operon (Byrd et al., 2009). Psl was shown to be vital in *Pseudomonas* cell-surface attachment when carrying out mutation studies, but also revealed strain to strain Psl variations in mature biofilm structure, i.e. PA01 biofilm structure is Psl expression dependent, but not PA14 (Colvin et al., 2012). Further investigations found that *Pseudomonas* surface attachment and subsequent biofilm formation on

72

glass was greatly impaired in Psl synthetic pathway mutation studies, confirming its importance in both cell-cell and cell-substratum binding interactions in both flow and static conditions (Ma et al., 2006). This conclusion was made visually evident using confocal laser scanning microscopy, where Psl was detected in a helical conformation attached to the cells prior to surface interaction. Psl was also visualised on the periphery on micro colonies, resulting in a Psl free 'void', which is later used for the assembly and dissemination of microbes in mature biofilms (Ma et al., 2009).

The Psl was only recently shown to be a pentasaccharide consisting monosaccharides of three residues; three D-mannose, one L-rhamnose, and one D-glucose (Byrd et al., 2009), with the below structural repeat (Figure 1.24). The synthesis of Psl requires other polysaccharide pathways which produce precursor sugar residues. These include; the alginate, rhamanose, and galactose synthetic pathways (Franklin et al., 2011).

[->3)-β-D-Man*p*-(1->3)-β-D-Man*p*-(1->3)-α-L-Rha*p*-(1->3)-β-D-Glc*p*-(1->)]$_n$-
2
↑
1
α-D-Man*p*
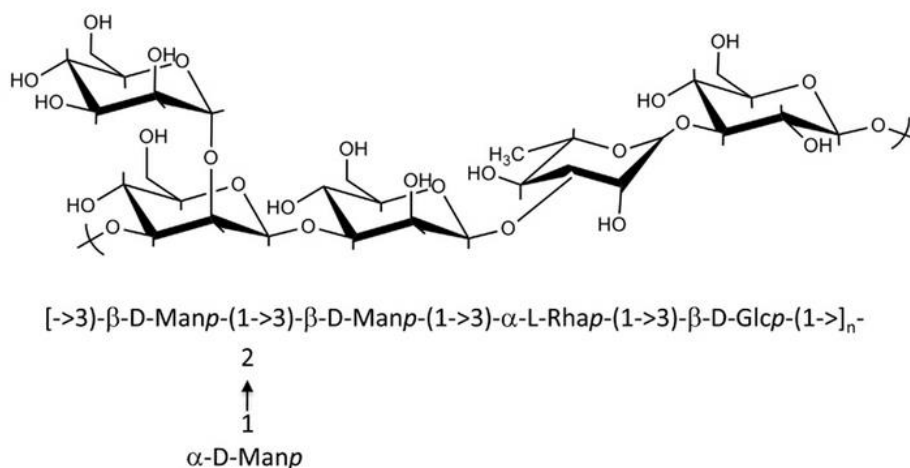
Figure 1.24. *PA* Psl polysaccharide (Franklin et al., 2011).

Zhao et al found recently that during the surface mobile phase (twitching) of *PA,* Psl was being excreted onto the surface (Zhao et al., 2013) during type 4 pili mediated migration (Wang et al., 2013). Another facet being that other colony members were recruited to these 'paths', resulting in a positive feedback mechanism. This culminated in large scale self organisation (Zhao et al., 2013), and this phenomena is likely to be important in the formation of micro colonies, and possibly in cell migration within biofilm superstructure. The development of Psl surface structures has been described as being similar to that of a spider's web (Wang et al., 2013). Interestingly a similar behavior has also been detected with eDNA expression and colony self-organisation (Gloag et al., 2013). Psl has also been shown to have a protective role in a biological context,

with its increased expression inhibiting neutrophil phagocytosis, and the immune complement cascade (Mishra et al., 2012).

The apparent cooperative nature of Psl, resulting in the recruitment, organisation, and subsequent co-localisation of microbial members may go some way in explaining why those cells that do not express Psl were more susceptible to antibiotic attack, with the inverse also being true. Psl therefore has been called by one author; the 'social' enabling polysaccharide (Irie et al., 2016).

The EPS Pel Polysaccharide

The Pel polysaccharide structure is currently not known, but is thought to arise as a product of a seven gene possessing operon (Franklin et al., 2011), that maybe important in pellicle formation (Franklin et al., 2011, Friedman and Kolter, 2004), with further works suggesting Pel may also be important in the formation of non-mucoid biofilms (Daniel J. Wozniak, 2003). Some authors report a significant decrease in biofilm mass in some *Pseudomonas* strains following critical Pel gene deletion (Colvin et al., 2011). Pel is likely to be glucose rich, in contrast to both alginate and Psl. Pellicle formations have been observed in this project (data not included) and were similar to those reported by others (Friedman and Kolter, 2004). These structures were paper like and ridged, the formation of which has been attributed to Pel expression, although not all authors observe this (Colvin et al., 2011). There is some evidence that Pel can behave as a redundant factor for the loss of adhesins in some *Pseudomonas* subtypes (Vasseur et al., 2005), and that it has a role in cell to cell interactions as well as in providing a scaffolding structure during initial early biofilm development (Colvin et al., 2011). The Pel operon appears to lack sugar precursor synthetic genes, that suggest a reliance on the relative abundance of sugars, synthesised independently (Franklin et al., 2011).

The EPS eDNA Spatial Arrangement, Function, and Known Structure

eDNA is abundant in nature, and is ubiquitous in the environment in relatively high concentrations suggesting an innate stability. It can be found at concentrations of some 2µg/g in the soil (Niemeyer and Gessler, 2002), and can account for 70 percent of the total DNA found in marine sediments (Dell'Anno et al., 2002).

eDNA is another important component in *Pseudomonas* biofilms (Allesen-Holm et al., 2006, Matsukawa and Greenberg, 2004) and is also most likely in alternate species biofilms. Indeed varying amounts of eDNA excretion have been seen in differing microbial species (Steinberger and Holden, 2005) and *PA* has been shown to be capable of expressing large amounts of eDNA (Hara, 1981). It was originally thought that the DNA component in biofilms came from lysed biofilm

colony members (Sutherland, 2001), and in fact, in some mono-species biofilms, for example *Staphylococcus epidermidis*, autolysis of colony members is thought to be a source of much eDNA (Qin et al., 2007).

It has been shown that eDNA plays important roles in both cell to cell interactions and in initial cell adhesion events (Busscher et al., 2008, Das et al., 2010) and this adhesion is likely due to acid-base chemical interactions (Das et al., 2010). One group reported that adding DNAase at the initial stages of biofilm development, negatively impacted maturation, but found that the mature biofilm structure was largely unaffected (Whitchurch et al., 2002). It has been suggested that eDNA also enhances gene transfer efficacy between biofilm members (Molin and Tolker-Nielsen, 2003).

Fascinating recent work has found that eDNA plays a central role in the self-organising advance of the biofilm leading edge, helping to organize cells into channels ensuring efficient supply of cells to an advancing front and that following DNAse exposure biofilm expansion was reduced some 76 percent and thus greatly reduced intercellular coordination (Gloag et al., 2013). This finding that *Pseudomonas* biofilm eDNA is localized at the leading edges of a biofilm is in contradiction with findings by Ma et al (Ma et al., 2009), who found that eDNA was typically found in the hollow cores of biofilms. This difference may be due to the two research groups using different stains PA103 and PA01 respectively, or perhaps different growth conditions, or both. However, taken together the work carried out by both groups does make sense, in that immature biofilms would be more affected by DNAase treatment than a mature biofilm if eDNA played a role in colony front advancement.

eDNA has been visualised as having an important role in clumping behavior in planktonic cultures (Allesen-Holm et al., 2006), with large quantities (4.5mg/ml) of eDNA being expressed (Hara, 1981). Some authors conclude that it is the most abundant EPS constituent in *Pseudomonas* biofilms, where eDNA was five and 15 times more abundant than protein and carbohydrate respectively (Matsukawa and Greenberg, 2004). It has been found in some biofilms that eDNA abundance can be some 50 percent greater than that of nuclear DNA (Steinberger and Holden, 2005). Its abundance appears species dependent, with unpredictable synergistic expression patterns being apparent when analysing mono and multispecies biofilm eDNA accumulation, when cultured in unsaturated conditions (non liquid flow, but high humidity conditions, on agar plates with membranes). The regulation of eDNA expression has been found to be mediated via quorum sensing (Allesen-Holm et al., 2006).

Mai and colleagues discovered that eDNA expression was spatially separate from the Psl polysaccharide dominant regions in *Pseudomonas* biofilm (Ma et al., 2009), suggesting some coordination between the two components in the *Pseudomonas* mushroom morphology, which may or may not be applicable to carpets morphologies. Also again, in some species, the corporative nature of the EPS components has been observed, for example; in the species *Staphylococcus aureus*, increases in eDNA resulted in the increased abundance of the amyloid fold, but not increased expression of PSM amyloidgenic protein (Schwartz et al., 2016), suggesting some catalytic capacity for some eDNAs.

Interesting recent work by Wilton and colleagues has clearly shown that eDNA has the ability to increase the resistance of *Pseudomonas* biofilms to aminoglycoside antimicrobial agents, due to the acidification of the local environment. This was shown in planktonic cultures, complete with restored susceptibility, on pH adjustment to more neutral conditions (Wilton et al., 2016).

The sequences of eDNA are not known, however some studies have compared the relative size of biofilm genomic fragments with eDNA present in biofilms, and found that there was a greater quantity of eDNA of longer chain length, than that of nuclear DNA, as determined via PCR and agarose gel analysis (Steinberger and Holden, 2005). Steinberger and Allesen-Holm working with *Pseudomonas*, and Qin with *Staphylococcus epidermidis*, have both concluded that eDNA is very similar to that of chromosomal DNA (Qin et al., 2007, Steinberger and Holden, 2004, Allesen-Holm et al., 2006).

Given the stated importance of this biofilm structural component, its presence and spatial distribution was monitored during this current project.

Protein in EPS

Protein is another abundant and potentially vital biofilm component. This point was somewhat evidenced by (Matsukawa and Greenberg, 2004), who found it to be the third most abundant EPS constituent. It is also perhaps the most unstudied of the known matrix components. The activation of multiple and convergent signaling as well as biosynthetic pathways results in many expressed proteins linked to the biofilm phenotype that have been detected and found to be vital in initial biofilm formation in some *Pseudomonas* stains (O'Toole and Kolter, 1998b). Some biofilms have been found to be very vulnerable to protease attack, indicating that in some instances, their partial / complete digestion can be detrimental to biofilm structure (Beenken et al., 2010).

One example of a biofilm expressed protein is the Biofilm-Associated-Protein (BAP), which was first discovered by (Cucarella et al., 2001) in *Staphylococcus aureus* and shares a significant amount of sequence homology with other microbial species, including *Pseudomonas* (25 percent) where it has been found to play differing roles in the biofilm phenotype (Waar et al., 2002, Latasa et al., 2006). In a *Pseudomonas* biofilm it is principally involved in cell adhesion events and substratum attachment, and possesses a hydrophobic transmembrane domain (Cucarella et al., 2001). Again, corroboration between two EPS components have been detected in *Staphylococcus aureus* where increases in the synthesis of polysaccharide PNAG were highly correlated with that of BAP; this correlation was also confirmed via gene knockout studies (Cucarella et al., 2001). Such corroborative behaviours are likely to be conserved in most species including *PA*.

Amyloid proteins have recently been found to play an important role in many microbial biofilms including *PA* (Dueholm et al., 2010), and are likely to play an important structural role. They are a diverse group of proteins called amyloidogenic proteins that are capable of producing the amyloid fold (DePas and Chapman, 2012). The amyloid fold favors simpler amino acids for example glycine and alanine, forms spontaneously and their stability has been suggested to have been important in the creation of life on earth (Carny and Gazit, 2005). Amyloid quaternary structures, can be 2-20nm is diameter, be of infinite length and tend to be mostly unbranched (Shewmaker et al., 2011). Indeed their structure typically has a preponderance of β-sheet motifs that aid their self-assemblage by non-covalent interactions (Chapman et al., 2002, Shewmaker et al., 2011), and it has been shown that these aggregating self-ordering proteins stabilise biofilm structure (Shewmaker et al., 2011, DePas and Chapman, 2012).

Amyloids are found throughout nature including humans, where they are associated with some disease processes, for example Alzheimer disease (Gamblin et al., 2003), where hyper-phosphorylation of amyloid Tau protein leads to aggregates and tangles that are very difficult to breakdown (Iqbal et al., 2005) via protease activity (Novak et al., 1993, Shewmaker et al., 2011). This ability for the protein to aggregate, coupled with its resistance to degradation, is likely to be the reason amyloid type structures are employed by microbes in biofilms, to play possibly a stable structural role.

As introduced previously, proteinaceous materials are almost certainly vital in both the formation and stability of biofilms, and thus warrant monitoring.

1.26 Surface Material Selection and Information

A small range of test materials were chosen for this project. They were selected for a combination of their relative abundance, costs, physical properties (Table 1.5) and industrial usage. The materials initially selected for the bulk of the microbial research work in this project were 316 stainless steel, 304 stainless steel, polycarbonate, PMMA, polyethylene, and polytetrafluoroethylene (PTFE). Later in the work plan, modified novel surfaces were brought into the project, which include the NILT Technology surfaces and the Sharklet™ polymer films, as well as other thin film surface modifications to polytetrafluoroethylene, polycarbonate, and 316 stainless steel. Film modifications include gold coating, PTFE-AF and SilWet thin film coating.

Polymer materials are widely used in the scientific, medical and industrial environments because they are low cost, light weight, recyclable, possess favourable mechanical properties (Table 1.5) and can offer good biocompatibility. In contrast metals are typically much more expensive, denser, and the ratio of strength to weight is not always favourable. They also can be more liable to bio-fouling as is the case for stainless steels (Pereni et al., 2006). Polymers offer the combination of innate corrosion resistance and high strength, with example applications being park benches, aerospace components, biomedical devices, automotive fuel tanks and car components (Yaneff, 2003).

1.26.1   Stainless steel

316 stainless steel offers better corrosion resistance than stainless steel 304, and also offers excellent pitting resistance combined with very good chemical resistance. It is by most metrics the gold standard in industrial corrosion resistant materials, with a concomitantly higher material price. The difference between the slightly inferior stainless steel 304 arises due to the presence of between 1-2 percent higher molybdenum content in 316 (see Table 1.5). 316 stainless steel is widely used in the paper, chemical, textile and photographic industry (Steel, 2007). This material is also often the material of choice in the construction of industrial chemical plants (Wright et al., 2013). This preference is likely due to both historic and familiarity reasons, coupled with wide spread use of polymers being a somewhat recent phenomenon in industrial application.

1.26.2   Poly(methyl methacrylate) (PMMA)

Poly(methyl methacrylate) (PMMA) is commercially known as Perspex® and is a clear, thermoplastic polymer. It is used extensively for optical and light industrial applications, though it is susceptible to surface scratching and crazing. It is available commercially in both pellet form

for injection moldings, as well as a range of extruded and rolled forms including sheets and rods. Medical uses include: bone cement, cranioplastic implants and intraocular artificial lens (Dankert, 1986). Outstanding properties include weatherability and mouldability. The most serious deficiencies are a low impact strength and poor chemical/solvent resistance.

1.26.3 Ultra-High Molecular Weight Polyethylene (UHMW-PE)

Polyethylenes are a family of semi-crystalline materials with excellent corrosion resistance and chemical resistance, good fatigue and abrasion resistance, and a wide range of properties (due to differences in length of the polymer chain.) Polyethylenes are easy to distinguish from other polymers because they float in water. They are 1/8 the weight of steel, high in tensile strength, and are as easy to machine as wood. Ultra high molecular weight polyethylene (UHMW-PE) is the ideal material for many wear susceptible parts in machinery and equipment, as well as a superb lining in material handling systems and storage containers. UHMW-PE is a self-lubricating, hydrophobic and shatter resistant. It meets both FDA and USDA acceptance criteria for food and pharmaceutical equipment and is a good performer in applications up to 180 °F (82 °C) or when periodically cleaned with live steam or boiling water to sterilise (W.S. Hampshire, 2016). Polyethylene production is the largest of all the polymers at 50 million metric tonnes per year in 2003 (Yaneff, 2003), which is now predicted to reach 99.6 million metric tonnes by 2018 (Share, 2014). Polyethylenes possesses good resistance to organic solvents, degreasing agents and electrolytic attack. They have a higher impact strength, but lower working temperatures and tensile strengths than polypropylene. They are lightweight, resistant to staining, and have low moisture absorption rates (W.S. Hampshire, 2016). Polyethylene is used in the medical sector for intravascular devices, cerebrospinal fluid shunts, orthopedic implants (Dankert, 1986). Polyethylene is recyclable as it is a thermoplastic polymer.

1.26.4 Polycarbonate

Polycarbonate is a transparent amorphous thermoplastic which has a very high impact resistance, but is partially prone to scratching. Thus, in some applications for example in spectacle lenses, they have an additional scratch resistant coating. Polycarbonate is also typically used to replace glass in impact prone applications such as safety glasses and impact resistant screens. It has good electrical insulating properties. It is also used to make DVDs and bullet proof cars (Bayer, 2009). It thermoplastic and is therefore recyclable.

1.26.5   Polytetrafluoroethyelene (PTFE-Teflon)

Polytetrafluoroethyelene is a high crystallinity thermoplastic polymer which is used in the medical sector for vascular grafts, arteriovenous shunts, intravascular devices and abdominal wall prosthesis (Dankert, 1986). It is used in the coating of non-stick pans in domestic applications. It is widely used in the electrical industries, as an insulator. PTFE is recyclable. The majority of the applications for this fluropolymer arise due to both its high temperature resistance and its low surface energy.

Material	Molecular Weight of Repeat Unit) (D)	Molecular Weight (D) -typical	Typical polydispersity (M_w/M_n)	Density $(g\ cm^{-3})$	Glass Transition Temp (°C)	Melting Temp (°C)	Tensile Modulus (MPa)	Impact Strength (MPa)	Refractive Index 25°C	Crystallinity and morphology	Surface Energy γ_s (mJm^{-2})	Chemical Structure
Polycarbonate	254	11,000	2.7	1.2	149.85	155	2380	850	1.5	Amorphous	42.9	
Polyethylene (UHMW)	28	> 1,000,000	1.07>10	0.92-0.99	-120.15	118-146	60-290	30-200	1.4	Semi crystalline	31.1	
PMMA-Perspex®	100.12	120,000	N/A	1.2	85-165	160	3100	48-76	1.5	Amorphous	41.0	
PTFE	50.01	$1\text{-}5\times10^7$	N/A	2.0	-63	335--345	340	187	1.4	Semi crystalline	25.6	
PTFE-AF2400	Not known	Not known	Not known	1.67	240	360	950-2150	N/A	1.3	Amorphous	15.6	
Polypropylene	42.07	300,000-600,000	5-12	0.9-0.91	9.8	185	34.5	N/A	1.5	Semi crystalline	29	
304 Stainless Steel	N/A	N/A	N/A	7.99		1315-1510	580	N/A	N/A	N/A	N/A	Chromium 17.5-24%, Nickel 8-15% Molybdenum 0-2.5%, Iron 53.48-74.5% Trace: N, P, S, C, Si, Mn, Cu
316 Stainless Steel	N/A	N/A	N/A	7.99		1371-1399	580	N/A	N/A	N/A	N/A	Chromium 16.00 - 18.00, Nickel- 10.00 - 14.00, Molybdenum 2.00 - 3.00, Iron-Balance, Trace: C, S, Si, N, P, Mn

Table 1.5. Summary of known properties for project materials. (systems, 2015, Steel, 2007, Oxford University Press, 1999, Calleja. G., 2013, Sutar., 2014)

1.27 Surface Preparation for Materials

1.27.1   DuPont[TM] Teflon[TM]-AF 2400 (PTFE-AF)

DuPont[TM] Teflon®-AF (PTFE-AF), is an amorphous fluorinated copolymer, and thus structurally related to standard PTFE, (see Table 1.5) so exhibits very similar properties. The uniqueness of this amorphous material is that it is soluble in a small number of perfluorinated solvents, for example 3M FC-75. This means can be used to cast and coat as a thin film. Another useful property is that it has an optical transmission of >95 percent (Chemours-Company, 2016a), making it a useful coatings material in optical applications. It also has the lowest known dielectric constant of any polymer (Chemours-Company, 2016c). It has a reported contact angle of 105° for water and a surface energy γ_S of 15.6 (mJ/m^{-2}) (Chemours-Company, 2016a).
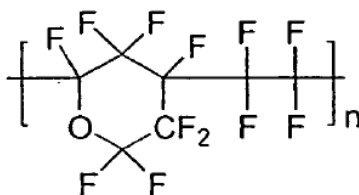

Figure 1.25. Chemical structure of PTFE-AF. Taken from Bikson (Bikson et al., 2004).

1.27.2   AbilSilWet L77

AbilSilWet L77 is a water soluble proprietary polyalkyleneoxide modified heptamethyltrisiloxane copolymer that is used as a non-ionic wetting agent. AbilSilWet is regarded as a superspreading fluid, due to its very low surface tension of 20.5 mN/m^2 at 0.5%w/v. Its applications include being an additive to crop pesticide sprays, where it reduces water usage whilst enhancing the wetting of leafs, increasing product efficacy (De. Sangosse, 2004). Silwet has even been shown to even wet PTFE and penetrate hydrophobic substratums (Ivanova et al., 2010) and thus such surface modifications on 316 stainless steel may warrant investigation.
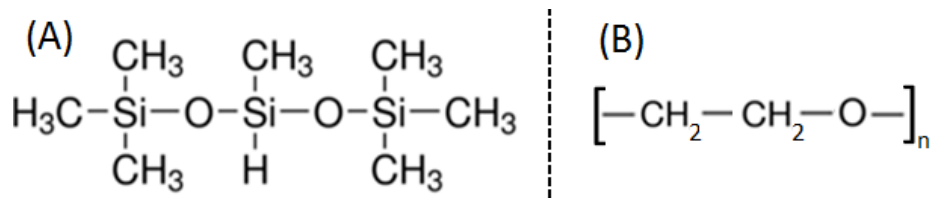
Figure 1.26. **A** Chemical structure of heptamethyltrisiloxane. **B** Chemical structure of polyalkyleneoxide.

1.27.3 NIL-Technologies (NILT)

NILT is a polypropylene based thin film (approximately 200µm thick) that has been engineered to form very specific proprietary surface topology. The water contact angle of the precursor planar polypropylene was reported to be 100°, however following modification the resulting contact angle was reported to be >150° (NIL. Technology. Corp, 2016), making it a classically super hydrophobic and lotus leaf like surface (Shirtcliffe et al., 2010). Surface topographic features are 18-20µm in diameter, with a height of 8-10µm (NIL. Technology. Corp, 2016). Interestingly, the modification of materials that are already hydrophobic is based on duplicating the nano and micro structures that have evolved in nature, in this case that of super hydrophobic plants exhibiting the lotus leaf phenomenon (Lee et al., 2006b).
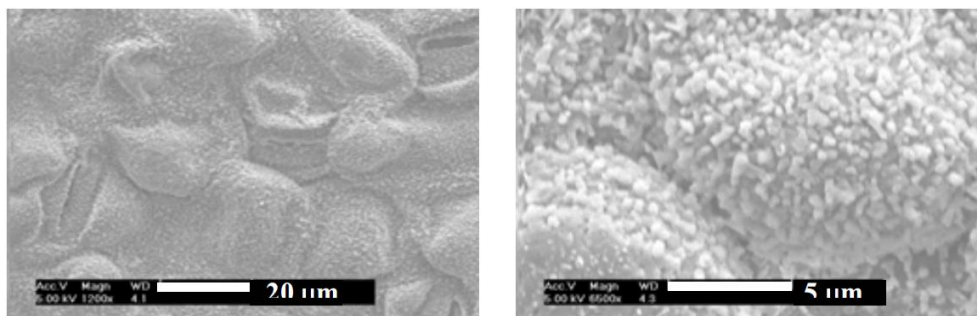

Figure 1.27. SEM of tulip tree leaf, at both 1200x and 6500x (Lee et al., 2006b).
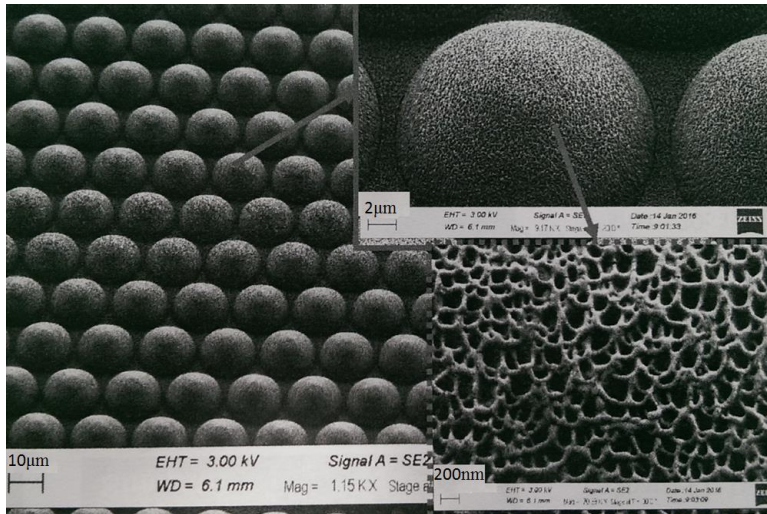
Figure 1.28. SEM of NIL Technology polypropylene surface, at 1150x, 9170x, and 70,000x, with 20nm gold film (NIL. Technology. Corp, 2016).

1.27.4   Silica Powder Abrasive

A Silica based abrasive was used in this study to examine what effects such an additive would have on the removal of *PA* biofilm in a high shear cleaning scenario (Chapter 9). Zeodent® abrasives are a group of water insoluble silica powders that are used in the dental formulation business to aid the removal of stains from the surfaces of teeth, whilst causing minimal damage to the structure of teeth.

Zeodent®119 is a propriety precipitated synthetic amorphous silica, that has an average particle size of 8-10µm, and when suspended 5%w/v in water, a published pH of 6-8 (Huber. Engineered. Materials. Corp, 2015). Zeodent®119 has a Brass Einlehner Abrasion value of 5-6 (White. et al., 2004).

1.27.5   Sharklet^{TM} Polymer Film

This technology is marketed as a material that inhibits microbial attachment, growth and biofilm formation solely through topographical effects, and as such was of interest to the project. The patented Sharklet^{TM} pattern is formed on an poly(dimethylsiloxane) substratum (Mann et al., 2014), with regular dimensions of 2µm width, rectangular features, with a small 2µm gap between them, which are 4µm in height (Chung et al., 2007) (Carman et al., 2006). The poly

(dimethylsiloxane) elastomer (Chung et al., 2007) has a reported γ_S of 15.7 to 23.0mJ/m^2 (Oxford University Press, 1999). Dimethylsiloxane is typically used in pacemakers, catheters, and cerebral spinal shunts (Gottenbos et al., 2000). The reasoning behind the design of the pattern is based around natural self-cleaning anti-adhesive surfaces as discussed above (Chapter 1.27.3), but as the name suggests the Sharklet™ pattern is based on mimicking the approximate topography and geometry of shark skin (Chung et al., 2007). Decreases in the binding of *Staphylococcus aureus* and subsequent prevalence of biofilm have been observed using extended growths relative to smooth control surface (Chung et al., 2007). A great deal of surface topography variations have been previously examined for the initial attachment of *Ulva linza* spores on PDMS substrates, including circular pillars, star pillars and channels of various dimensions (height 1.5 to 5µm, width 2 to 20µm, spacing 2 to 20µm) and the Sharklet™ topography dimensions were shown to be superior at retarding spore attachment (Carman et al., 2006). Decreases of some 90 percent of surface attached microbes were observed in the hospital clinical environment following a 6 month trial relative to appropriate controls (K P Schmid, 2011). Other impressive anti-microbial adhesion observations both in the laboratory and clinical environments have also been reported (S T Reddy, 2011, R M May, 2011, Reddy et al., 2011, Mann et al., 2014, May et al., 2014).
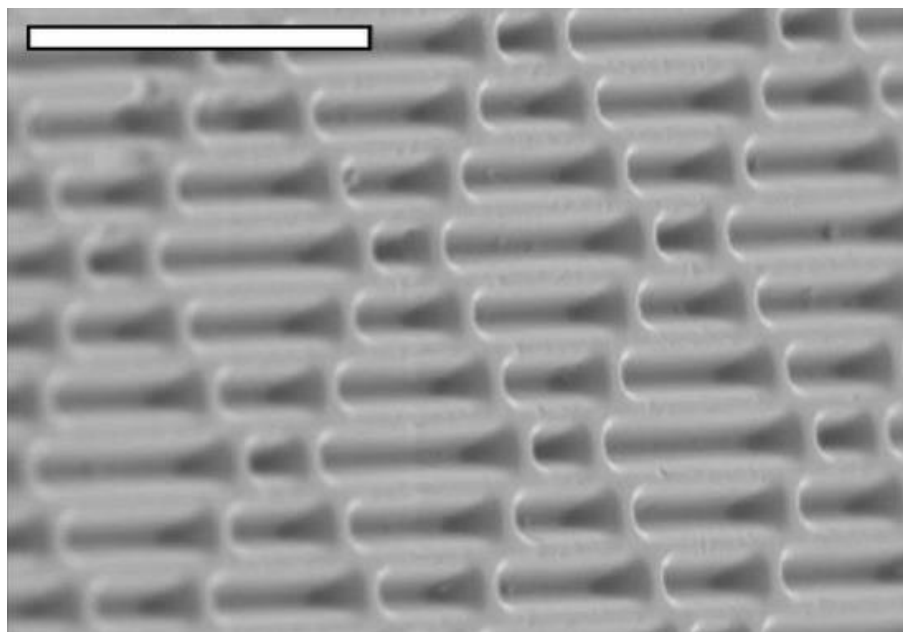

Figure 1.29. Taken from Mann et al (Mann et al., 2014). Scale bar represents 20µm.

This fascinating topographical patterned material, coupled with the cited papers relating to bacterial decreased bacterial adhesion events, warranted investigation within the context of the work presented in this thesis.

1.28 Origin of Microbial Contamination in Industrial Plants

Microbial contamination of industrial manufacturing processes comes about in a number of ways. Either via a large contamination event, or by a continuous contamination process, or perhaps a few residual microbes having survived a cleaning procedure (Verran and Whitehead, 2006), having been hidden within the process equipment e.g. dead leg of plant piping.
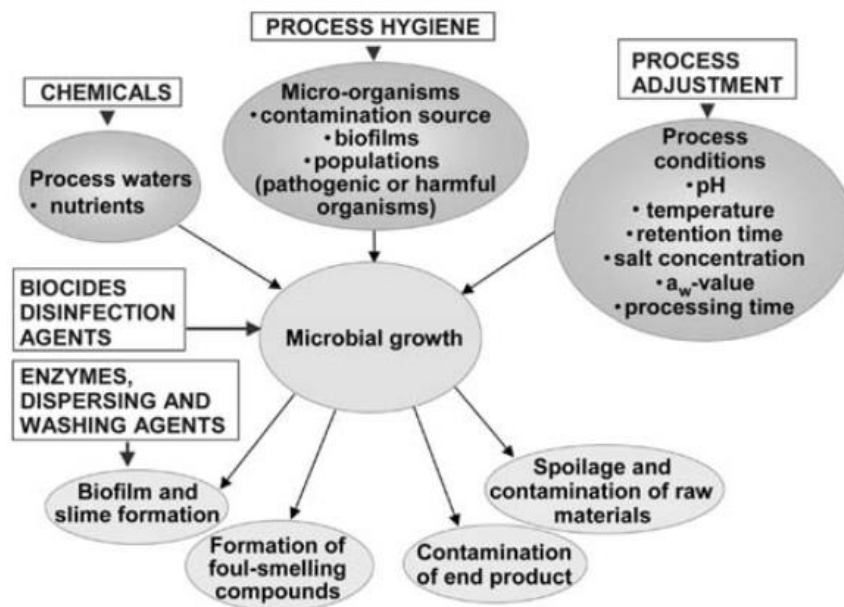

Figure 1.30. Source, control and problems associated with microbial contamination within industrial process setting and resultant outcomes (Maukonen et al., 2003).

Microbes can enter a manufacturing process in a number of ways including:

- through raw materials
- air in the processing plant
- contaminated water
- contaminated cleaning agents
- process surfaces
- factory personnel

The control of undesirable microbes within industry is a multi-stage process, but ultimately is aimed at either reducing the numbers of microbes and their activity, or controlling their deposition on process equipment. This control is achieved through the promotion of good hygiene, running of the process line in a rational manner, and using effective biocides and disinfectants in line with optimised cleaning regimes (Maukonen et al., 2003).

Cleaning is of paramount importance in industry and must take into account both the planktonic and sessile life style of microbes, and as such cleaning should not only remove the biofilm but kill the bacteria when released to prevent seeding elsewhere in the manufacturing system.

As discussed in Section 1.22, flow rates and mass transport are very important, thus any means that are effective at limiting the transfer of microbes to the surface of an internal pipe surface will help limit colonisation rates. To achieve this using lower liquid flow rates helps by increasing the size of the surface-fluid boundary layer the bacteria have to cross in order to reach the surface, whilst limiting the rate of transfer of bacteria at the boundary layer interface. Also limiting turbulence would also help, this could be done by using stainless or electro polished steel instead of mild steel, creating a smother less turbulent fluid, but also reducing the occurrence of T-bends in the plant piping which can introduce local turbulence in the plant, all of which help to transfer microbes and surface conditioning agents to the surface.

1.29 Industrial Biofilm Formation- An Industrial Perspective

P&G is a large multi-national company trading in most countries on the world, with a net market capital worth of approximately US$224Bn. The business is divided into four separate divisions; Grooming, Health Care, Fabric Care and Home Care, and finally Baby Care and Family Care.

Microbial contamination of P&G industrial plant is a challenge from both prevention and a cleaning-sanitisation perspective. Approximately 80 percent of their microbial contamination is believed to arise from poor quality of water (Wright et al., 2013). This microbial challenge spans not only liquid formulation businesses but the vast majority of businesses for example; oil and gas distribution, drinking water distribution, medical devices, commercial shipping and heat exchangers (Carpentier and Cerf, 1993, Costerton. W. J., 1987).

The microbial load tolerance within P&G liquid products has an upper quality safety limit of 100cfu/ml, with some types of microbial species not being tolerated at all. This is far lower than some competitor products which tolerate upto 1000cfu/ml.

One example of a microbial contamination event occurred in November 2009 when a product recall was issued for Vicks Sinex nasal spray (product of the OTC medicines division) in three countries; the US, UK and Germany. This recall was due to the detection of the bacteria *Burkholderia cepacia* in the product made in their production plant in, Germany. There were no reports of illness, however, the bacteria had been previously linked to increased pathogenicity and death in CF patients (Govan and Deretic, 1996). An increased level of risk resulted from the presence of this particular bacterium and because the product that was contaminated was an aerosol generating device that could enhance the delivery of these bacteria to a known microbial sensitive site. Interestingly, P&G showed that this organism likely using Gluconate (Chlorohexidine digluconate) (which is used as a preservative in P&G) as a carbon source. P&G observed that with increasing bacterial levels the level of this agent decreased accordingly, suggesting its consumption or degradation. The cost of recall for this product was believed to be ~ $25M, including plant sanitisation and associated costs (Wright et al., 2013). This is merely one example from one company, which undermines the potential costs to industry and risks to the public that microbial product contamination pose.

The cost of closing, cleaning and sanitising one production plant costs approximately US$5M and such cleaning regimes need to be conducted with some regularity as a preventative measure to ensure that stringent product quality metrics are met, especially when increased bacterial presence within the system is detected.

There is a requirement by regulatory bodies throughout the world for products to accurately describe their contents and ingredients, and companies are responsible and liable for anything

present in the product especially if it is not on the list of ingredients including any bacterial contamination. However, many liquid products made in large scale production plants i.e. washing up liquids and hand sanitisers, are made in non-sterile environments, albeit clean environments. Creating a sterile environment is not possible due to practical considerations. To enter these clean room production environments there are hygiene and clothing requirements including the use of lab coats, overshoes, beard and hair nets and the need to wash hands with an alcohol gel. Despite these measures, contamination of plant equipment is inevitable and does occur. Although the contamination risk that arises from production personnel represents a relatively low potential source of bio-contamination, it is real and is minimised further by taking precautionary measures.

Increased microbe contamination can also affect product stability, resulting in a reduction in shelf life, but also the build-up of potential toxins and/or gasses (presenting an explosion risk), and it is these factors that are the main concern within the home and laundry care division of P&G from a biofilm standpoint.

There are many challenges within industry. Within P&G and the industry as a whole there has been an increasingly popular move to make products from substrates that are derived from more natural sources and thus more bio-degradable and sustainable. In addition there has been a push to reduce the amounts of preservative present within liquid formulations. Also, over time there has been a reduction in 'hostile' chemistries used in the manufacture of some products, thus creating a better environment for microbial life to thrive. These initiatives are principally driven by market forces rather than from a bio fouling perspective (Wright et al., 2013). These more naturally sourced substrates often contain an increased microbial load, which coupled with the decrease in preservative used, greatly increases the risk that biofilms will be become established within the industrial plant, but also actively live and prosper within the liquid products. This constitutes a 'perfect storm' that in the future may limit product manufacture quality and the types of antimicrobial agents available for use, similar to what is currently being observed with the emergence of antibiotic resistance strains in hospitals worldwide.

In recent times there has been a move to standardise existing and new plant design, to minimise dead legs in the plant piping, and thus minimise biofilm establishment rates. This has been brought about due to the costs of commissioning plants and their changes in use over time, often they are adapted as products and requirements change. This in turn creates areas with dead ends and increased branching, which are harder to clean and can induce turbulence.

A sample of used 316 stainless steel manufacturing plant was obtained and analysed using WLI and found to have a R_a of 1.6±1µm, which is way above the recommended hygiene standard R_a for 316 stainless steel of < 0.8µm (EHEDG, 2009). It is interesting to note that no such standard roughness for polymers such as polycarbonate exists.

Figure 1.31. 316 stainless steel inlet/outlet blank sample of used manufacturing plant, taken from a well-used 100L vessel.

Biofilm reduction from a rate colonisation, growth and cleaning perspective represent a major challenge to industry, and remains a very active area of research.

1.30 Techniques Introduction

1.30.1 Confocal Laser Scanning Microscopy

Confocal laser scanning microscopy is an advanced microscopic technique employed in many areas of biology. The concept was first described in 1961 (Minsky, 1961). The technique is essentially based around fluorescence technology, whereby light of a known wave length is used to excite fluorescent molecules that then emit at a new lower wavelength. These fluorescent molecules can either be expressed *in situ* attached to a molecule of interest i.e. GFP, or fluorescent probes or dyes can be used which associate with a target of interest. Also, some targets may naturally fluoresce as for example riboflavin (Zipfel et al., 2003) and many others. The premise being that unbound fluorescent probe can be removed or there is enhanced

fluorescence following binding, either way the target is pronounced. In standard fluorescence microscopy, the microscope detector detects all of the light being emitted, all at once, with spatial resolution in the X and Y dimensions only (2D). This approach is great, for examining surfaces, where perhaps only 2 dimensional data differentiation is required. In such an example all of the z dimension data is lumped together, which can be beneficial, application depending.

The advantage of confocal microscopy is the ability to discriminate in the Z dimension, in addition to the X and Y dimensions (3D). The collection of in focus Z plane data at a user defined optical thickness and step height, allows for the creation of 3D images that can allow of the localisation or co-localisation of different structural components in space, and with time lapse confocal microscope, over time as well. This optical sectioning does not require the sample to be physically sectioned, conferring many advantages.
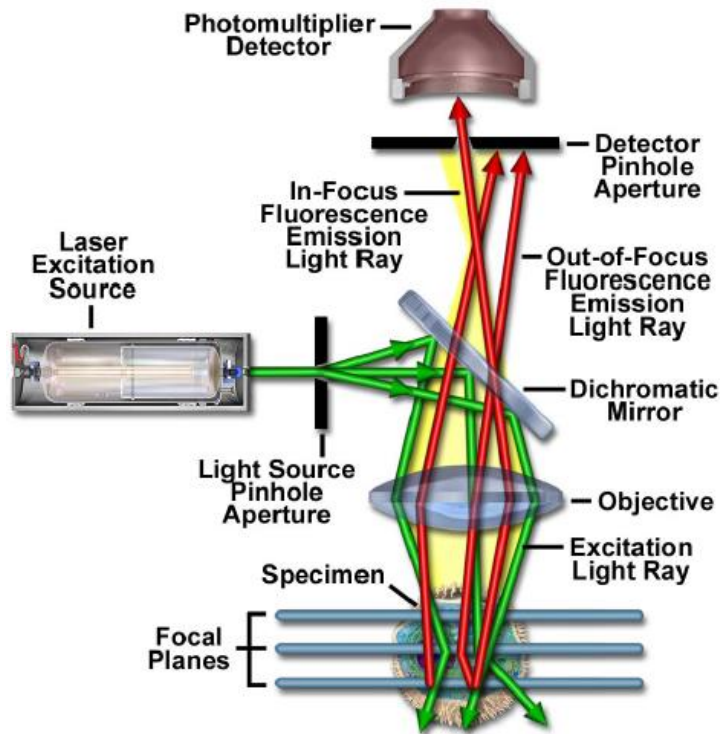
Figure 1.32. Diagrammatic representation of confocal laser scanning microscope, showing the laser beam path and major components (Claxton. N.S., 2005).

The ability of the technique to work is based principally on 2 pinholes, one positioned just after the laser source, and the other just before the photon detector. The first pinhole ensures only cohererent electromagnetic radiation of the desired wavelength passes through; this light is then focused and directed to the specimen. Typically, there is a great deal of reflectance both below and above the focal plane (out of focus light, Figure 1.32), but as this light is not confocal with the second pinhole, only in focus light passes through to the detector (Claxton. N.S., 2005). Due to the enormous amounts of data that are collected by these instruments it wasn't until the mid-eighties (White., 1987) that confocal microscopes were commercially available.

$$dz \, (\mu m) = \sqrt{\left(\left(\lambda * \frac{n}{NA^2}\right)^2 + (AU * n * \sqrt{2} * 1.22 * \lambda / NA^2)^2\right)} \qquad \text{Eqn. 6}$$

Confocal microscopy optical thickness equation and a calculation for fluorescent probe Syto®9 (λ=Emission; 580nm), n=Refractive index (water = 1.33), (NA=Numerical Aperture (25x Lens 0.95). For Table of optical z slice Parameters see Appendix B.

$$NA = n * Sin \, \theta \qquad \text{Eqn. 7}$$

n=refractive index, Sin θ is half angular aperture

The numerical aperture (NA) is a quantity that describes the angle of the light that is collected by the objective. The higher the NA then the greater the angle that can be measured. Typically, the higher magnification of an objective have a higher NA (Mike and Joe, 2005).

1.30.2   Confocal Laser Scanning Probe Selection

Chemical probe selection for confocal microscopy utilising upto three probes can be complex. There are many factors, for example; probe-conjugates availability, excitation-emission considerations, including FRET, overlapping emission profiles and differing buffer compatibility. This project was concerned with detecting changes in gross biofilm colony morphology. The biofilm constituents chosen for analysis were the microbe (which could include eDNA), carbohydrate, and protein abundance.

Probes selected for use in this project were:

Syto®9 (Thermo Fisher Cat No. 34854)

ConA-Alexa® Fluor®633 (Thermo Fisher Scientific Cat No. C21402)

Sypro® Orange (Thermo Fisher Scientific Cat No. S6651).

Concanavalin A-Alexa Fluor®633 Conjugate Confocal Microscopy Probe
Concanavalin A is a Lectin extracted from the common Jack Bean (*Canavalia ensiformis*), that like all Lectins exhibit very specific sugar binding properties, in this case specifically binding to α-mannopyranosyl and α-glucopyranosyl residues (Scott et al., 1992, Molecular Probes, 2006,

Goldstein et al., 1965, Aldrich, 2016). Conveniently, both mannose and glucose residues are principle components of all three known polysaccharides expressed in *PA* (see Chapter 1.25.1). ConA exists as a homo-tetramer at neutral physiological, and has a combined molecular weight of approximately 100kD (Aldrich, 2016). It has been used extensively in many fields from targeted drug design (Scott et al., 1992), to biofilm research (Sweity et al., 2011, Strathmann et al., 2002).

The Alexa Fluor® probes are sulfonated rhodamine derivatives, that have been developed to have enhanced quantum yield, photo-stability and excitation coefficients; they are also less environmentally sensitive (Claxton. N.S., 2005). A wide range of excitation / emission spectral ranges are available conjugated to a variety of probes. The Alexa Fluor® 633 has a molar extinction coefficient of 159,000$cm^{-1}M^{-1}$(ThermoFisher Scientific, 2010), but the quantum yield and fluorescence life time of this molecule are not known.
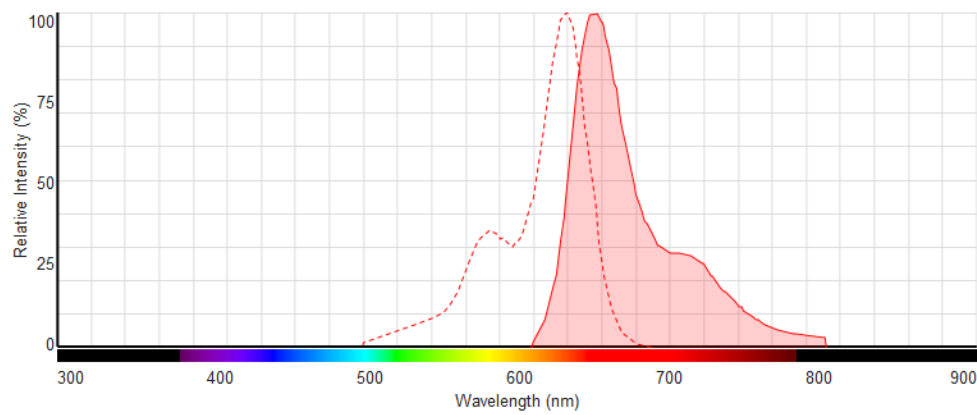

Figure 1.33. The excitation (red line) and emission spectrum (pink shading) for Alexa Fluor®633 (ConA) (ThermoFisher Scientific, 2015).

Syto®9 Green Fluorescent Nucleic Acid Confocal Microscopy Probe

Syto®9 is a cyanine based probe that is typically sold as a kit by Thermo Fisher for the detection and quantification of live and dead bacteria (BacLight™ Cat No. L7007). The Syto® probes are based on a partially saturated indole nitrogen heterocyclic molecule, consisting of two aromatic hydrocarbon rings interconnected by a polyalkene bridge (Claxton. N.S., 2005), these are available conjugated to numerous probes. Syto®9 reagent binds to both viable and non-viable microbial cells, as well as gram positive and negative (Fisher Scientific, 2004) bacteria, and to

both to DNA and RNA, with little difference in the emission/excitation between the two. However, differences in the relative intensities of Syto® have been observed between gram positative and negative microbes (*Pseudomonas* and *E.coli* verses *S. aureus and Bacillus subtilis*) with gram negatives stain intensity approximately 18 times greater (Stiefel et al, 2015).   Syto® stains penetrate virtually all membranes, with very low intrinsic fluorescence due to the unbound probe quantum yield being <0.01 (ThermoFisher Scientific, 2014). The quantum yield when bound to DNA is 0.58 and an molar extinction coefficient of >50,000cm^{-1}M^{-1} (ThermoFisher Scientific, 2014), thus giving an increase of some 58 fold in fluorescence when bound to DNA; one paper reporting increases in fluorescence of 100 fold and DNA association constant of 1.8 x10^5/M (Stocks, 2004). The DNA/RNA binding sequence and mechanism is not known (ThermoFisher Scientific, 2016), and neither is the fluorescence life time of this molecule known.
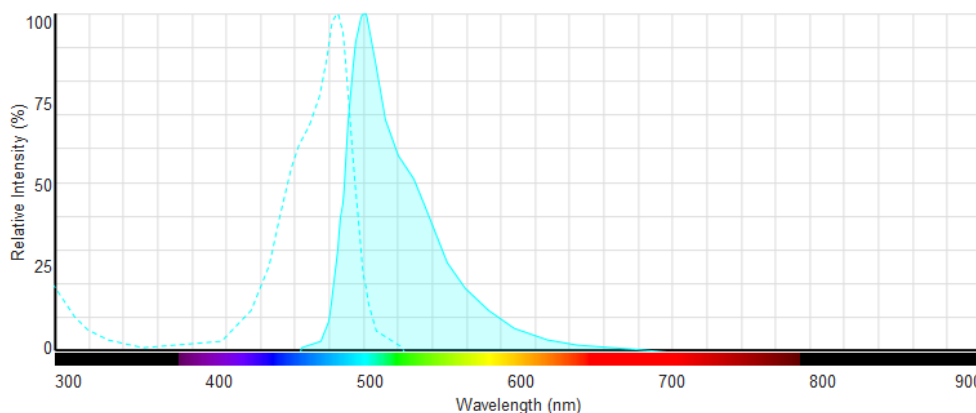

Figure 1.34. The excitation (cyan line) and emission (cyan shading) spectrum for Syto®9(ThermoFisher Scientific, 2015)

Sypro® Orange Protein Confocal Microscopy Probe

Sypro® orange stain is a molecule that interacts non-covalently with proteins, with a sensitivity when staining SDS-PAGE gels of 1-10ng of protein (Steinberg et al., 1996b). Sypro® is thought to bind to the exposed hydrophobic regions of proteins (Hawe et al., 2008). Quantum yield when bound has been determined to be approximately 0.5 (Azadi et al., 2013), however the molar extinction coefficient is not known. Previous research (Steinberg et al., 1996a) has shown that Sypro® does not bind to DNA or carbohydrate (Fisher Scientific, 2003), and that the probe could be used with both native PAGE and 2 dimensional gel electrophoresis, suggesting its suitability

as a probe to selectively target proteins for visualisation in biofilms in the absence of SDS, as its typically used (Fisher Scientific, 2003). The fluorescence life time of this molecule is not known.
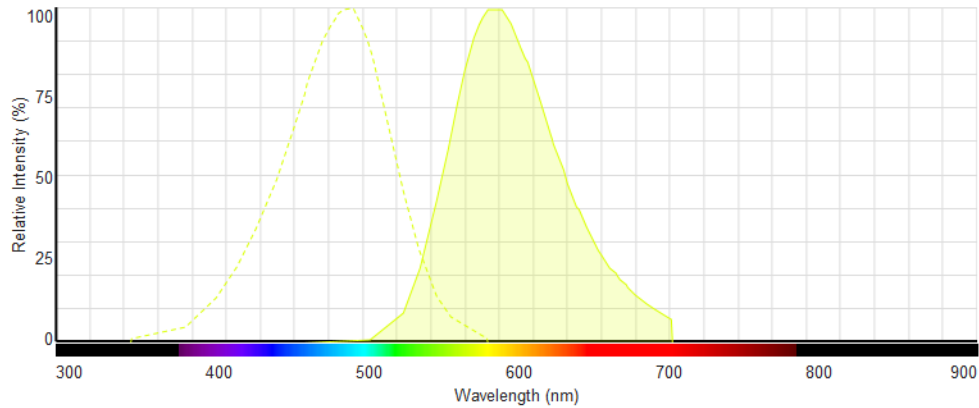

Figure 1.35. The excitation (green line) and emission (green shading) spectrum for Sypro®(ThermoFisher Scientific, 2015).
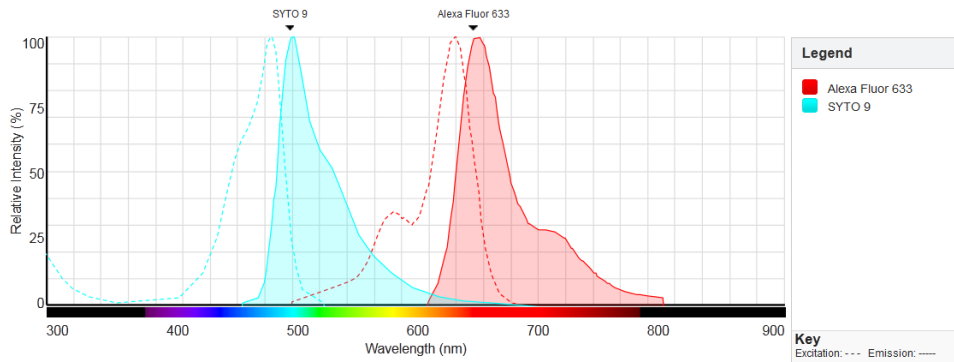

Figure 1.36. The excitation and emission spectrum for Syto®9 and Alexa Fluor® 633 (ConA). Adapted from (ThermoFisher Scientific, 2015). This figure is relevant to the confocal work performed using TCS SP2, stain method 1 Figure 2.5.
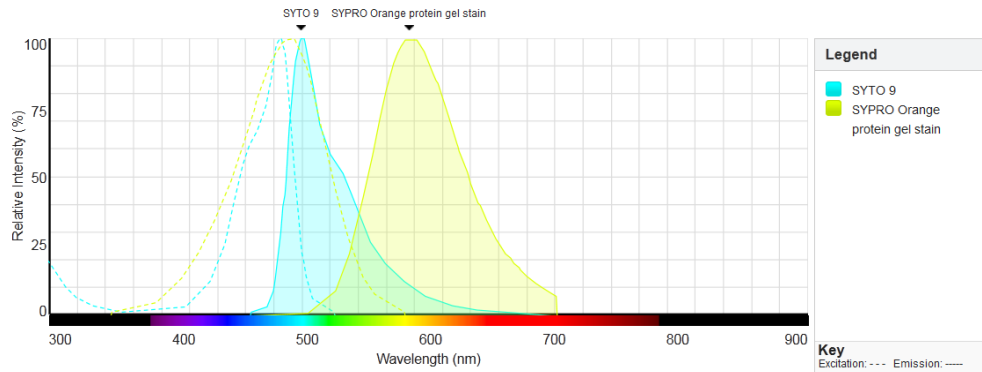
Figure 1.37. The excitation and emission spectrum for Syto®9 and Sypro® (ThermoFisher Scientific, 2015). This figure is relevant to the confocal work performed using TCS SP2, stain method 1 Figure 2.5.

Excitation laser lines for Syto®9 and ConA-Alexa Fluor® 633 were 488 and 633nm respectively. Detection bandwidths used were 495 to 510 and 640 to 660 respectively. SyPro® Orange was excited using a 476nm laser light.

Probe/Stain Combination	Excitation Laser Line Used	Percentage Primary Probe Emission at Stated Wavelengths		Percentage Second Probe Emission Overlap with Primary Probe at Primary Probe Detection Bandwidth at Stated Wavelengths	
Syto®9 / ConA-Alexa Fluor® 633	488nm / 633nm respectively	495 to 510nm	640 to 660nm	495 to 510nm	640 to 660nm
		94 to 79% (<86.5%)	*3 to 2% (<2.5%)*	**0 to 0% (0%)**	*83 to 89% (>86%)*
Syto®9 / SyPro® Orange	488 / 476nm respectively	495 to 510nm	570 to 623nm	495 to 510nm	570 to 623nm
		<u>94 to 79% (<86.5%)</u>	17 to 4% (>10.5%)	<u>1 to 3% (>2%)</u>	89 to 62% (<75.5%)

Table 1.6. Shows the laser wavelength used for each probe or dye, the emission wavelength range selected and the percentage overlap of the respective second probe. Averages are in brackets. Comparables are highlighted for easier comparison. This Table is relevant to the confocal work performed using TCS SP2, stain method 1 Figure 2.5.

Combining probe information and examining the spectral overlap in the emission spectrum of the two co-incubated probes produces Table 1.6. Very little spectral emission overlap is determined (>3%) between Syto®9 versus Alexa Fluor® 633 and Syto®9 versus Sypro® Orange, however a non-trivial amount (approximately 1/7 or 14% signal bled into Sypro® Orange (false positive)) of overlap is found within 640 to 660nm. However, the vast majority of the Sypro® Orange dataset (86%) is valid, and so could be included in gross data analysis when thesholding.

1.31 – Biofilm Quantification Program – *Comstat 2.1*

Due to the enormous complexities of visually interpreting changes in biofilm morphology, either following culturing of mature biofilm or their subsequent removal, *Comstat2.1* analysis software was used with the confocal data sets. This facilitated quantification of various physical biofilm morphology attributes that may not be apparent by visual examination, whilst allowing a scientific

quantitative statistical analysis to be performed on biofilm architecture. An example of a mature biofilm is given in Figure 1.39.

Comstat 2.1 is a confocal laser scanning microscopy analysis program that is an add-on module to *ImageJ*, an image analysis software suite which is freely available on the internet. *Comstat* was specifically designed to analyse biofilm morphology and was developed by Heydorn in 2000 (Heydorn et al., 2000). Another revision, *ComStat 2*, being released in 2008 (Vorregaard, 2008), followed by the 2.1 software release in 2015. It is simple to use software and can analyse a great deal of confocal imagery at speed with high reproducibility. By using such a program, it removes much potential user bias and fatigue, for example when setting thresholds for many thousands of images. *Comstat* was developed for and is widely used by the biofilm community, with many hundreds of publications citing the software including, works carried out on *Pseudomonas* biofilm morphology changes on board the ISS (Kim et al., 2013).

There are many output variables obtained from the software, these include; biomass ($\mu m^3/\mu m^2$), maximum film thickness (μm), average biomass thickness (μm), roughness (R_q), fractal dimension, percentage area occupied in layers. In this project only biomass, average biomass thickness and maximum thickness parameters were evaluated. This was because these are the basic physical metrics of a biofilm that could be used to measure biofilm change in response to cleaning or growth.

The *Comstat* software works by applying a threshold, which is automatically determined using the Otsu method, or by the user. Once an image threshold has been applied all pixels with a lower threshold, are assigned a number zero, and those ≥ the threshold are assigned number one. The result is all zeroed data is effectively removed as background, and all data assigned number one, (biomass) is included in the data analysis (Heydorn et al., 2000). This 'biomass', is of course fluorescent probe specific.

The Otsu method was devised in 1979 by Nobyuki Otsu (Nobuyuki., 1979). It is an automatic thresholding function that serves to subtract the background from images, ensuring only the object of interest is under study.

A connected material function can also be used in the *Comstat* program following the thresh-holding and allows for the removal of any 'biomass' that is not attached to the substratum. Any

material not connected to the substratum has its pixels set to zero (Heydorn et al., 2000). By using these settings only classical biofilm (surface attached biological material) is analysed.

The biomass (bio-volume) is calculated as the sum of the pixels in a stack, multiplied by the voxel size [(pixel size)$_x$ (pixel size)$_y$ (pixel size)$_z$] divided by the area of the substratum in the stack. This yields the overall bio-volume in the stack and an estimate of the hydrated biomass (Heydorn et al., 2000).

Average thickness and maximum thickness parameters are ascertained by determining the maximum height above each pixel illuminated at the substratum on the x,y plane, which ignores internal voids (Heydorn et al., 2000).
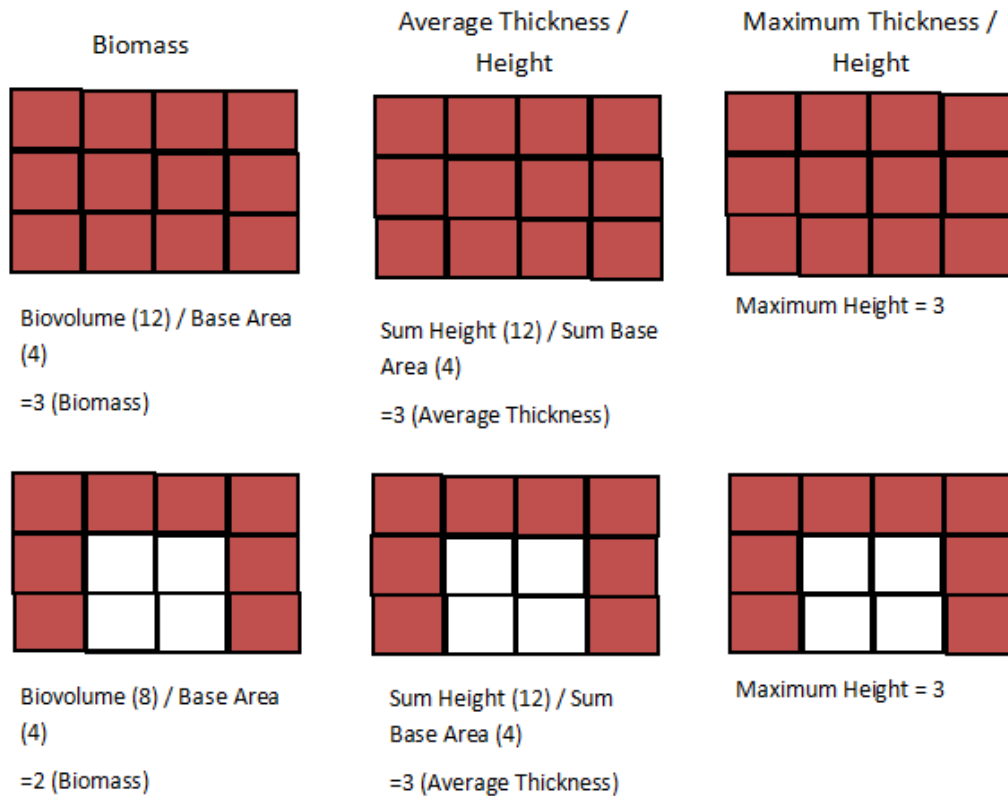

Figure 1.38. Simplified schematic of the different biofilm metrics calculated by Comstat.

It is noteworthy that the parameters obtained are channel specific, i.e. stain specific. So such estimates of biomass, will depend on the probe employed in the method. This is actually exploited

in this project to determine changes in expression level and spatial distribution of biofilm components, specifically cell mass, protein, and carbohydrate contribution, in the biofilms.
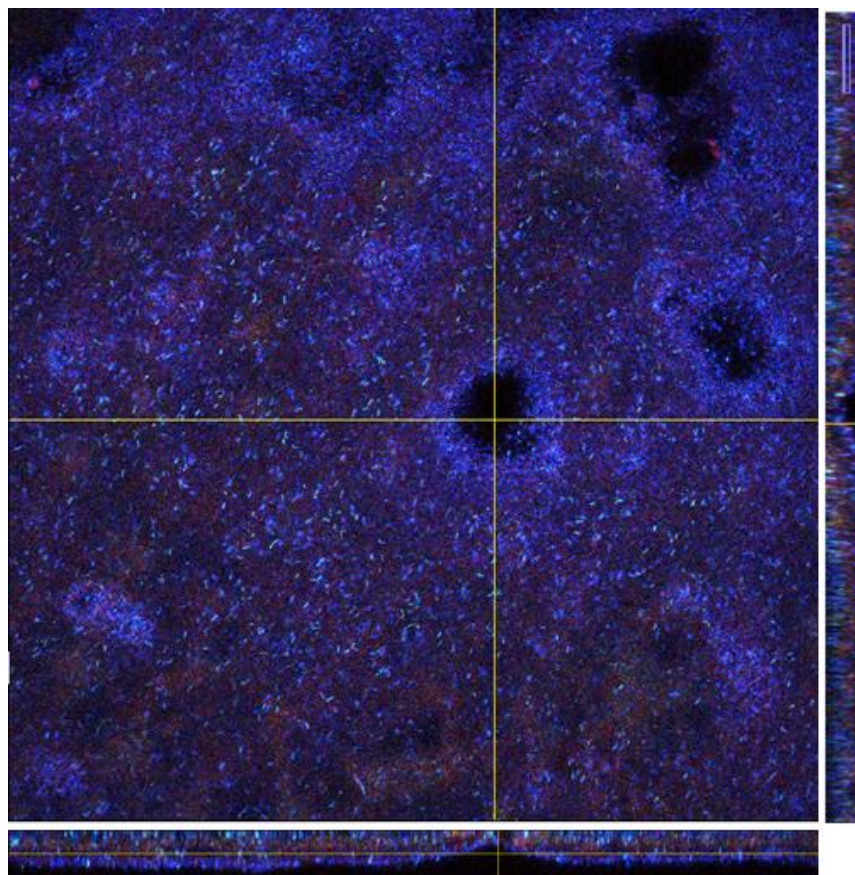

Figure 1.39. Top down and orthogonal slice view of confocal image composite stack showing mature *Pseudomonas* biofilm on PC-SC, showing all three excitation/emission channels. 1024x1024, taken using Leica confocal TCS SP8 microscope. Images are 465µmx465µmx33.15µm in size. Samples was stained as detailed in Figure 2.5-2.

In order to evaluate the relative change in mature biofilm whilst taking advantage of the 3 probes employed for the evaluation of the mature biofilm phenotype, the individual metrics obtained from each probe were combined (summed). Relative decease in the combined metrics were determined relative to negative controls. This enabled the gross physical evaluation of the change in biofilm, in response to cleaning (Chapter 9) or substratum surface properties (Chapter 8).

Comstat can also be used for the determination of the percentage area occupied in either a stack or in single images, and it was used to this effect in the initial binding assay to evaluate the initial

attachment of microbes to different substratum's, using the more advanced TCS SP8 confocal microscope.

1.32 Surface Energy and Contact Angle (CA) Analysis

Contact angle is a method used to determine the 'wettability' of a surface using a liquid, and can allow the surface energy of a solid substrate to be semi empirically determined (Stadler et al., 2003).

Contact angle measurement is a technique that can determine the degree of surface hydrophobicity. The contact angle of the test liquid as measured through the liquid from the surface-liquid-vapour phase boundary is what is of interest. A larger angle would indicate a greater degree of hydrophobicity and vice versa when using a water probe. The contact angle of a surface is very sensitive to contamination, and thus it can be used as a measure of surface cleanliness.
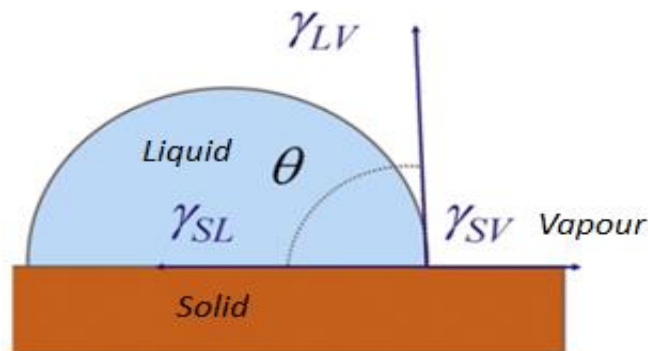

Figure 1.40. Contact angle measurements (Shirtcliffe et al., 2010).

$$\gamma_{LV} \, Cos \, \theta = \, \gamma_{SV} - \gamma_{SL} \qquad\qquad \text{Eqn. 8}$$

Young's Equation (Eqn. 8) is shown above. Young's equation relates the surface tensions of the solid under study, the liquid and contact angle and thus recognises that the resultant contact angle seen in experiments is the result of equilibrium at the three phase contact line for the solid-vapour

(SV), solid-liquid (SL) and liquid-vapour (LV) surface energies or surface tensions (Etzler, 2003, Young, 1805).

Young's equations do not take into account the potential roughness or chemical heterogeneity of the substrate. For these additional factors, the works of Wenzel (Wenzel, 1949, Wenzel, 1936), and Cassie and Baxter need to be consulted (Cassie and Baxter, 1944). Both Wenzel and Cassie-Baxter energy states are due to local free surface energy minimums, with sometimes only a small finite energy barrier between them (Kusumaatmaja et al., 2008) .

Wenzel's equation assumes that the probe in contact with a rough surface occupies the valleys therein, thus increasing its surface area and amplifying the surface chemistry effects, creating either enhanced wetting or hydrophobicity (Eqn. 9). Also, arising from Eqn. 9 is that changes in the observed contact angle on a rough surface are dependent on change in $\Delta\theta_e$, thus increases in surface roughness enhances the contact angle in this model. θ_e is the equilibrium contact angle on a smooth flat surface of the same material. In such a situation where a very high contact angle is achieved, the water probe will adhere to the surface, during inversion, even if the surface is super hydrophobic (Shirtcliffe et al., 2010, David et al., 2003). In the Wenzel model the θ_e of a flat surface of <90° results in a shift towards complete wetting, with the inverse being true (McHale et al., 2004).

$$cos\theta_e^W = rcos\theta_e \qquad\qquad \text{Eqn. 9}$$

In the Wenzel Equation *r* > 1 is the ratio of the true surface area of the solid to its horizontal projection (surface roughness contribution) and $cos\theta_e^W$ is the Wenzel contact angle.
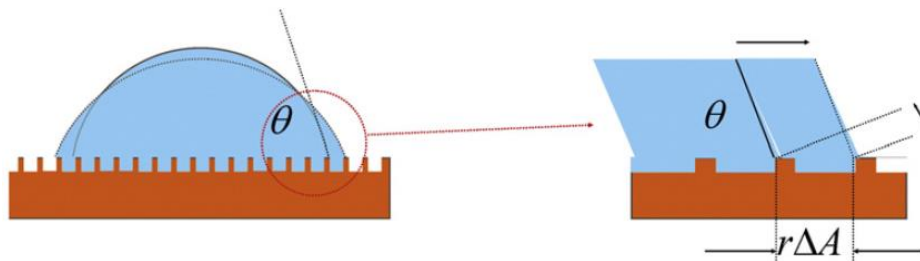

Figure 1.41. Surface wetting in Wenzel model (Shirtcliffe et al., 2010).

$$\Delta\theta_e^W = r \left[\frac{sin\theta_e}{sin\theta_e^W} \right] \Delta\theta_e \qquad\qquad \text{Eqn. 10}$$

$\Delta\theta_e^W$ is the change in observed contact angle on a rough surface compared to a smooth surface.

However, not in all situations does a probing liquid follow the contours of the substratum, in some instances a probe sits across a composite surface, consisting of the tops of peaks and the subsequent air gaps (McHale et al., 2004). These drops 'bridge' across the tops of the peaks in topography and create a 'super' hydrophobic surface. In this Cassie-Baxter model, during sample inversion the probe droplet will roll off (Cassie and Baxter, 1944), this is due to low resistance from the air pockets (Patankar, 2004). This phenomenon whereby a probe cannot penetrate a surface occurs is due to capillary action (David et al., 2003) resulting in a self-cleaning surface or lotus surface. This effect can be seen when surface structures have roughness's in the order of 30μm (Bico et al., 2002), similar to the scales of the engineered NIL Technology surfaces used in this project (NIL. Technology. Corp, 2016). In this model the contact angle cos θ determined is the average of the two surfaces, namely the air gap and actual substratum surface.

$$Cos\theta_e^C = \varphi_s Cos\theta_e - (1 - \varphi_s) \qquad\qquad \text{Eqn. 11}$$

In the Cassie-Baxter equation φ_s =<1 is the fraction of the surface tops of the solid. $(1 - \varphi_s)$ is the fraction corresponding to the air gaps.
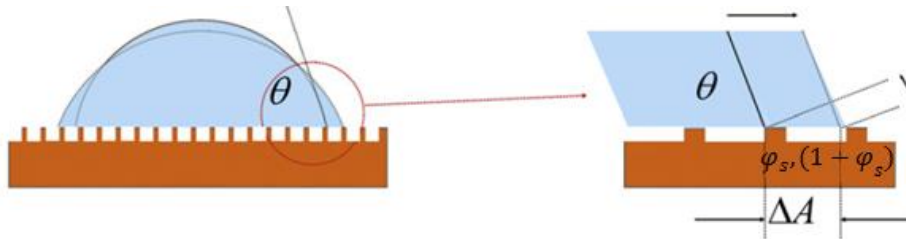

Figure 1.42. Substratum wetting in Cassie-Baxter model (Shirtcliffe et al., 2010).

McHale and colleagues suggest that for a given surface as the roughness is increased, initially Wenzel model behaviour is observed, followed by Cassie and Baxter wetting behaviour, and the propensity of a probe to 'stick' to an inverted surface as a possible means of determining which

model is appropriate (McHale et al., 2004). Wenzel surfaces have high contact angle hysteresis, whereas Cassie-Baxter have low contact angle hysteresis (David et al., 2003).

It is important to note that it is thought that the air gaps beneath the probe are not trapped in any way, and that the propensity of the probe to remain suspended on the peaks of the substratum is governed only by the cost in surface free energy in wetting the sub peak structures (Patankar, 2004).

Contact angle measurements are capable of quantifying different surface energy contributions via the use of different liquid probes.

Work of adhesion calculations are used to measure the free energy between the solid (test surface) and the fluid, and were proposed by Fowkes (Fowkes, 1962, Fowkes, 1964). Work of adhesion can be calculated using the contact angle of just two liquid probes; commonly water (H_2O) and diiodomethane (CH_2I_2). Using these two probes liquids, both the dispersive and polar contributions to the total surface energy can be calculated. There are other methods available for measuring contact angles, and numerous other analyses available. The Fowkes' equation is however, considered the most robust for measuring surface energies (Williams, 2013) (Hejda, 2010).

$$W_{S-L} = 2\sqrt{\gamma_S^d \gamma_L^d} + 2\sqrt{\gamma_S^p \gamma_L^p} = \gamma_{L-V}\,(1+cos\theta) \qquad\qquad \text{Eqn. 12}$$

Fowkes's equation for the work of adhesion is given above (Eqn. 12) where γ_S^d is the dispersive surface energy of solid, γ_L^d is the dispersive surface energy of liquid, γ_S^p is the polar surface energy of solid and γ_L^p is the polar surface energy of liquid (Williams, 2013, Etzler, 2003).

The sum of γ_S^d and γ_S^p as determined using Eqn. 12, gives the total surface energy γ_S of the material under examination. Since the polar and dispersive surface tension components γ_L^d and γ_{SL}^p of these two probe liquids are known, if the contact angles for both liquids are measured for the solid of interest, this data can be used to determine the surface energy components of the solid; γ_S^d and γ_S^p. The surface tension of DIM and H_2O as well as other commonly used contact angle probes are given below (Table 1.7).

	γ_L^p	γ_L^d	γ_L
H_2O	21.8	51.0	72.8
Diidomethane (DIM)	0.0	50.8	50.8
Formamide	19.0	39.0	58.0
Ethylene Glycol	29.0	19.0	48.0
Glycerol	30.0	34.0	63.0
n-decane	0.0	23.8	23.8

Table 1.7. Details of the surface tension components of commonly used probes at 25°C used in the determination of a solid's surface energy (Hejda, 2010, Bueno, 2005).

1.33 White Light Interferometer

A white light interferometer is an optical instrument for measuring the height and topography (roughness) of different surfaces. It works by examining the time it takes for light to be reflected back from a sample substratum into a detector, following the light being previously split and reflected from a flat reference surface, essentially by examining the interference pattern detected following light reconstruction.

Interferometry was first developed by Thomas Young and demonstrated in approximately 1802 (Young, 1802), and used to confirm the wave like characteristics of electromagnetic radiation. Optical interferometry utilises the wave like property of light, but in theory any radiation that has wave like properties would work, for example acoustic or other electromagnetic waves lengths (i.e. radio).

In summary interferometry relies on the splitting of the incident light source into two beams, with both traversing a medium (air); one reflecting off the sample substratum with its differing topography, and the other reflecting off a flat reference surface. The two beams are then recombined, and directed onto a CCD camera where the interference wave pattern can be detected and deciphered.

This technique has diverse applications from eliciting topographical metrological information from surfaces (Cross et al., 2009) to recently helping to detect gravitational waves from two merging stellar black holes (Abbott, 2016).

A white light interferometer can gather data in the z direction with a resolution of <0.1nm, and x/y resolution of <160nm (Veeco, 2007), data capture is fast, and because there is no contact between the sample and the device, the sample is not damaged.

The downside of this method is that it cannot be used to measure surfaces that require visualisation through a liquid, this limitation is due to refractive index anomalies. Also, surfaces with very high angled slopes cannot be resolved as it results in the non-reflection of the white light signal back into the optics. Also surfaces that do not reflect light are fundamentally problematic with this approach.

In this thesis the method will be used to investigate the surface topography of different substratums on which biofilms will subsequently form.

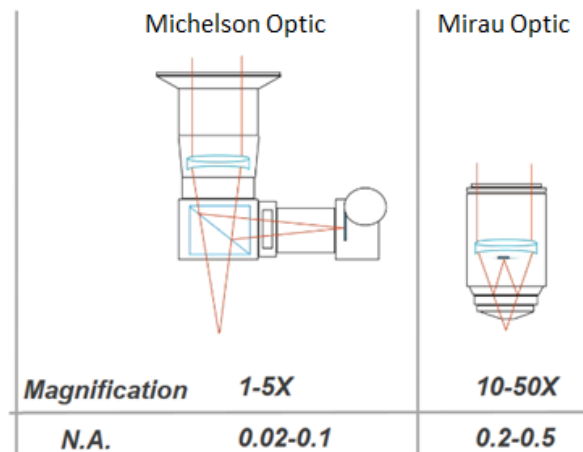|	Michelson Optic	Mirau Optic
Magnification	1-5X	10-50X
N.A.	0.02-0.1	0.2-0.5

Figure 1.43. Diagram of the two different optical methods available on standard WLI, highlighting the different paths/lengths taken by light en-route to the reference surface. The usage of each approach is dependent on the magnification required (Mangolini., 2010).

There are two principle operational modes, the use of which depends on the roughness of the surface under study.

Vertical scanning Interferometry (VSI) uses a broadband light source that can be effectively used for measurement of rough surfaces, differing by as much a 10mm, and giving resolution in the nano meter range. In VSI mode the device scans vertically though the z focal plane and uses data from that scanning to calculate the height of the sample as a function of x and y coordinates (Veeco, 2007).

Phase-shifting Interferometry (PSI) uses a narrow band monochromatic light source (535nm). This method is typically employed on quite smooth surfaces, such as mirrors and polished surfaces that differ by less than 35nm in height and delivers sub nanometer height resolution. The interferometry technique is limited in z height resolution because at greater than $λ/4$ per detector pixel then height ambiguities of multiples of half wavelengths exist (Veeco, 2007, Mike and Joe, 2005). This mode works by mechanically altering the path length, of a fixed standard surface within the instrument when focused on a surface, and analysing the differences in reflected light so that surface topography data is obtained (Veeco, 2007).

This technique has been used before when studying biofilms, for example in examining *Streptococcus mutans* tooth enamel MIC studies where significant changes in surface topography were detected by both the MIC and the presence of biofilm superstructure itself (Cross et al., 2009). However, this method is somewhat limited when investigating biofilms and does not discriminate between biofilm components, but detects only gross surface structural characteristics, for example biofilm height (if you can also image the substrate under the film) and surface topography/roughness.
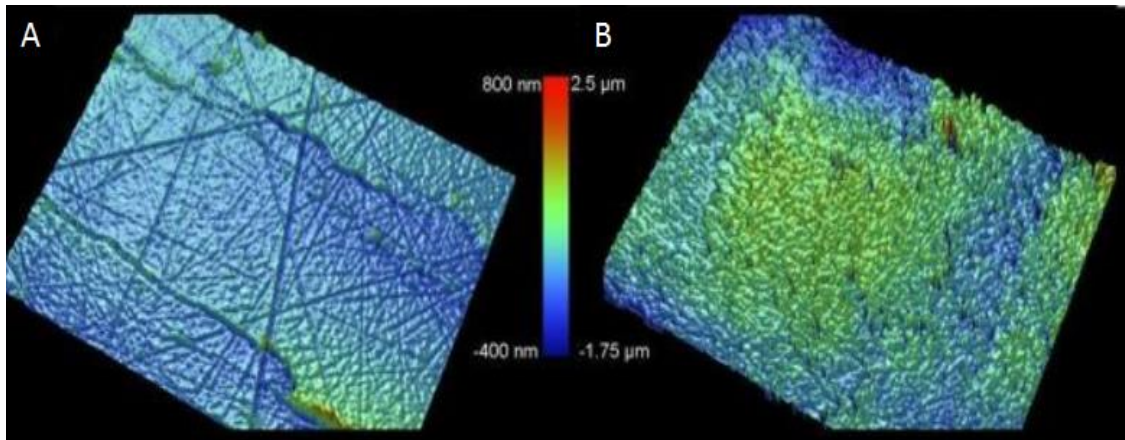
Figure 1.44. Image of the smooth polished enamel surface with and without 72hr old *Streptococcus mutans* biofilm. x y scan dimensions 1200x940µm (Cross et al., 2009).

The above figure is an example of the type of data that could be collected from experiments in this thesis on biofilms, and indeed was the initial technique of choice. Cross and colleagues were able to elicit changes in average surface roughness, and height changes as a result of biofilm establishment (Cross et al., 2009). However, the information set on biofilms reported is very limited in comparison to what can be obtained in confocal laser scanning microscopy studies.

While light interferometry is however excellent at determining the surface topography of different substrate materials, eliciting surface roughness parameters R_a, R_q, R_t, and R_z, which are very useful when investigating interfacial interactions including adhesion. A full description of these parameters is given below.

R_a Parameter

This parameter is typically called the centre line average or the arithmetic average height. The definition of R_a is the average absolute deviation of the roughness irregularities $Z(x)$, from the main line over one sampling length (Gadelmawla et al., 2002).
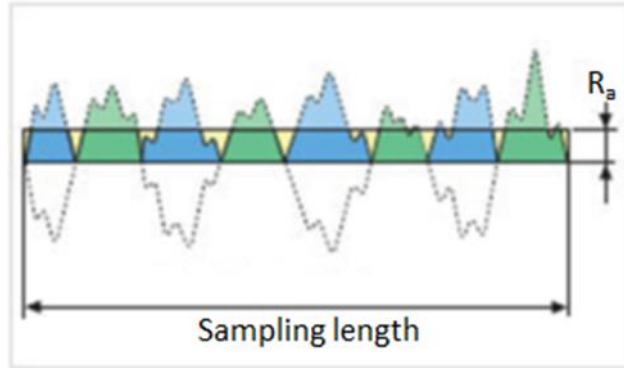
Figure 1.45. Diagrammatic representation of R_a (Olympus, 2016).

$$R_a = \frac{1}{l}\int_o^l Z\,(x)\,dx$$ Eqn. 13

This parameter gives very good overall description of height variations across the sample, but it is not sensitive to small or medium changes in the data (Sedlaček et al., 2009). Large rare features, such as scratches would not drastically influence change in R_a. It is R_a that has typically been used to establish roughness metrics that are for example used for hygiene control and manufacturing standards (EHEDG, 2009, Gadelmawla et al., 2002).

R_q Parameter

Known as the root mean square (or RMS) of $Z_{(x)}$. This parameter is more sensitive than R_a to large deviations from the mean line. The R_q is defined as the standard deviation of the distribution of surface heights R_a (Sedlaček et al., 2009, Gadelmawla et al., 2002).
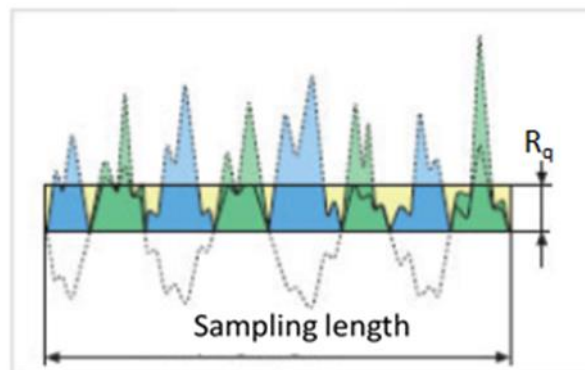

Figure 1.46. Diagrammatic representation of R_q (Olympus, 2016).

$$R_q = \sqrt{\frac{1}{l}\int_o^l Z^2\,(x)\,dx}$$ Eqn. 14

R$_t$ Parameter

R$_t$ is also known as R$_{max}$. This parameter is sensitive to the high peaks of deep scratches for example. R$_t$ is defined as the vertical distance between the highest peak (Z$_p$) and lowest valley (Z$_v$) along the entire assessment length of the profile (Gadelmawla et al., 2002).
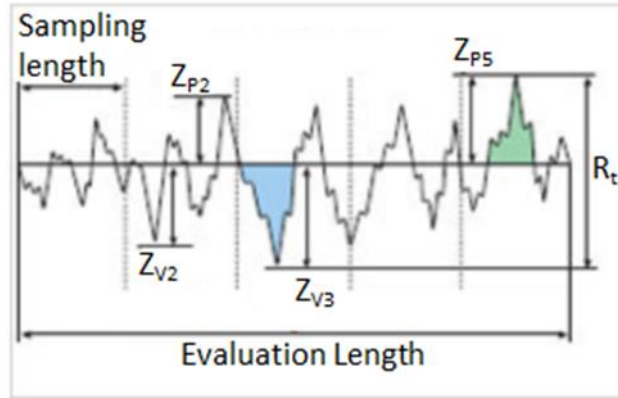

Figure 1.47. Diagrammatic representation of R$_t$ (Olympus, 2016).

$$R_t = \max(Z_{Pi}) + \max(Z_{Vi})$$
<div align="right">Eqn. 15</div>

R$_z$ Parameter

The R$_z$ is the maximum height of topography features in the sample. The R$_z$ is defined as the difference in average height of the ten maximum peak height values from the top ten maximum valley depth values (Olympus, 2016, Gadelmawla et al., 2002, Mitik-Dineva et al., 2009). This metric has been suggested to be important in initial biofilm colonisation of a surface, indeed more important than perhaps R$_a$ (Milledge, 2010).
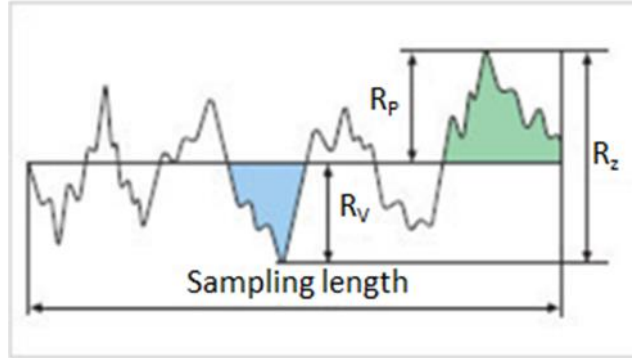
Figure 1.48. Diagrammatic representation of R_z (Olympus, 2016).

$$R_Z = R_P - R_V$$

<div align="right">Eqn. 16</div>

1.34 Introduction to the Quartz Crystal Microbalance (QCM)

The quartz crystal microbalance (QCM) is an acoustic method that detects mass change on a material surface and can detect mass change in the ng range (Dixon, 2008). It has also been widely used to measure film thickness in the nm range (Johannsmann, 2007).

QCM can be used to study the attachment between bacteria (or other cells) and the sensor surface. This technique is both non-destructive and non-disruptive (Zhou et al., 2000). It is widely used in the study adsorption phenomena within solid-liquid interactions but also in solid-vapour interactions. QCM is at its simplest essentially used as a mass sensor. QCM has been used in a wide range of applications from quantifying thin film depositions from a vapour phase (Zhang et al., 2017) to analysing conditioning film deposition and microbial adhesion (Chen et al., 2010).

The quartz crystals are used for their piezoelectric properties (Dixon, 2008), but also they possess high stress limits, high temperature resistance, high rigidity and linearity coupled with low hysteresis and they are typically AT cut due to properties such as low temperature depended frequency shifts around room temperature (Marx, 2006). The quartz is approximately 330μm in thickness and is sandwiched in-between two gold layers, which when an AC current is applied, results in the rapid expansion and contraction (oscillation) of the crystal. The thicker the crystal the lower its fundamental resonance frequency, crystals of approximately 330μm thickness have

a fundamental resonance frequency of about 5MHz, and this is a compromise between frequency (relating to sensitivity) and thickness (relating to usability) (Dixon, 2008).

The principle relationship that arises from QCM use, which correlates changes in oscillation frequency of the piezoelectric crystal with change in mass, is given by the Sauerbrey equation and was formulated in 1959, and describes this relationship (Eqn. 17) (Sauerbrey, 1959)).

$$\Delta m = \frac{C}{n} \Delta f$$
Eqn. 17

The Sauerbrey Eqn. 17 (conventional mass binding) (Olsson et al., 2011) Δm = change in mass, Δf = change in Frequency, n = resonance frequency overtone number (harmonic number) and is multiples of fundamental crystal resonance frequency, C = mass sensitivity constant (~ -56.6 Hz µg/cm^2 for a 5MHz quartz crystal for SRSthinkers crystal, and -17.7ng/cm^{-2} s^{-1} for Q-sense QCM system)

$$C = \frac{T_q\,P_q}{f_0}$$
Eqn. 18

Mass sensitivity constant equation is Eqn. 18 (Dixon, 2008). T_q = thickness of quartz of approximately 330µm, P_q = Density of quartz 2.648g/cm^{-3}, f_0= fundamental resonance frequency in Hz.

The Sauerbrey equation describes conventional mass loading, which assumes that the adhering particle is rigid, has no viscous dissipation properties, and is evenly distributed over the crystal surface. These particles must be relatively small (nm dimensions) when compared to the crystal dimensions (<2% f_0) (Dixon, 2008).

Within the limits of the Sauerbrey equation, the thickness of the deposited material can also be calculated:

$$T_f = \frac{\Delta m}{\rho_f} \qquad\qquad \text{Eqn. 19}$$

Equation 19 is derived from Sauerbray's equation (Eqn. 17) and is used to calculate film thickness in gas phase (Systems, 2010a). P_f is the density of the film material in g/cm^3, T_f is the thickness of the film in cm.

1.34.1 Liquid Adsorption Measurements using QCM

QCM can be readily used in liquids, however the density and viscosity of the liquid in contact with the sensor and greatly impact the resonance and dissipation of the quartz crystal sensors.

Kanazawa's equation (Eqn. 20) is able to predict the change in the resonance frequency of an unloaded crystal in a viscous medium:

$$\Delta f = -f_u^{\frac{3}{2}} \left[(\rho_L n_L) / (\pi \rho_q \mu_q) \right]^{1/2} \qquad\qquad \text{Eqn. 20}$$

This equation shows the influence of the solution properties on the crystal (Eqn. 20) (Systems, 2010a). F_u is the frequency of oscillation of unloaded crystal, P_q is the density of quartz (2.648 g/cm^{-3}) μ_q is the shear modulus of quartz (2.947 x10^{11} g/cm^{-1}s^{-2}) ρ_L is the density of the liquid in contact with the sensor, η_L is the viscosity of the liquid in contact with the sensor.

However, for soft particle layers, for example cells or polymers, dissipation constraints must be included. Dissipation describes the interaction of the adhered particle and sensor surface with the near environment or bulk fluid, and as such, input of kinetic energy from the resonating crystal across to the particle can be greatly dissipated into the bulk environment which reduces or dampens the resonance signal and inferred mass binding result (Fishbane et al., 1996). So in short, thin layers of viscous particles behave differently to stiff particles attached to the quartz crystal.

QCM has been used to analyse the binding of microbes to differing surfaces with some success. However the interpretation of the data can be difficult due to coupled resonance anomalies, where the sensor frequency may actually increase with increasing mass (Marx et al., 2001, Galli Marxer et al., 2003), or conversely increased dampening may occur due to the viscoelastic effects of the

adsorbed film (Olsson et al., 2011). In either case this technique is limited to the near surface range of approximately 250nm (Marx, 2003), or about one bacterial cell layer (monolayer).

The work reported here is on detecting the formation of conditioning films upon different surfaces. However, these same complexities in data interpretation are true for these thin films. To assist in analysing this complexity, Figure 1.48 was used from Zhou et al (Zhou et al., 2000). This paper provided an analysis which allows for the easy determination for whether an adsorbed film is elastic (requiring the Sauerbrey equation) or not (Marx, 2003), with a small deviations being tolerable with films of approximately 200nm thick or less giving an approximately 5 percent error (Lucklum et al., 1999). Some authors reported that a slope of 0.2 (D(R)/F) yielded little change in frequency due to changes in viscosity (Muramatsu et al., 1995).
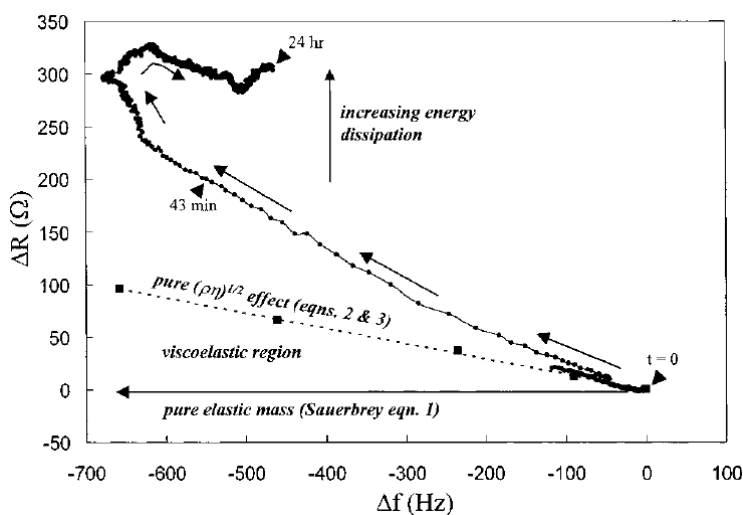

Figure 1.49. Interpreting a ΔR versus Δf plot (Zhou et al., 2000); (Su and Li, 2005, Marx et al., 1999).

Two QCM instruments were used in this project, a QSense E1 and a Stanford Research Systems QCM200. Both record changes in frequency but one monitors dissipation (D) and the other monitors resistance (R), respectively which are equivalent (Zhang et al., 2009).

1.35 Aims of the Study

The overarching aim of this project was to increase understanding of the physiochemical relationship between surfaces and two important stages of the biofilm life cycle; the early initial attachment phase and mature biofilm stage.

This is a multifaceted project requiring surface selection and thin film modification, microbial assay development and validation, and finally the investigative aspects; investigating surface mediated *PA* attachment, mature phenotypic biofilm colony change, and ease of biofilm removal.

<u>Surfaces and Thin Film Modifications</u>

- Source a range of polymer and metal surface materials that are commonly used and representative of a range industrial manufacturing and home applications.
- Develop both rough and smooth variants of each surface material ensuring a wide range of roughness and γ_S values, and also source and confirm thin film modifications that augment γ_S. This will enable the thorough investigation of whether these surface physiochemical metrics influence on biofilm.

<u>Microbial Assay Development</u>

- Develop and validate assays using available tools that allow for an assessment of the early attachment of microbes to a surface that is quick to perform, in situ and non-destructive, and an assay that can assess both biofilm structural morphology (thickness and biomass) and removal of mature biofilm in cleaning 'high shear' experiments.

<u>*PA* Biofilm-Surface Experiments and Recommendations</u>

- Examine the relationship between both surface roughness and γ_S with *PA* early surface attachment.
- Investigate whether there are any *PA* mature biofilm morphological phenotypic differences that can be attributed to differing physiochemical surface metrics.

- Explore the relative ease of mature biofilm removal (cleaning) from different surface materials and examine possible mature biofilm % loss correlations with both surface roughness and γ_S. This will explore whether the biofilm-surface interface (possible weakest link) remains important, even following full surface mature biofilm establishment.

- Investigate the early surface attachment of *PA* on modified (by thin film addition) stainless steel and polymers surfaces, relative to un-modified control to examine γ_S mediated-*PA* early attachment responses.

- Investigate the ease of mature *PA* biofilm removal on modified (by thin film addition) surfaces stainless steel and polymers, relative to un-modified control to examine γ_S mediated-*PA* interface fluid shear responses.

- Make recommendations as to the types of surfaces, modifications or physiochemical metrics that could be used to limit *PA* (microbe) attachment and enhance surface cleaning.

CHAPTER 2 Experimental Methods and Materials Section

2.1. Laboratory Reagents

All of the reagents used in this work were either microbiology, research or analytical grade and were purchased from reputable suppliers.

Water used during all experiments and when making buffers was ultra-pure Milli-Q grade.

2.1.1 Buffer Recipes

Growth Medias

All growth medias and buffers that were required to be sterile for experimentation were autoclaved for 121°C for 15 minutes.

Tryptic Soya Buffer. Supplier: Biomerieux (TSB). Cat no. 42100. Prepared solubilising TSB powder in Milli-Q 25g/l. This is referred to herein as FS-TSB. Final pH was adjusted to 7.3 ± 0.2 at 25°C, using either Hydrogen chloride or sodium as required.

Tryptic Soya Agar (TSA). Suppler: Biomerieux. Cat no. 43019. Prepared by solubilising both TSB powder in Milli-Q 25g/l and agar 15g/l in Milli-Q water. Final pH was adjusted to 7.3 ± 0.2 at 25°C, using either hydrogen chloride or sodium hydroxide as required.

AB Minimal Medium with Glucose Supplement. Prepared to the following concentrations; $(NH_4)_2SO_4$ (15.1 mM), $Na_2HPO_4 \cdot 2H_2O$ (33.7 mM), KH_2PO_4 (22.0 mM), NaCl (0.051 M), $MgCl_2$ (1 mM), $CaCl_2$ (0.1 mM), and trace metals (100 µl/liter). The trace metal solution contained $CaSO_4 \cdot 2H_2O$ (200 mg/liter), $FeSO_4 \cdot 7H_2O$ (200 mg/liter), $MnSO_4 \cdot H_2O$ (20 mg/liter), $CuSO_4 \cdot 5H_2O$ (20 mg/liter), $ZnSO_4 \cdot 7H_2O$ (20 mg/liter), $CoSO_4 \cdot 7H_2O$ (10 mg/liter), $NaMoO_4 \cdot H_2O$, and H_3BO_3 (5 mg/liter). Recipe taken from (Pamp and Tolker-Nielsen, 2007)

2.1.2 Microbes Used

PA BioBall™, NCTC 12924. Supplier: Biomerieux 1.1×10^8 CFU. Lot number B2286, and B2153. ATCC equivalent strain 9027. DSM 1128.

PA14 kindly supplied by Dr Huw Williams, Faculty of Natural Sciences, Department of Life Sciences, Imperial College London.

2.1.3 General Reagents

Bioball™ rehydration liquid. Supplier: Biomerieux. Cat no. 410386.

Saline Solution (Sterile 0.85%). Supplier: Biomerieux Cat no. 44320.

2.1.4 Confocal Reagents and Accessories

Syto®9 green fluorescent nucleic acid probe. Cat no. S34854. Supplier: Life Sciences Solutions, Thermo Fisher Scientific.

SYPRO® orange protein gel stain (5,000X Concentrate in DMSO). Cat no. S6651. Supplier: Life Sciences Solutions, Thermo Fisher Scientific.

Concanavalin A, alexa fluor® 633 conjugate-5mg probe. Cat no. C21402. Supplier: Life Sciences Solutions, Thermo Fisher Scientific.

2.1.5 Substratum Surface Materials

2.1.5.1 CDC Reactor Coupons

Standard CDC coupons were sourced from Biosurface Technologies Corporation. 421 West Griffin Drive, Suite 2, Bozeman, Montana 59715 USA.

304 stainless steel disc coupon. Cat no. RD128-304.

316L stainless steel disc coupon. Cat no. RD128-316.

Polycarbonate disc coupon. Cat no.RD128-PC.

Teflon disc coupon. Cat no. RD128-PTFE.

UHMW polyethylene disc coupon. Cat no. RD128-PE.

Polymer and Metal Sheets Used For In-house Coupon Manufacture

Polymer coupon materials were sourced from Gilbert Curry Industrial Plastics Co Ltd, 16 Bayton Road, Bayton Road Industrial Estate, Exhall, Coventry, CV7 9EJ, United Kingdom. Non Standard Metal Precursor materials were sourced from Orion Alloys Ltd Unit A1, River Way Industrial Estate, River Way Harlow, Essex CM20 2DP, United Kingdom.

Polycarbonate clear lexan exell D sheet 300mm x 300mm x 2mm thick. Gilbert Curry Industrial Plastics Co Ltd.

Natural polyethylene PE300 sheet 1000mm x 2000mm x 1.5mm thick. Gilbert Curry Industrial Plastics Co Ltd.

PTFE virgin sheet 600mm x 600mm x 1.5mm thick. Gilbert Curry Industrial Plastics Co Ltd.

PTFE Sheet 600x600mm x4mm thick. Gilbert Curry Industrial Plastics Co Ltd.

316 stainless sheet 2x1m mirror polish on one side, Orion Alloys Ltd.

304 stainless sheet 2x1m mirror polish on one side, Orion Alloys Ltd.

2.1.6 Novel substratums and Thin-Films and Abrasives

NIL Technology Substratum NILT2609 LMT 12/1-2016, polyproplyene with MLA+BS. Nano patterning and nano imprint lithography. Kindly supplied by Kevin Wright (P&G).

Sharklet™ poly(dimethylsiloxane) film. Kindly supplied by Eric Pathe (Sharklet™ Technologies, inc, USA).

Domino Encapulate AbilSilWet L77- Domino Encapsulate, was kindly supplied by Kevin Wright (P&G).

2.1.7 Sandblasting Glass Bead Abrasive

Glass bead abrasive. Supplier: Machinemart.co.uk. Product Code 000332095. Manufacturer sku 3052095. Particle size 200-300μm particle size. https://www.machinemart.co.uk/p/20kg-glass-bead-abrasive/.

Silica powder abrasive. Supplied by Kevin Wright (P&G). Zeodent® 119HY. RO-003. 11000015.

2.2. Streak Plating of Microbial Cultures

This standard method was used to obtain a pure culture sample from a mixed culture or isolate a single CFU. A nutrient growth agar relevant to the microorganism of interest was prepared. A 5µl inoculation loop was inserted into the culture of interest and streaked onto the sterile agar plate up to 10 times in a small area of the agar plate. The agar plate was then turn 90º, and approximately two of the preceding streaks were streaked into a new area of the plate. This was repeated several times finishing in the centre of the agar plate.
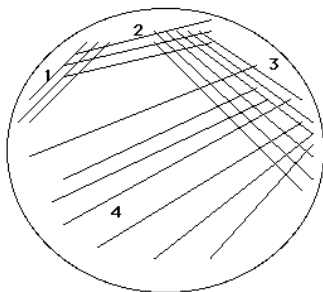
Figure 2.1. Diagram of plate streaking. Numbers indicate starting point (1) and end point (4).

After streaking was completed the inoculated plates were incubated at 37ºC overnight. Individual colonies were then taken and further processed as required.

2.3. Spread Plating of Microorganisms

This microbial method is used for the quantitative determination of a culture, yielding the number of CFUs in the culture being tested. A series of 10 fold dilutions of the test microorganisms were prepared using sterile buffers. Dilutions could either be carried out in PBS or in sterile media relevant to the microorganism understudy. 10µl of each dilution was pipetted onto prepared agar plates and performed in triplicates. Using a fresh sterile L-shaped spreader each time the inoculum was spread evenly over the agar plates in sterile conditions. The inoculated agar plates

were then incubated at 37ºC overnight. Colonies were then counted, and the numbers of CFU were calculated per millilitre.

2.4. Gram staining

Gram staining is a biochemical procedure used to identify whether a bacterial cell is one of two predominant structural types. A bacterial cell wall possessing sufficient peptidoglycan to retain the crystal violet dye stains gram positive, whereas those that do retain crystal violet are gram negative.

A 5µl sterile loop of bacteria was spread on a slide and heat fixed carefully using a Bunsen burner (It was important not to burn the sample but simply to dry it). The sample slide was flooded with crystal violet for 1 minute, when rinsed with distilled water. The sample slide was then flooded with iodine for 1 minute then rinsed with distilled water. Decolouriser was then applied (alcohol) for 5-10 seconds then rinsed with distilled water. Safranin counter stain was then applied for 1 minute and then rinsed off with distilled water. The sample was then viewed under the microscope.

2.5. Modifying Substratums via Sand Blasting

Sand blasting was used to create standard surface roughnesses across the entire set of test materials under investigation. Sandblasting was also used to create a metal template for use in moulding the polymer surfaces.

Sandblasting work was carried out using a Clarke SB30 sandblasting cabinet (MachineMart.co.uk; product code 051710065), using 200-300µm glass bead abrasive. The nozzle of the sandblaster was moved across the surface of the sample first horizontally and then vertically 3 times each to provide a visually even surface finish.

When sandblasting metal surfaces it was observed that the metal would deform in a convex manner, making it unusable. To counter this, the reverse side of the metal sheet was sandblasted, which then corrected this abnormality. Following this surface treatment the substratum samples were then analysed using white light interferometry and/or contact angle analysis as required.

2.6. Compression Re-Moulding of CDC Reactor Coupons

316 stainless steel metal templates were pre-sand blasted to achieve a standard increased surface roughness (R_a). These samples were then used to remodel the polymer surface topography of the CDC coupons in a heated press under appropriate temperature and pressure. This transfer process was designed to achieve more consistent roughness across polymer and metal substrates tested.

All moulding experiments were carried out at room temperature using a platen press and special coupon mould. A roughened 316 stainless steel was loaded into a platen press, and the polymer coupon of interest was placed on top. A second post sandblasted 316 stainless steel metal sheet was then placed on top, and the pressure increased to the desired level for the time required.

If a polymer exhibited viscoelastic flow under pressure then the CDC coupon dimensions would change during the unconstrained pressing process. To avoid this, a specially designed and engineered mould was used to hold the CDC coupons. This would allow polymer compression to occur without change in overall coupon dimensions, especially diameter. The CDC experimental coupons are typically 12.5-13.0mm in diameter, 3.7mm thick and disc shaped. The mould was a small sheet of 316 stainless steel with two 13.00mm holes- see Figure 1.2. The mould was 3.2mm thick, allowing 0.5mm of the external polymer coupon to be proud of the mould surface, and thus allow compression.

Figure 2.2. Coupon mould designed to allow compression of CDC coupons. Dimensions 3.2mm thick, holes are 13.00mm in diameter.

When using the mould, two polymer coupons were inserted into each coupon holder hole. The device was inserted in between two roughened stainless steel sheet templates, and then

compressed for the desired pressure and time. Following coupon surface remodelling, coupon sizes were checked to confirm that they fit into the standard coupon holder used in the CDC reactor.

2.7. PTFE-AF Coated 316 Stainless Steel Smooth Coupons

PTFE-AF thin film coatings on 316-SC coupons were made using a dip coating method. A 1% w/v solution of PTFE-AF, in Fluorinert® FC-40 perfluorinated solvent (3M), was prepared by dissolving the solute for a period of 7 days at room temperature in a clean glass beaker (Chemours-Company, 2016b). Using tweezers freshly cleaned 316-SC coupons were lowered into the PTFE-AF solution for 3 seconds, and then withdrawn. The coupons were then placed into an oven, edge on (perpendicular), and allowed to dry 100°C for 2 hours. Coupons were then ready to use.

2.8. Abil "SilWet" L77 Coated 316 Stainless Steel Smooth Coupons

Abil SilWet thin films were prepared by dipping (perpendicular using tweezers) the 316-SC coupons into freshly prepared 10%w/v solution in water, for 5 seconds. This dipping was followed by a 3 times dip rinse in sterile water. It was then ready for immediately use. For a dry prepared Silwet coated surface, the freshly dipped Silwet 316-SC coupon was placed in an oven to dry overnight at 32.5°C and was then ready for testing.

2.9. Gold Sputter Coating of Coupons

Gold sputter coating is a common method used to gold coats samples for SEM analysis. Gold is electrically conducting and so its deposition is essential to visualize biological samples, or non-conducting surfaces. The equipment used here was a Quorum K550 sputter coater using argon gas. Sputtering works by bombarding a target, in this instance a gold surface with ionised argon, the gold then migrates towards the specimen surface of interest via a plasma.
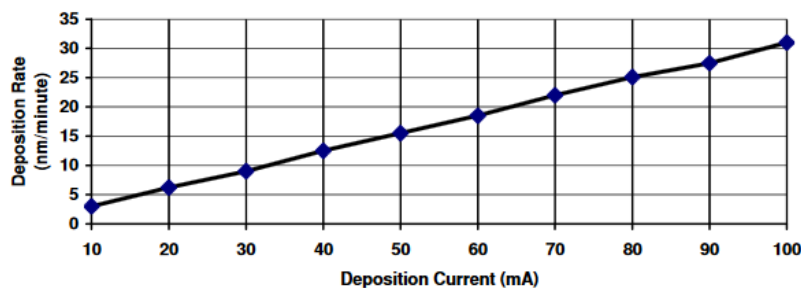
Figure 2.3. The deposition current versus gold deposition rate in nm per minute (Emitech, 2007)

The gold thin film thickness can be controlled by varying either the deposition current and/or the total time for sample coated. For all samples coated in this thesis a deposition time of 3 minutes and currently of 30mA was selected, which give a film thickness of approximately 30nm.

2.10. Culturing *PA* in Novel Flow Cell (FC)

The flow cell described here was manufactured as described in Chapter 4. All FC growth stages were carried out at room temperature (15≥25°C), or 37°C, as indicated. The principle FC growth medium was either LB growth medium or AB minimal medium as indicated.

2.10.1.   Flow Cell Preparation, Use and Harvesting

The surface topography of the coupon of interest was determined using WLI prior to experimentation. The FC was assembled and orientated with the inlet lower than the outlet, to aid in air removal. Sterilisation was achieved by flowing 70% ethanol through the FC at 200μl/min for 10 minutes. This was followed by sterile water and sterile LB growth medium for 10 minutes at 200μl/min. 50μl of master cell bank (PA01) was inoculated into a 20ml LB medium sterile universal and incubated for approximately 4 hours until the OD@600nm was 0.6 ±0.2, whereupon the inoculum was passed though the FC at 200μl/min. This was then followed by either AB minimal medium or LB, as per experiment. Inlet media bottles where changes when needed. Harvesting (removal of medium) was carried out by inverting the FC and pumping air into the system at 50 μl/min, to minimise colony disruption. FC was then dismantled and surface imaged using an appropriate method.

2.11. Quartz Crystal Microbalance - QSense E1

All QSense experiments were conducted using a flow cell window module (QSense QWM 401), following the manufacturers operating instructions using a 200µl/min flowrate at 20°C, with degassed solutions, for both test and running buffers. Results were imported into Microsoft Excel for analysis.

2.12. Contact Angle Analysis using Krüss Easy Drop

Contact angle measurement is a technique that can allow the determination of the surface energy of solid substrates. The Krüss Easy Drop instrument uses a video camera to measure the contact angle through a droplet of liquid placed the surface of interest. A larger contact angle would indicate a greater degree of hydrophobicity using water as the probe. The contact angle of a surface is very sensitive to contamination, and thus it can be used as a measure of estimating surface cleanliness.

There are many ways to measure the contact angle, and the commonly used advancing contract angle method is described here.

A Gilmont micrometre syringe was used to control the flow of the probe liquid of interest to form a droplet onto the surface under study. Different syringes were only used for specific liquid probes to prevent cross contamination. The appropriate syringe was secured in place above the sample stage, aligning the needle centre of the camera view.

The substratum sample was then placed onto the measurement stage, and a single drop of probe placed on the test sample. The probe droplet was then brought into view and focused using the manual camera adjusters, ensuring the edges of the droplet was clearly visible. The light source brightness was adjusted so that the droplet appears dark, relative to the background- see Figure 2.4. This contrast is important as it allows the software to detect the droplet edges for contact angle determination via a fit of Laplace's equation to the drop shape. The limits of the droplet detection window were also set, i.e. substratum surface and upper droplet size limit see Figure 2.4.
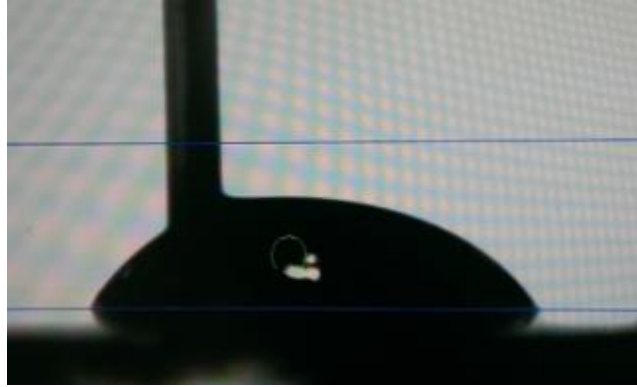
Figure 2.4. Image of diiodomethane (DIM) on a polycarbonate surface. Contrast between droplet and background for software detection purposes is emphasised, and droplet detection window is shown by the horizontal blue lines.

The syringe needle was placed into the centre of liquid probe and the drop volume was increases so as to create an advancing contact angle. The computer software was set to take a contact angle reading every second for fifteen seconds or as required. Data was then copied into Microsoft Excel for analysis.

2.13. White Light Interferometer - Wyko NT9100

White light interferometer is an optical method for measuring different topographical variables of different surfaces, and ultimately works by comparing white light that has been split in two, and then recombined, following, reflectance from a flat (known) reference surface and reflectance from the sample (unknown) surface. This recombined light is then analysed, yielding topographical information about the sample surface.

Before operating the interferometer the sample stage level was calibrated; this was performed as per manufactures instructions. This step is important as if the sample is not level the surface topography will appear at an angle too.

To operate the Interferometer, the sample was placed onto the sample staging area. Either PSI or VSI mode was selected depending on the nature of the sample. The light intensity was adjusted, to ensure that no red (over exposure) was occurring, but that the surface is clearly visible.

In PSI mode, the scan was performed once the fringes were located, however in VSI mode a back-scan was required, that covered the focal depths (sample height) within the field of view. The back scan setting was found by locating the initial fringes of the sample, then by adjusting the height of the focal plane, to the point at which the last fringes were seen in the intensity view. The difference between the z parameters of the two positions +20µm was the back-scan limit.

The scan was then performed and the data analysed with tilt correction selected using the manufactures software to correct any tilt error.

2.14. The CDC Reactor

A CDC reactor (Biosurfaces Technologies Corp, cat no CBR90) is a small (approximately 400ml working volume) bench-top chemostat based system used to culture biofilms. Eight coupon mounting rods protrude into the growth chamber, each of which can hold three coupons, giving a total of 24 sampling opportunities. Each coupon is 12.7mm in diameter and 3.0 mm thick. The internal environment is maintained by the addition of a continuous volume of fresh growth media into the vessel, with spent media being constantly removed. The system is typically used by experimentalists looking to work with bioreactors in high shear environments.

2.14.1.   CDC Reactor Method / Protocol

The glass CDC bioreactor vessel, head plate and coupon holders were cleaned with laboratory detergent (Micro90 detergent, Sigma Aldrich Z281565), and rinsed with milliQ water, and assembled according to the manufactures instructions. 350ml 10%v/v TSB media was prepared and put into the CDC reactor ready for autoclaving, and coupon addition. All substratum coupons were cleaned prior to experimentation by boiling in 5%v/v Tween 80 for 30 minutes, they were then rinsed in milliQ water until bubbles are no longer present. Coupons were then placed into 70%v/v ethanol solution for 1 hr. Coupons were secured into the coupon holders ready for sterilisation by autoclave. Following the complete assembly to the reactor according to manufactures instructions, the media inlet and outlets were clamped, and the ends of the tubing wrapped in tinfoil. The entire apparatus was then placed into an autoclave bag, complete with secured coupons and autoclaved for 20 minutes at 121°C. The CDC reactor was placed into a class 2 cabinet and the autoclave bag was removed. The *PA* Bioball^{TM} was re-suspended in 150µl rehydration fluid, and then injected into the reactor, which was then placed into the incubator (32.5°C). The stirrer was set to '1', equating to 174rpm ±10. The system was then left overnight

in batch mode. Typically samples (batch samples) were taken on the second day, following overnight running, for early stage biofilm formation assessment. Additional mature biofilm samples were taken on day 4 post inoculation. Coupons once analysed were first autoclaved at 125°C for 15 minutes, and then scrubbed using a soft sponge, before storing.

2.15. Growth and Analysis Biofilm Using Novel Flow Cell

The surface topography of the coupon substratums was determined using WLI prior to experimentation, using method in Chapter 2.16. All FC biofilm cultures were carried at room temperature (15≥25°C).

50μl of master cell bank (PA01) was inoculated into a 20ml LB medium sterile universal and incubated for approximately 4 hours until the OD@600nm was 0.6 ±0.2, whereupon the inoculum was passed though the FC at 200μl/min, this was then followed by either AB minimal medium or LB, as per experiment.

Prior to sample harvesting, a fresh 4%v/v formaldehyde solution was prepared in PBS pH adjusted to 6.9 (Bacallao et al., 1995). Flow was maintained for a period of 1hr at 0.2ml/min, and then left over night (16hr) to fix the biofilm samples. PBS was then injected to remove the formaldehyde. Harvesting (removal of medium) was carried out by inverting the FC and pumping air into the system at 50μl/min, to minimise colony disruption. A flow was stopped and the sample inlet and outlets capped. The flow cells were then double sealed and transported and dismantled for imaging.

2.16. Confocal Microscopy Methods

2.16.1.   Mature Biofilms

Biofilm Sample Preparation
Following the careful removal of the biofilm coupons from the CDC reactor, the samples were placed with the biofilm sample surface facing up, in a pre-labelled petri-dish. Loosely bound or non-attached biofilm was then immediately removed via a rinse step; 1ml of sterile water was carefully pipetted onto the biofilms containing coupons and allowed to run off into the dishes. Residual water was then removed by dabbing the edge of the coupon with a tissue.

Stain Method 1

The first of two probes (10µM Syto®9) was carefully pipetted (250µl) onto the biofilm and then incubated at room temperature for 20 minutes in the dark, which minimises photo-bleaching effects. The probe was then carefully removed by dabbing on the side of the coupon with tissue paper, and the rinse step was repeated. The second probe, (150µg/ml ConA, or 2x Sypro®) was then added, and incubated as previously described above. The samples were rinsed in sterile water as stated above and then stored for a maximum of 6 hours in the dark, ready for analysis (see Figure 2.5 for overview).

Stain Method 2

All three probes to be used were prepared in PBS (Syto®9 10µm/ml, ConA150µg/ml, Sypro® 2x final). 250µl was pipetted onto each coupon and left a period of 30 minutes in the dark at room temperature. Probe was then rinsed off as described above, prior to confocal scanning.
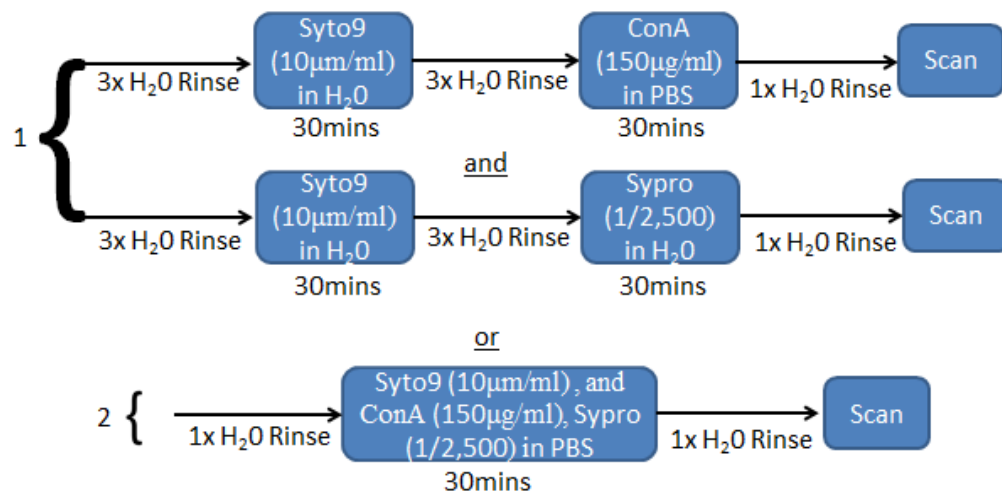
Figure 2.5. Confocal probe staining procedure, including staining steps and probe concentrations. Probe staining protocol 1 was carried out on the confocal microscope TCS SP2. Probe staining protocol 2 was used on works carried out on the TCS SP8 confocal microscope.

2.16.2.　　　Microbe Initial Attachment Assay Method

Sample Preparation and Incubation

Coupons to be tested were cleaned as per Chapter 2.17.2, immediately prior to use, and placed into sterile petri dishes. 200µl of inoculum (pre-diluted to OD=0.2 @600nm and 20%v/v TSB final) was pipetted onto each test substratum and incubated in the sealed petri dish for the desired period. Following the attachment incubation, unbound cells were removed by dipping each coupon into three consecutive sterile tubes of water using tweezers, ensuring the coupons were perpendicular to the water wash during submersion. The coupons were then placed into fresh petri dishes ready for staining.

Stain Method

Pre-prepared Syto®9 stain (200µl 1/1000 final dilution in water) was carefully pipetted onto the coupons and incubated for a period of 30 minutes at room temperature in the dark. Samples were then ready for imaging using the TCS SP8 confocal microscope.

2.17. Confocal Microscope Setup

Two confocal microscopes were used during this investigation, a Leica TCS SP2, and a Leica TCS SP8 confocal laser scanning microscope.

2.17.1.　　　Leica TCS SP2 and SP8 Setup

Leica TCS SP2/SP8 was setup according to manufactures instructions. The instrument was turned on at least 30 minutes before readings were taken to allow the lasers and detectors to reach operating temperature. The Leica control software was loaded, and the appropriate lens selected both physically and in the software, the lens was typically 63x or 10x (or 25x for SP8) water emersion lens. The lasers required for the experiment were then selected. The surface was visualised and brought into focus using the manual optics and the z height for the start of the scan was then inputted into the software. This was repeated for the top of the biofilm, but using the fluorescence signal detected from the outer surface of the biofilm as imaged on the confocal microscope computer.

During experiments when a 63x lens was used a pinhole setting of 1.0AU was selected, and for all 10x magnification experiments a pinhole of 0.5AU was used. A resolution of 512x512 pixels

per inch was used. z scan step height was also typically set to 1µm. The typical lens used on the SP8 was the 25x water immersion lens, using with a dz of 1.0µm

Once the data was collected, it was downloaded and processed using *Comstat 2.1*. See Chapter 1.31.

CHAPTER 3 Novel Flow Cells and Initial Biofilm Experiments

A flow cell was required for the biofilm growth work. This requirement came about because of the need to be able to use different surface substrates i.e. polymer and metals that had been pre-treated. The system available to the project in the beginning, the Bioflux™ 1000, was limited in that only a single polymer surface could be tested (as supplied by the manufacturer); this was of limited use. Therefore, new flow cells were manufactured using a CNC machine.

The brief for the flow cell was the following:

- Flexibility to control the fluid flow regimes i.e. change between laminar or turbulent flow.
- Easy to clean, and chemically stable.
- Allow easy access to the biofilms contained within, with the possibility of in-situ microscopy.

All flow cells were all made from brass which is relatively chemical inert, and stiff, which would enable sufficient tightening of the screws to allow the gasket to form a tight seal.

The flow chamber in all the flow cells was formed by cutting away a section of a gasket (1mm thick) to form a channel. This way flow cells of different dimensions could be readily obtained, making the system highly adaptable.

3.1 Flow Cell Version 1

In this early version the single gasket has dual purpose; it creates the flow cell channel, but also seals around the glass window and surface substrate. Glass windows are present on both top and bottom, which sit into small recesses that present both glass slides to the gasket to enable a good seal to be formed.
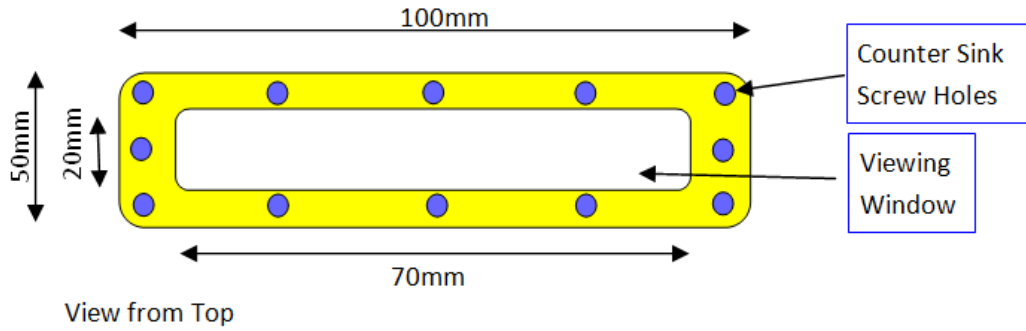
Figure 3.1. Version 1 of the flow cell-plan view.
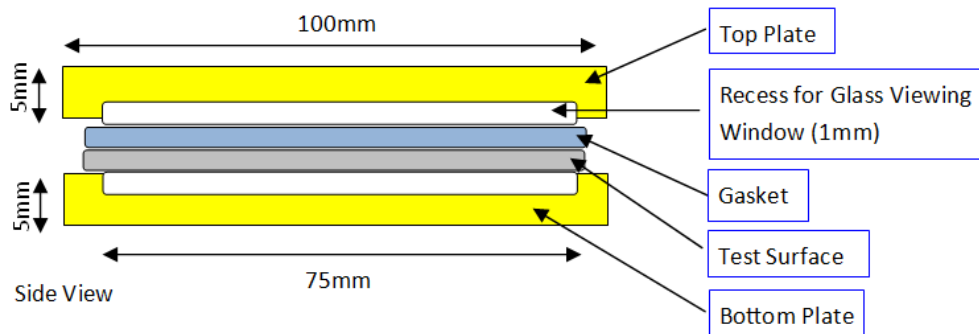
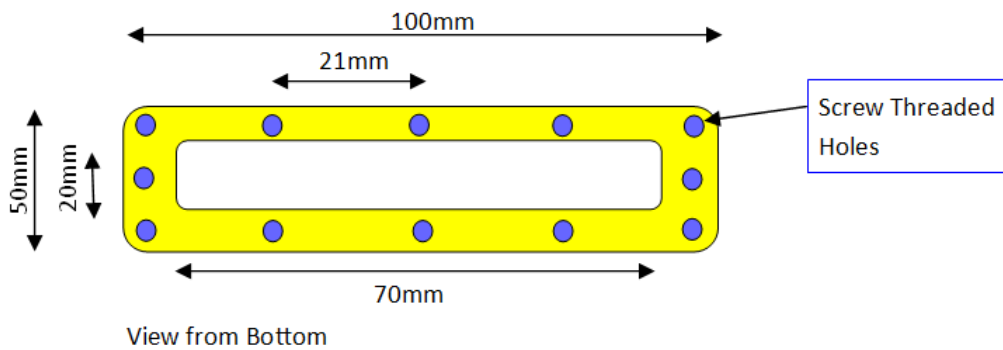Figure 3.2. Version 1 of flow cell – side elevation.
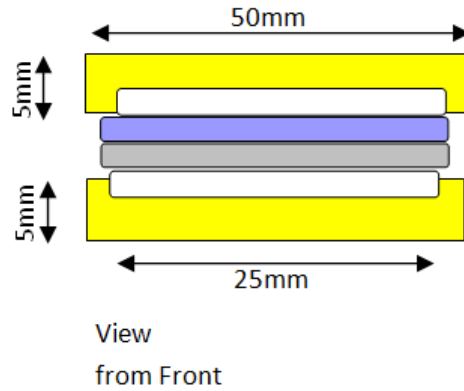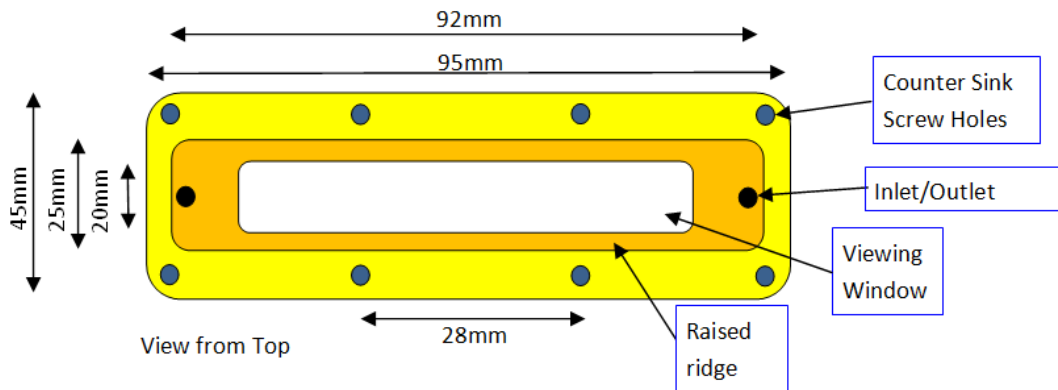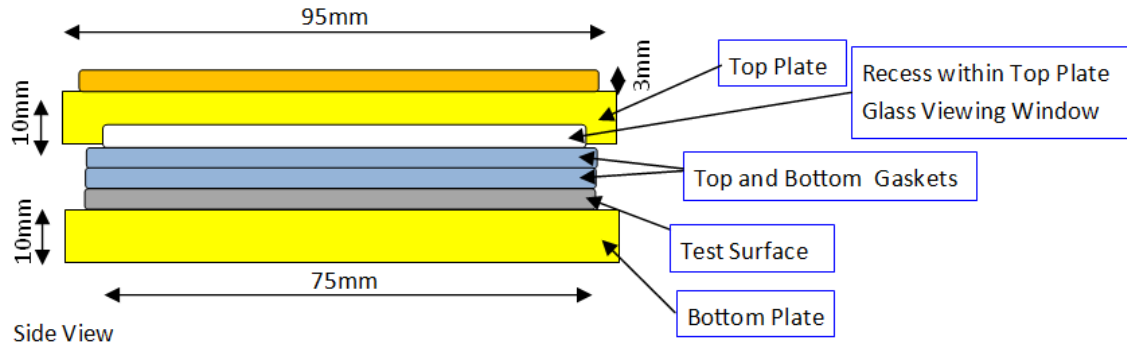

Figure 3.3. Version 1 of flow cell- bottom view.

Figure 3.4. Version 1 of flow cell. Viewed from the front.

Figure 3.5. Photo of Version 1 of flow cell.

During the test stage of this first generation flow cell, introducing and removing the test reagents was carried out using two syringe needles. These were used to piece the outer part of the gasket at either end of the flow cell. This enabled the flow of fluids from the 'inlet' through the preformed flow channel and out through the 'outlet'. This turned out to be rather difficult to carry out, due to lack of visibility. Furthermore, once the needles were inserted persistent leaking was detected, from both windows (top and bottom). Furthermore, upon tightening down the screws to address the leaking the windows, a window would often fail. Also the use of needles when working with microbes is not recommended due to safety considerations, and using needles would in introduce inter flow cell variability. To address these challenges, a second generation flow cell was commissioned.

3.2   Flow Cell Version 2

In this second generation flow cell, a fixed sample inlet and outlet were added to aid sample delivery, and reduce system variability. The fitting were made compatible with luer fittings (typically found on FPLC systems), and a double gasket system was used to help prevent leakages, and deliver and remove fluid under flow. A larger recess for the glass viewing window was cut into the top plate only to reduce pressure on the glass whilst enhancing the seal, but to also simplify the gasket design to be used in this system. The bottom plate was filled in (window removed), as gross flow cell transparency was not required, and its presence introduced a higher chance of leaking. Due to rigidity of the brass construction material the numbers of securing screws was reduced from 12 to 8. Flow of fluid passes through the inlet tube, down into the leur fitting and through a hole cut into the top gasket, down into the second, lower gasket were the fluid flows along the channel and then the reverse out of the outlet.

A raised ridge was placed upon the top plate so allow for the length of the plastic leur fittings.

Figure 3.6. Version 2 of flow cell-plan view.

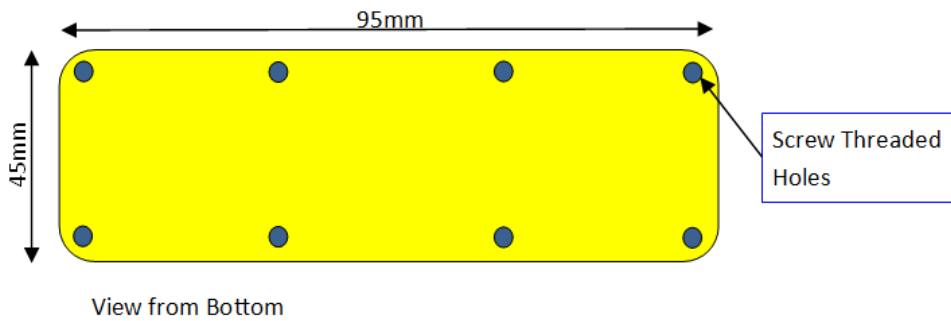Figure 3.7. Version 2 of flow cell –elevation view.
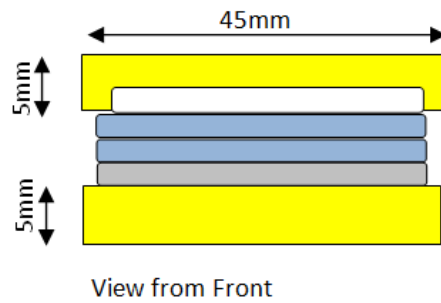

Figure 3.8. Version 2 of flow cell- bottom view.

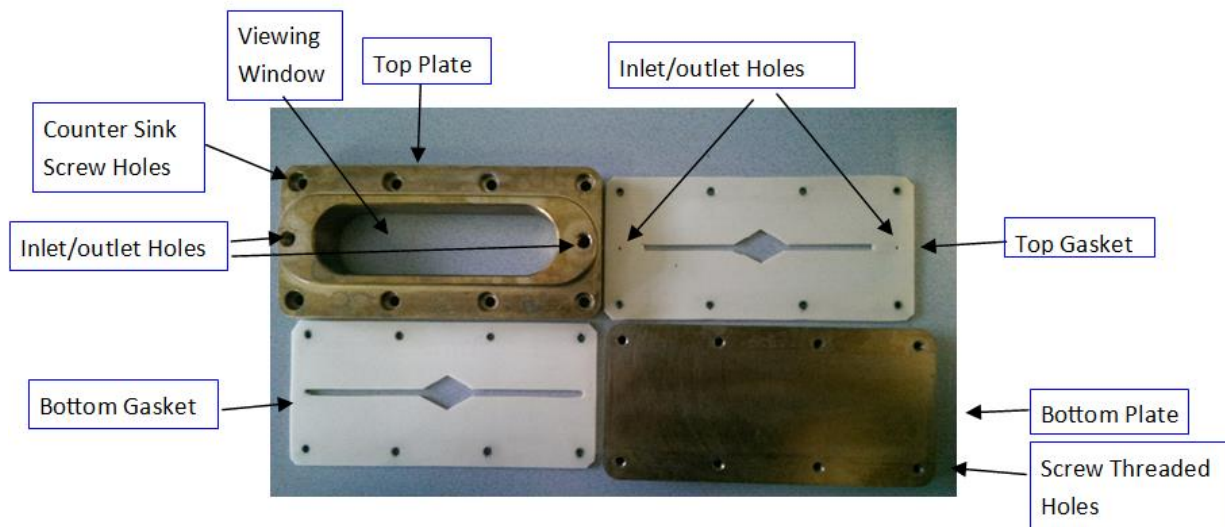Figure 3.9. Version 2 of flow cell-front view.

131

Figure 3.10. Photos of Version 2 of flow cell.

This second generation flow cell was supposed to address the problems of sample delivery and removal across the flow cell but also to fix the leaks detected at the windows of flow cell version one. Some leaking between the two gaskets was evident, and it was difficult to get fluid flow from the inlet to the outlet visually. A great many leaks were also apparent. Also, the breaking of the glass window still remained a consistent problem. Delivery of the media into the flow cell was also a problem, due to constriction due to deformation of the channels when under pressure. This was likely due to the compression required to seal the system being too great.

3.3   Flow Cell Version 3

This version of the flow cell was the final iteration. This final version successfully addressed the leaking and glass window stress (breaking) problems. Firstly the size of the viewing window was reduced (from 75x20mm to 53x12mm), and the inlet-outlet sample delivery system was changed again. This time samples were delivered through the side of the bottom plate and then up into the flow cell gasket chamber, which was sealed with an O ring. Due to the viewing window becoming smaller, coupled with the thickness of the top plate; a chamfer (45º) was introduced. This would ensure that the glass window was adequately supported, and would allow for access for microscope optics should they be required.
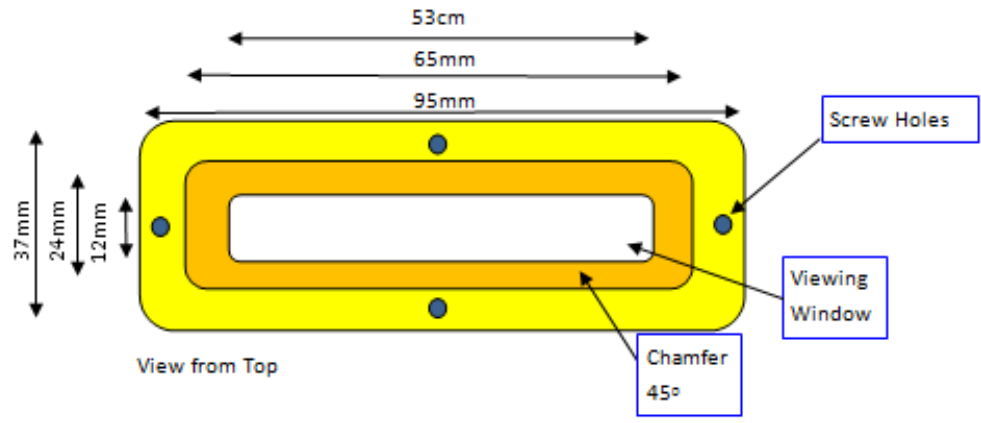
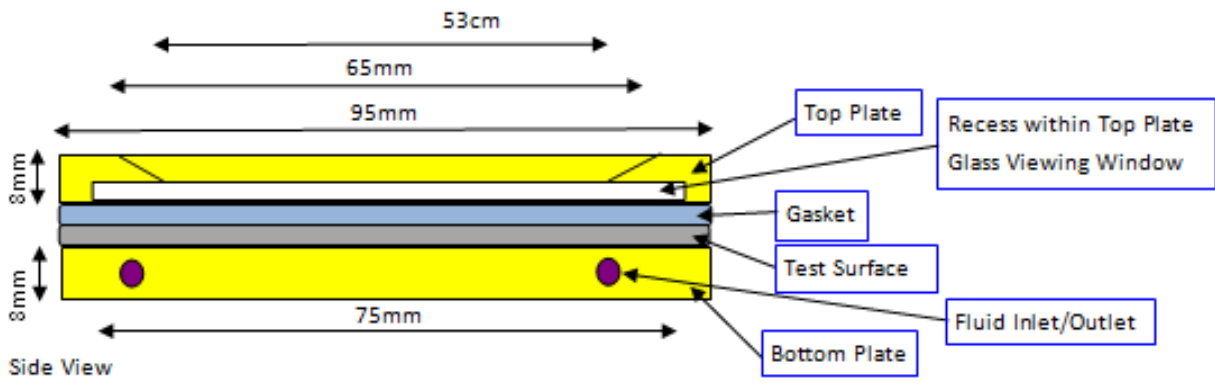**Figure 3.11 Version 3 of flow cell-plan view.**
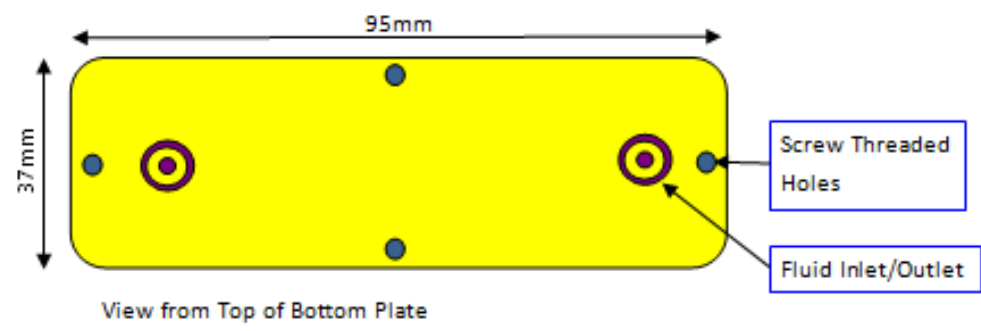

Figure 3.12. Version 3 of flow cell –side view.
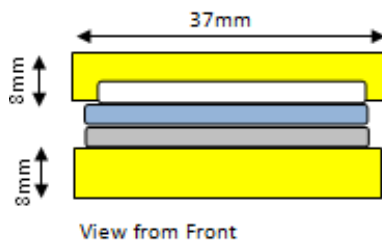

Figure 3.13. Version 3 of flow cell-bottom view.

37mm

8mm

8mm

View from Front

Figure 3.14. Version 3 of flow cell-front view.

Top Plate

Viewing Window

Chamfer 45°

Screw Holes

Screw Threaded Holes

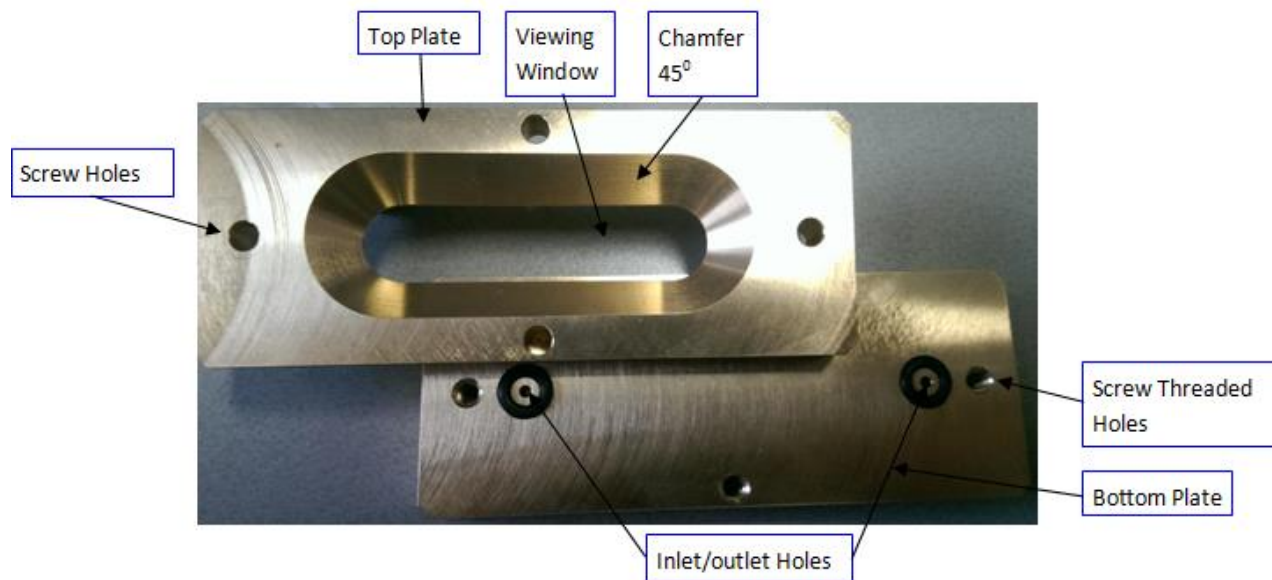Bottom Plate

Inlet/outlet Holes

Figure 3.15. Photo of Version 3 of flow cell.

3.4 Initial Biofilm Growth Experiments using Novel Flow Cell

These initial biofilm growth experiments were to establish suitable procedures and techniques for the growth and harvest of the resultant microbial colonies intact for analysis using the novel flow cell. Two different media formations were tested (AB minimum and LB), at two different temperatures. During initial experiments it became apparent that experimental throughput would be a problem, with not enough replicates being able to be produced in a short time. Also, the flow cell gasket configuration resulted in the inlet and outlet channels being rapidly blocked by biofilm (Figure 3.16), which reduced flow and thus any predicted fluid flow field parameters, and is likely a problem in all microfluidic flow cells used in biofilm culturing experiments.

Figure 3.16. Picture of a smooth 304 stainless steel substratum with PA01 cultured for 2 days in AB minimum growth medium at room temperature. Points of interest are the microbes appearing to be growing well in the inlet and outlet area of the flow cell.

An example of a biofilm grown in the final flow cell iteration using WLI is shown below for reference.
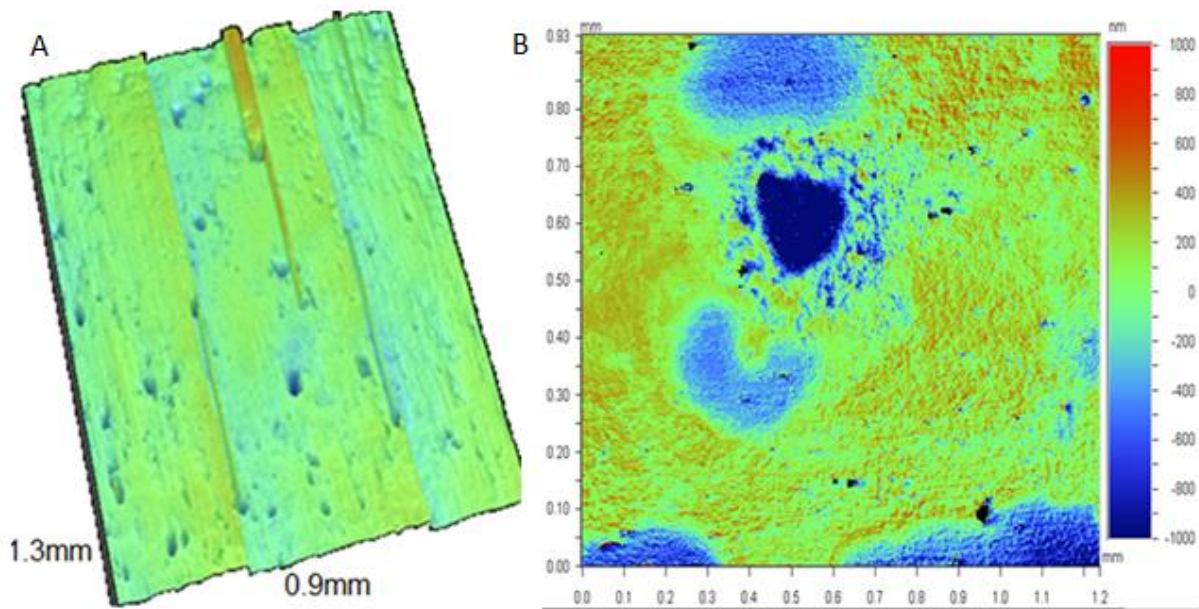
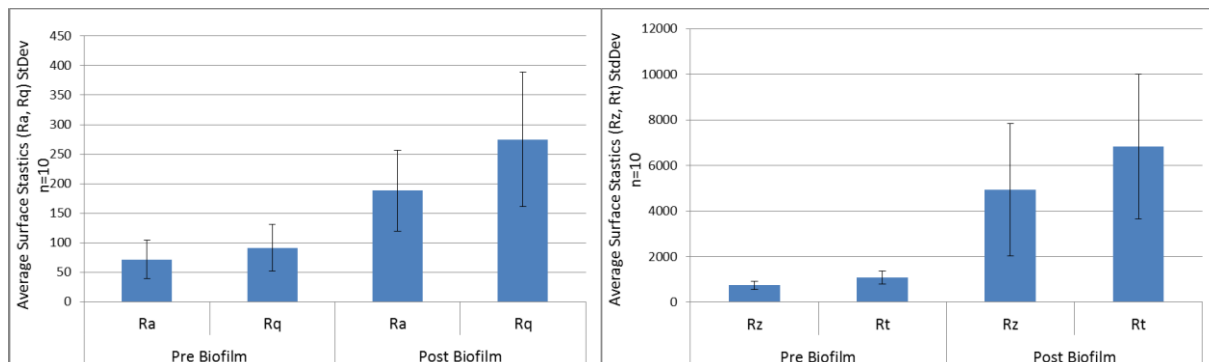Figure 3.17. WLI images of 304, pre (A) and post (B) 2 day PA01 biofilm growth. Images using 5xmag VSI.

Figure 3.18. Roughness data obtained pre and post 2 day biofilm growth on 304 stainless steel.

In addition to the above issues with the flow cell, the use of WLI for the analysis of the biofilms did not produce rich datasets as only roughness parameters could be obtained. However, upon examination of both the WLI image data and the calculated roughness parameters (Figure 3.17 and Figure 3.18 respectively) increases in surface roughness (biofilm + substratum vs substratum

136

only) could be detected, and is statistically significant with both the R_t and R_z metrics. Similar observations have been made by other authors (Cross et al., 2009), discussed in Section 1.33 and is visually apparent in Figure 1.44.

It was possible to potentially ascertain the maximum gross height of some of the biofilms if small scratches were to be imposed upon them as a substrate reference marker. However, even this metric would have been open to significant operator bias, and was not scientifically robust. With these comments in mind, confocal microscopy was selected as a more useful biofilm quantification tool.

3.5   Conclusion

In conclusion the use of microfluidic flow cells of the nature developed here, would not be able to produce the numbers of replicates required within acceptable time scales. Coupled to this, the challenge of reducing biofilm growth within the flow cell inlet and outlet (seen in Figure 3.16) that interferes with fluid flow rates and dynamics remains.

A possible fourth flow cell iteration that would result in increasing the numbers of experimental replicates of the flow cells is to create a hybrid system that takes the best of the Bioflux® 1000 and the best of the flow cells developed here. One could imagine a single multi flow cell system that looks similar to that of the Bioflux® system that incorporates upto 24 flow cells, but that would allow interchangeable/customisable surfaces and gaskets (as used here) allowing for substratum modification and fluid flow manipulation.

The use of white light interferometry in analysing biofilm produces only surface biofilm/substratum roughness data that does not relate the biofilm to the substratum in a reproducible, meaningful way, for example if a biofilm where to completely cover a substratum, and thus confocal microcopy, which overcomes this challenge will be used in future experiments.

CHAPTER 4 Substratum Surface Characterisation and Preparation

Coupons were sourced from three suppliers, Biosurface Technologies, Gilbert Curry Industries, and Orion Alloys. All coupons were initially sourced from Biosurface Technologies (the CDC reactor manufacturer), but following surface roughness determination using WLI, the variability across individual and different coupons was too great. Raw substratum materials were sourced from Gilbert Curry Industries (polymers) and Orion Alloys Ltd (steels) as detailed in Section 2.1.5.2, to facilitate in-house coupon fabrication.

The objective was to obtain and engineer a range of materials that possessed differing roughness's and surface energies, either in their virgin state or following thin film surface modification.

The substratum materials chosen for the study were the metals; 316 and 304 stainless steel, mild steel, and polymers; polyethylene, polytetrafluroethylene (Teflon^{TM}), PMMA, and polycarbonate.

4.1. Centre for Disease Control Biofilm Reactor Coupons

A number of coupons were initially purchased from Biosurface Technologies, the manufacture of the CDC reactor. Upon receipt of the coupons their roughness was determined using WLI.

Each coupon inserted into the CDC reactor presents two surfaces that can be colonised by the bacterium- top and bottom surface. The roughness of both surfaces was compared.
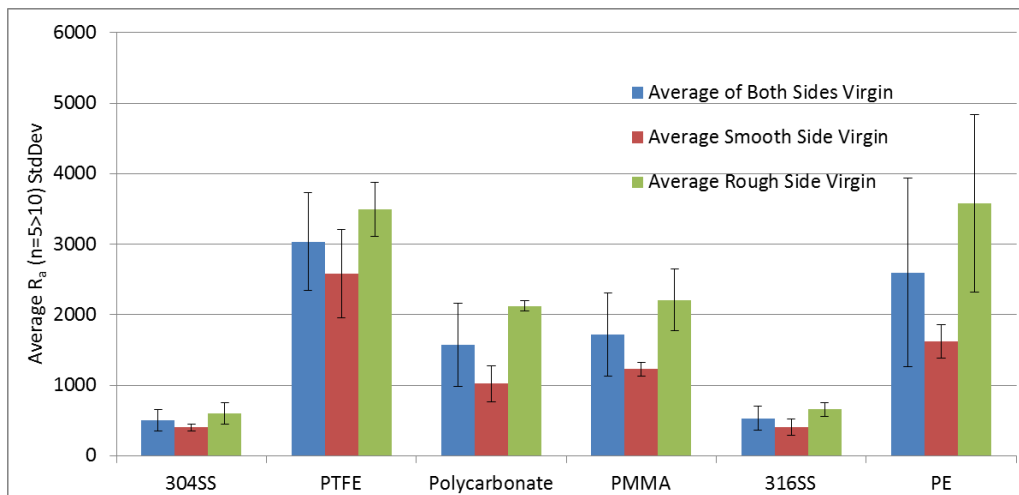
Figure 4.1. Surface roughness on Biosurface Technology coupons as received determined using WLI.

The results showed large but not statistical significant differences between the different coupon sides. However, upon visual inspection clear differences were evident in the topographical structures. One example is shown below in Figure 4.2 below.
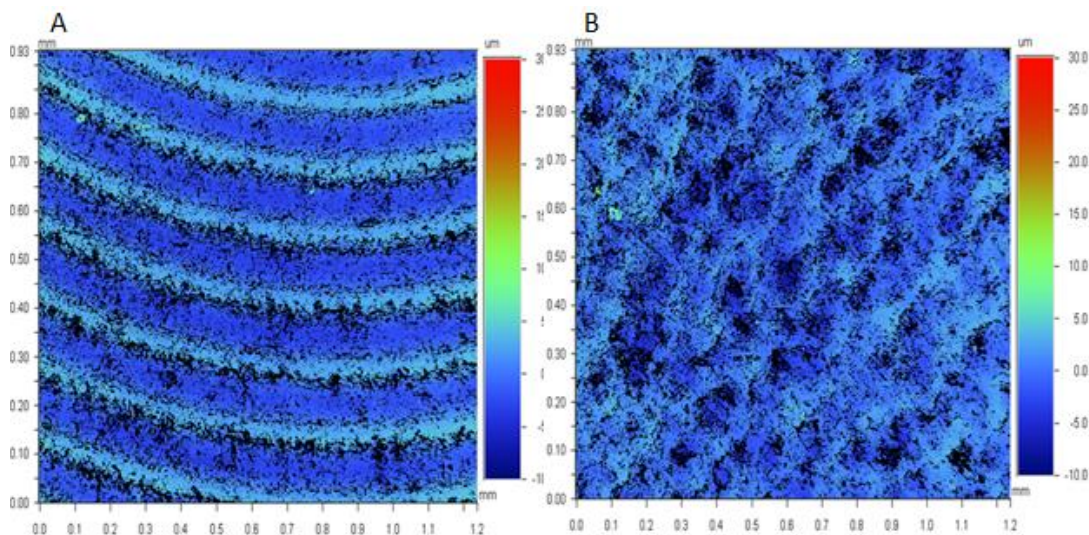

Figure 4.2. PMMA coupon from Biosurface Technologies. (A) Rough coupon side. (B) Smooth coupon side, (R_a=1.87µm and 1.23µm respectively).

In the above example, although the roughness of the two sides of the PMMA coupon are statistically very similar (see Figure 4.1) they are in fact quite different topographically. Similarly, variations in topography were seen across many individual coupons and across coupon sets. The largest concern was the variation across individual coupons appeared to have arisen during manufacturing and specially machining. Such surface disparities could have induced unknown and uncontrolled variation in results which could have made experiment interpretation more difficult. To overcome these unanticipated challenges, I manufactured my own coupons in-house and moulded their topography to suit the needs of the experiment. One benefit of manufacturing my own coupons was that coupons could be made with different topographies (a rough and smooth variant), could have identical surface chemistries, but also within a coupon and across coupons the topography would be more similar.

4.2   Manufacture of In-House Coupons

The objective was to procure, analyse and manipulate a number of substratum materials, both metals and polymers that possessed a range of both surface energy and topographical characteristics. The materials that were chosen for the study were the metals; 316, 304 stainless steel, mild steel, and the polymers polyethylene, polytetrafluoroethylene (Teflon^{TM}), PMMA and polycarbonate. The relative costs, ease of obtainment, current uses by industry and medicine as well as their physical properties, as discussed in Chapter 1.26 were considered as part of the material selection process. Both a 'smooth' and 'rough' variant of each substratum material was prepared in order to test this variable.

To produce the coupons from the purchased metal and polymer sheets, different cutting techniques were required. The steels and polycarbonate were cut using a high power precision laser cutter, and both polytetrafluoroethylene and polyethylene were cut out using a half inch hand punch and large hammer. Any burrs were removed manually using a hand file.

WLI and contact angle was used to characterise the substratums, the results of which are detailed below.

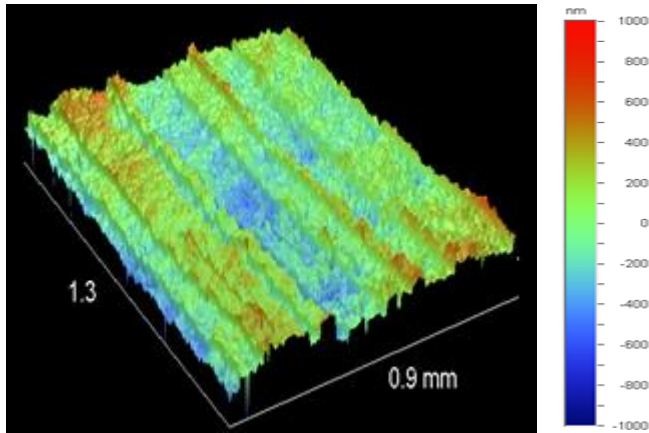## 4.2.1 Virgin Substratum Roughness

Figure 4.3. Natural PE (virgin). Image taken at 5x magnification using VSI.
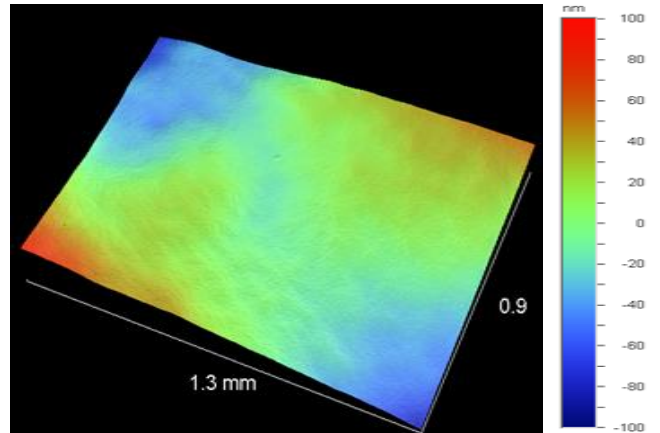

Figure 4.4. Polycarbonate (virgin). Image taken at 5x magnification using PSI.
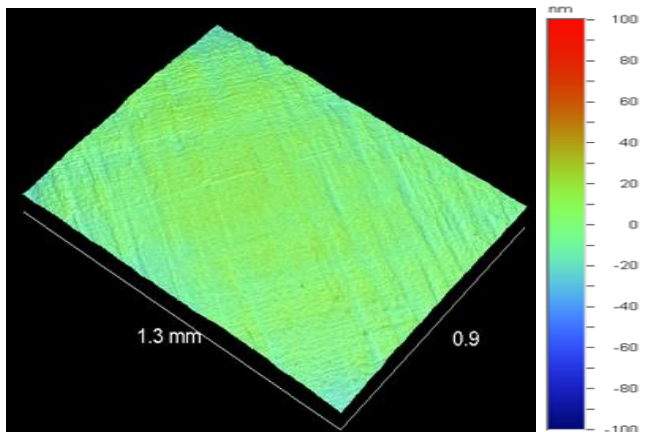

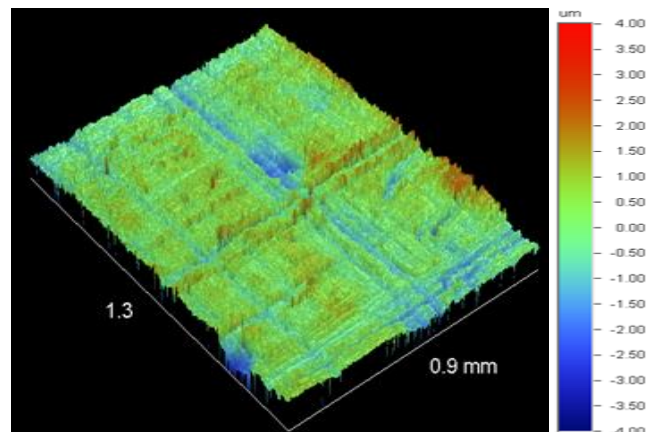Figure 4.5. PMMA (Virgin) taken at 5x magnification using VSI.

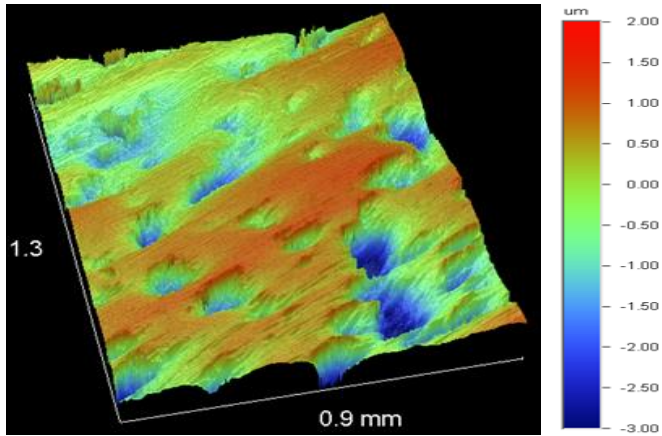Figure 4.6. PTFE (virgin) taken at 5x magnification using VSI.

Figure 4.7. Mild steel (virgin). Taken at 5x magnification using VSI.

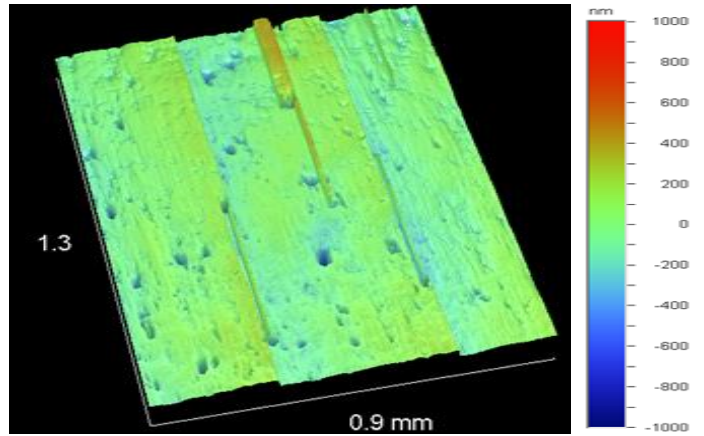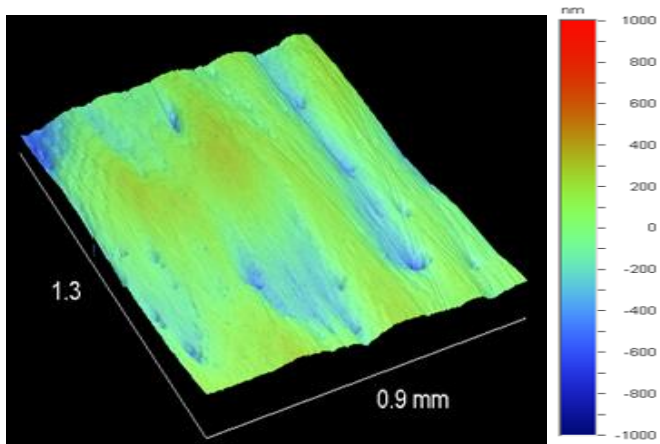Figure 4.8. 304 stainless steel (Virgin). Taken at 5x magnification using VSI.

Figure 4.9. 316 stainless steel (virgin). Taken at 5x magnification using VSI.
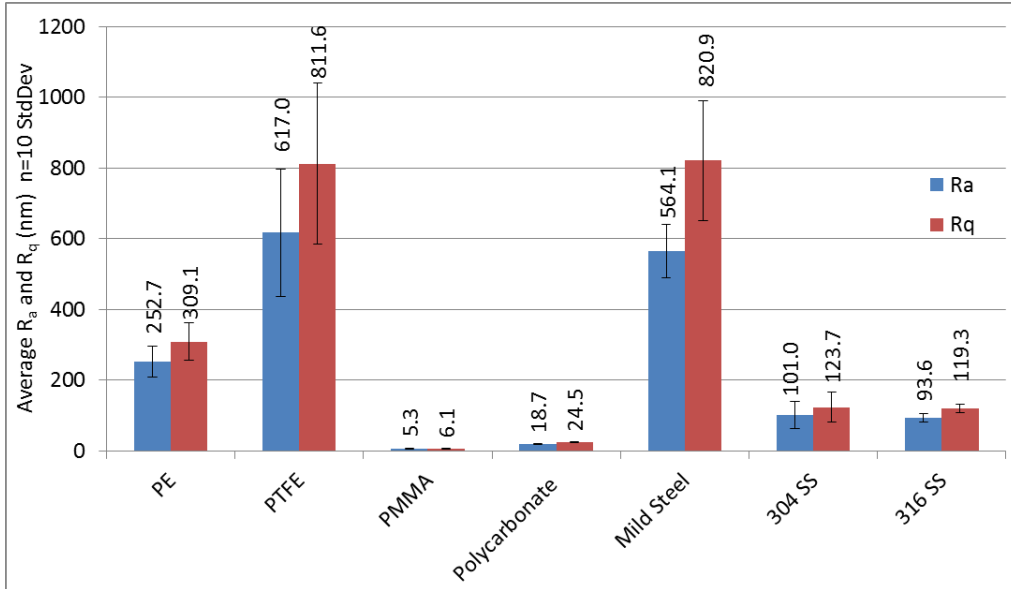
Figure 4.10. Average surface topographic data R_a and R_q, for virgin unmodified substrates as determined using WLI.
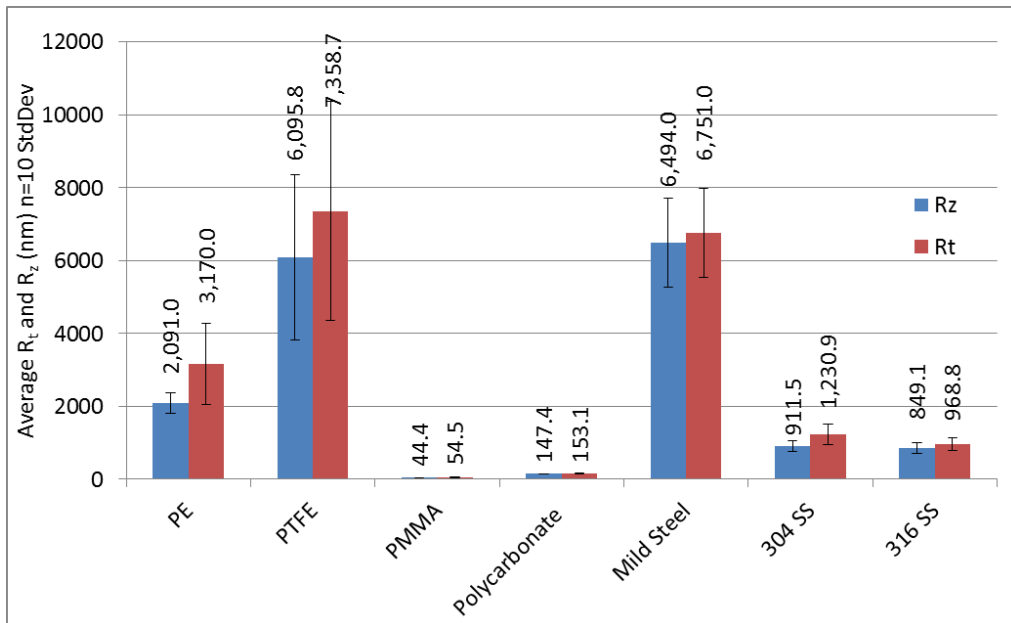
Figure 4.11. Average surface topographic data R_z and R_t, for unmodified virgin substrates as determined using WLI.

4.2.2 Discussion – Initial Surface Roughness Determination

The two roughest surfaces (as delivered) were PTFE and mild steel, and coincidentally both had statistically equivalent roughnesses (R_a; 617±180nm and 564±75nm respectively). They were by far the roughest substratum materials tested in this thesis (see Figure 4.10 and Figure 4.11). PMMA and the stainless steels (304 and 316) were equally 'smooth', with PE appearing as an intermediate (see Figures 4.10 and 4.11). In order to create a rough variant for a given material sandblasting was used, as detailed in Chapter 2.7.

4.2.3 Virgin (Unmodified) Substratum Contact Angle Data

Figure 4.12. Advancing and receding contact angle for water and diiodomethane on the virgin substrates.

Using the average advancing contact angles shown above, the following surface energies were calculated (Table 4.1) using Fowkes' work of adhesion Eqn. 12.

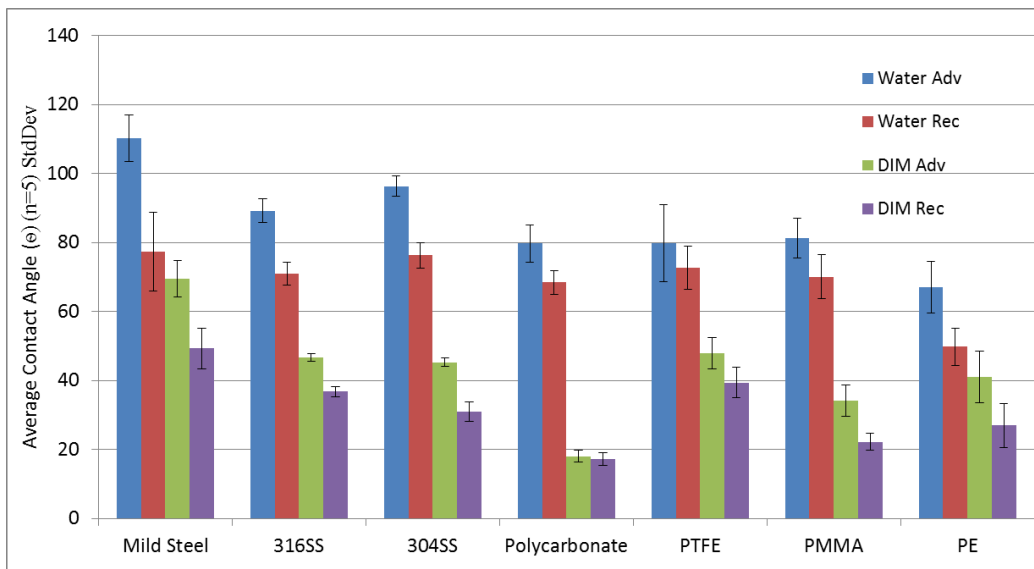| Material	$\gamma^p{}_S$, $\gamma^d{}_S$, γ_S (mJ/m²)				
	Ref1	Ref2	Ref3	Ref4	Current Work – Sandblasted Coupons
316SS	8.4, 35.0, 43.5 (Yang et al., 2010)	3.3, 26.3, 29.6 (Hao et al., 2005)	1.6 ,40.9-42.5 (Bueno, 2005)	1.52, 41.75, 43.27 (Matjie et al., 2016)	1.5,36.2,37.6
304SS	-,-, 36.5 (Lerebour et al., 2004)	0.0,38.0,38.0 (Hedberg et al., 2014)	-,-,-	-,-,-	0.3,36.9,37.2
Mild Steel	4.2,64.6,68.8 (Lawrence and Li, 1999)	-,-,-	-,-,-	-,-,-	0.7, 32.6 ,33.3
PTFE	1.6, 18.4, 20.0 (Landrock. A, 2015)	1.1, 16.9, 18.0 (Yaneff, 2003)	3.5, 18.5, 22.0 (Bueno, 2005)	-,-,-	4.4, 35.4, 39.9
PE	0, 35.7, 35.7 (Landrock. A, 2015)	-,-, 35.7 (Yaneff, 2003)	-,-, 31.0 (Baier, 1972)	0.3, 35.7-36.0 (Oxford University Press, 1999)	9.0, 39.1, 48.1
PC	6.5, 27.7, 34.2 (Landrock. A, 2015)	1, 44, 45 (Yaneff, 2003)	-,-, 42.9 (Oxford University Press, 1999)	-,-,-	2.1, 48.3, 50.5

Table 4.1. Surface energy of unmodified surfaces. Experimental and literature date.

4.2.4 Discussion – Surface Energy of Virgin Substrates

A range of surface energies were elicited from the materials studied. 316, 304 stainless steel and PC were quite similar to that reported in the literature (Table 4.1). However, larger deviations from the literature values were observed within the polymer group, notable examples being; PTFE experimental γ_S was determined to be 39.9 mJ/m^2, versus literatures value of ~18.0 mJ/m^2. PE the experimentally determined γ_S mJ/m^2 of 48.1 versus literature value of 37.5 mJ/m^2 (Table 4.1).

It was plausible that these large discrepancies in the surface energies of the polymers was due contamination of the material surfaces during manufacturing. Polymeric and chemical processing aids are commonly used in polymer manufacture and are known to be prevalent on the surface.

4.2.5 Surface Roughness of Sandblasted Coupons

Sandblasting was performed using a Clarke SB30 sandblasting cabinet with a glass bead abrasive, with an approximately 200-300μm particle size, as described in Chapter 2.7.
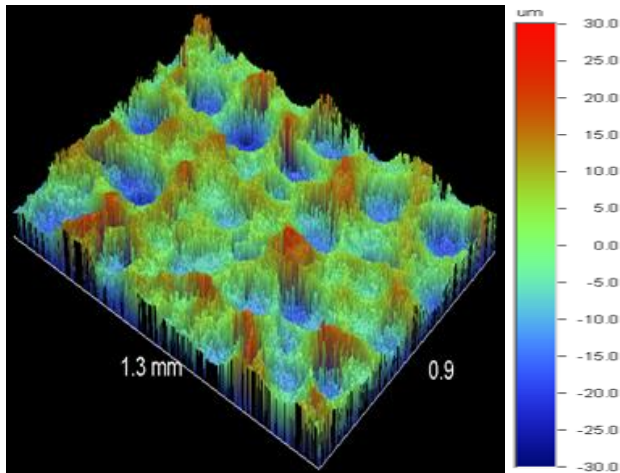
Figure 4.13. Image of PTFE surface post sandblasting. 5x magnification using VSI.
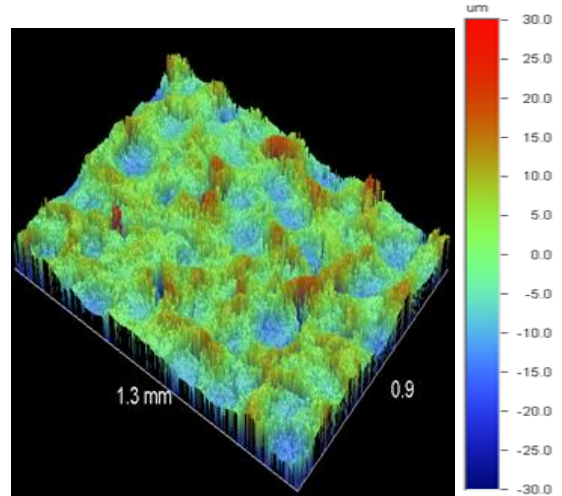
Figure 4.14. Image of PE surface post sandblasting. 5x magnification using VSI.

Figure 4.15. Image of PMMA surface post sandblasting. 5x magnification using VSI.

Figure 4.16. Image of polycarbonate surface post sandblasting. 5x magnification using VSI.

Figure 4.17. Image of mild steel surface post sandblasting. 5x magnification using VSI.

Figure 4.18. Image of 316 stainless Steel surface post sandblasting. 5x magnification using VSI.

Figure 4.19. Image of 304 stainless steel surface post sandblasting. 5x magnification using VSI.
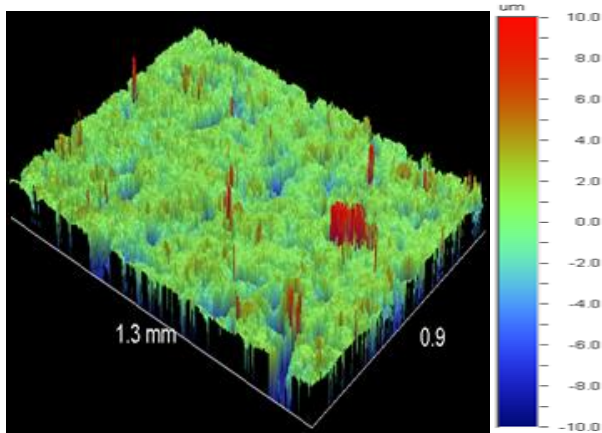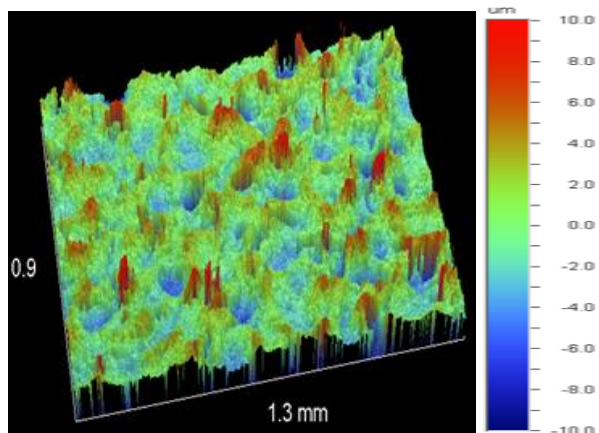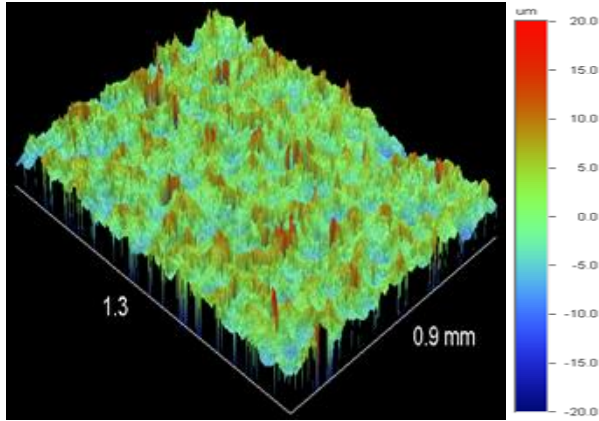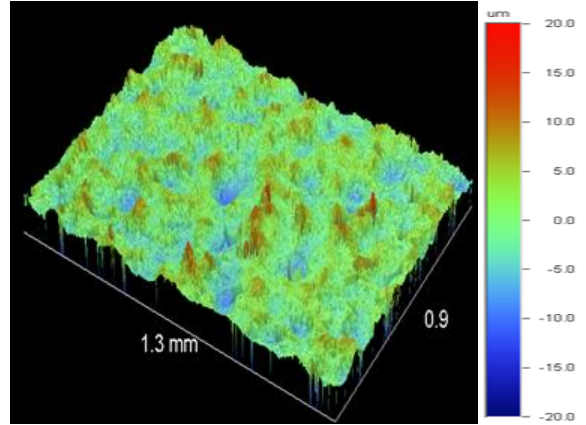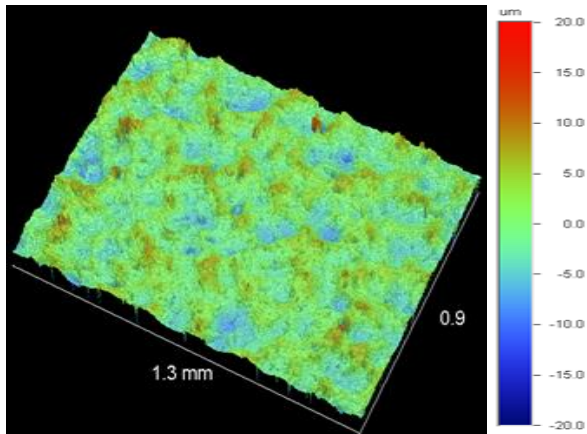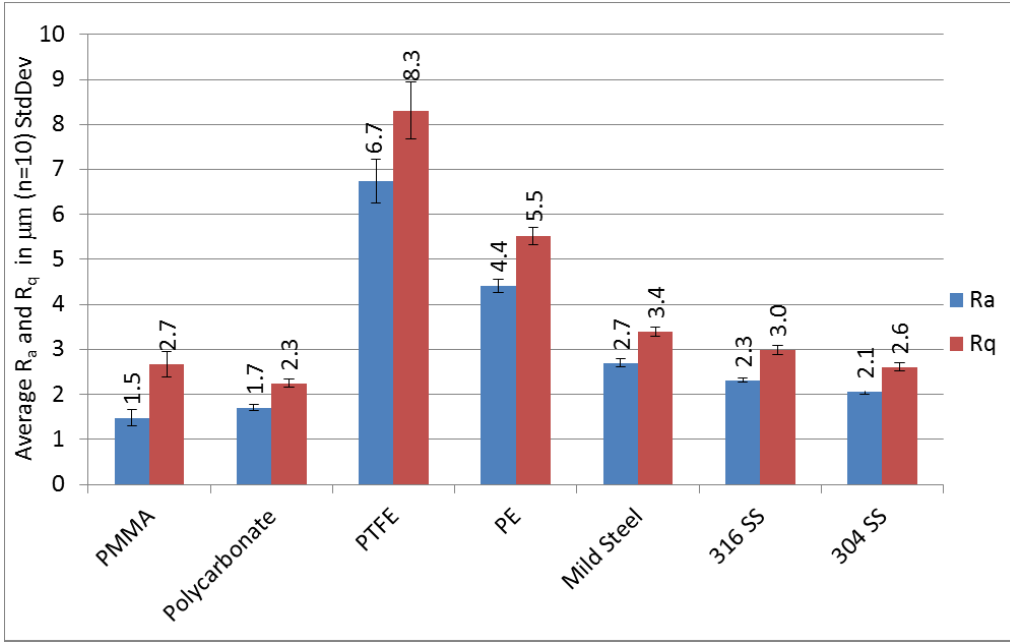
Figure 4.20. Surface topography parameters R_a and R_q, for sandblasted substrates.
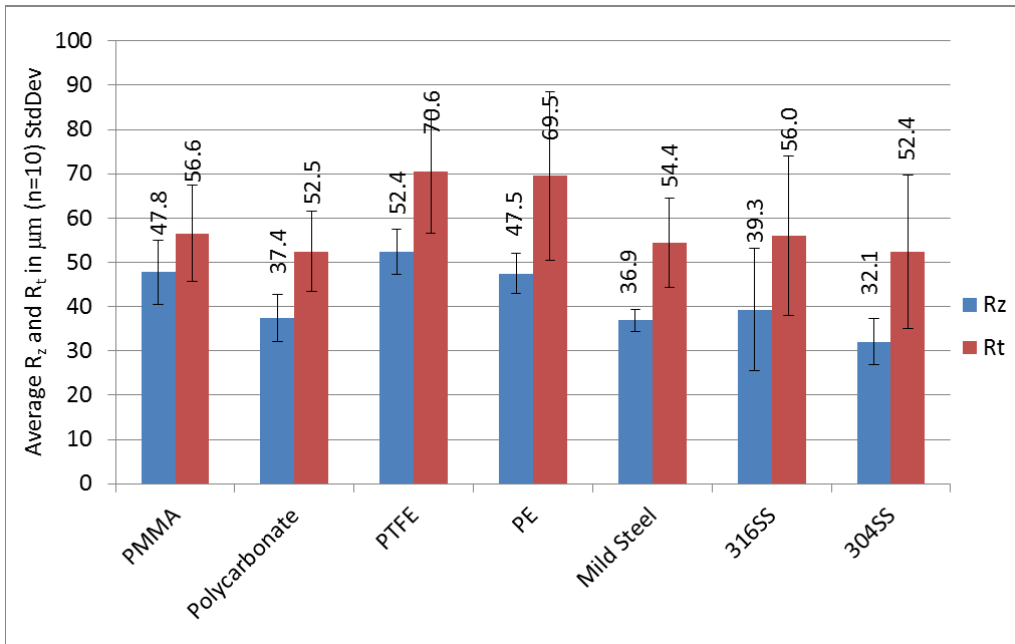

Figure 4.21. Surface topography parameters R_z and R_t, for sandblasted substrates.

4.2.6 Discussion - Surface Topography of Sandblasted Substrates

Sandblasting successfully remodelled the surfaces of the different materials. Importantly, the remodelling appeared to be consistent for each of the different materials, when examining the R_a and R_q (Figure 4.20), statistical differences were observed. This is likely due to a combination of impact strength and melting temperature of the various materials tested. Conversely, the R_t and R_z (Figure 4.21) for the differing materials were all remarkably similar, which was somewhat unexpected. This similarity is likely due to the nature of both the R_t and R_z measurement (stated in Chapter 1.33) i.e. sampling the extremes of surface topology. For example R_z is derived from the 10 largest troughs to peak heights. This is likely coupled to the fact that the momentum of the glass beads used in the sandblaster was similar (approximately same size and travelling at same speed). These beads radically altered the surface topography as shown for PTFE in Figure 4.20 which is relatively soft (and so heavily cratered) or facilitating rarer but large damage events of similar scale as PMMA. Whether a substratum was heavily, or only a little pitted would give a similar metric, as is the case in Figure 4.21.

Following the observation of the effects of sandblasting (comparison of Figure 4.10 and Figure 4.20) on the different substratum materials, it was thought that there was a risk that surfaces would not only be topographically remodelled, but be chemically altered too. This could be by the embedding of sand particulates into subsurface-surface of the polymers, which was not desired.

To overcome the risk of introducing sand particles into the polymer substratums surface-subsurface, another option for remodelling their surfaces was to use sandblasted stainless steel 316 as a mould for the polymers, using a platen press (Chapter 2.8). In this methodology only the stainless steel surfaces would be topographically altered using the sandblaster and used in the biofilm experiments.

4.2.7 Surface Energy of Substrates Post Sandblasting

The surface energy determinations for the sandblast modified substratums were carried out using the same procedure as per Chapter 2.15.
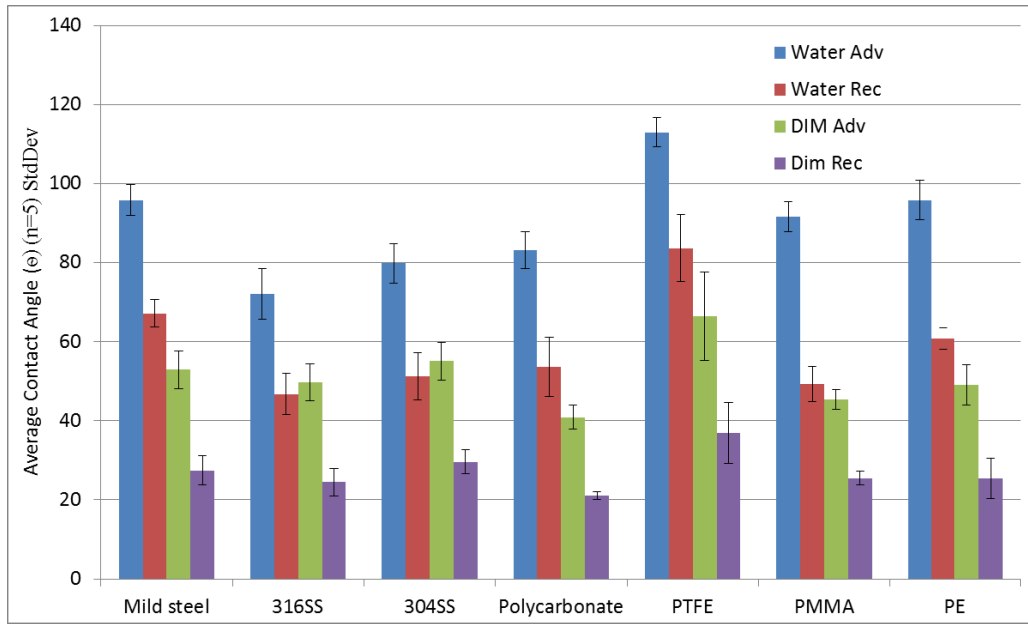
Figure 4.22. Advancing and receding contact angle for water and diiodomethane (DIM) on the sandblasted substrates.

	$\gamma^p{}_S,\ \gamma^d{}_S,\ \gamma_S\ (mJ/m^2)$
Material	Current Work – Sandblasted Coupons
316SS	8.0, 34.5,42.5
304SS	5.5, 31.4, 36.9
Mild Steel	0.7, 32.6, 33.6
PTFE	0, 24.0, 24.0
PE	0.5, 34.8, 35.3
PC	2.6, 39.2, 41.8

Table 4.2. Surface energy of sandblasted surfaces as calculated using Fowkes' work of adhesion (see Eqn. 12).

4.2.8 Discussion - Surface Energy Post Sandblasting Modification

The surface energies of the sandblasted substratums was found to be more closely related to those found in the literature compared with the as received virgin surfaces (comparing Table 4.2 and Table 4.1). It is noteworthy that substratum roughness is not normally reported alongside the surface energies of different materials found in the literature.
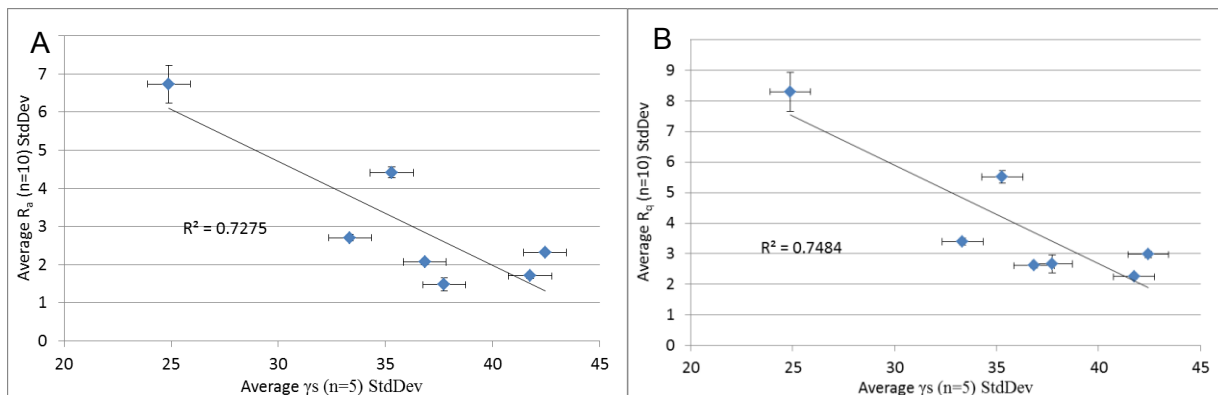
Figure 4.23. Graph of sandblasted substratums roughness versus total surface energy.

152

During the analysis of both the surface energy and surface topography data, especially for the sandblasted surfaces, there appeared to be a first order general correlation. The raw data was analysed using the scatter plots above (Figure 4.23). It appears that both roughness parameters R_a and R_q correlate with surface energy, R^2=0.73 and 0.75 respectively. This is likely again to the nature of the metrics as explained in Chapter 1.33. The effect of roughness on contact angle and thus the calculated surface energy is likely due to Wenzel type liquid-solid interactions explained in Figure 1.41.

4.3   Polymer Substratum Remodelling using Platen Press

A platen press (discussed in Chapter 2.8) in conjunction with the mould (shown in Figure 2.2) was used to remodel the polymer substratums surfaces using two unmodified and two post sandblasted 316 surfaces as a mould counterface, where required.

Numerous combinations of rough and smooth mould templates were used on the various substratum materials with the aim of creating a 'smooth' and 'rough' variants for each material. All experiments were conducted at room temperature, but the load varied as did the duration of the applied compression.

The rough polycarbonate material was modified using a 5 tonnes pressure for 4 minutes, with the rough polyethylene coupons required 2 tonnes for 2 minutes.

PTFE was difficult to compress because of its tendency to cold flow, therefore handmade virgin PTFE sheet made coupons were used as smooth PTFE coupons, and the virgin PTFE coupons sourced from Biosurface Technologies (Section 2.1.5.1) were used as the rough variant.

The smooth variants for the polyethylene, polycarbonate, 316 and 304 stainless steel were unmodified surfaces sourced from Gilbert Industries, or Orion Allows respectively.

4.4 The Rough and Smooth Coupons using Compression Moulding

4.4.1 Coupon Surface Roughness
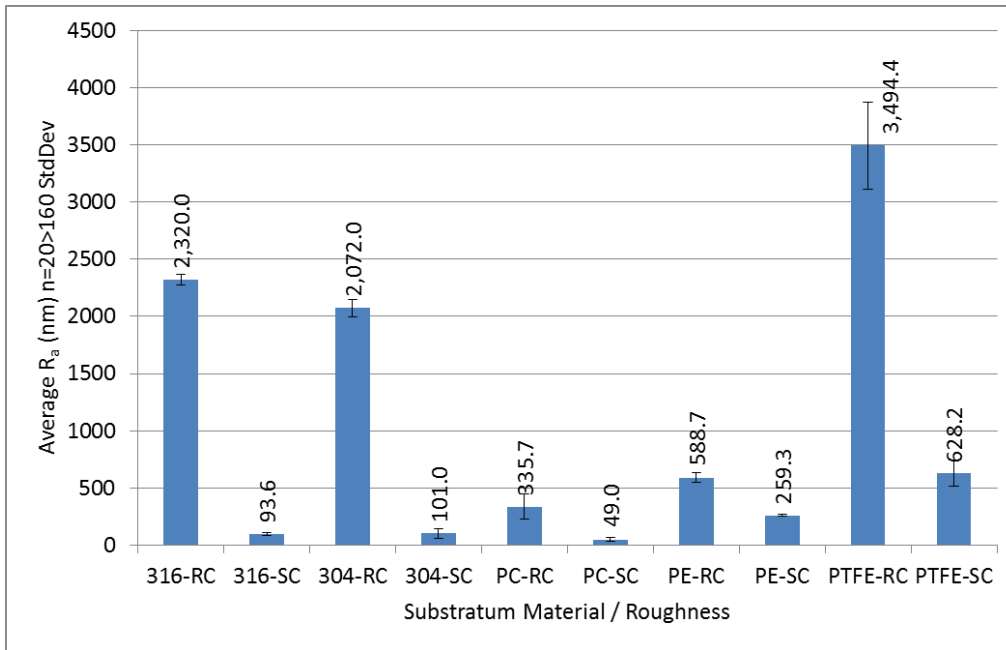
Figure 4.24. The roughness of all substrates used in the study.
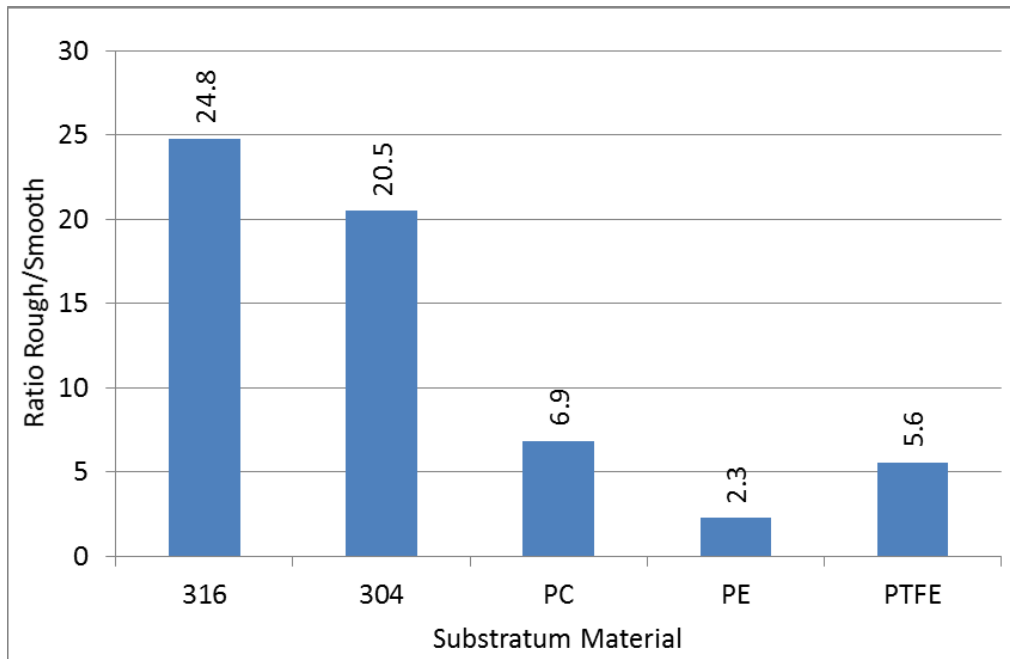
Figure 4.25. Ratio of average roughness (R_a) of rough to smooth substrates.

In summary, the PTFE coupons were cut from unmodified virgin PTFE coupons made from Gilbert Industries PTFE sheet (smooth variant), and unmodified virgin PTFE coupons from Biosurface Technologies were used as the rough variant.

Polyethylene coupons were made in-house cut from polymer sheet from Gilbert Industries, the smooth variant was unmodified, but the rough substratum coupons were made using a platen press set to 2 tonnes for 2 minutes, using post sandblasted 316 stainless steel as a mould.

Polycarbonate coupons were made in-house cut from polymer sheet sourced from Gilbert Industries. Smooth variants were unmodified, but the rough variants were made using a platen press set to 5 tonnes for 4 minutes, using post sandblasted 316 stainless steel as a mould.

Both the 304 and 316 stainless steels were made in house, cut from steel sheets purchased from Orion Alloys. The smooth variant was unmodified material, but the rough variant was sandblasted as discussed above.

A range of surface roughness were obtained complete with a rough and smooth variant for each material variable, with a roughness factor increase between 2.3 and 24.8x observed (see Figure 4.24 and Figure 4.25).

Approximately 30 coupons of each substratum were fabricated and used in the biofilm experiments. Some of these coupons were further modified with thin film coatings. See Chapter 4.5.

4.4.2 Coupon Surface Energies
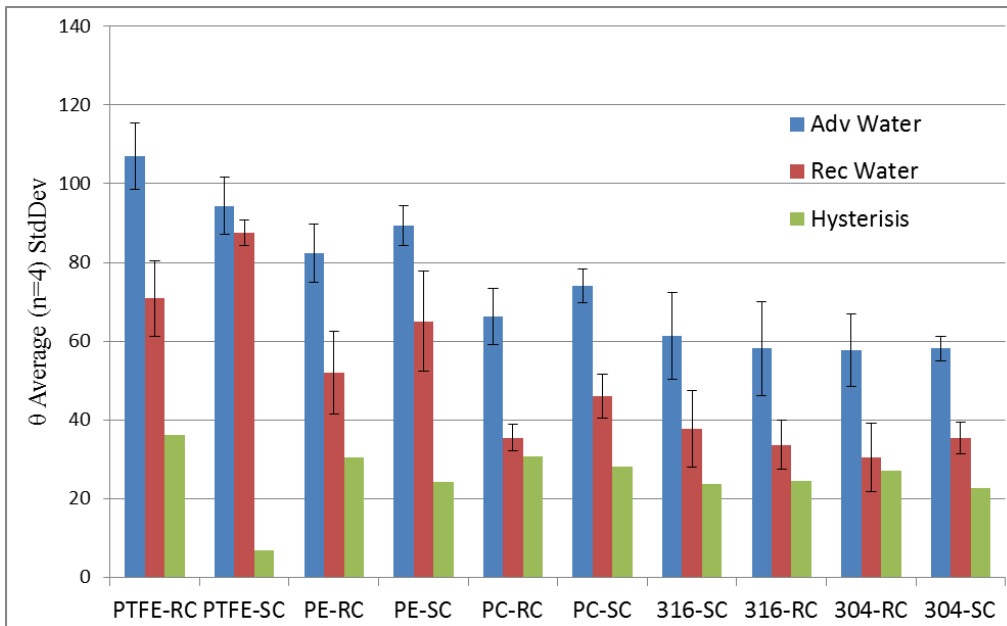
Figure 4.26. Water contact angles for the rough and smooth coupon surfaces
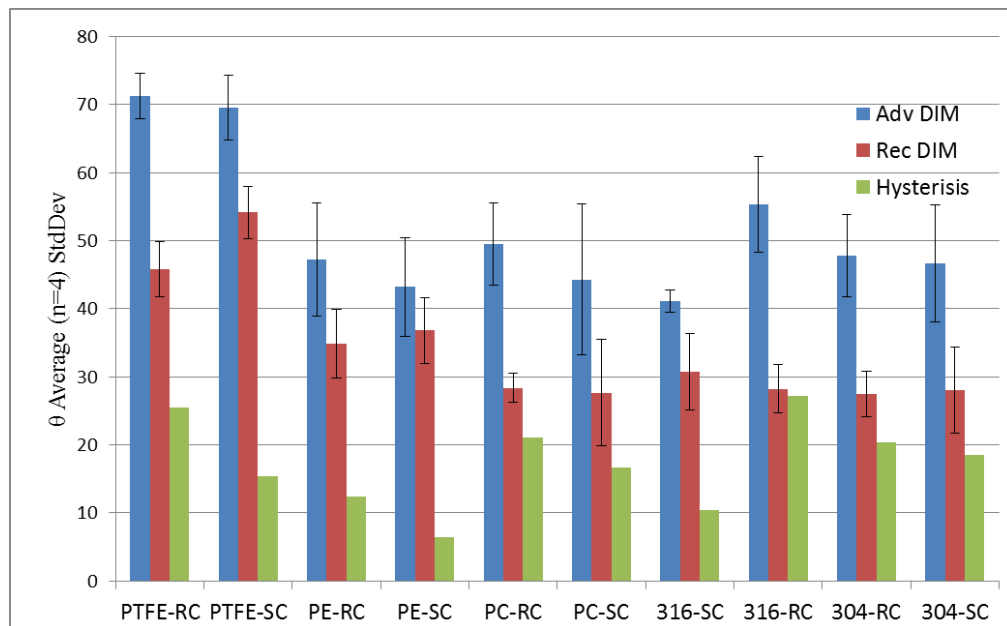
Figure 4.27. DIM contact angles for the rough and smooth coupon surfaces

	γ^p_S, γ^d_S, γ_S (mJ/m^2)	
Material	Current Work	
	Smooth Coupons	Rough Coupons
316	11.9, 36.3, 48.3	17.0, 31.3, 48.3
304	14.9, 36.1, 51.0	15.5, 35.5, 50.9
PTFE	2.4, 23.2, 25.6	0.28, 22.2, 22.4
PE	1.3, 38.0,39.2	3.4, 35.8, 39.2
PC	6.2, 37.4, 45.5	11.0, 34.6, 45.5

Table 4.3. Surface energy data for the rough and smooth surfaces determined experimentally (see Eqn. 12).

Comparing the surface energy (Table 4.3) as determined using Fowkes' work of adhesion equation (Eqn. 12) with the advancing water and DIM contact angles finds that that they quite comparable to those quoted in the literature (Table 4.1).

4.5   Coupons Coated with Thin Films and Engineered Materials

A number of coupon materials were selected for modification by use of a thin film coating. PTFE, PC and 316 stainless steel coupons were gold coated using a sputter coater. The purpose was to determine whether the application of a thin film coating would turn a classically hydrophobic substratum, now with a new hydrophilic thin gold coating, go on to augment microbial adhesion. This study was compared with a hydrophilic substratum control; 316 stainless steel. The gold film thickness was approximately 30nm (see Chapter 2.11). SilWet and PTFE-AF thin film coatings were also deposited on 316 stainless steel, to increase and decrease the γ_S of 316 stainless steel respectively.

In addition two proprietary engineered polymer materials were also evaluated, these were NILT and Sharklet[TM]. These materials were discussed in Chapter 1.27.3 and Chapter 1.27.5 respectively.

4.5.1 Surface Energy of Thin Film Coated Substrates and Engineered Materials
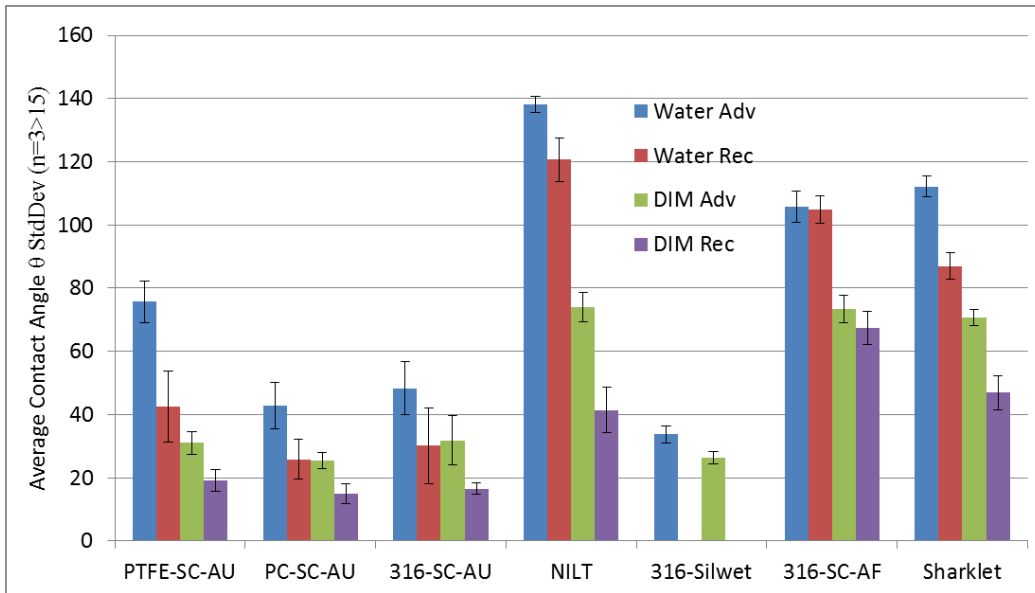
Figure 4.28. Advancing and receding contact angles for both water and DIM probe on coated substratums.

PTFE-AF water advancing contact angle has been reported to be 110° (Chemours-Company, 2016a), which is within the range obtained in the above experiments of 108° (Figure 4.28).

	γ^p_S (mJ/m^2)	γ^d_S (mJ/m^2)	γ_S (mJ/m^2)
PTFE-SC-AU	4.1	43.8	47.9
PC-SC-AU	19.4	46.0	65.5
316-SC-AU	17.5	43.5	60.9
NILT	2.8	20.7	23.5
316-SC-SilWet	24.2	45.6	69.8
316-SC-AF	0.5	20.8	21.3
Sharklet™	0.0	22.5	22.5
Gold (Cognard, 1984)	~5	~45-60	~50-65

Table 4.4. Surface energy values determined experimentally using Fowkes' work of adhesion (see Eqn. 12), for the thin film modified surfaces.

Following the deposition of the gold, onto the surface of the PTFE, PC and 316 an increase in γ_S was observed for all substratums (γ_S;PTFE 25.6 to 47.9, PC 43.6 to 65.5, and 316SS 51.0 to 60.9 mJ/m^2), confirming that the thin films were present on the surfaces. The increases in γ_S are also what would be expected when gold coating a hydrophobic material, and were similar to the range reported in the literature 45-65 mJ/m^2 (Cognard, 1984). The gold thin films were also visually apparent. The differences in the surface γ_S observed for the different materials maybe due to the materials roughness influencing the contact angle θ, as explained in Chapter 1.32.

After the deposition of the PTFE-AF thin film onto the 316 stainless steel, a decrease in surface energy was observed (γ_S 48.3 to 21.3 mJ/m^2). γ_S for PTFE-AF has been reported to be 15.6 mJ/m^2 (Chemours-Company, 2016a), which is lower than the 21.3 mJ/m^2 reported here and so is in-line with literature observations, which confirms the thin film deposition of PTFE-AF. Interestingly, the Sharklet^{TM} (γ_S 22.5mJ/m^2) surface has almost identical surface energy parameters to PTFE-AF, and is similar to the γ_S range reported 15.7 to 23.0mJ/m^2 for poly(dimethylsiloxane) (Oxford University Press, 1999, Carman et al., 2006).

4.5.2 Surface Roughness of Thin Film Coated Coupons
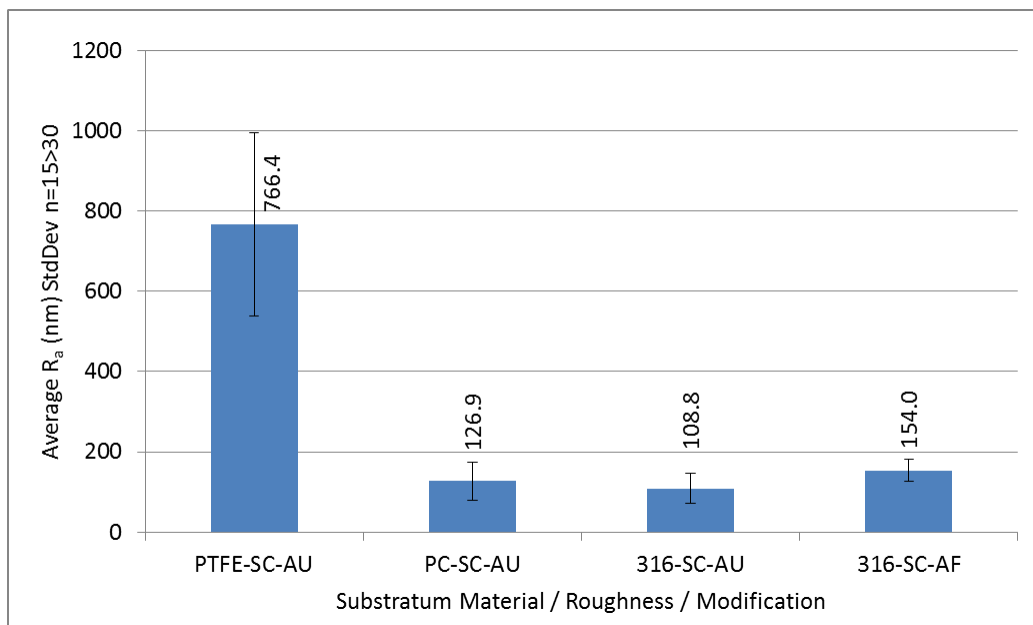
Figure 4.29. Surface roughness of modified substratums

The thin film surface modification did not result in a statistically significant increase in roughness when gold coating PTFE, or 316 stainless steel. However, slight increases in roughness were observed for PC-SC-Au and 316-SC-AF. These were not significant in the overall scope of this study.

4.6   Conclusions

The objective was to source and engineer a variety of materials that possessed a range of experimentally determined roughness's and surface energies, and examine thin film surface modifications of some of these materials. Material average roughness (R_a) ranges achieved were between 49nm and 3.94µm, with intra-material roughness ratios between 1:2.3 (PE) and 1:24.8 (316) (Figure 4.24 and Figure 4.26 respectively). The different materials cover a relatively large γ_S range: 21.3 – 65.5mJ/m^2 (Table 4.4). These materials were then used in succeeding Chapters to examine the early attachment of *PA*, investigate any differences in gross *PA* biofilm structure when cultured upon them, and examine the ease of *PA* biofilm removal.

CHAPTER 5 Microbial Initial Binding Assay Validation

An initial binding assay was developed to evaluate the extent to which *PA* attaches to the different substratums under study, as a mean of studying the first stage in biofilm formation. This measurement was determined by using confocal microscopy in combination with a fluorescent probe that stains all cells (Syto®9), whether dead or alive, by binding to the microbes. Fluorescence from DNA-Syto®9 conjugates has been observed to be up to 100 times greater in comparison to unbound Syto®9 (Stocks, 2004). The confocal microscopy images were captured using a Leica TCS SP8 confocal microscope, setup to have an optical slice thickness, dz, of 15µm (see Eqn. 6 and Appendix B for calculations), to capture all the data from the surfaces under examination. Image data was then analysed and the percentage substratum area occupied parameter extracted using *Image J* with the *Comstat2.1* add-in (See Chapter 1.31 for details).
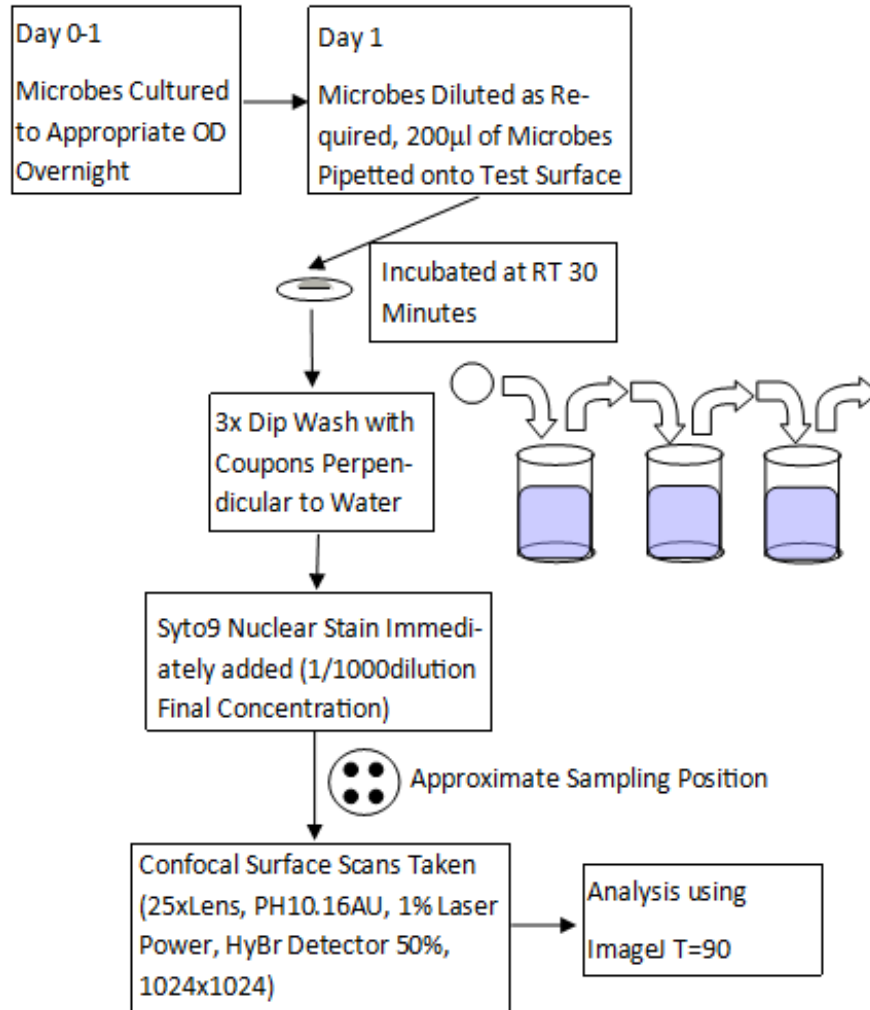
Figure 5.1. *PA* initial binding assay experimental work flow.

5.1 Microbe Initial Binding Assay Validation

The negative control is perhaps the most important component of any assay validation. Here the substratum's were treated as per the initial binding assay method work flow, but only sterile full strength TSB was added for 30 minutes (i.e. no microbes), followed by Syto®9 probe staining for 30 minutes. This test was to check both background coupon surface reflectance's as well as probe surface anomalies that could potentially give rise to false positive results.
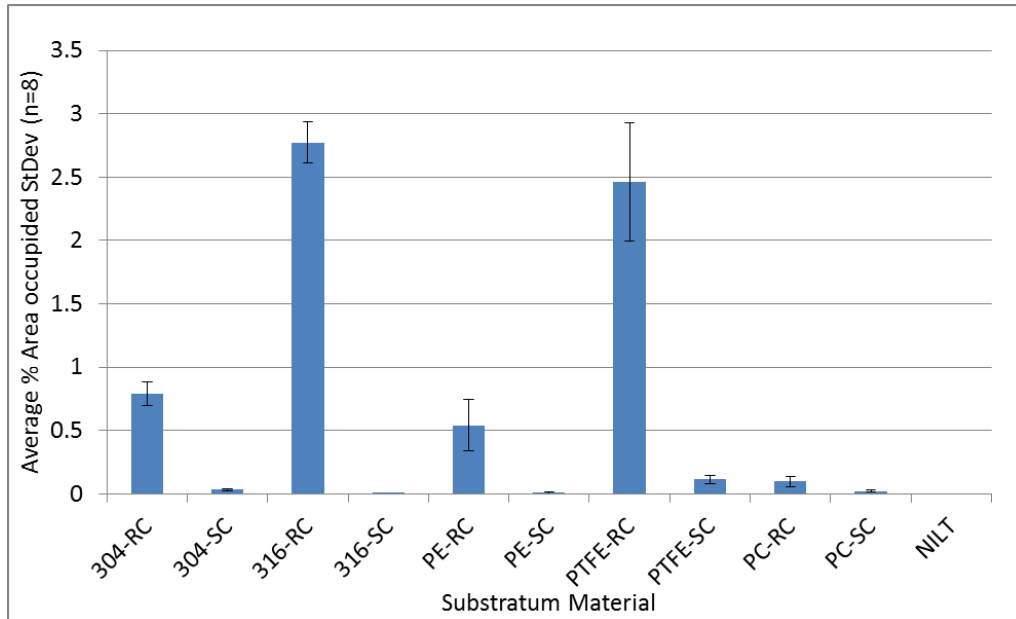
Figure 5.2. Initial binding assay negative control for different surfaces.

The negative control result for the coupons post cleaning validates that both the cleaning protocol used to remove *PA* from the surface is effective, and that the majority of the signal obtained following surface exposure to *PA* is from the microbes themselves.
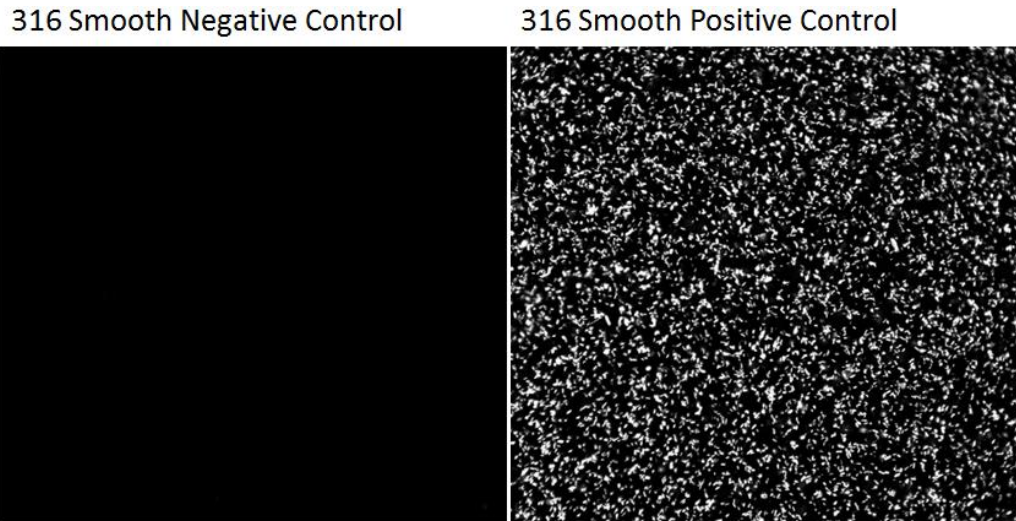
Figure 5.3. Example images of negative control (Syto®9 only) and positive control (*PA* + Syto®9) for 316-SC coupons.

To confirm that the microscope was detecting only microbes at the surface, a high resolution image stack was taken, with a dz of 1μm (0.36AU), with a z step increasing height of 1μm.
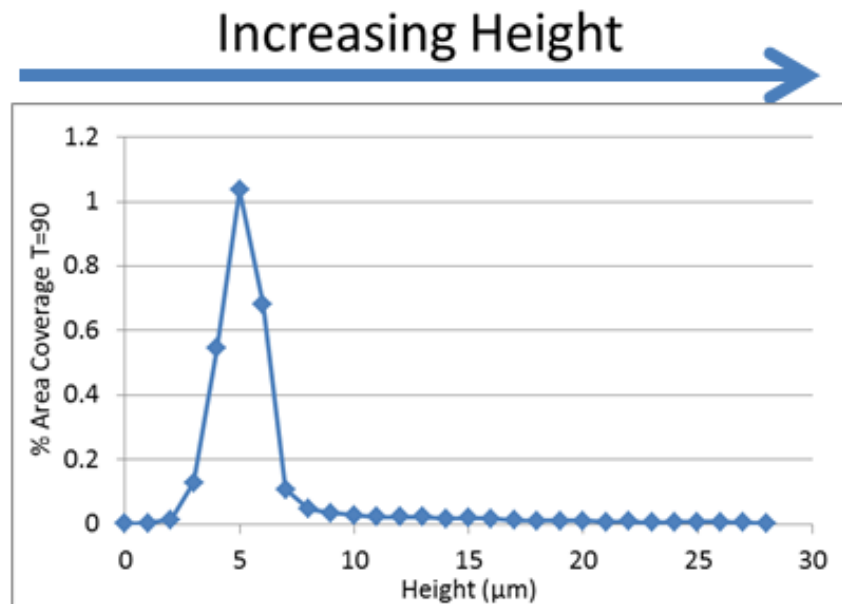
Figure 5.4. Confocal microscopic z stack for *PA* bound to 304-SC (30 minute incubation with 1μm dz, 1μm z step height increment).

164

Figure 5.4 above does confirm that the microbes are located at the surface within approximately 3µm. This deduction can be made due to the fact that 99% of the microbes are within 3µm of the surface and due to the lack of microbes being observed greater than 3µm from the surface. This data is important as it confirms that the assay method where by, a droplet of microbes of a pre-determined OD is placed on the surface is successfully removing the unbound and free floating microbes. Only those that are attached are being detected.

To ensure that the microbe fluorescent data is collected regardless of the topographical variation a dz of 15µm was used. A dz of 15µm was chosen because the average R_a of the different materials used in this project fall well within this range (R_a <3.5µm, (Figure 4.24)) and would ensure all of the microbe attachment would be captured regardless of topography. Given that no significant microbes are detected in the bulk following the attachment and rinsing steps (Figure 5.4), having a standard dz simplifies and increases the speed of the assay.
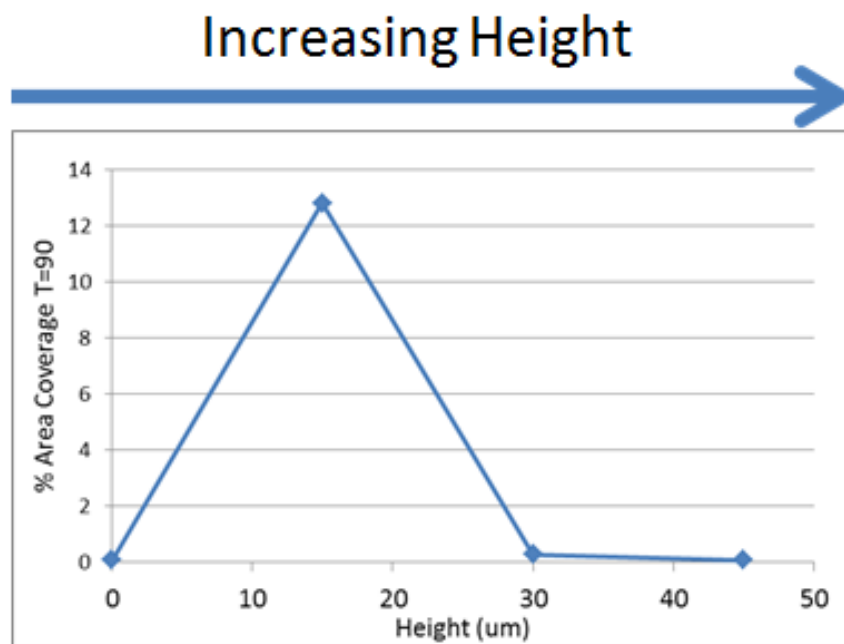
Figure 5.5. Confocal microscopic z stack for *PA* bound to 304-SC (30 minute incubation with 15µm dz, 15µm z step height increment.

The above is a typical example of initial binding assay data (Figure 5.5), collected using a dz of 15µm. Figure 5.5 also confirms the observation made in Figure 5.4 (dz 1µm) that very few

microbes are present in the near bulk environment, which increases the confidence in the measurement.

To further validate the assay, a number of serial dilutions (1/10) were performed using a starting culture of *PA* OD 0.1 @600nm. The standard initial attachment assay method was used, and 100μl of each dilution was spread on TSA and incubated ON for 18hrs at 32.5°C before counting the CFUs. This experiment was to confirm that the initial binding assay could detect *PA* in a quantitative manner, and relate this back to a standard microbiological quantification test. The concentration of TSB was fixed at 20 percent across the dilutions. Each dilution was thoroughly mixed prior to aliquoting onto the test surface or sterile TSA. This procedure was carried out 3 times and the results averaged.
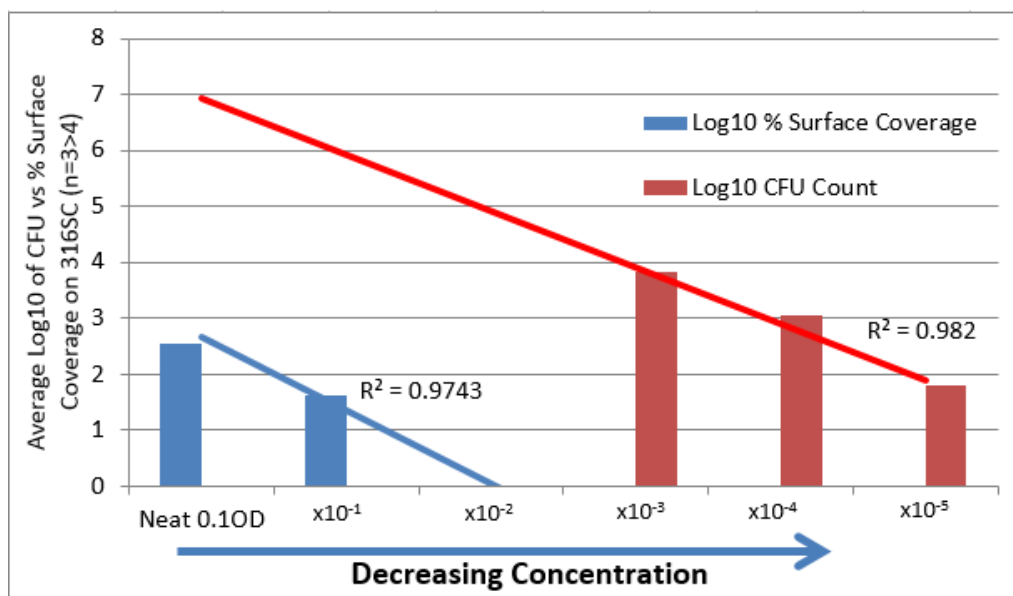
Figure 5.6. Comparison of CFU agar counts versus initial binding assay of serial dilutions (1/10) *PA*, with a dz of 15μm.

In the above method comparison (Figure 5.6), the result of the 10x dilutions can clearly be seen in both the Initial binding assay and TSA CFU counting method, with both showing good linearity eg an R^2 of 0.97 and 0.98 respectively. There is however no overlap between the two methods. This issue is due to neat (OD0.1@600nm) and 10^{-2} dilution being too concentrated to count the CFUs, and 10^{-3} to 10^{-5} being too dilute to detect with the initial binding assay. Both however are

shown to be correlating with the dilution factors used. This confirms that the initial binding assay is able to discriminate quantitatively.

5.2 Discussion and Conclusion to Initial Binding Assay Validation

It has been shown in this series of experiments that background surface fluorescence following coupon exposure to Syto®9 probe is exceeding low, and that any subsequent signals must be from the microbes under study. This analysis is aided by setting the confocal microscope detector to 50 percent, and by setting the threshold cutoff to 90 in *Comstat2.1*; thus selecting only for the most fluorescent (brightest) sources which are the microbes. Utilising the unique properties of the confocal microscope, the microbes have been shown to be bound to, or proximal to the surface (within 3μm) using 316 stainless steel as an example substratum material. The comparison of the CFU count and initial binding assay, when examining a serial diluted microbe containing broth, shows that the assay is able to quantitatively detect the microbes attached upon a surface. These experiments thus validate the initial binding assay is functional and suitable for investigating the initial binding of microbes on to different surfaces.

CHAPTER 6 Initial Attachment of *PA*

6.1   Initial Binding Analysis of *Pseudomonas* on Rough and Smooth Coupons

The effect of surface roughness and surface energy on the attachment of microbes has mixed and often contradictory results in the literature. Surface topography testing centered on 316 stainless steel and other substrates has given rise to many contradictory reported datasets (see Chapter 1.20).

The early stage biofilm assay developed was to assess the initial binding of *PA* to the different substratum's under investigation. The confocal microscope (Leica TCS SP8) pin hole was set to 10.16 AU for microbe surface detection experiments, complete with a 25x water immersion lens, yielding a large dz of 15µm, to ensure all surface data was collected across all surfaces, regardless of topography. To detect the microbes, fluorescent probe Syto®9 (1/1000 dilution in H_2O) was used with a 1024x1024 pixel resolution.

In order to determine the effect the surface energy, topography, and surface chemistry of different substratums, prepared coupons of known surface parameters were tested. See Chapter 4.4 and Chapter 4.5 for substratum details.

A *PA* starter culture was incubated overnight for 16-20 hours at 32.5°C, under anaerobic conditions. The OD was checked and a proportion of the culture was diluted to an OD of 0.1@600nm in water or TSB immediately prior to testing, ensuring that the media concentration was 20%v/v FS-TSB. *PA* coupon contact time was 30 minutes. The experiment consisted of 3 independently repeated experiments, each testing at least 3 coupons, each coupon being scanned for fluorescence at 4 different positions i.e. n=36.
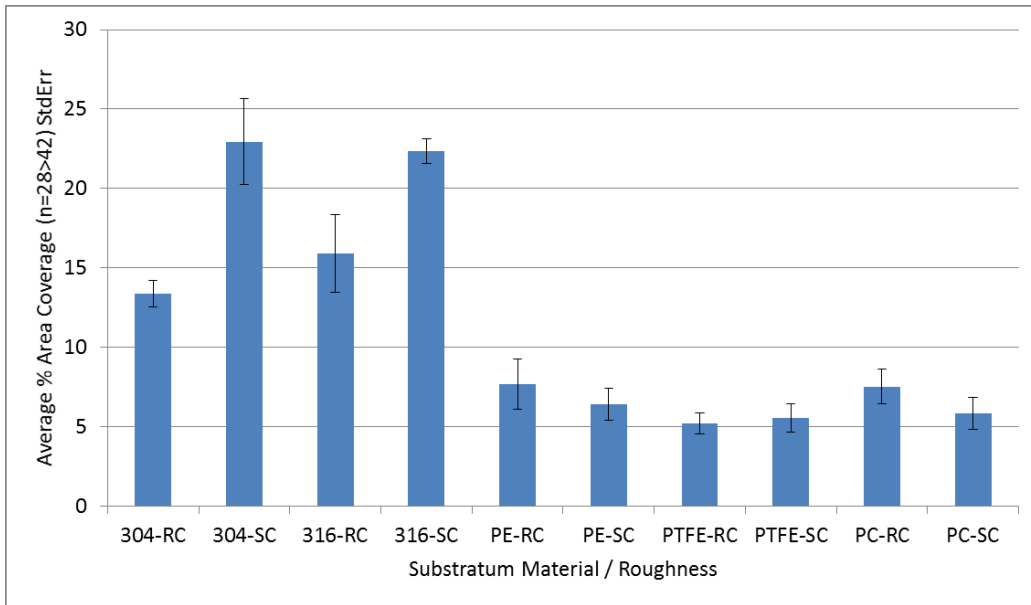
Figure 6.1. Initial binding coverage on different substratum materials.
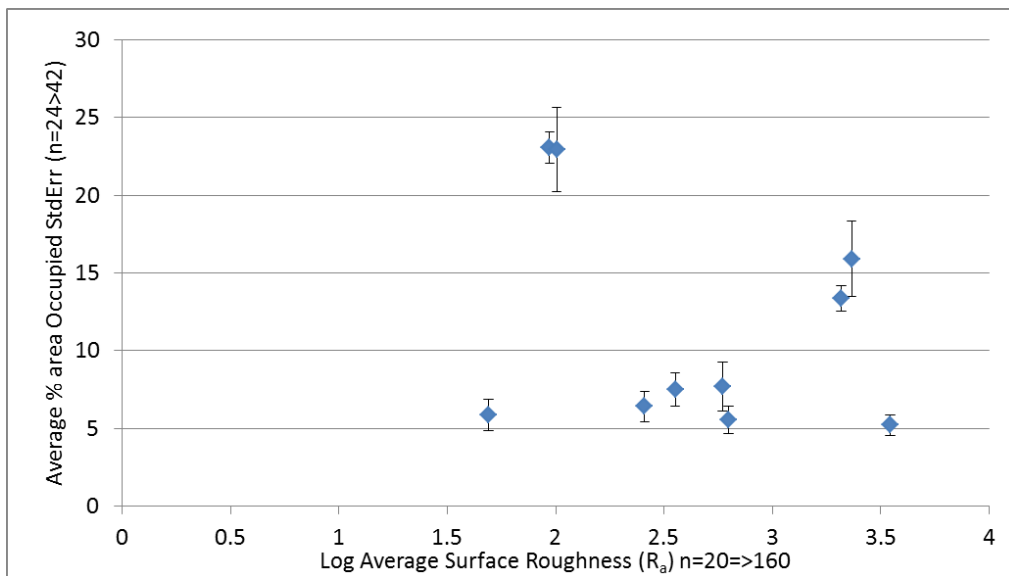
Figure 6.2. Initial binding coverage versus log of average surface roughness
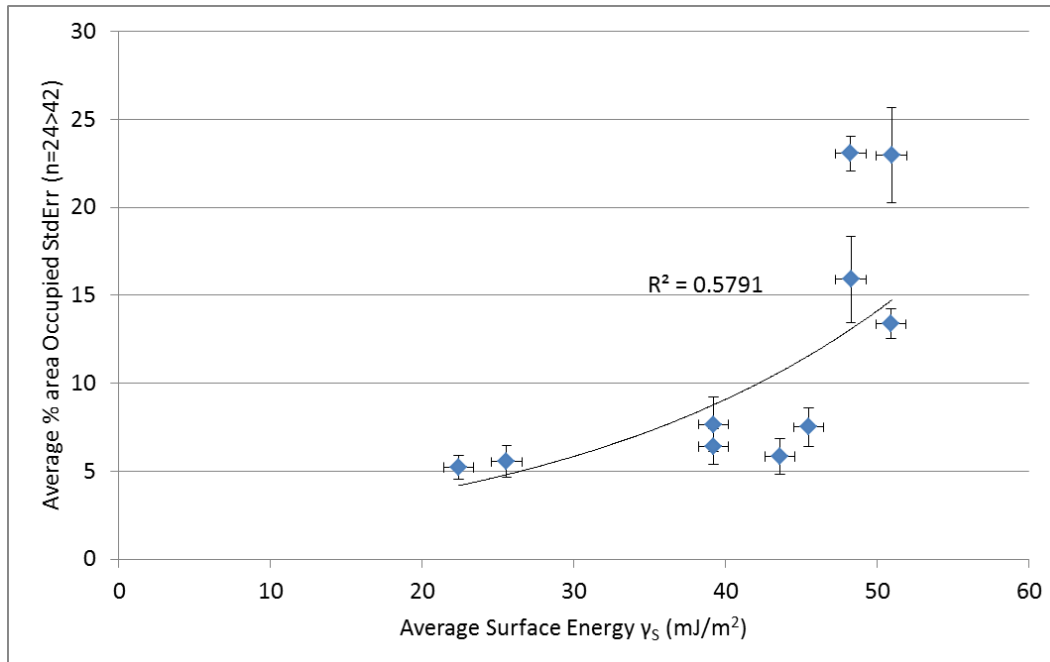
Figure 6.3. Initial binding assay results versus substratum total surface energy γ_S.

6.1.1 Discussion - Initial Binding Analysis of *Pseudomonas* on Rough and Smooth Coupons

Upon examination of the data, it is evident that all of the metal coupons tested showed enhanced binding, with approximately 3x more *Pseudomonas* on these substratums when compared to the polymers. PC smooth relative to 316 smooth showed a reduction in initial microbial binding of some 72 percent. Both smooth metal variants, showed increased microbe binding, when compared to rough metal surfaces; no statistical difference between 304 and 316 stainless steel was observed (Figure 6.1). No significant differences in *Pseudomonas* binding was observed between the different polymers. However, all rough polymer variants exhibited slightly higher microbe area occupancy then the same smooth polymers; these differences where small and are not statistically significant (Figure 6.1).

Upon examining the relationship between *PA* percentage area occupied and average surface roughness (R_a) (Figure 6.2), it is clear that no relationship exists, also this lack of correlation has been reported by many authors (Barnes et al., 1999), (Guðbjörnsdóttir, 2005, Hilbert et al., 2003,

Mueller et al., 1992, Tide et al., 1999), and is discussed at length in Section 1.20.2. Following the removal of the two most apparent outliers in the data (Figure 6.2 - outliers indicated in red), still no apparent correlation is evident. An interesting side note is that these possible outliers (from a hypothesised roughness correlation) are both metals (316-SC and 304-SC stainless steel), which coincides with previous observations in the literature of a loss of roughness correlation (Barnes et al., 1999), (Guðbjörnsdóttir, 2005, Hilbert et al., 2003, Mueller et al., 1992, Tide et al., 1999) with metal substratums specifically, this is discussed in Section1.20.2. A slight positive correlation (Figure 6.3) was observed with γ_S. This correlation is further discussed in Chapter 6.6, following the addition of further experiments where modifications to some of the substratum further extend the dataset, giving stronger apparent correlations.

6.2   Initial Binding Analysis of *PA* on Modified Coupons– Thin Films

The aim of this experiment was to evaluate the response in initial binding of *PA* to previously reported materials following the modification of some the surfaces.

The surfaces selected for modification were smooth 316 stainless steel, smooth polycarbonate, and smooth PTFE. These were selected because they covered a range of roughness's and surface energies, that following modification may yield interesting *Pseudomonas* initial binding observations.

Modifications to the surfaces include the addition of a 30nm thin film of gold to PC and PTFE, which would result in a lower hydrophobicity, and the addition of PTFE-AF thin film to 316 stainless steel which would increase the coupon's hydrophobicity. For details of these modifications see Chapter 4.5.

Figure 6.4. Initial binding assay results for thin film modified substratums. Red boxes group relevant unmodified substratum with appropriate thin film modified substratum.

Figure 6.5. Percentage difference of microbial binding relative to control for thin film modified substratums. Red boxes group relevant unmodified substratum with appropriate thin film modified substratum.

6.2.1 Discussion - Initial Binding Analysis of *Pseudomonas* - Modified Coupons and Thin Films

The smooth 316 stainless steel coupons yielded initial binding data consistent with the previous set of experiments; at 22 and 23.5 percent surface area occupancy respectively (Figures 6.1 and 6.4). This consistent behavior is also true for both PC smooth (6 percent, and 6.5 percent surface area occupancy respectively), and PTFE smooth 6 percent and 7.8 percent surface area occupancy, respectively, (sees Figure 6.1 and 6.4).

Gold coating of the 316 stainless steel coupons gave similar *PA* initial binding data to the uncoated materials; 22 percent surface area occupancy. However, a significant increase in cell attachment was observed for gold coated PC, exhibiting a 74 percent increase in microbial retention (see Figure 6.5). This increase in *PA* initial attachment to PC appears related to increases in both γ_S (44 percent increase) and γ^d_S (22 percent increase). No significant effect was detected when gold coating the PTFE coupons (see Figure 6.4), even with large detected increases in γ_S (Table 4.3

and Table 4.4). This lack of *PA* binding response maybe due to the surface of the PTFE being considerably rougher than that of the PC (628.8nm vs 49nm respectively) which could have resulted in the up even distribution of the gold thin film.

A large effect was detected following the deposition of PTFE-AF on 316 smooth coupons. In this instance a decrease of 88% *PA* binding was detected (see Figure 6.5). The decrease in *PA* was found to relate correspond the relative decrease in all three surface energy metrics (γ_S = 66.4, γ^d_S 46.7 and γ^p_S 96.8 percent).

It can be concluded that the metal or polymeric nature of the substrate surface on which the microbes attached is clearly a factor in the extent of initial microbial attachment, and that surface energy metrics appear important in the amount of *PA* attachment after 30 minutes.

6.3 Initial Binding Analysis of *PA* - Modified Surfaces and Topographically Engineered Polymers

The aim of this experiment was to evaluate the initial binding response of *PA* for a series of modified coupons, including two commercial engineered materials. There are:

- Polypropylene surface (NILT)
- Sharklet^{TM} substratum.
- SilWet surface modified substrates (air dried and freshly dipped)

316-SC stainless steel coupons were selected as a positive control reference and were used as the base substrate for all three modifications. A negative control for NILT and Sharklet^{TM} was included (Syto$^®$9 stain, no *PA*, see Figure 6.6). For details of these modifications see Chapter 4.5.
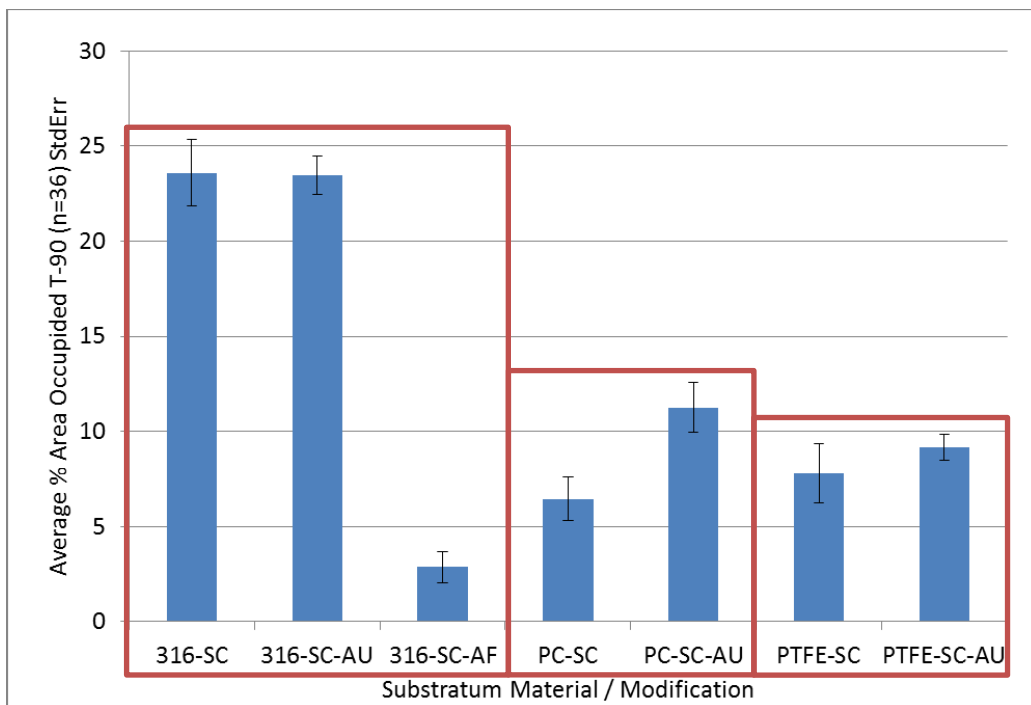
Figure 6.6. Initial binding assay results for modified 316-SC substratums. Red boxes group relevant unmodified substratum with appropriate thin film modified substratum.
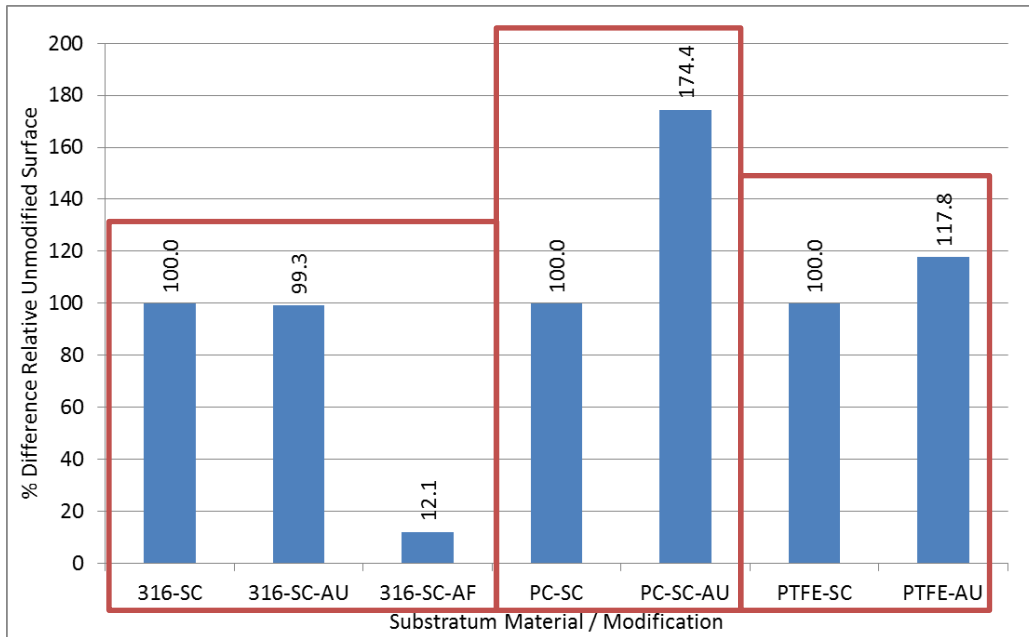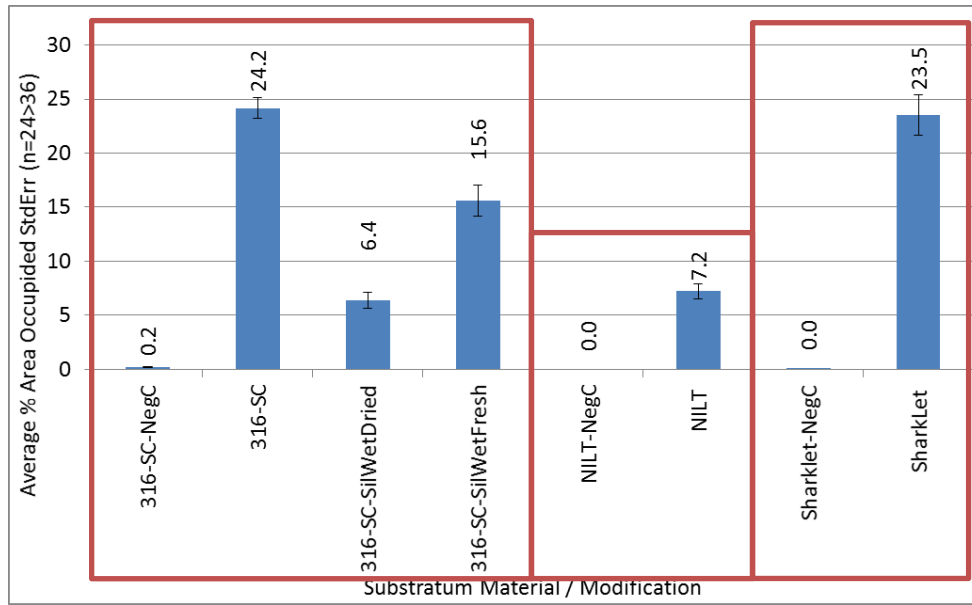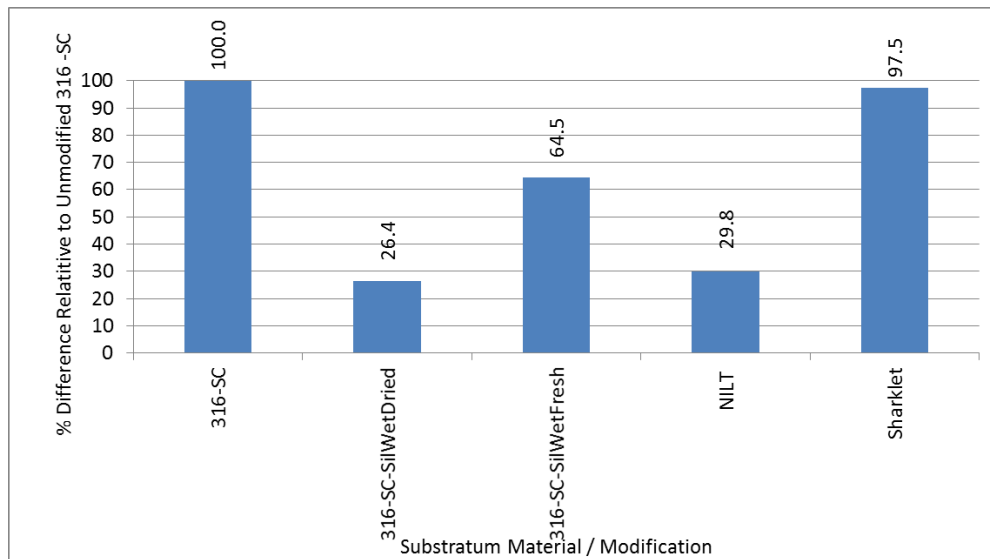

Figure 6.7. Percentage difference of microbial binding to modified 316-SC and engineered substratums.

6.3.1 Discussion - Initial Binding of *Pseudomonas* on Modified Surfaces and Topographically Engineered Polymers

The 316-SC set of positive control replicate set (Figure 6.6) compared to previously conducted experiments (Figure 6.1 and Figure 6.4) are in very good agreement, further validating this assays reproducibility across experiments reported.

Both Silwet preparation methods (pre-dried and freshly coated) on 316-SC stainless steel yielded a decrease in microbial binding relative to the negative control, with a 75 and 35 percent decrease respectively. However, during these experiments it was evident that the Silwet was partially (visually) leaching from the surface, thus the effectiveness of this film on the binding of *Pseudomonas* is complicated by the behavior. However, independent work investigating the binding and subsequent growth of both *Staphylococcus* and *Pseudomonas* on Silwet modified stainless steel showed a small positive effect, when compared to negative controls when cultured in a CDC reactor (Biomed, 2016a).

The NILT polypropylene substratum exhibited lower binding than 316-SC, by 70 percent (Figure 6.7). However, these levels of binding observed, when compared to that of unmodified PTFE and unmodified polycarbonate appear to be quite typical and fall within the polymer binding range of 6-11 percent surface area occupation, suggesting the engineered nature of NILT is ineffective in this specific liquid based application (comparison of Figure 6.1 and Figure 6.6).

The Sharklet^{TM} micro-engineered surface was surprisingly good at facilitating the attachment or trapping of *Pseudomonas*, to its surface, and was similar to that of standard 316-SC stainless steel. This poly(dimethylsiloxane) substratum is by far the worst of the polymers tested in this study, which was quite unexpected; given it has very low γ_S of 22.5mJ/m^2, similar to that of PTFE-AF coated stainless steel and PTFE. Previous research on attachment to Sharklet^{TM} substrates involving *Staphylococcus aureus* has shown decreases in microbe attachment following the engineering of the pattern relative to plain flat poly(dimethylsiloxane), in TSB media as performed here. One significant difference being these experiments were conducted in non-static fluid environments (petridishes on a rocker for 21 days (Chung et al., 2007). The poly(dimethylsiloxane) material has similar γ_S reported herein to that of the literature 22.5mJ/m^2 of 15.7 to 23.0mJ/m^2 (Oxford University Press, 1999) respectively. Ergo, one would expect similar bio adhesion performances, if accepting the Baier surface energy-bio-adhesion hypothesis

detailed in Chapter 1.20.1. One hypothesis is that the engineered topographical features are approaching the size of the microbes themselves (0.5-0.8 x1.5-3μm) (Todar, 2013a), and so the microbes maybe becoming physically trapped which would reduce the rinsing efficiency of the assay. This observation has been previously observed by Tebbs, Flint and Whitehead (Tebbs et al., 1994, Flint et al., 2000, Whitehead et al., 2005), whereby surface topographical features that approached the size of the microbes appeared to enhance attachment or entrapment. This would also explain why there are larger numbers of microbes present just above the surface (Figure 6.10), as they dislodge from within the topography and swim about in the bulk. The cause of the high binding to the Sharklet™ remains at this stage a point of debate.

6.4 Spatial Distribution of *Pseudomonas* on NILT Coupons

Due to the apparent three dimensional structure of the engineered NILT substratum, as detailed in Chapter 1.27.3, a further experiment in addition to the initial binding assay was performed, whereby the spatial distribution of the microbes contributing to the total approximate 7.2 percent area occupied (reported in Figure 6.6) was determined.
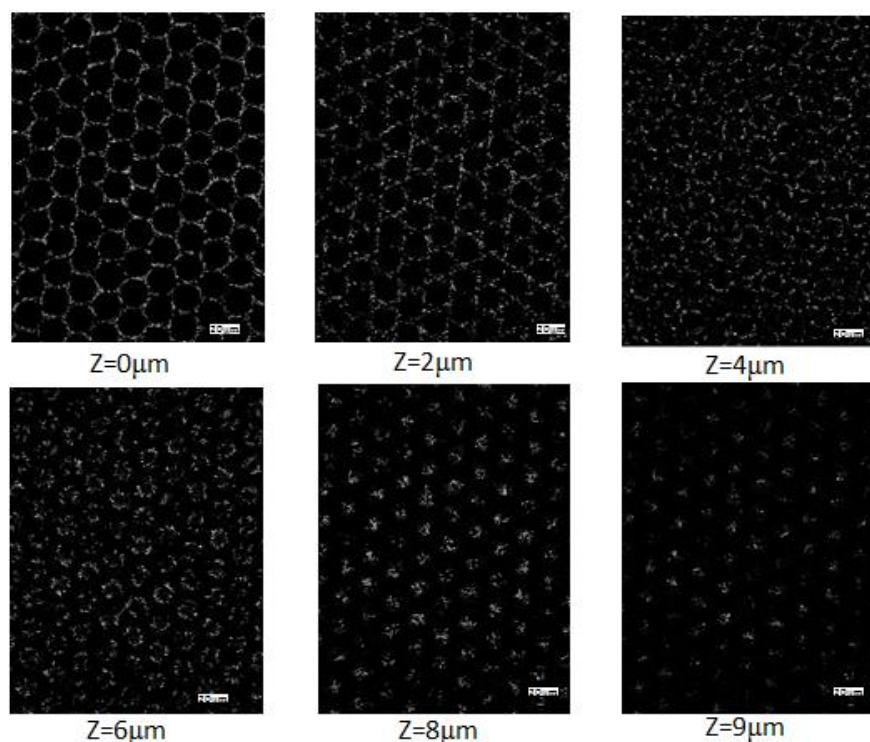
Figure 6.8. Raw data images of NILT taken using confocal laser scanning microscope (1μm dz, 1μm step height) using 25x lens, following 30 minute incubation with *PA*.

177
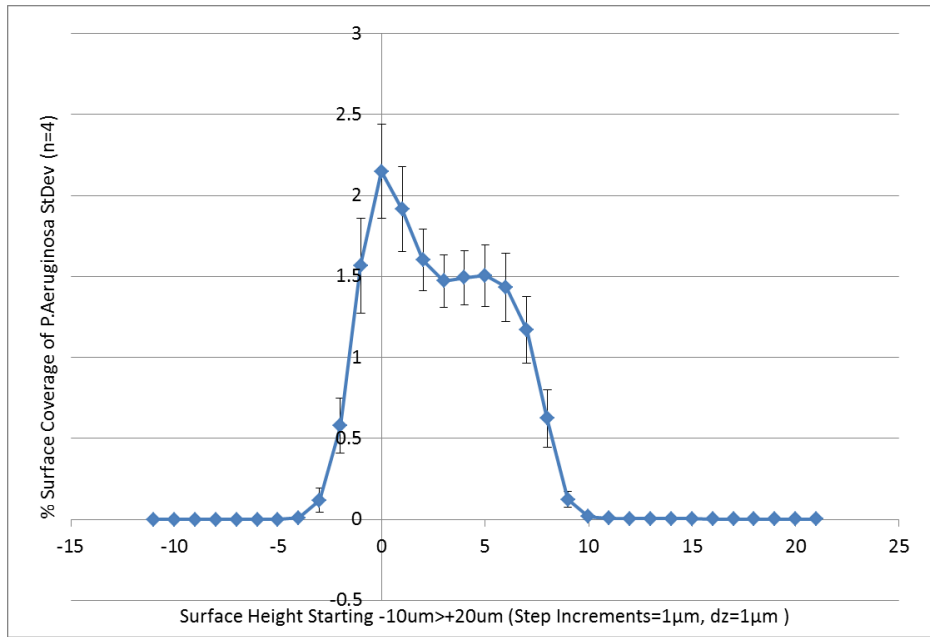
Figure 6.9. Initial binding assay for *PA* on NILT substratum

The results presented in Figures 6.8 and 6.9 confirm the micrometer structure of the NILT engineered surface, with the convex lens topography having an approximate diameter of ~20µm, and a height of -10µm as stated in Chapter 1.27.3. These dimensions were determined indirectly by examining the immobilized stained pattern of the surface attached *PA*. It is also noteworthy that, no significant signal was detected above the substratum (or below), which indicates that the rinsing method employed is effective and only the attached microbes of interest are being visualised.

Interestingly, *PA* appears to occupying the entire surface including the inter-convex lens regions, with a higher number of *Pseudomonas* found in these regions attached to the surface. These numbers then decrease, with increasing height, before reaching a plateau, representing the microbes attached to the slopes of the convex-lens, then the numbers drop off entirely once scanning above the surface topographical features. These observations whilst interesting, also confirm the non- flat (Wenzel-like) material wetting behavior (Figure 1.41), as the microbes are occupying all available surface area of the substratum topography, including the deep valleys, that would have been unoccupied if Cassie-Baxter wetting was occurring.

6.4.1 Discussion –*PA* Attachment to NILT Substratum

A careful examination of the topographically engineered NILT surface revealed an increase in the quantity of *Pseudomonas* that are found in the valleys of this textured material. Upon closer inspection it was observed that higher microbial masses were found to settle in the lowest areas (Figure 6.9). The NILT surface exhibited Wenzel wetting wherein the liquid probes in contact exhibit a large contact angle hysteresis due to surface roughness (see Figure 4.28). In addition the liquid probes were observed not to slide off these types of surface when the substrate was inclined.

The NILT substratum has been independently shown to be readily colonised by both *PA* (Figure 6.16) and *Staphylococcus aureus*, which was reported for both laminar and turbulent flow regimes (Biomed, 2016b). This behavior was also reported for stainless steel coated with Silwet thin films following both 24 and 72 hours of microbial growth (Biomed, 2016a).

Pseudomonas aeruginosa on NILT
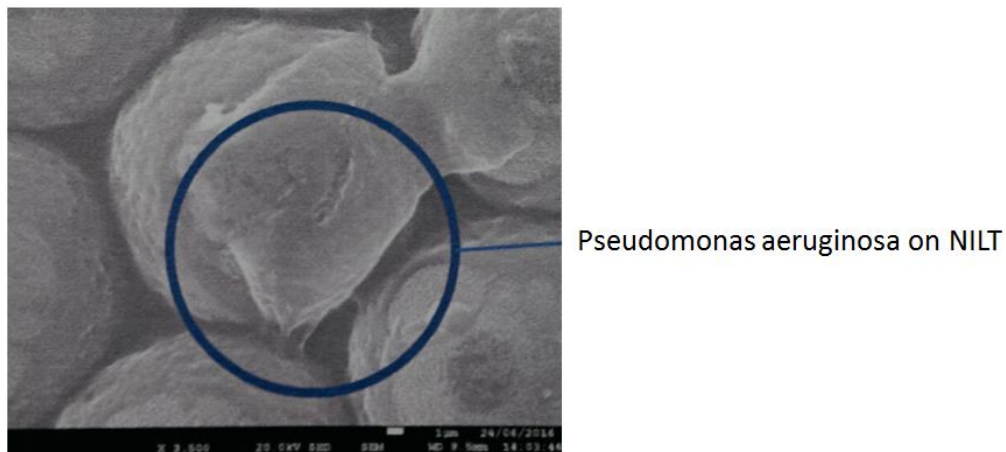
Figure 6.16. SEM of *PA* biofilm on NILT micro-engineered surface. Modified from (Biomed, 2016b)

6.5 Spatial Distribution of *Pseudomonas* on Sharklet[TM] Substratum
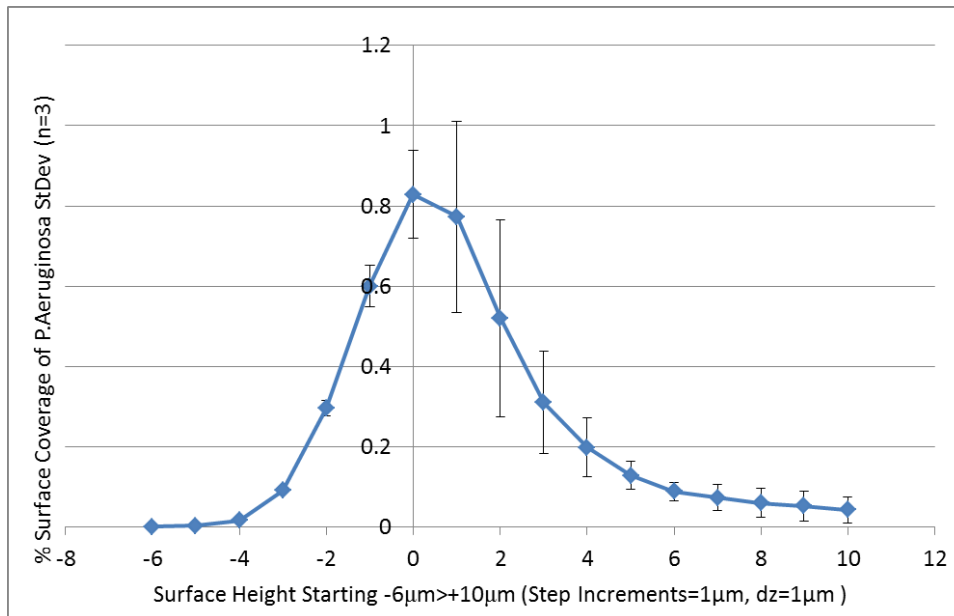
Figure 6.10. Initial binding assay of *PA* on Sharklet[TM]

The results from Figure 6.10 confirm the reported height of the Sharklet[TM] surface features, which are stated to be approximately of 3μm in height (Chung et al., 2007). It is noteworthy that, a decreasing microbe signal was detected above the substratums 3μm, which was higher than observed with NILT. This may initiate the slow detachment or dissemination of the microbes from the surface over time.

6.6 Main Discussion–Initial Attachment of *PA* and Surface Energy Components

Throughout all of the *Pseudomonas* initial binding experiments, a standard control substratum has been used; 316-SC. This control substrate was to ensure consistency across the experiments, which was very reproducible (average 22.3 percent, StdDev 7.21, StdErr 0.77 n=87). This result coupled to the relatively low negative control background surface reflectance and fluorescence (Figure 5.2) and the quantitative nature of the assay, when compared to a

standard plate counting method, validates the robustness, and reliability of this initial attachment assay.

Of interest is the observation of some authors (Flint et al., 2000, Boulangé-Petermann et al., 1997, Guðbjörnsdóttir, 2005, Barnes et al., 1999) who have reported a high degree of microbe attachment to both 304 and 316 stainless steel compared to other metals and polymers, for example those observations made in Figure 1.17. This work suggests that stainless steel, from an initial attachment perspective, should not be the material of choice in process applications or public areas where there is a desire to have less microbes present.

Substrate roughness do not appear to have a significant effect on microbe binding. This is evident from the scatter plot of all tested substratums (Figure 6.14) where no correlation between average surface roughness (R_a) and initial microbial attachment was detected (R^2 of 0.07). A similar observation was made by Li and Logan (Li and Logan, 2004), who reported an R^2 of 0.14. This work is highly suggestive that the role of surface chemistry is far more important than the surface topography where initial *PA* attachment is concerned. Only slight increases in initial microbial binding was detected for the polymers with increases in coupon roughness, but these were not significant (Figure 6.1). This trend was not the case for 316 and 304 stainless steel. For these materials increased *Pseudomonas* binding on the smooth surfaces was observed, in comparison to the rough variants. This observation however seems counter intuitive (see Figure 6.1). The relative unimportance of roughness in the attachment of microbes to surfaces has been widely reported experimentally in the literature for a range of substrate roughnesses:

- 0.1 to 0.8µm (Barnes et al., 1999, Guðbjörnsdóttir, 2005)
- 0.01 to 0.9µm (Hilbert et al., 2003)
- 0.002 to 0.015µm (Mueller et al., 1992)
- 0.08 to 0.25µm, 0.5 to 3.3µm (Pereni et al., 2006)
- 0.1 to 3.2µm (Flint et al., 2000)
- 0.01 to 1.0µm (Boulangé-Petermann et al., 1997)

These studies substantiate the observations reported herein, that across the average surface roughness (R_a) range covered in this report from 0.049 to 3.49µm there was no correlation between roughness and microbial attachment. But as discussed in Chapter 1.20.2, substratum roughness maybe relevant in surface cleaning efficacy.

It is also noteworthy that all of the polymers tested yielded very similar *Pseudomonas* initial binding results. This observation was somewhat unexpected, given that PTFE has almost half the total surface energy of both PC and PE, therefore the PTFE substratums should have significantly less *PA* attached; but this was not the case. This observation has also been reported in the literature by others (Gottenbos et al., 2000), where a range of polymers including PE, PMMA, PP and PTFE all yielded similar initial attachment results. However, *Pseudomonas* PTFE-AF colonisation was lower as evidenced by the lower initial attachment levels observed (Figure 6.4).

Following the coating of a 30nm gold film on PTFE-SC, PC-SC, and 316-SC coupons resulted in surface energy increases however, minimal differences in the microbial initial binding was detected in both gold coated PE-SC, and 316-SC. This trend was not the case for PC; where by an increase in microbial binding of 74 percent was observed.
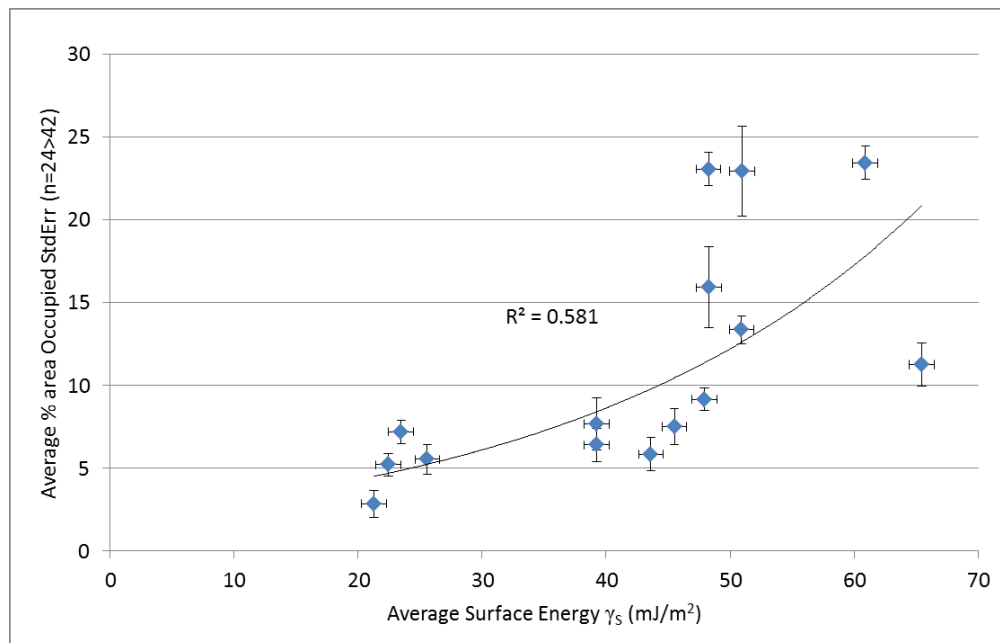
Figure 6.11. Percentage area occupied versus total surface energy γ_S
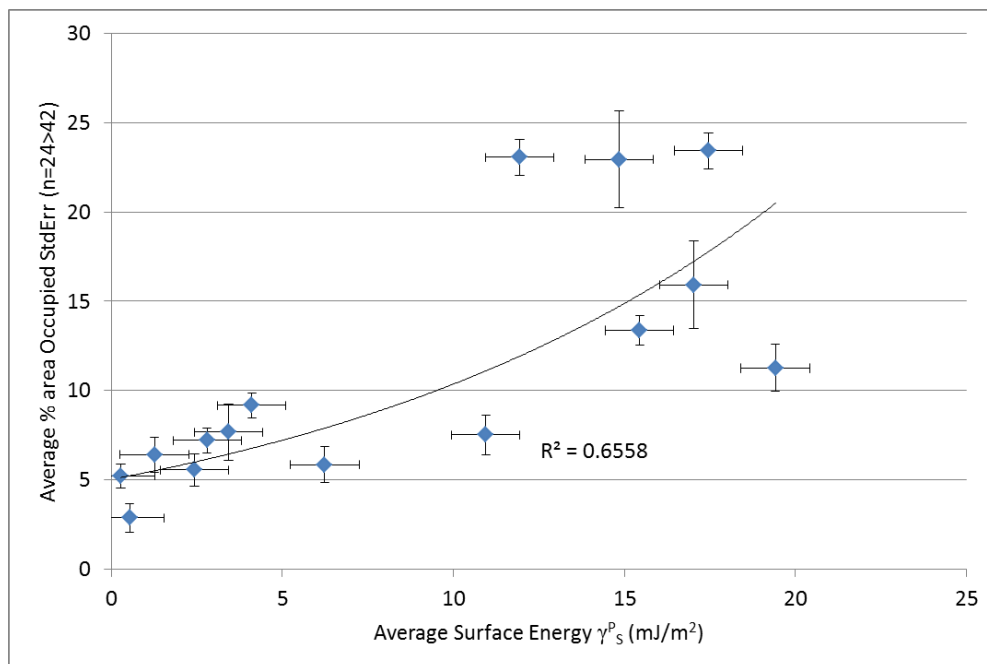
Figure 6.12. Percentage area occupied versus polar surface energy γ^p_S
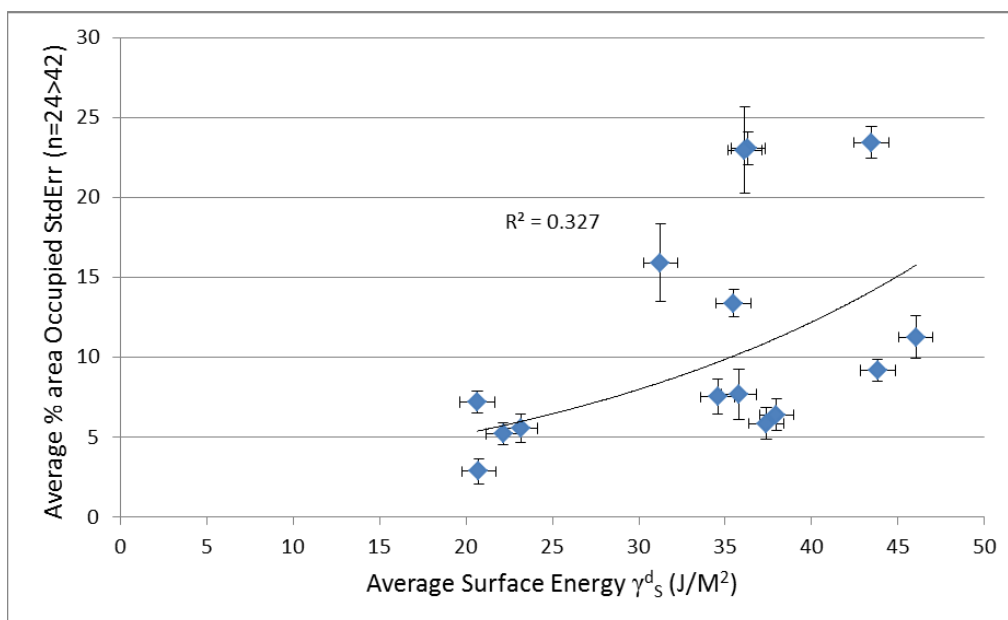
Figure 6.13. Percentage area occupied versus dispersive surface energy γ^d_S
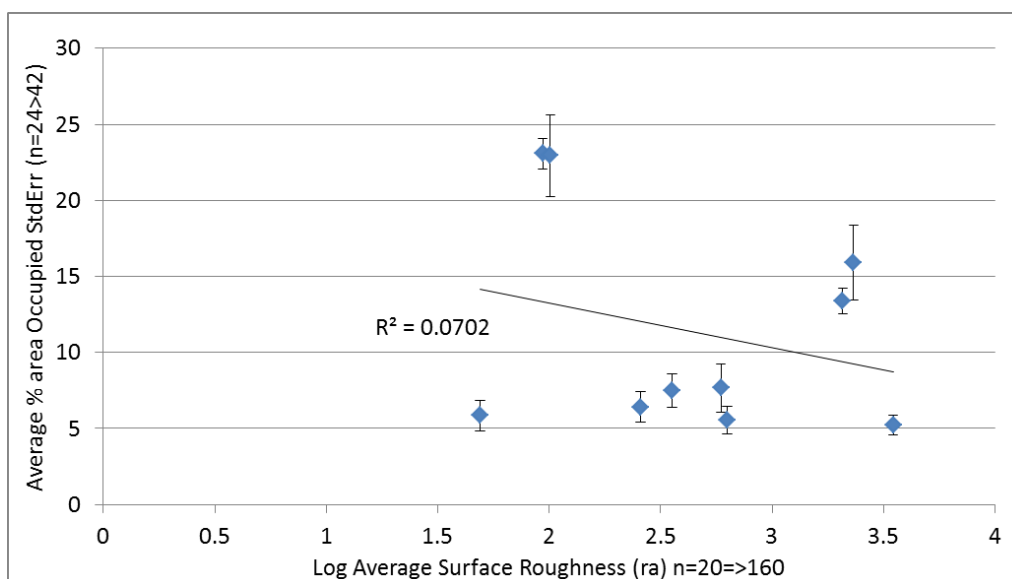
Figure 6.14. Percentage area occupied versus log average surface roughness (R_a). The role of

Increases in both γ_S, and in particular the γ^p_S component, did enhance initial microbe binding. A global analysis was performed on all of the data which generated a correlation of P=<0.001, R^2=0.581 of and P=<0.05, R^2=0.655 respectively for γ_S, and γ^p_S, see Figure 6.11 and Figure 6.12. A much weaker correlation (P=0.07, R^2=0.327) was detected with γ^d_S (Figure 6.13). This suggests that although the γ^d_S energy values are higher than the γ^p_S energy values, the short range polar (chemical, acid-base) specific interactions seem to be more important for microbial adhesion.

A significant discovery of this current work was the effect on *Pseudomonas* initial attachment on 316-SC following the deposition of the PTFE-AF thin film. 316-SC was used as the standard surface in these experiments due to its consistently high and reproducible initial microbe binding levels of approximately 24 percent occupancy. Following PTFE-AF deposition 316-SC exhibited only 2.5 percent initial *Pseudomonas* binding; a 10 fold decrease in binding relative to the base material. This observation requires some explanation. Firstly, 316-SC prior to modification exhibits a γ_S of 48.3mJ/m^2, consisting of γ^p_S 11.9 mJ/m^2 and γ^d_S 36.3 mJ/m^2. By examining Figures 6.11

184

and Figure 6.12, it is evident that the total surface energy, and moreover the polar component that are the principle surface variables that drive the initial attachment of *PA* on the substratums. It is these two factors that are greatly altered following PTFE-AF thin film deposition, becoming a γ_S 21.3 mJ/m² and γ^p_S 0.5 mJ/m². Thus, the hypothesis behind the 88 percent observed decrease in binding of *Pseudomonas* is primarily due to the decrease in the polar surface energy component γ^p_S of the substratum, though there is also a link to the total surface energy γ_S. Indeed, as discussed in the introduction (Chapter 1.20.1) many authors have reported a strong substratum γ_S -bio-adhesion attachment correlation, with one team reporting a correlation of $R^2=0.94$ with *Pseudomonas* (Pereni et al., 2006).
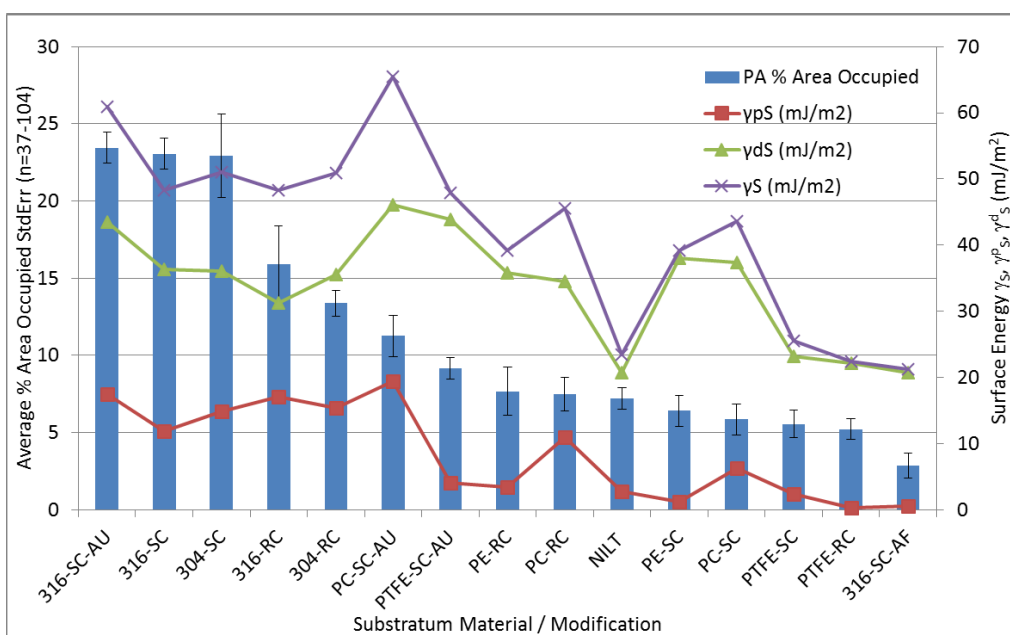
Figure 6.15. PA initial binding data (percentage area occupied) compared with substrate surface energies γ_S, γ^p_S, γ^d_S.

Two interesting observations arose following the global analysis shown in Figure 6.15.

- Following the gold coating of either steel or polymers substratums, a detectable increase in the attachment of *Pseudomonas* to both those materials. This point was more evident in the gold coated polymers, for example both PC and PTFE, as they became more 'metal like' i.e. increases in the *PA* initial binding results were found.

185

- Conversely, the addition of the PTFE-AF thin film resulted in 316-SC exhibiting, not surprisingly, more polymer like behavior from a microbial binding perspective.

CHAPTER 7   Microbial Biofilm Growth Assay Validation
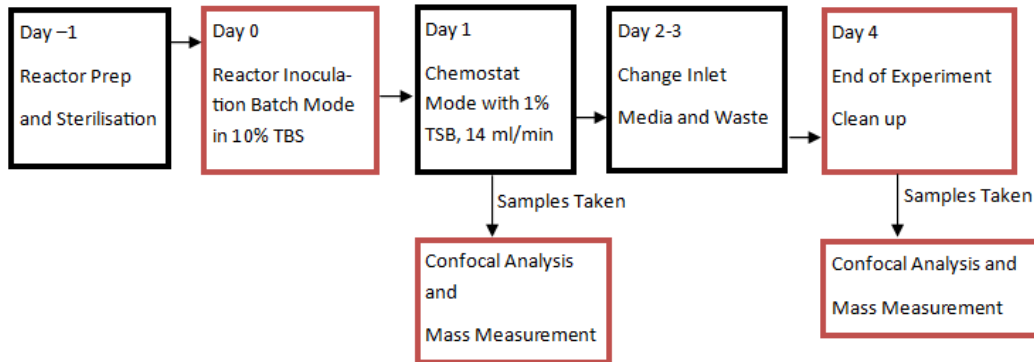
Figure 7.1. Diagram of microbial biofilm growth assay. Inoculation of the CDC was via a dissolved *PA* Bioball™.

This microbial growth assay was designed to provide not only the overall biofilm mass, but also changes in gross biofilm morphology. Morphology in the context of this assay refers to changes to the abundance in 3 major biofilm constituents. Namely microbial abundance (Syto®9), polysaccharide abundance (ConA), protein abundance (Sypro®) and the sum of all three. The physical parameters obtained for each of these components were:

- biomass thickness ($\mu m^3/\mu m^2$)
- maximum film thickness (μm)
- average film thickness (μm)

These parameters were determined by analysing the confocal image data sets using *Comstat 2.1* software (see Chapter 1.31). These parameters gave spatial information on the relative distribution of the biofilm components of interest which were then related to the known surface properties on the test coupons used.

Microbial biofilm assays were initially conducted using the Leica SP2 confocal microscope. Two dye combinations were used for simplicity; Syto®9 green stain with Sypro®, and Syto®9 green with Alexa 633-Fluor® Concanavalin A (Figure 2.5). Depending on the experiment, a sample would be taken at day 1 (as indicated in Figure 7.1), to investigate the initial colonisation of the surface

understudy, or only at the end of the experiment on day 4 (Chemostat mode post 72hr). Later experiments utilised the more advanced Leica TCS SP8 confocal microscope where a single dye combination experiment using Syto®9, Alexa 633- Fluor® Concanavalin A, and Sypro® in PBS was possible (Figure 2.5-2).

Typically a step height increment of 1µm was used to elicit biofilm component spatial detail with a dz of 1µm (see Eqn. 6 and Appendix B for calculations).

7.1 *PA* CDC Reactor Growth Curve

Before conducting CDC reactor experiments, where the growth of biofilm on the coupon surface was to be measured, the growth rate of the organism needed to be ascertained in a planktonic culture. This determination was to ensure that the dilution rate used during the CDC chemostat experiment stage was greater than the cellular dividing time. This ensures that the chemostat (continuous addition and removal of fresh/waste media respectively) phase of the CDC reactor experiment is principally allowing growth of pre-deposited microbes on the surface during the batch phase, and that they are not being continuously growing and being re-deposited from the reactor bulk.

9ml of TBS in a 20ml universal container was inoculated in *PA* and incubated at 32.5ºC overnight, in anaerobic conditions. This inoculum was then used as seed for a sterile CDC reactor containing 350ml 1%v/v TSB, which was pre-warmed to 32.5ºC overnight. The inoculated CDC reactor was incubated at 32.5ºC at 174rpm. Samples were regularly taken and the OD@600nm noted.
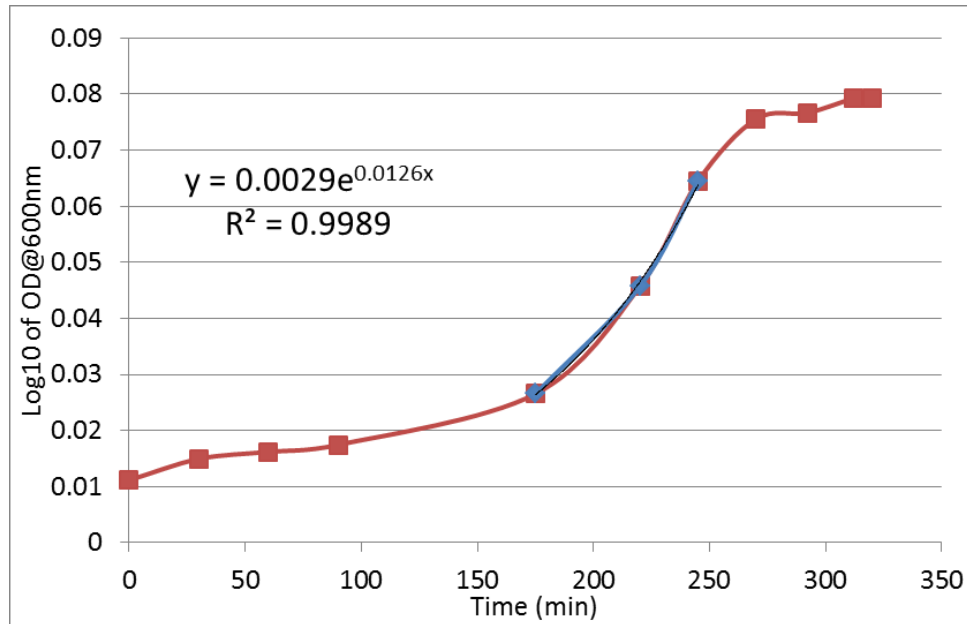
Figure 7.2. *PA* growth curve in CDC reactor. R^2 and exponential equation are relevant to the exponential part of the curve only.

Using the above data the doubling time of the bulk culture was calculated to be approximately 50 minutes, when growing the bacteria at 32.5°C in 1%v/v TSB at 174rpm in a CDC reactor. Thus, an inlet/out let flow rate corresponding to a dilution rate greater than this time was used. A flow rate in all experiments during the chemostat stage was 14ml/min, corresponding to a 1:1 dilution every 24 minutes.

7.2 Negative Control for the Mature Biofilm Growth Assays using Confocal Microscopy

Initially the substratum coupons were stained using the appropriate dye in the absence of microbes. The staining procedure used was dependent on the microscope used, see Figure 2.5. This control experiment checked both background surface reflectance and probe surface anomalies that could give rise to false positives, and would possibly be used for future subtraction, from biofilm growth or biofilm removal data.

189

It is important to remember that during analysis an auto threshold function (Otsu's thresh-holding) was used, and that should any probe-substratum interaction be even faintly detectable, given the absence of bright sources, such as the target microbes, or biofilm components, these low fluorescent and/or reflective signals will disproportionately skew the negative control. Given the nature of these experiments, where different thicknesses of biofilm will result, these cannot be corrected for, i.e. subtracted. But these negative controls remain an important reference point during the removal of biofilm in later experiments, where the removal of the probe target in cleaning experiments, are replaced by the weak signal background of the surface, which could be considered a null surface. All of the extensive results from these control experiments are given in Appendix D.

7.2.1 Biofilm Component Probe Negative and Positive Control

The aim of this control experiment was to determine whether the excitation/emission wavelengths used in this project resulted in auto-fluorescence from any of the components of *Pseudomonas* biofilm, of course without the addition of the staining probes. But following the addition of the confocal probes (see Figure 2.5-2) to observe the fluorescent signal being recovered, on the very same biofilm unstained biofilm.

A *Pseudomonas* biofilm was cultured using the standard method stated in Chapter 2.17 in a CDC reactor on a standard 316-SC stainless steel coupon. The coupon containing a 'mature' biofilm was harvested at +4 days (see Figure 7.1). The sample was then rinsed using the standard protocol, but not stained. The biofilm was immediately imaged using the Leica TCS SP8 microscope. The very same sample was then stained using the stain protocol 2 (Figure 2.5) and then imaged again.
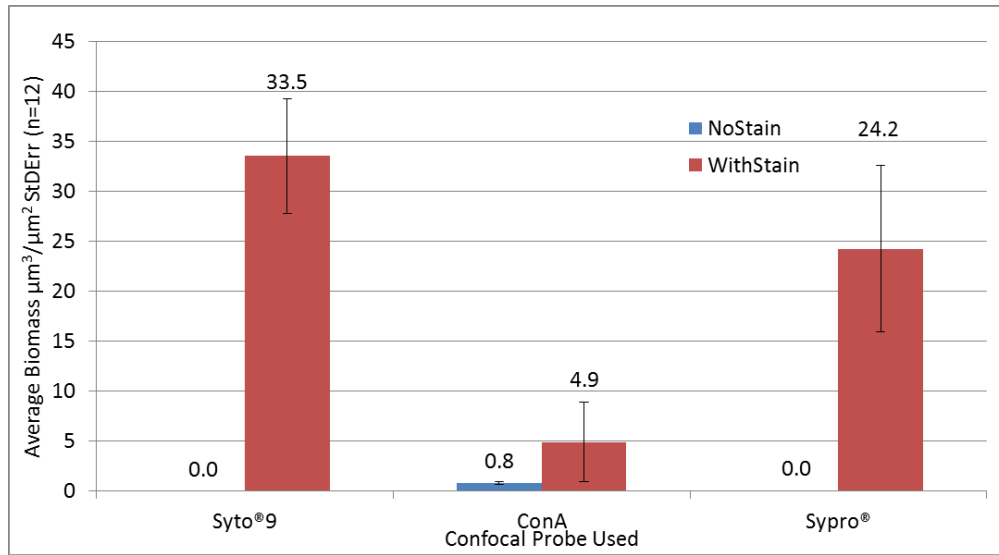
Figure 7.3. *Pseudomonas* biofilm confocal probe negative and positive control for average biofilm biomass
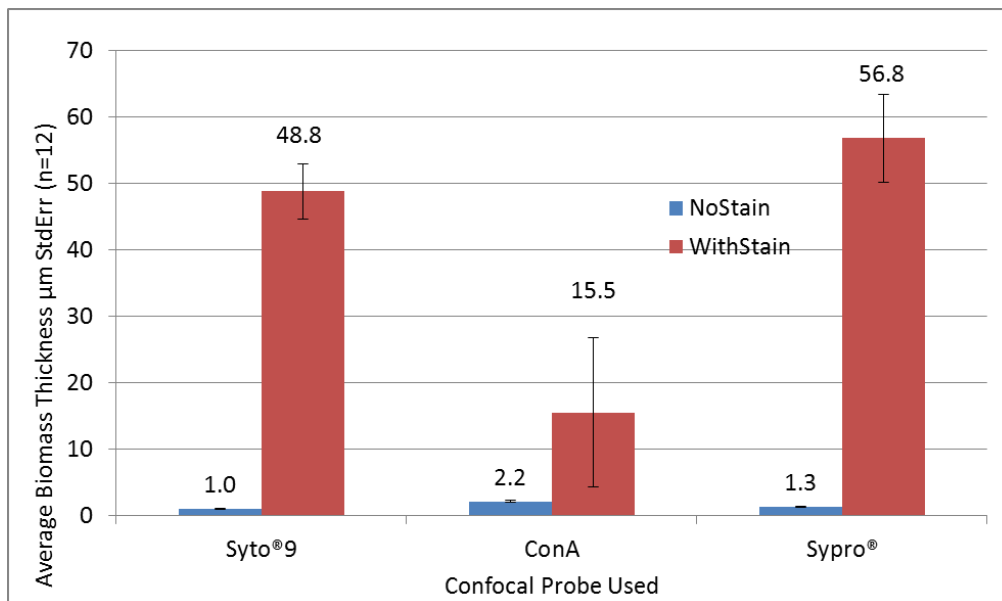
Figure 7.4. *Pseudomonas* biofilm confocal probe negative and positive control for average biofilm thickness
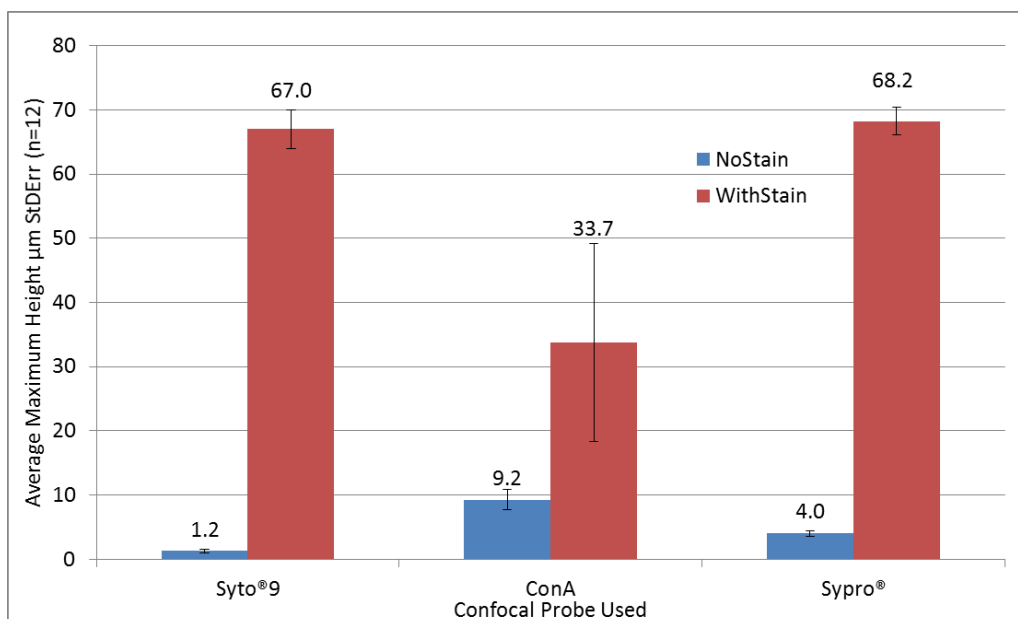
Figure 7.5. *Pseudomonas* biofilm confocal probe negative and positive control for maximum biofilm thickness.

7.2.2 Coupon Physical Mass - Negative Controls

In addition to the confocal film thickness measurement, a direct measurement of the dried biofilm mass was also undertaken. In order to get an accurate mass reading for the dried biofilm for any substratum, a negative control was required for each material, to enable the subtraction of any change in mass due to uptake or loss of water. Each coupon was soaked in 1% TSB for 24 hours, then dried for 2 hours at 100°C, then weighted. Coupons were weighted pre and post treatment.
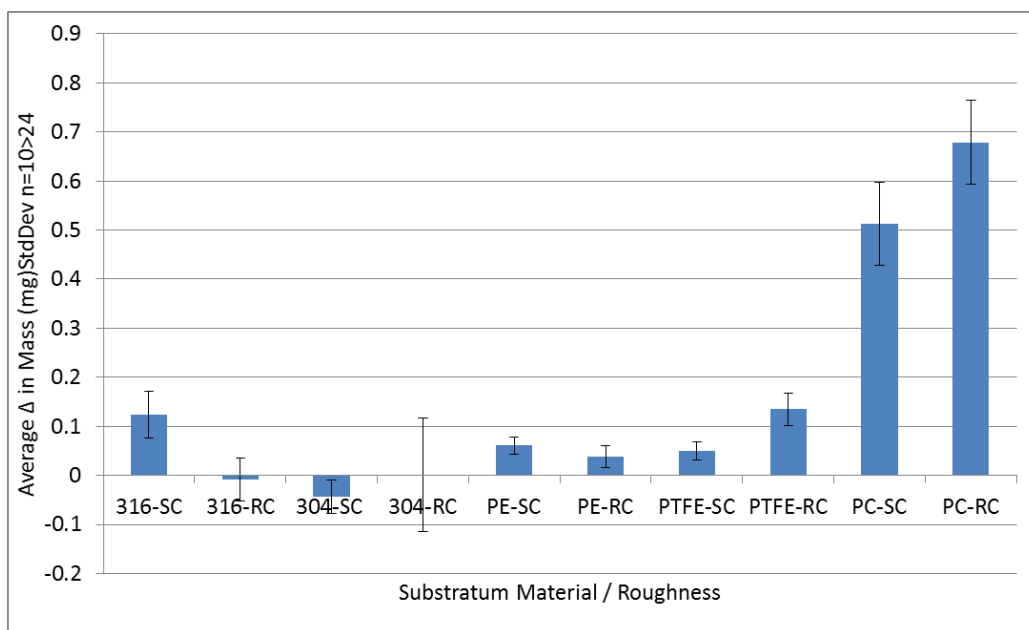
Figure 7.6. Average change in mass (mg) of different substratum negative controls (no microbes), following soaking for 24 hours in 1%TSB, before being dried for 2 hours at 100°C.

7.2.3 Discussion – *PA* Growth Assay Negative Controls

The negative control obtained for the TCS SP2 confocal microscope showed some variability across the different substratums, with the metals showing typically higher readings, which was particularly evident in the biomass thickness metric in the rough coupons of 304 and 316 stainless steel (Figure C1.1). This discrepancy is likely due to a combination of both substrate surface roughness and reflection. Typically the Syto®9 results were consistent between the two different probe configurations (Figure 2.5-1) (comparing Figures C1.1 with Figure C1.4). ConA detection appeared to be more consistent across both materials and detection variables compared to Sypro® on the TCS SP2, but all or some of these 'signals' could be background and are most likely overstated (in the absence of biofilm) given the auto thresh holding used by the *Comstat* analysis software.

As discussed above, these negative controls are only relevant when the substratum is exposed, following a cleaning event. When a biofilm is in place, much of the surface reflectivity was absent, or greatly reduced, thus in these negative control results, output variables (i.e. biomass)

ascertained using the auto-thresholding function may be disproportionally overstated, thus should not be removed from actual biofilm data.

Generally, the difference observed between the negative controls of the two different confocal microscopes was very large (comparison of Figure C1.4 and Figure C1.7). This is due to the removal of much of the reflected light from the sample data, thus increasing measurement of the target fluorescent light, over background reflected light in the newer SP8 instrument. In short the SP8 systems offer much more superior performance.

The negative and positive controls for the biofilm component probes (Figures 7.3 to 7.5) confirm that in the absence of the confocal staining probes, no biofilm auto-fluorescence was observed. None or very little signal was detected from the 316 coupon surface that was analysed and then compared to the positive control. This low level signal that was detected was due to a small amount of residual surface reflectance by the coupon surface. This result confirms that no auto-fluorescence is occurring from the different native constituents of 'mature' *Pseudomonas* biofilm when using the excitation/emission wavelengths used in the standard method.

The change in physical mass negative control (Figure 7.6) shows that with the majority of materials used; their masses are relatively unchanged following immersion in TSB for 24 hours, and subsequent drying, with typically a modest ±<0.1mg change in mass be recorded. This was not true for the PC coupons, where a large increase in mass was detected in the order of 0.5 to 0.6mgs. This larger change in mass simply reflected the relatively large hygroscopic behavior of PC relative to the very hydrophobic PE and PTFE. This change in mass was not likely attributable to the Araldite™ glue used, as this was used in both metal coupons also, where little mass change was detected. During physical mass measurement analysis's, these negative controls will be subtracted from the biofilm mass measurements, yielding the true biofilm mass. It is important to note that the dried physical mass measurements will only give an indication of the mass of the biofilm on the test surface of interest. Unlike the confocal image analysis which will be confined to the particular coupon test surface understudy. Biofilm will by their very nature colonise the entire surface of each 3 dimensional coupon. This will greatly complicate the interpretation of any material in comparative physical mass analyses, due to loss of biofilm in the petri dishes during confocal probe staining and coupon transport and handling, which is unavoidable. In addition to this issue, during high shear cleaning experiments different areas of each coupon, separate from

the test surface will experience alternate shear rates, which could further hamper data interpretation.

Taken together, this negative control grouping suggests that subsequent experimental results would be valid, within the limits of the experiments conducted.

7.3 Reproducibility of Growth of *PA* on 316 Stainless Steel

The aim was to determine whether *PA* growth on a given substratum was reproducible not only within an experimental set, but also over 3 independent weeks. 316 stainless steel was selected because it is widely used in industry and has also been widely used in academic biofilm investigations. Confocal microscope (Leica TCS SP2) with a 63x water immersion lens was used, with a pinhole of 0.5AU giving a dz of 1.2µm, step increments were set to 0.5µm.
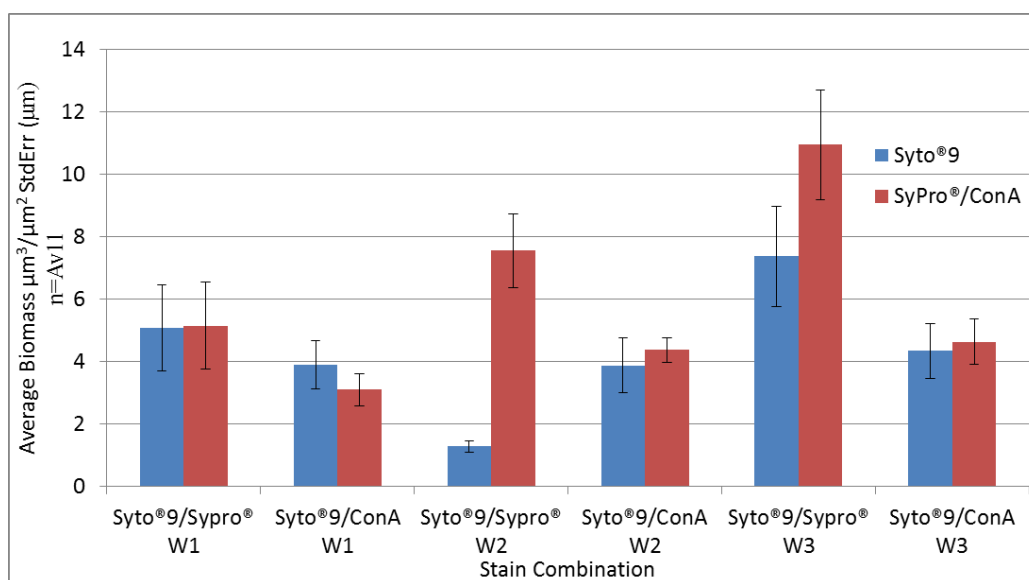
Figure 7.7. Growth of *PA* on 316 stainless steel. 3-4 coupons over 3 weeks. Biomass ($\mu m^3/\mu m^2$) metric shown. W1=week1, W2=week 2, W3=week3. Slashes differentiate red bar as either Sypro® or ConA as appropriate.
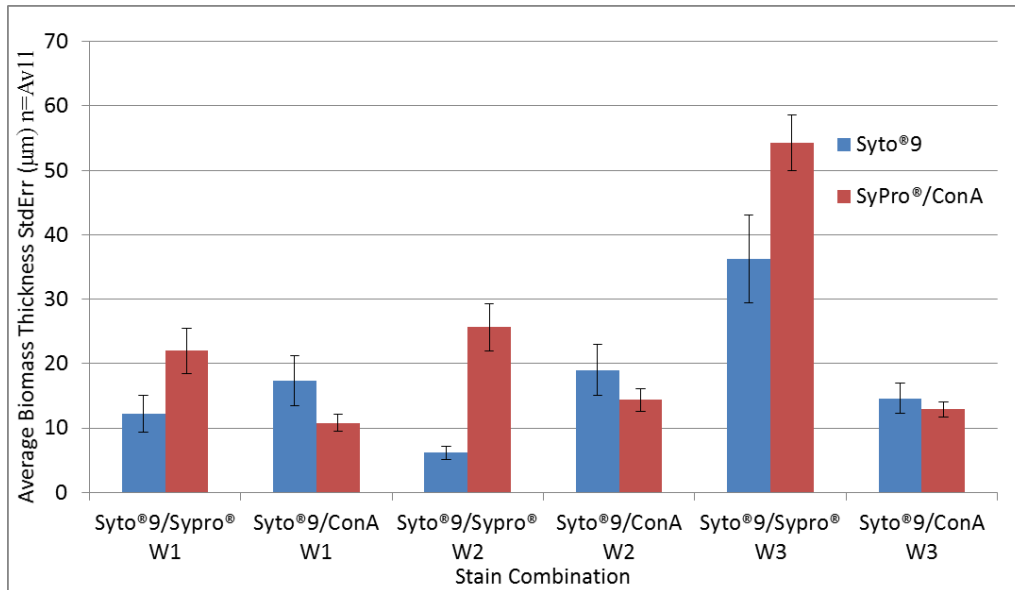
Figure 7.8. Shows the average biomass thickness (µm) for each probe. W1=week1, W2=week 2, W3=week3. Slashes differentiate red bar as either Sypro® or ConA as appropriate.
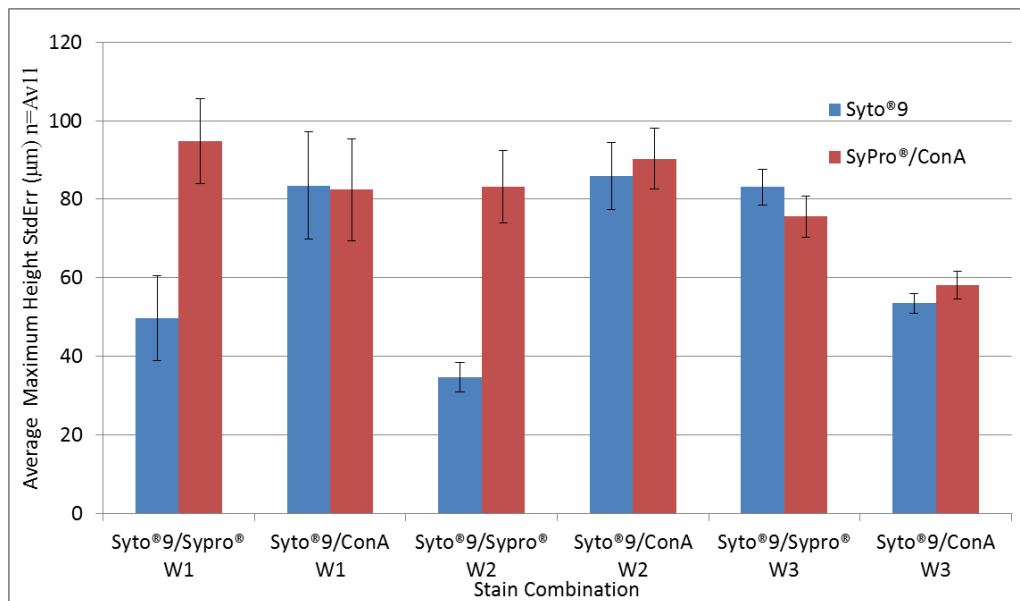
Figure 7.9. The maximum biofilm height (µm) determined for each probe. W1=week1, W2=week 2, W3=week3. Slashes differentiate red bar as either Sypro® or ConA as appropriate.
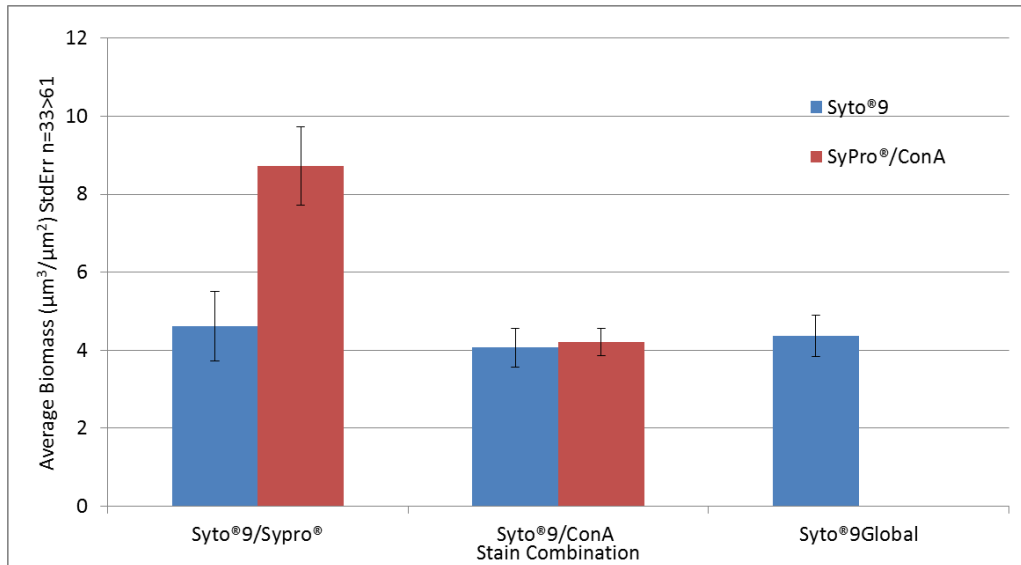
Figure 7.10. Average of all biomass data taken over 3 independently replicated experiments.
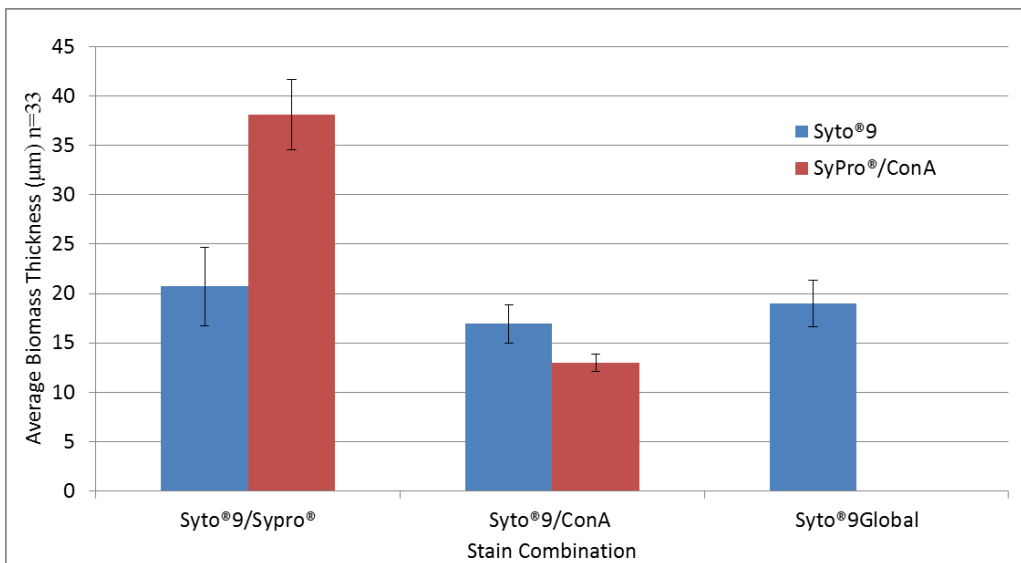
Figure 7.11. Average of all average biomass height data taken over 3 independently replicated experiments.
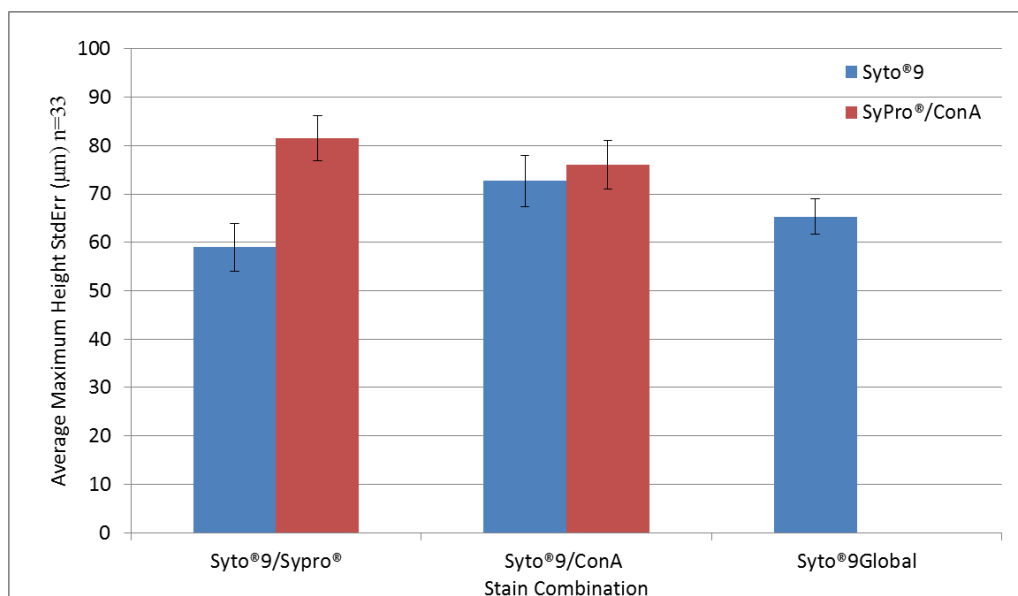
Figure 7.12. Average of all maximum height data taken over 3 independently replicated experiments.

7.3.1 Discussion – *PA* Growth Assay Reproducibility on 316-SC Stainless Steel

Some week to week variability was detected in the data, however, given the complex nature of biology, this variation was not unexpected (Figure 7.7). ConA data appeared to have the lowest inter experiment variability, and was statistically indifferent across the output variables for biomass, average height; Figure 7.7 and Figure 7.8 respectively. Across all three independent experiments, excluding W3-Syto®9/Sypro®, small weekly variations were observed which were acceptable and were within or close to statistical variations. W3-Syto®9/Sypro® did standout from the rest of the data, and is likely an anomaly, but this would be averaged out, when analysing across, three or more independent experimental repeats. The observed biofilm biomass and average thickness observed are of the similar to those reported in the literature (Kim et al, 2013).

7.3.2 Conclusion - *PA* Growth Assay Reproducibility on 316-SC Stainless Steel

Thus, the use of confocal microscopy, to investigate biofilm morphology changes is feasible when minimum of three intra experimental replicates are repeated three times independently. Repeating experiments, in an independent manner ensures that any observations are not a random anomaly (as perhaps seen in the W3-Syto®9/Sypro® replicate), but a real change in the data trend.

Thus, all subsequent works will have conclusions based on data across averaged across three or more independent experiments, run on different weeks.

CHAPTER 8 Growth of Mature *PA* on Different Substratums

8.1 *PA* Growth Rough and Smooth Substratums

The growth and morphology of microbial biofilms has to our knowledge not been investigated in the context of differing substratums with variable surface energies and roughness. The aim here therefore was to culture *PA* on a range of substrates with known roughness and surface energies. Then relate their growth behavior back to the substratum properties using confocal probes (Syto®9, ConA, Sypro®) as discussed in Chapter 1.30.2. The TCS SP2 microscope was setup to have a dz of 11.3µm, and a step height increment of 1µm, using a 10x water immersion lens, with a pinhole of 0.5AU. Duel staining protocol 1 was used in this work.

Both confocal film thickness, biofilm and actual biofilm mass data were collected at both day +1, and +4. But due to the inability of the TCS SP2 confocal microscope to differentiate from reflected light from the different surfaces, and fluorescent stained biofilm material, the +1 inoculation data (early stage biofilm data) was not included. However, direct mass measurements were included, as this was not affected by this optical problem.

Materials tested include polyethylene, polycarbonate, PTFE, 316 stainless steel, and 304 stainless steel, each coupon having a defined rough (RC) or smooth coupon surface (SC), as detailed in Figure 4.24.

Substratum	Syto®9	Sypro®	ConA-Alexa Fluor®
316-RC	28	16	12
316-SC	20	12	8
304-RC	28	12	16
304-SC	23	11	12
PTFE-RC	20	8	12
PTFE-SC	24	12	12
PC-RC	24	8	16
PC-SC	24	12	12
PE-RC	20	16	4
PE-SC	20	16	4

Table 8.1. Number of replicates measurements *n* for each coupon.
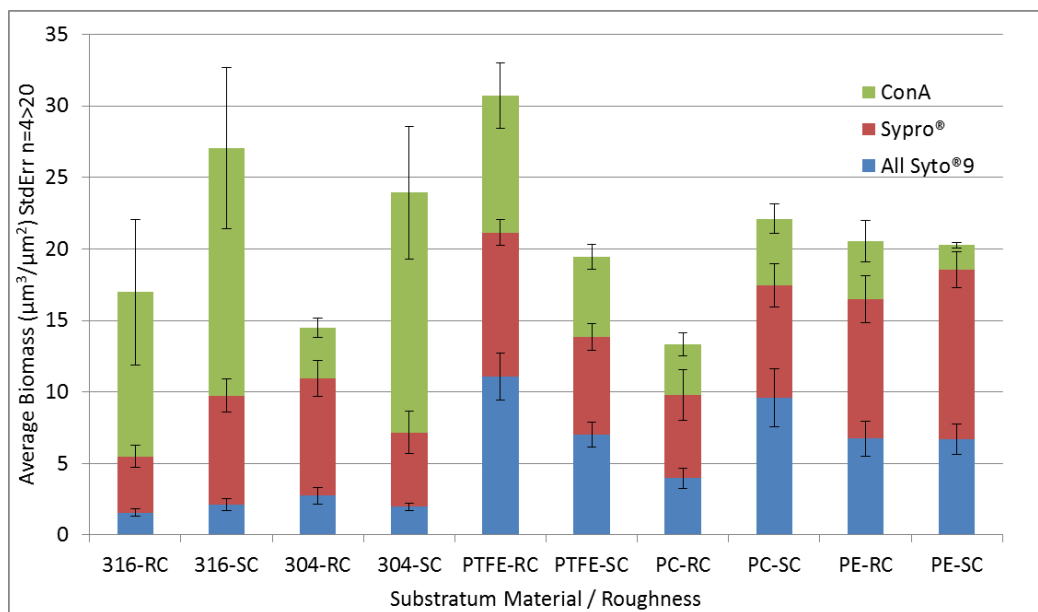
Figure 8.1. *PA* biofilm- summed average biomass data.
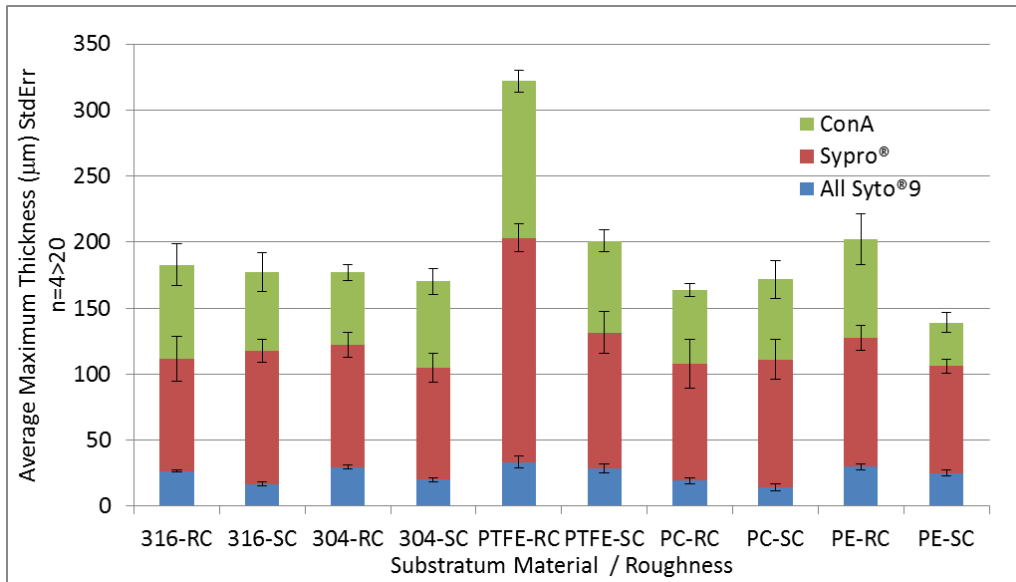
Figure 8.2. *PA* biofilm - average maximum thickness data.
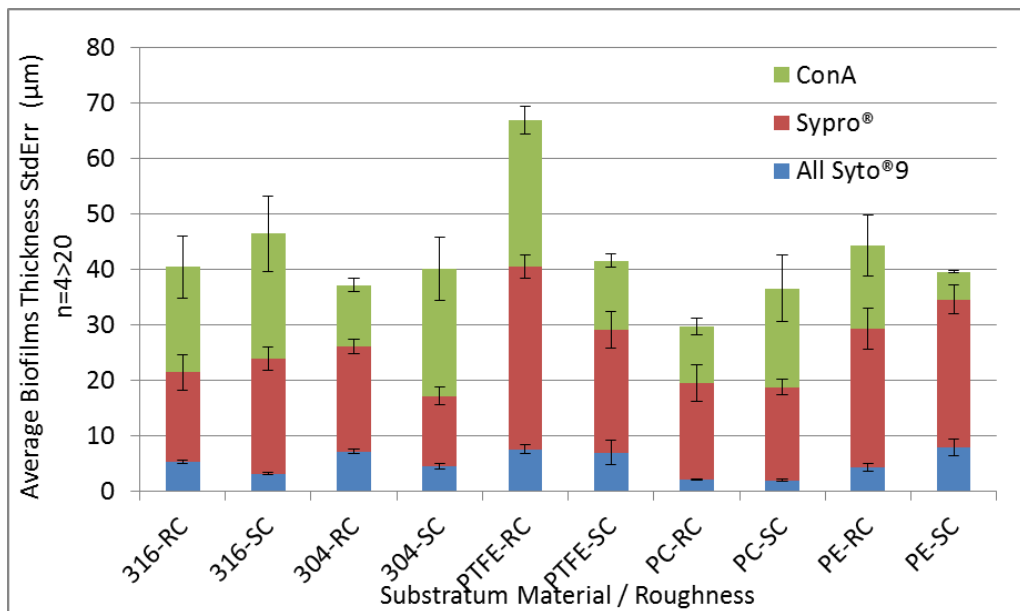
Figure 8.3. *PA* average biofilm thickness data.
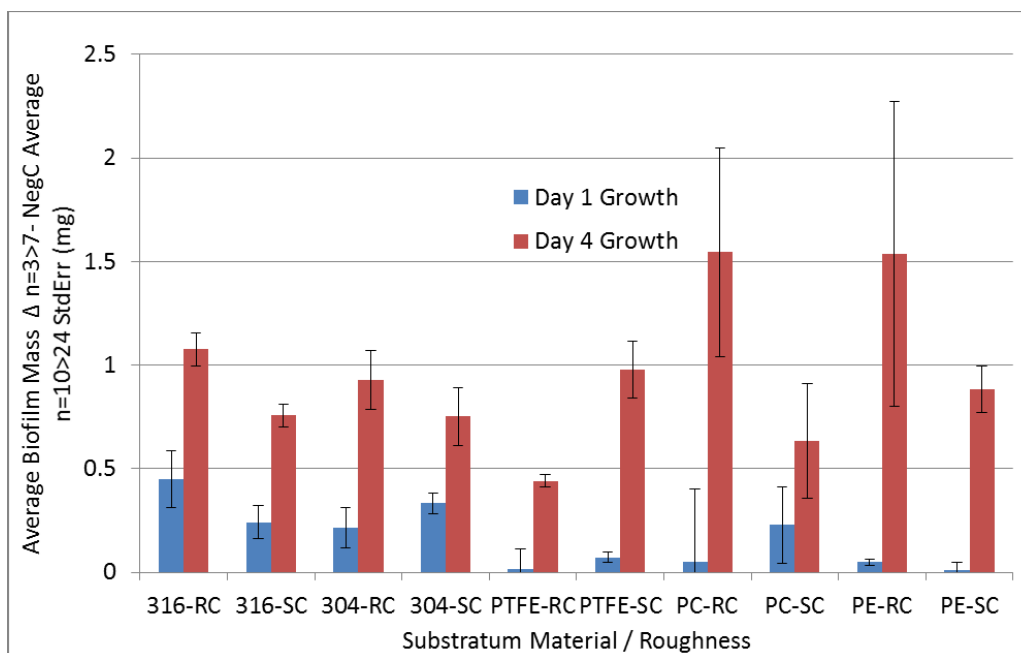
Figure 8.4. *PA* biofilm - actual dried mass for Days 1 and 4.

8.1.1 Discussion – *PA* Growth on Rough and Smooth Substratums

Across all of the substratums tested, differences in the composition of the biofilms were observed. Upon examining the summed biomass data (Figure 8.1) the *Pseudomonas* biofilm cultured on metal (316, and 304 stainless steel), had a greater amount of polysaccharide (ConA), and a lower overall microbial population. For the biofilm grown on the polymers (PTFE, PC, and PE) the inverse was apparent. Interestingly, the amount of protein present in the different biofilms was similar.

Examination of the maximum height and average height data (Figure 8.2 and Figure 8.3, respectively), shows that the maximum height of both the polysaccharide and protein component are consistently higher than the maximum extent of the microbes themselves in the z plane, which confirms that the microbes are embedded within the EPS matrix, and do not sit upon it.

Interestingly, the summed maximum height data (Figure 8.2) yields the same summed maximum height, across all substratum materials and roughness tested, with the exception of the PTFE-RC which showed much thicker biofilm on average. The reason for this observation remains unknown,

with thick biofilms on PTFE relative to the other substratums not being observed again, during this project. Similarly, excluding PTFE-RC, the summed average biomass thickness shows, a gross conservation of behavior across all substratums and roughnesses tested. This observation is interesting because it appears that mature biofilms, (in this context meaning four day old biofilms) whilst consisting of different component proportions, exhibited similar gross physical characteristics (i.e. maximum height, and average biomass thickness), that are independent of the substratums surface energy, roughness and chemical makeup.

However, this observation was not observed with the summed biomass metric which reflects the actual biomass excluding voids and pores. There are a number of possible reasons for this difference:

- The biofilms did grow differently (i.e. different growth rates, or sloughing rates, due to substratum properties), but all reached highest physical limit (average height, maximum height), and were limited by the turbulent flow regime about their structures.
- When culturing biofilms different surfaces, the substratum is largely irrelevant.

Both of these possible explanations would also rationalise the differences in the biofilm biomass metric, whilst maximum height and average height would not. One report in the literature found that the rate of *Pseudomonas* growth upon different substratums including PTFE, PE, PP and poly(dimethylsiloxane), was the same when cultured in a simple flow cell system, with all of the polymers having similar levels of colonisation after 24 hours (Gottenbos et al., 2000).

In order to investigate the former explanation, the biofilm growth assay would need to be shortened in time so to detect the resultant variances evident in the initial binding assay between the different materials and their possible impact on the biofilm growth kinetics. However, such a study was outside the scope of the current project and is noted as an area for future study.

Another possible hypothesis for the latter explanation is based on the premise that conditioning films may be forming on the coupon surfaces that originate from the bulk media components. It is possible that these conditioning films maybe more important themselves from a bio-adhesion perspective than the physiochemical properties of the substrates. It could be that the properties of these conditioning films which would likely be similar given they arise from the same bulk components, and that it could be these films the microbes are interacting with in the surface environment. This hypothesis is discussed in Chapter 1.11.1 and investigated in Chapter 10,

whereupon on a limited number of surfaces were examined for their propensity to form conditioning thin films in the presence of the TSB growth medium used in all biofilm experiments.

Figure 8.4 shows increases in biofilm dried masses were observed from +1day to +4 days post inoculation for all test substratums which were statistically significant. This observation was to be expected for growing biofilms. The average dried mass per coupon is 0.95mg at +4 day. Overall however there are larger errors than desirable in this measurement for some samples, especially for both polycarbonate and the roughened polyethylene samples. The data shown in Figure 8.1 for the confocal biomass and the dried biofilm masses shown in Figure 8.4 could be expected to show some level of correlation, but none is evident. This disparity could arise due to the limitation of the direct mass measurement made during these experiments, where the total dried coupon associated biofilm is being measure. It is possible that greater biomass is attached to the reverse side of the coupon and in addition to this quantity, during coupon handling unknown biomass could be being lost. This would make direct biomass comparisons between the error prone physical mass metric and confocal biomass metric that, is only concerned with the CDC reactor inner coupon surface difficult at best.

No statistical difference was observed between the two metals tested (304, 316 stainless steel), at either sampling time. Increases in biomass, were seen, which appeared linked to the surface roughness, across all materials, excluding PTFE, however observed difference were not statistically significant, with the exception of 316 stainless steel (Figure 8.4).

Both rough PE and rough PC substratums exhibited greater biofilm mass, than there smooth counterpart, but only PC was statistically significant. The inverse was observed for PTFE substratums tested. What was disappointing was that the physical mass data collected, failed to correlate with the confocal data obtained. The reason for this remains unknown, but two main possibilities arise; either the drying method utilised is not specific enough to the surface understudy (inner CDC coupon surface), as biofilm will be cultured upon the entire surface of the 3 dimensional coupons not just the test surface so the two may appear unrelated, or no relationship exists between hydrated biofilm and dried biofilm.

In order to further evaluate the interactions of the biofilm with differing inanimate surfaces, some substratums were modified using thin coatings upon their surfaces and then biofilms were cultured upon their surfaces.

8.2   Growth of *PA* on Thin-Film Modified Substratums

Surface modifications included gold coating, of smooth polycarbonate, smooth PTFE, and smooth 316 stainless steel, but also coating a PTFE-AF film onto 316 stainless steel. During this series of experiments a 'negative control' surface reference was present in the CDC reactor, which was an unmodified sample of each material. For information on the coating process for the gold and PTFE-AF thin-films see Chapter 2.11 and Chapter 2.9, respectively.

A Leica TCS SP8 confocal microscope was used for the acquisition of this data set. A 25x water immersion lens, with a pinhole of 0.36AU corresponding to a dz of 1.005µm. A step height increment of 1µm was used. Probe staining protocol '2' was used, due to the improved data gathering capacity of the TCS SP8 instrument over the TCS SP2 (Figure 2.5). Standard *PA* growth conditions were used (see Chapter 2.17).

Substratum	Syto®9	Sypro®	ConA Alexa Fluor®
316-SC-NegC	32	32	32
316-SC-AU	32	32	32
316-SC-AF	36	36	36
PC-SC-NegC	31	31	30
PC-SC-AU	32	30	32
PTFE-SC-NegC	35	35	35
PTFE-SC-AU	36	36	36

Table 8.5. Number of replicate measurements *n* for each coupon
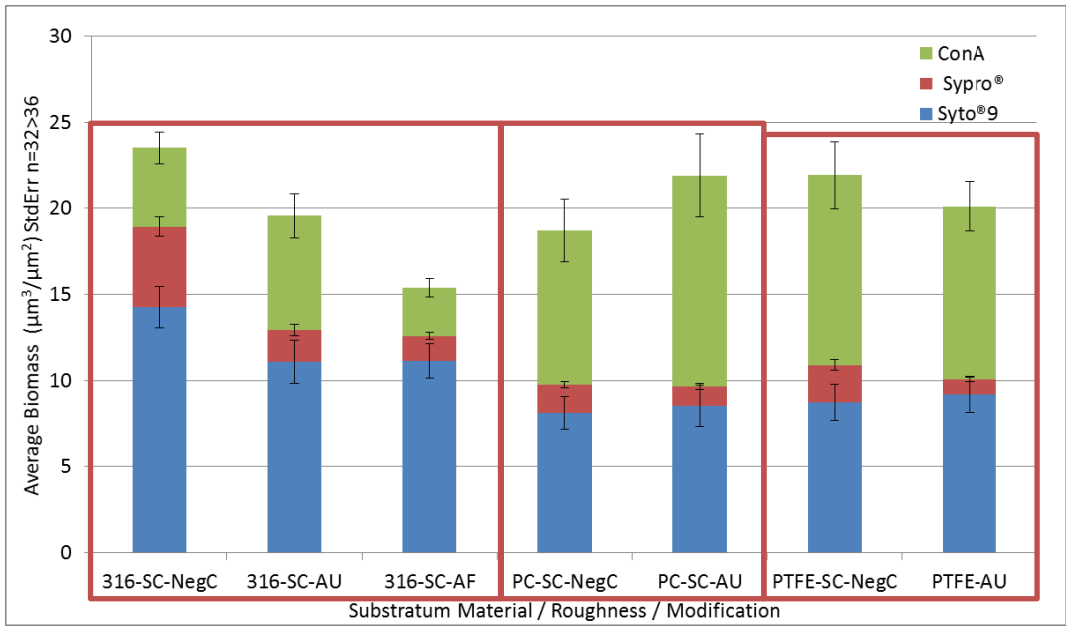
Figure 8.6. *PA* biofilm biomass (summed) on modified substratum. Red boxes group relevant unmodified substratum with appropriate thin film modified substratum
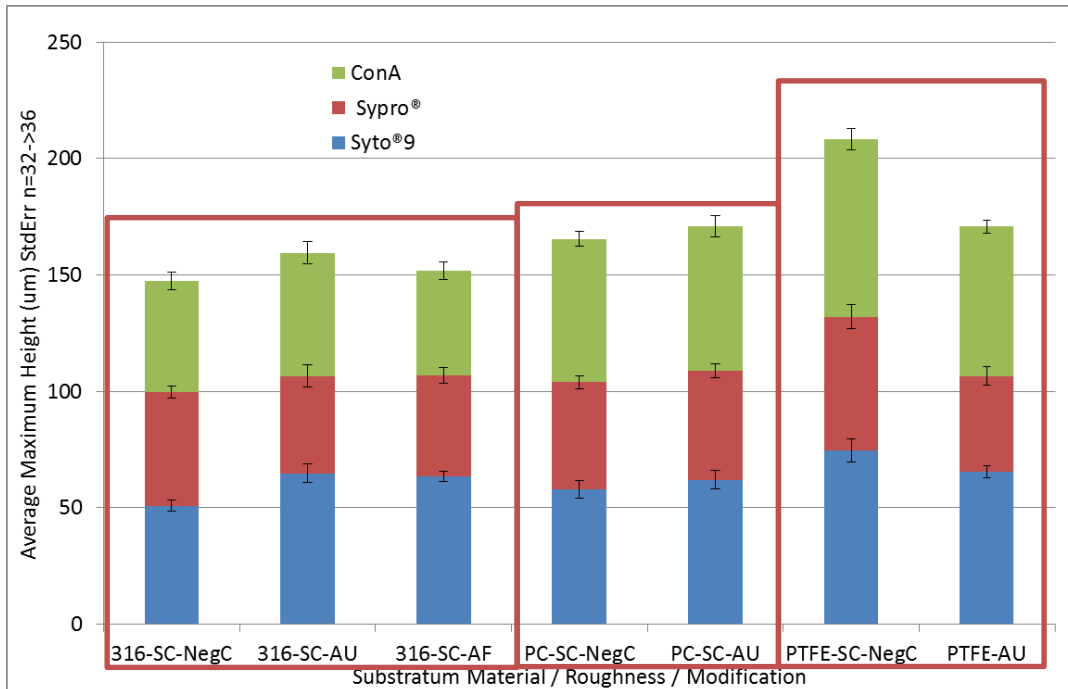
Figure 8.7. *PA* biofilm maximum height (summed), following growth on modified substratums. Red boxes group relevant unmodified substratum with appropriate thin film modified substratum
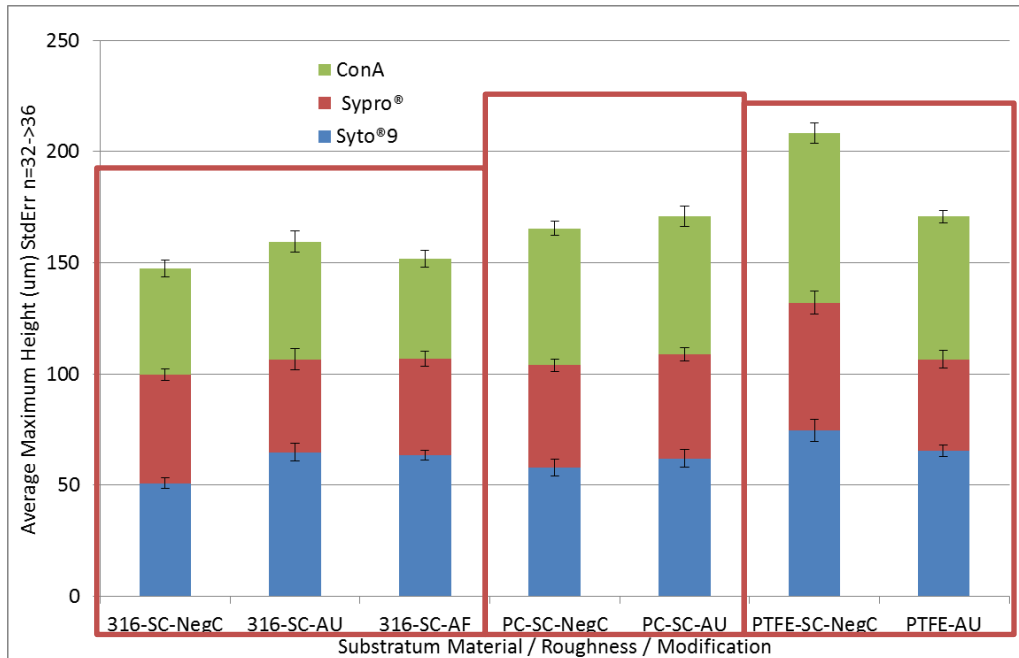
Figure 8.8. *PA* biofilm average biofilm thickness (summed), following growth on modified substratums. Red boxes group relevant unmodified substratum with appropriate thin film modified substratum.
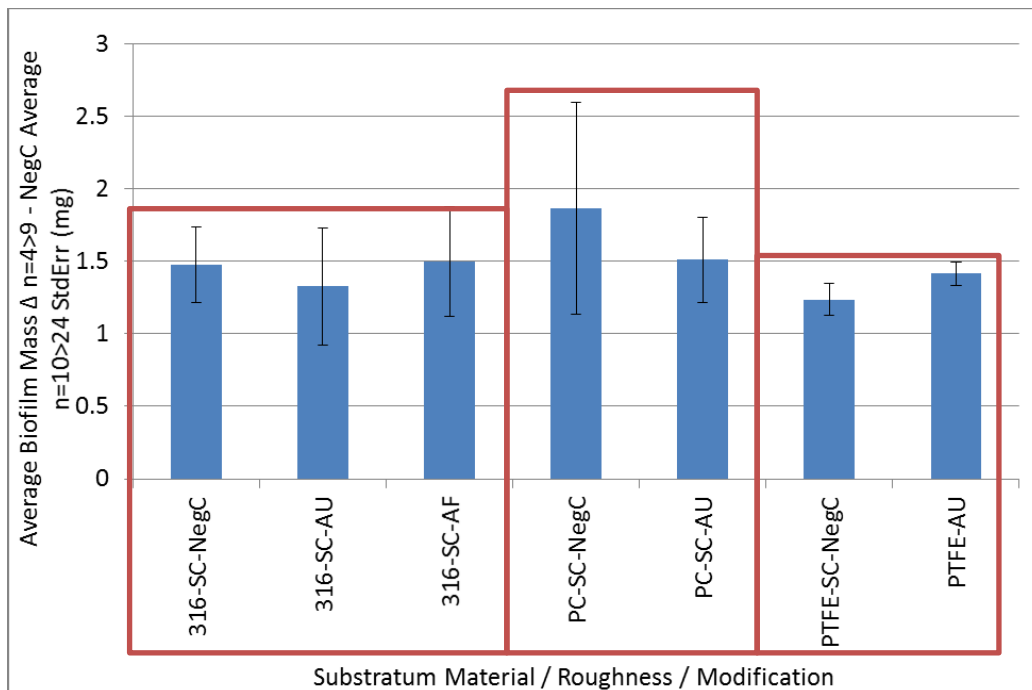
Figure 8.9. Biofilm actual dried mass following *PA* growth of modified substratums. Average biomass negative control (Figure 7.6) was subtracted from experiment data

averages. Red boxes group relevant unmodified substratum with appropriate thin film modified substratum

8.2.1 Discussion –*PA* Growth on Thin-Film Modified Substratums

Physical mass measurements (Figure 8.9) taken across the different modified substratums, proved to be very consistent across the different modified materials, and were not statistically different from one another. This data is consistent with previous experimental observations, on the defined substratums (Figure 8.4). One can deduce from the physical mass data, that the biofilm has the same overall physical mass, irrespective of the substratums or their thin-film modification, within the experimental uncertainties of this measurement.

Upon observing the summed variables (Figures 8.6, 8.7.and 8.8), one can see that the resultant data, look similar, with the exception of 316-SC-AF, which saw relative decreases in average biomass, and average height when compared to the unmodified 316-SC control. However, this trend was not reflected in the physical biofilm mass measurement data, or maximum height collected. The addition of gold to the surfaces of 316, PC-SC and PTFE-SC, had no apparent gross effect on the resultant biofilms (Figures 8.6 and 8.8) or the physical mass of the biofilm.

When examining the individual average and maximum biofilm height (Figure 8.7 and Figure 8.8 respectively) data, the principle biofilm component, the microbes (Syto®9) appear to be the majority component in on the metals, whether modified or native, whereas on the polymer substratums the microbe component and polysaccharide component numerically have a 1:1 relationship. This trend is in contrast to the previous experiments (Figure D1.2) where the polysaccharide and protein components were statistically present in a 1:1 ratio, with the microbes imbedded. This may be due to a change in the gross behavior, or because of a change in the microscope being used resulting in a perceived change in component spatial arrangement. It is also possible that each biofilm (on each coupon) in isolation will develop its own unique internal self-expressed environment, even on the same coupon during experimental repeats, due to surface being non-ideal, and also the individual positions and actual microbes being different resulting in different gross expression of components overall, representing a somewhat chaotic system.

To test the mechanical strength of the biofilm-substratum interface and gross biofilm structural resilience to physical perturbation, the next set of experiments involved growing *Pseudomonas*

biofilms using the standard growth method, then increasing the shear rate of the liquid in contact with the film.

CHAPTER 9 High Shear Cleaning with/out Abrasive Study on Mature *Pseudomonas* Biofilm

9.1 High Shear Cleaning Study on Mature Biofilm

In this Chapter the cleanability of coupons with biofilms attached was tested. Following the standard growth method detailed in Chapter 2.17, the biofilms were subjected to a cleaning regime. The experiment would test both the biofilms resistance to shear, and also the interfacial adhesion between the biofilm and the coupon surface. The purpose was to determine whether the surface energy of a substratum could be correlated with mature biofilm removal. Such a relationship would be useful in industrial manufacturing, but also in healthcare settings and marine shipping environments. In these situations surfaces are either subjected to high fluid shear for example; in the case of marine shipping during transport or in a fluid manufacturing environment during pigging or following induced fluid shear brought about by physical wiping as occurs in the consumer home.

For the cleaning study, both 316-SC and 316-RC coupons were used as they have a large roughness ratio of 1:25 (Figure 4.25) with a R_a of 93.6nm and 2320nm respectively coupled with a relatively large γ_S of 48.3mJ/m^2 for both variants. PC-SC has a similar R_a (49.0nm) to 316-SC, but an intermediate total surface energy of γ_S (45.5mJ/m^2) and also PTFE-SC because it has an intermediate roughness (628.2nm) but very low total surface energy γ_S (25.6mJ/m^2). Given the noted negative effect of the PTFE-AF thin coating on *Pseudomonas* initial adhesion (Chapter 6), 316-SC-AF coated coupons were also included (R_a=126.9nm, γ_S 21.3mJ/m^2).

CDC *Pseudomonas* biofilm growths are carried out at 174rpm, corresponding to a calculated Reynolds number of 174,000 and shear stress of 44N/m^2, calculated using Eqn. 21 and Eqn. 24, respectively (see Appendix A, Table A1). Following a sustained period of growth of 72hrs in chemostat mode (1%TSB addition 16ml/min), or 96hr if including the batch phase (surface inoculation phase), the RPM was then increased to 400rpm corresponding to a Reynolds number of 390,000 and 188N/m^2 shear stress for a period of 30 minutes. 400rpm was chosen because it was the highest rpm achievable prior to agitator resonance and the exposure of CDC coupons to air due to interactions with the fluid vortex.

Three to five coupons of each material were included in each CDC reactor replicate, complete with one negative control coupon that was removed prior to the increase in stirrer RPM. This experiment was repeated independently four times, and all coupon biofilms were analysed using confocal laser scanning microscopy and physical mass measurements.

The aim was to test the adhesion and cohesion of the biofilms attached to the coupons.
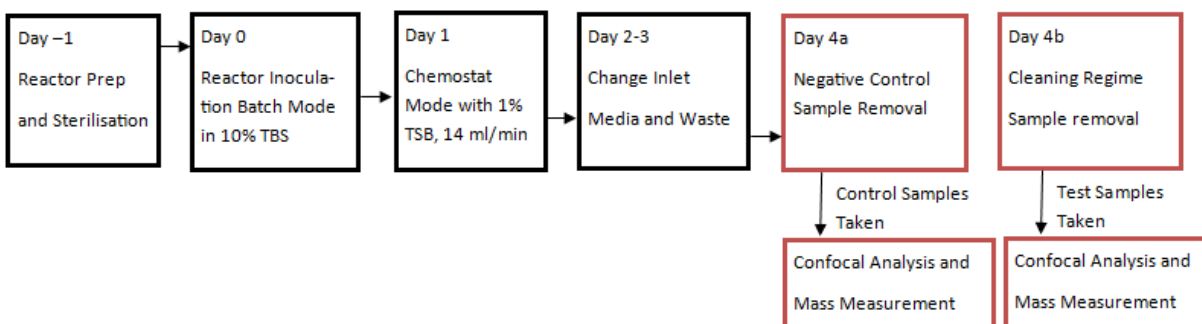
Figure 9.1. Structure of biofilm growth shear cleaning experiment.

Substratum	Syto®9/Sypro®/ConA Alexa Fluor®
316-SC	56
316-RC	65
316-SC-AF	52
PC-SC	48
PTFE-SC	52
316-RC-NegC	16
PTFE-SC-NegC	20
PC-SC-NegC	12
316-SC-AF-NegC	16
316-SC-NegC	20

Table 9.1. Number of replicates measurements *n* for each coupon in the high-shear cleaning experiment
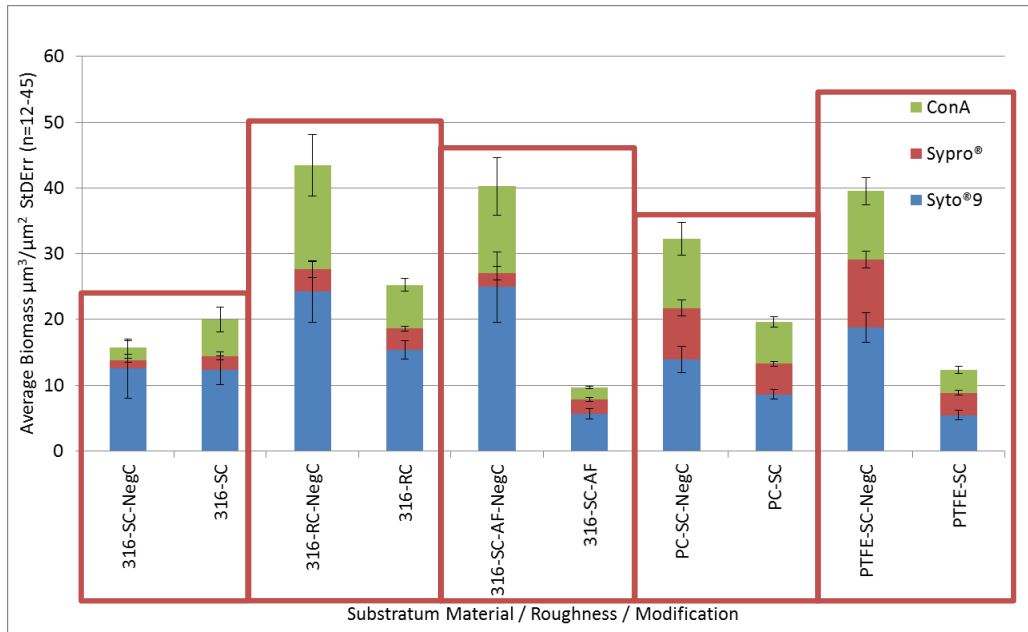
Figure 9.2. High shear cleaning results for summed biomass metrics. Within each box data is shown for a negative control (LHS) and the clean coupon (RHS)
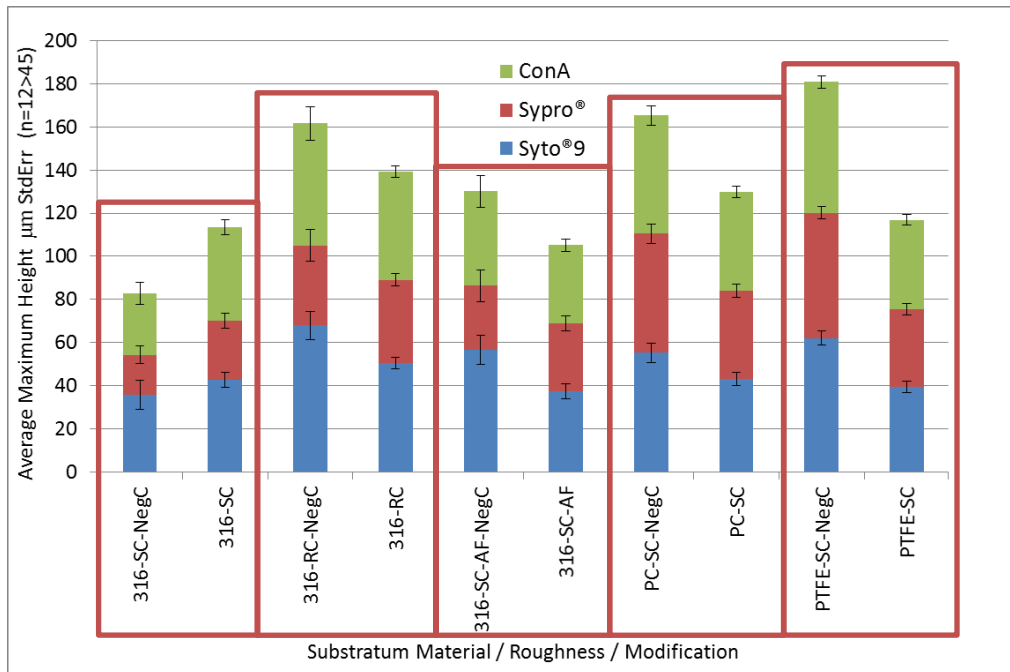
Figure 9.3. High shear cleaning results for summed maximum height. Within each box data is shown for a negative control (LHS) and the clean coupon (RHS)
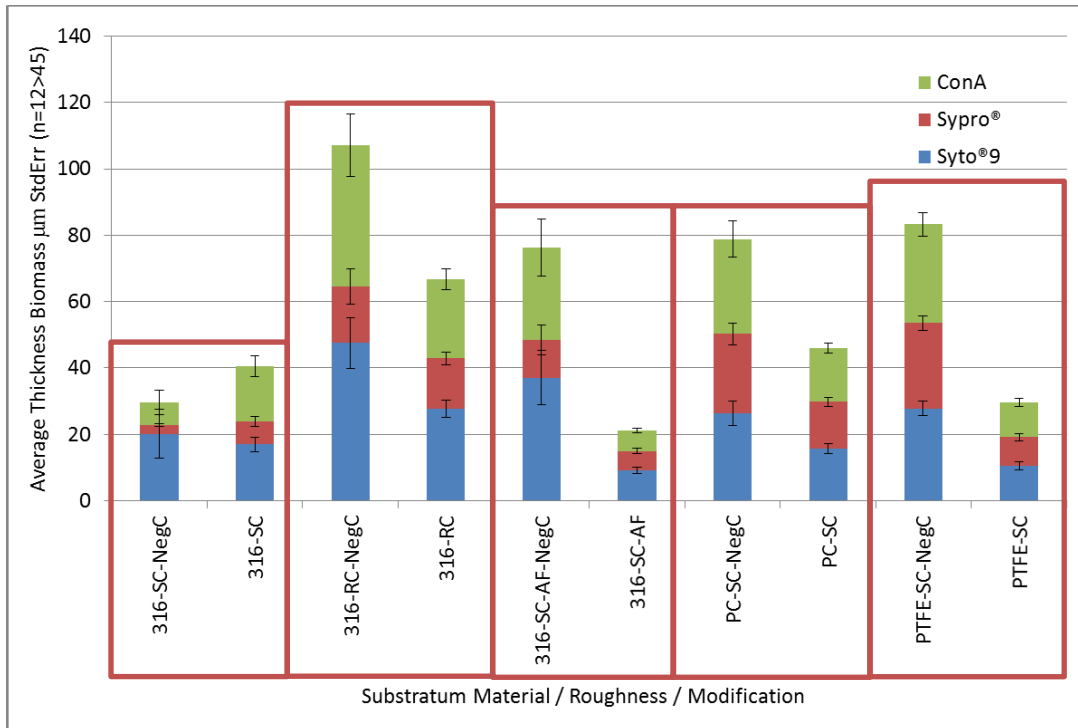
Figure 9.4. High shear cleaning results for average thickness. Within each box data is shown for a negative control (LHS) and the clean coupon (RHS)
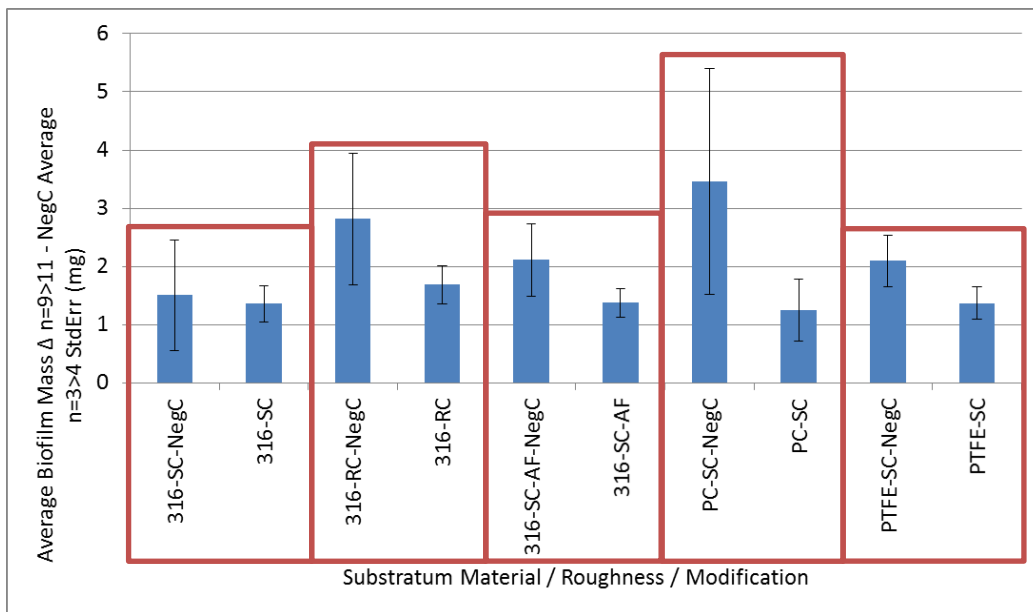
Figure 9.5. High shear cleaning experiment result showing average physical dried mass(mg). Average biomass negative control (Figure 7.6) was subtracted from experiment data averages to give the data shown here.

9.1.1 Discussion – High Shear Cleaning on Mature Biofilm

When examining the data, it is evident that 316-SC (Figures 9.2, 9.3 and 9.4) substratum gave a slightly larger biomass, maximum and average film thickness than the 316-SC-NegC control sample, respectively. However, these differences are comparable to the errors associated with each measurement. A second explanation is an intrinsic limitation in the methodology employed here in that only one 316-SC-NegC sample was tested during each experimental replicate. Thus, this single sample could be non-representative for 316-SC-NegC.

Dried physical mass measurements (Figure 9.5), did detect decreases in biofilm upon the different test materials, following high shear cleaning, however these differences were not statistically significant, due to the apparent large errors in the data. The occurrence of these large errors is discussed in Chapter 7.2.3.

For the 4 other samples tested (except for 316-SC) summed thicknesses and biofilm mass data exhibit a decrease in biofilm thicknesses and biofilm mass following the high shear cleaning relative to the experiment negative control sample.

The maximum biofilm height metric was less correlated compared to the biomass and average biofilm thickness metrics in the high shear cleaning test. This difference is likely due to the fact that the latter metrics are based on film averages across the sampling area, and are thus more representative of gross biofilm attributes. Conversely, the maximum biofilm height metric, is more a measure of an extremity of measurement, and so is less sensitive to average changes. This is comparable in concept to the R_a and R_z used in roughness measurements, discussed in Chapter 1.33.

The largest percentage decreases in the biofilm thickness and biofilm biomass after high shear cleaning were found on both virgin PTFE-SC and 316-SC-AF materials, followed by PC-SC and 316-RC as shown in Figure 9.2 and Figure 9.4 respectively.

Further data analysis was performed to determine whether there was any surface energy or topographical link with the percentage remaining biofilm after cleaning. Using only the summed confocal output probe data for each analysis metric, for a gross biofilm perspective the percentage biofilm remaining was calculated, relative to the intra experiment cleaning negative control. The percentage remaining biofilm was then plotted against, the various surface energy metrics. The same analysis was performed for the physical biofilm mass measurement.
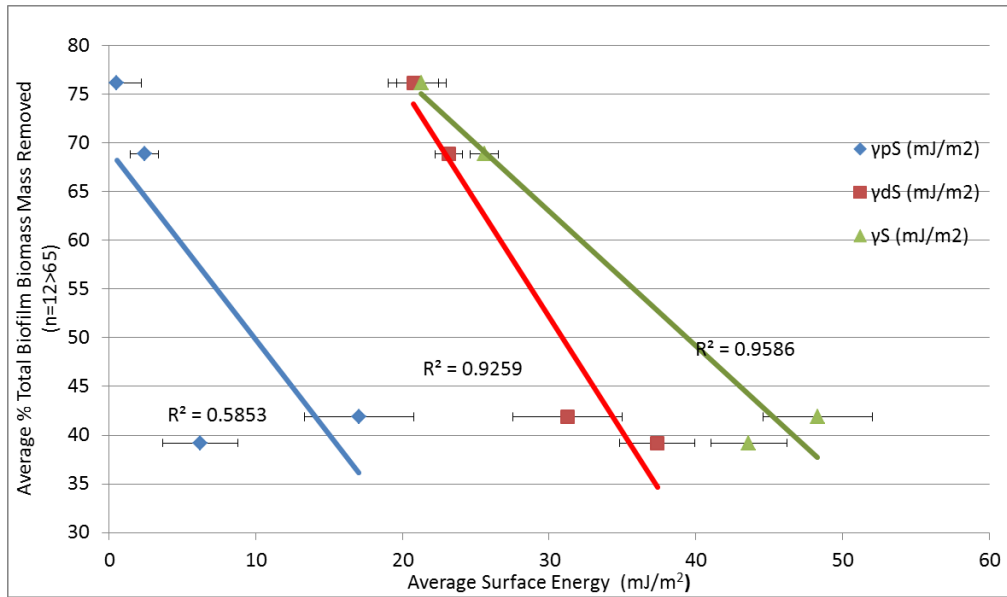
Figure 9.6. Percentage biomass remaining following high shear plotted against surface energy.
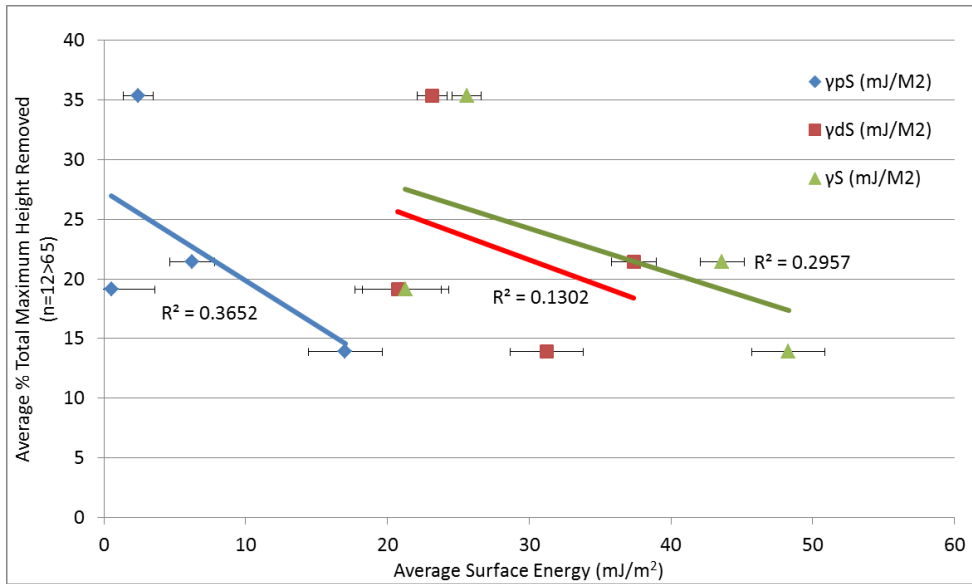
Figure 9.7. Percentage maximum height remaining following high shear plotted against surface energy.
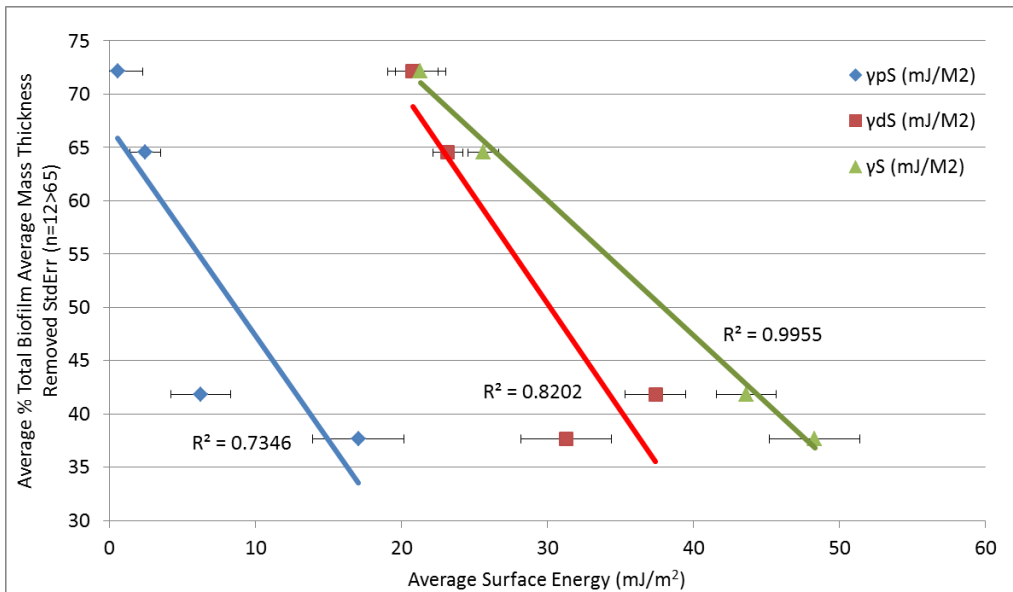
Figure 9.8. Percentage average biomass thickness remaining following high shear plotted against surface energy.
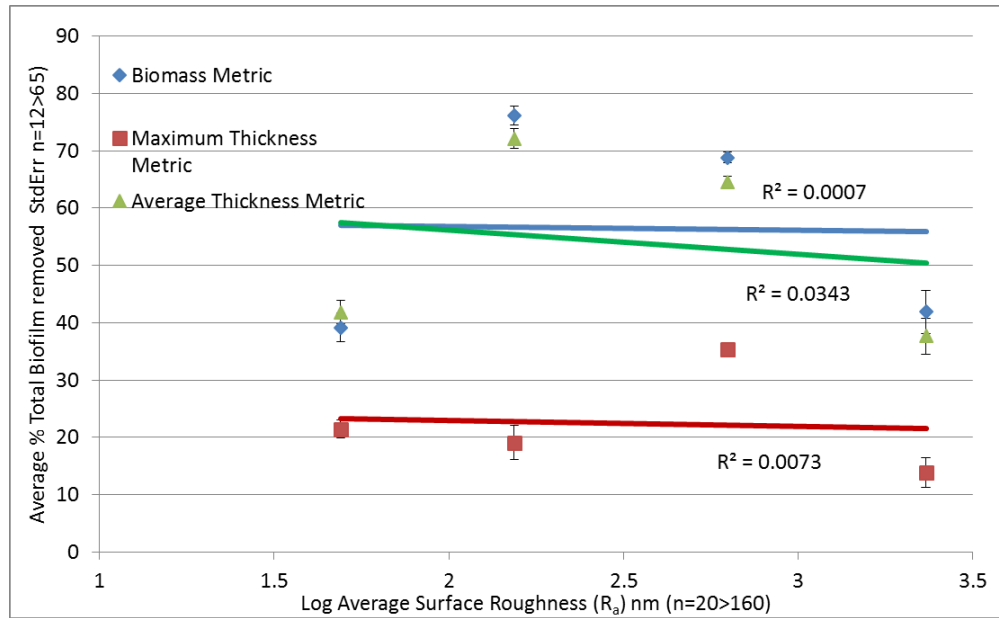
Figure 9.9. Percentage average biofilm remaining following high shear plotted against R_a.

The results show in Figure 9.6 and Figure 9.8 an apparent correlation between the average surface energy of different substratums and the average amount of biofilm removed from the different surfaces following the high shear cleaning event. Greater correlations are seen in both the biomass and average biofilm thickness metrics with γ_S (P=0.02, R^2 0.96 and P=0.0022, R^2 =0.99 respectively) and γ^d_S (P=0.037, R^2 0.93 and P=0.0943, R^2 0.92 respectively) (Figure 9.6 and Figure 9.8), but were also evident to a lesser extent with γ^p_S (P=0.234, R^2 0.58 and P=0.143, R^2 0.73 respectively). Poorer statistical correlations were observed with the maximum height metric, indicating that this metric is less associated with adhesion, not a surprising conclusion (Figure 9.7 as discussed in Chapter 9.1.1). No correlation was evident for the average physical mass measurements obtained which primarily reflects the errors associated with the methodology. These problems included the biofilm growing on all sides of their 3 dimensional structure, with all sides of the coupon experiencing different (and uncontrollable) shear rates which undermines the robustness of the method.

Lower surface energy substratums generally resulted in the increased average biofilm removal upon examining the different biofilm metrics (Figures 9.6, 9.7, and 9.8). This observation coincides

with the relationship found between initial attachment of microbes upon substratums with different surface energies (Chapter 6.6) and work published in the literature (Chang et al., 1977, Dexter, 1979b, Dexter et al., 1975), and corroborates the Baier's theory of bio-adhesion (Baier, 1972). No correlation was detected regarding average surface roughness (R_a) with high shear cleaning (Figure 9.9). In the literature roughness has been linked to the resistance of biofilms to cleaning (Frank and Chmielewski, 2001, Whitehead and Verran, 2006, Blel et al., 2008). However, these studies concentrated on the removal of primary monolayers of microbes from the surface and considered features that may retain individual microbes such as small surface defects (1 to 3µm), rather than the growth and removal of the biofilm superstructure over a given substratum, as reported here. Hence, this study is the first known observation of the increases in relative gross removal (mechanical failure of the biofilm-substratum interface) of mature biofilm being correlated to that of the substratum surface energy parameters.

Our hypothesis for this inverse relationship is that when increasing the shear upon a given substratum, there is an increased likelihood of failure occurring at the biofilm-substratum interface, on lower surface energy substratum (due to less attachment points being available), than on a higher surface energy substratum (stronger attachment points). The correlations observed here have been observed in natural experimental systems, whereby biofilms were cultured on an array of materials in a turbulent marine harbor environment for many months (Dexter et al., 1975, Dexter, 1979b). But these were comparative studies investigating material differences but not relative change when compared to a negative control.

9.2 High Shear Cleaning Study with Silica Abrasive Powder

To further test the cleanability of these selected substratums, the introduction of an abrasive silica powder (Zeodent®119) in combination with high shear was tested. Experimental conditions were identical to those detailed in Chapter 9.1, but with the inclusion of silica powder (7g/350ml =2%w/v) added to the CDC reactor during the 30 minute high shear cleaning stage.

Immediately prior to the increase in shear the CDC media outlet was shut, and the inlet media flow rate turn to zero. This was to ensure that the silica powder was not diluted during the course of the experiment. Three independent experiments were carried out, each with 3 to 5 test coupons from each test substratum, plus appropriate negative control (substratum removed prior to high shear/silica addition.

The aim of the experiment was to determine if enhanced cleaning would be detected in a high shear environment in the presence of an abrasive powder.

Substratum	Syto®9/Sypro®/ConA Alexa Fluor®
316-SC	36
316-RC	48
316-SC-AF	44
PC-SC	40
PTFE-SC	44
316-RC-NegC	12
PTFE-SC-NegC	12
PC-SC-NegC	12
316-SC-AF-NegC	12
316-SC-NegC	12

Table 9.2. Number of replicates measurements *n* for each coupon for various substratums used in the high-shear cleaning experiment with silica powder.
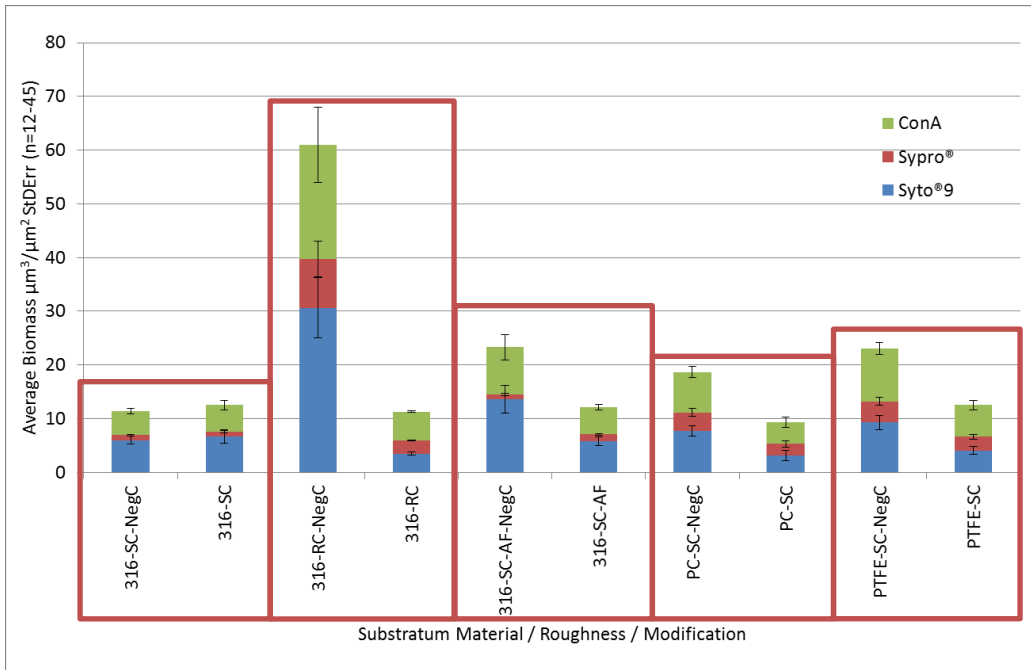
Figure 9.10. High shear cleaning experiment with the silica powder showing summed biomass metrics. Within each box data is shown for a negative control (LHS) and the clean coupon (RHS)
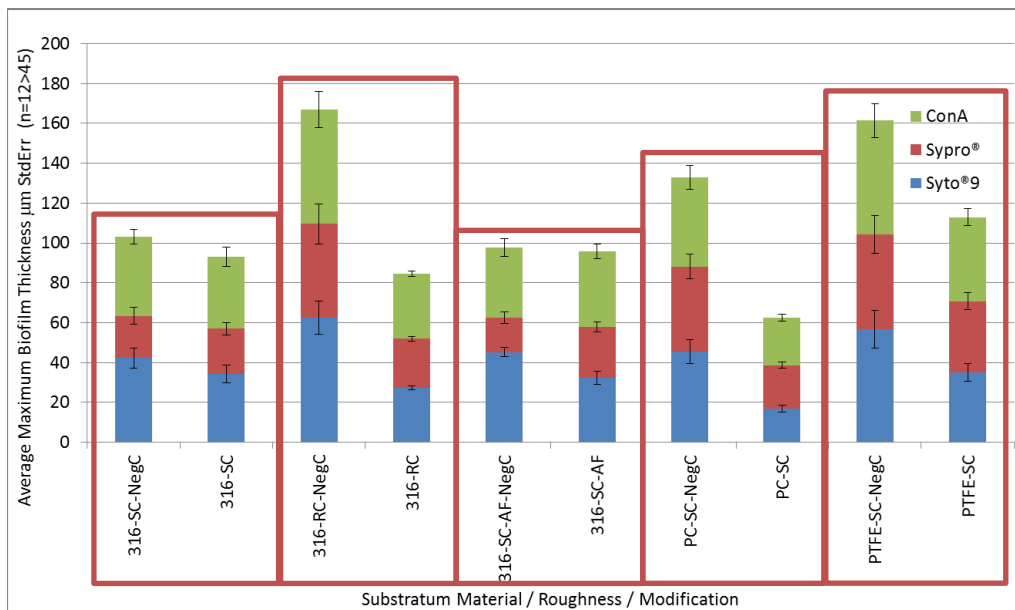
Figure 9.11. High shear cleaning experiment with silica powder result showing summed maximum biofilm thickness metric. Within each box data is shown for a negative control (LHS) and the cleaned coupon (RHS)
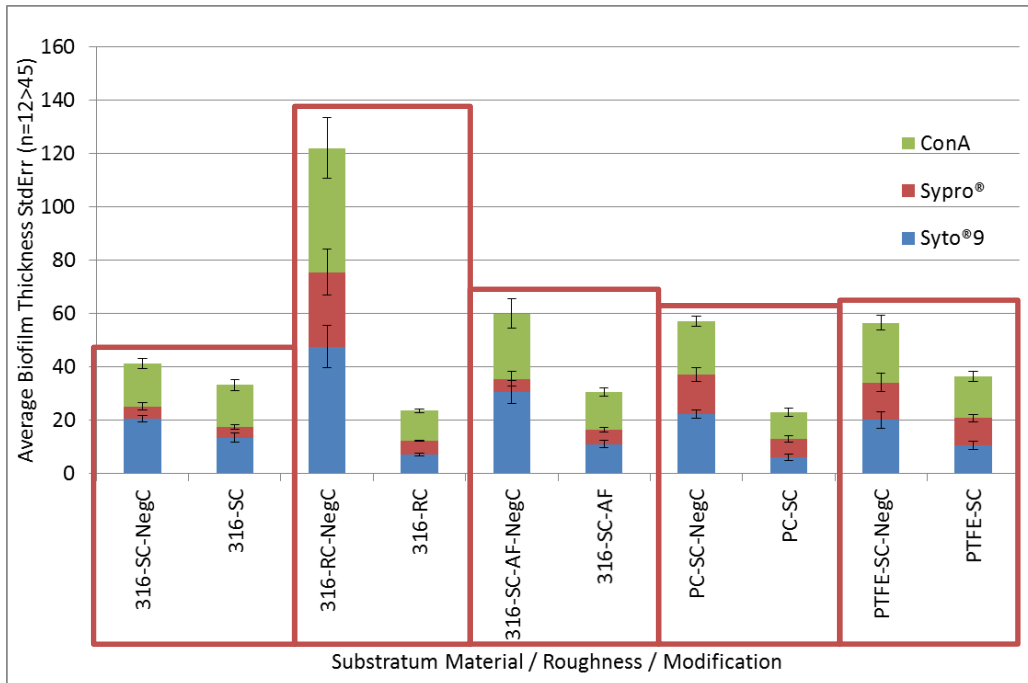
Figure 9.12. High shear cleaning experiment result with silica powder showing summed average biomass thickness metric. Within each box data is shown for a negative control (LHS) and the clean coupon (RHS)
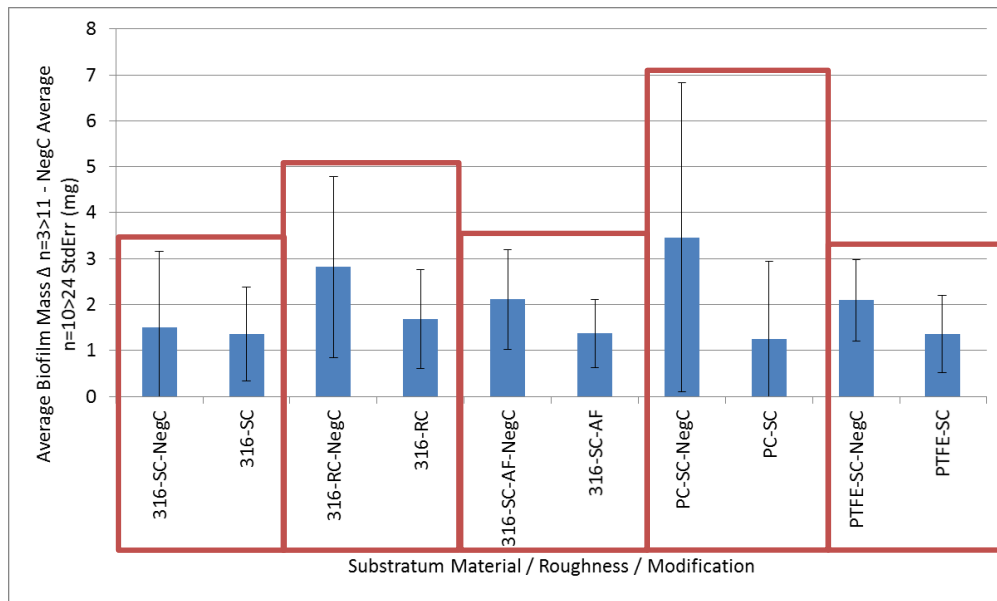
Figure 9.13. High shear cleaning experiment result showing average physical dried biomass mass. Average biomass negative control (Figure 7.6) was subtracted from experiment data averages. Within each box data is shown for a negative control (LHS) and the clean coupon (RHS)
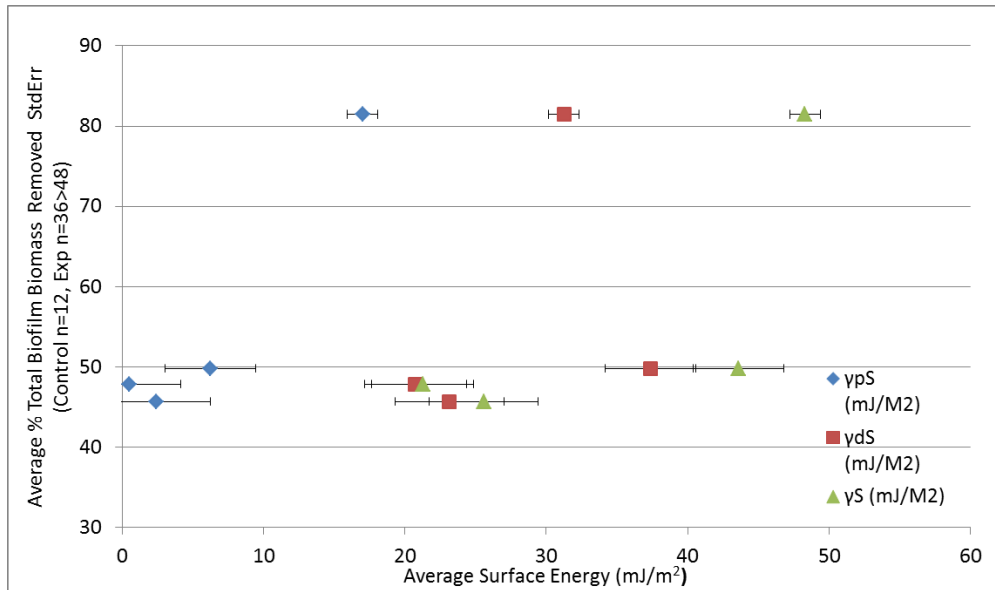
Figure 9.14. Percentage biomass removed following high shear with silica powder plotted against surface energy.
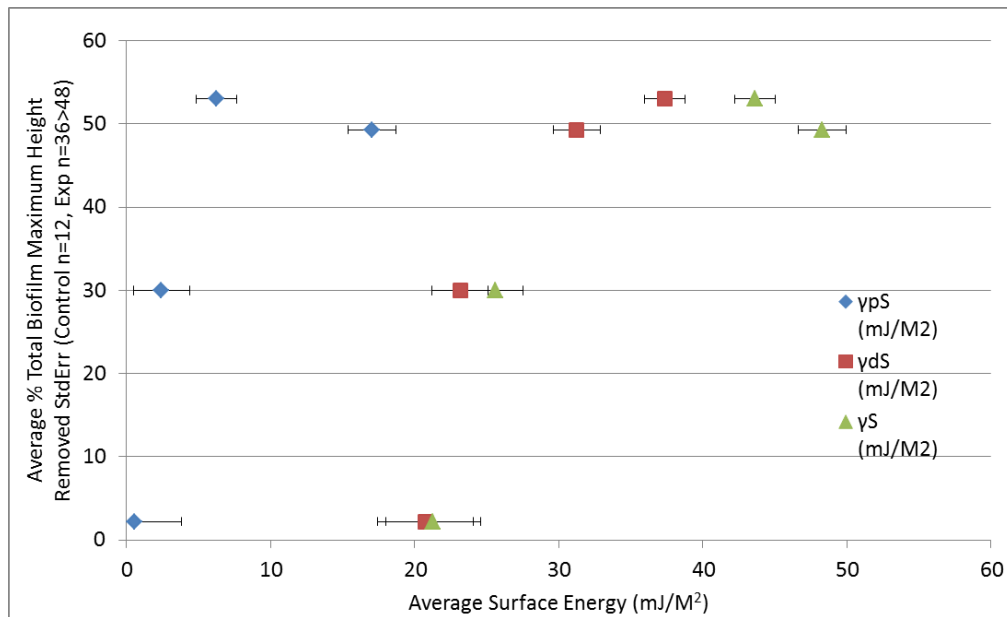
Figure 9.15. Percentage biomass removed following high shear with silica powder plotted against surface energy.
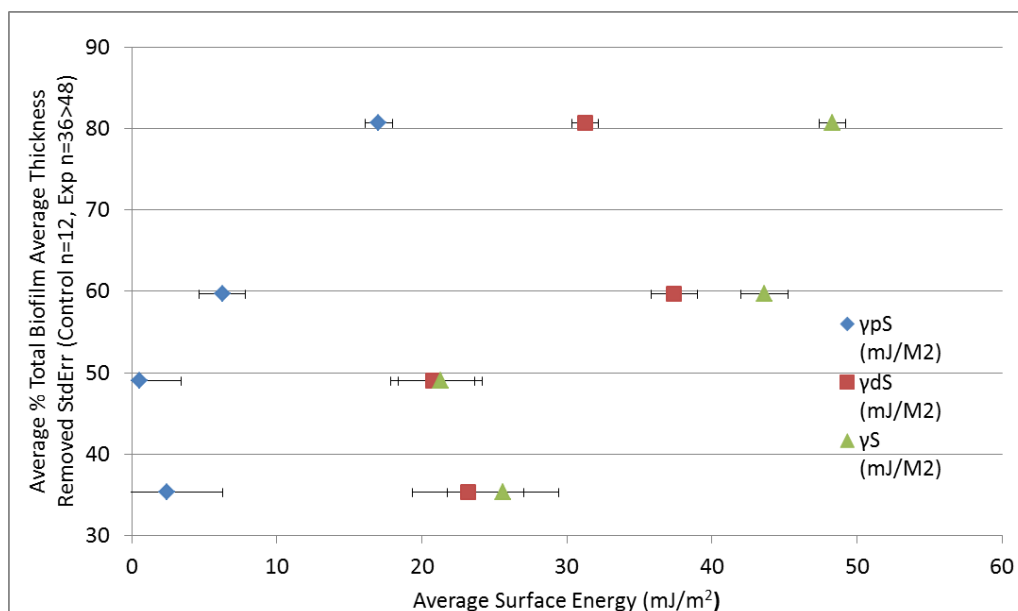
Figure 9.16. Percentage biomass removed following high shear with silica powder plotted against surface energy.

9.2.1 Discussion – High Shear Cleaning Study with Silica powder

The addition of the silica abrasive has resulted in the loss of the surface energy-high shear link that was observed in the previous set of experiments (Chapter 9.1), but also the trend observed the initial microbial binding studies (Chapter 6.6). The loss of the previously observed correlations is likely due to the additional effect of biofilm erosion occurring due to the presence of the silica particles. This phenomenon is much more a bulk material behaviour than surface based behaviour, and thus would not be expected to correlate to surface energy. Abrasives are widely used in the dental industry to enhance the removal of dental plaque from teeth, typically achieving 58 – 68% biofilm removal from teeth relative to controls (Mankodi et al 1998). Interestingly, similar percentage removal was observed from here (Figure 9.10), for most of the materials examined. It is noteworthy that although the surface energy correlated biofilm losses were lost, enhanced biomass removal using the abrasive was not observed (comparison of Figure 9.2 and Figure 9.10).

The dried physical mass measurements (Figure 9.13), did detect decreases in biofilm upon the different test materials, however these differences were not statistically significant, due to the large errors in the data. Some reasons for these large errors are discussed in Chapter 7.5.5.

CHAPTER 10 Conditioning Film Establishment

QCM, was used to determine whether a conditioning film was forming on both 316 stainless steel and gold sensors following the addition of sterile full strength TSB. TSB is the growth medium used in both the *PA* initial attachment and CDC reactor experiments. The formation of a TSB constituent thin-film is quite possible and relevant from a *PA* attachment and biofilm cleaning perspective. The QCM was also used to give a preliminary insight on some of the conditioning film properties. This includes the mass of the deposited film, surface viscosity indications. The QSense QCM was setup to use a fixed flow rate of 200µl/min at a temperature set to 20ºC. The sensors were equilibrated for 10 minutes in DDW water prior to sample injection. Full strength TSB was flowed over the sensor for 40 minutes, followed by 45 minutes water.
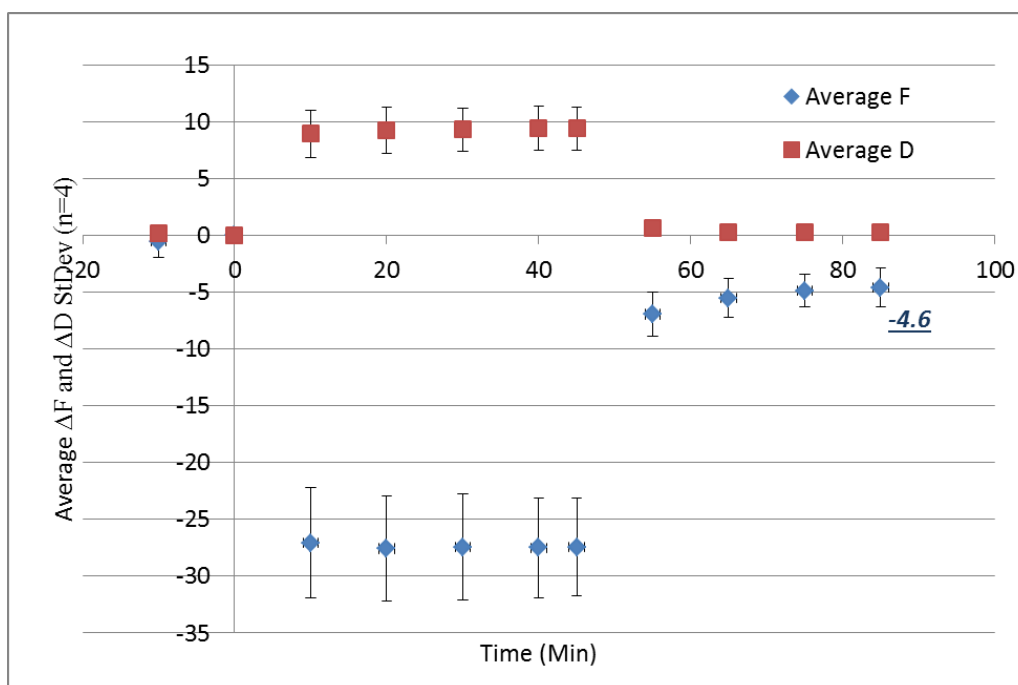
Figure 10.1. QSense QCM Result of FS-TSB forming a metastable film on a gold substratum. Analysis is on the 3rd overtone.
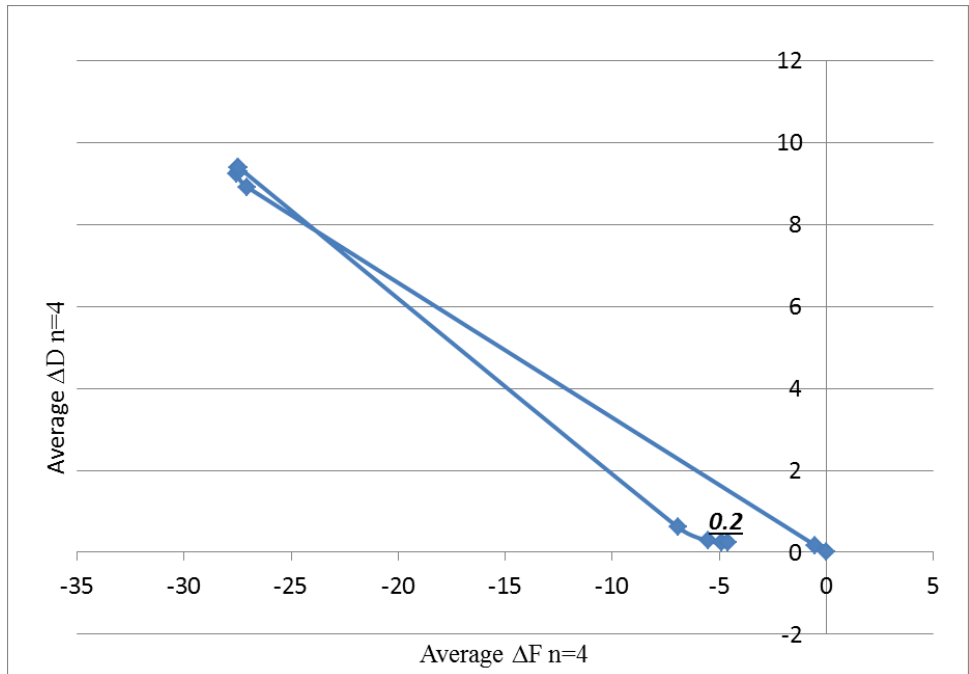
Figure 10.2. QSense QCM ΔF versus ΔD plot for FS-TSB on gold substratum. Analysis is on the 3rd overtone.
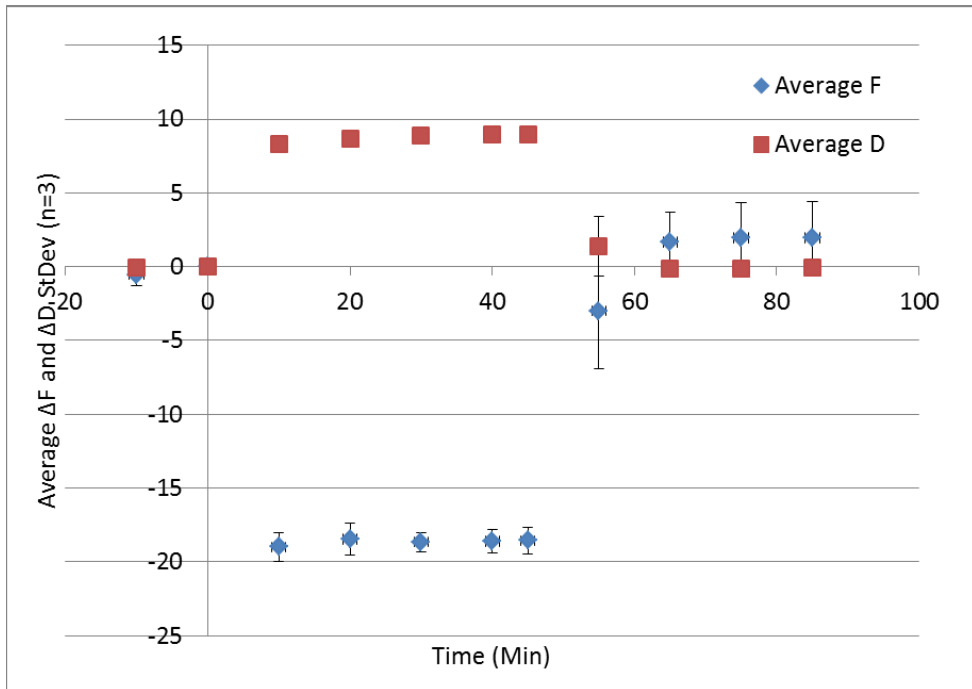
Figure 10.3. QCM on FS-TSB forming metastable film on stainless steel substratum. Analysis is on the 3rd overtone.
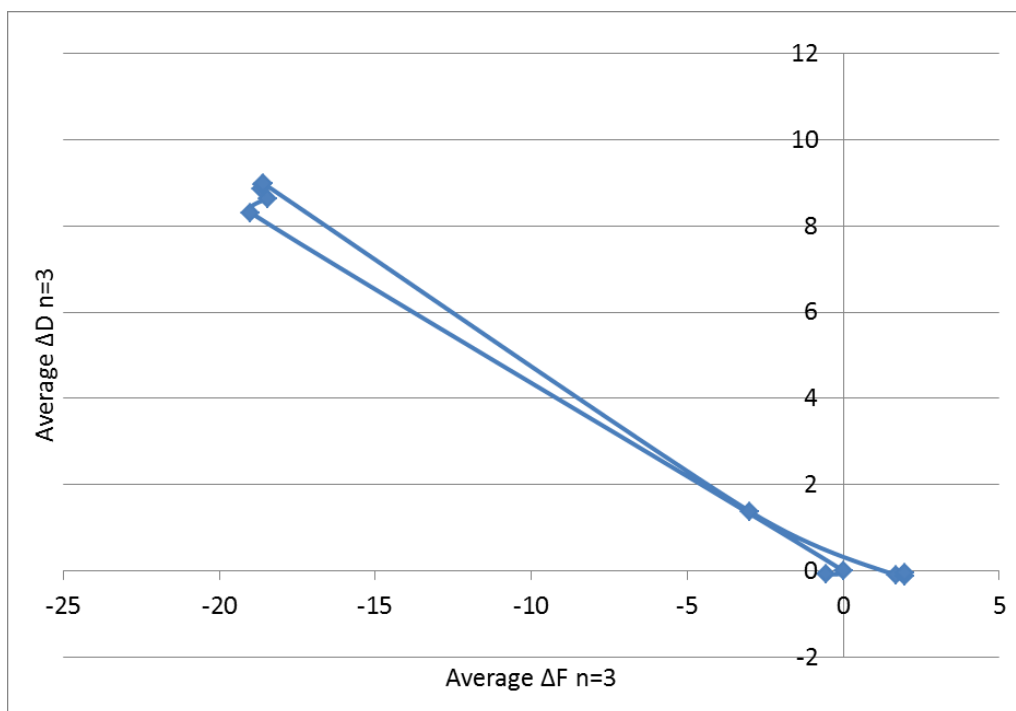
Figure 10.4. QCM ΔF versus ΔD plot for FS-TSB on stainless steel substratum. Analysis is on the 3rd overtone.

10.1 Discussion – Conditioning Film Establishment

Upon examining the results obtained in Figure 10.1 and Figure 10.3 it is evident that no detectable thin film formed on the stainless steel surface. However a small decrease Δf was identified on the gold sensor (Figure 10.1) corresponding to an average of Δf=-4.6 and ΔD=0.2. As detailed in Chapter 1.34 some authors have reported using the Sauerbrey equation to quantify substratum-thin films in water, when the Δf/ΔD ratio was less than 10 (Muramatsu et al., 1995). For the thin film detected on the gold substratum the ratio was 23, which therefore allows for the use of the Sauerbrey equation (Eqn. 17). A calculated mass of TSB film was 25.4ng/cm^2 was estimated for the conditioning film. It is important to note that the chemical nature of this thin-film remains unknown, but could be elicited with additional experimentation. This small experiment shows that conditioning films will not form on all surfaces equally, much like the initial binding of microbes, which adds to the perceived complexity of biofilm study.

CHAPTER 11 Discussion

11.1 Overall Discussion

In this study a range of substratums were selected to evaluate the establishment, growth and cleanability of *Pseudomonas* biofilms. The materials were polycarbonate, polyethylene, PTFE, 316 and 304 stainless steel. PMMA was also originally selected for study, but had to be dropped due to chemical and heat incompatibilities. Each substratum material was manufactured to create a 'rough' and 'smooth' variant, of known surface energy and roughness parameters. Steels are widely used in consumer product manufacturing and many other industries; including food preparation, but also in the medical sector. Polymers are also widely used in these same sectors. In most instances there is a need to understand more about the bio adhesive and bio-clean properties of these and other commonly available materials from a biofilm perspective. Additionally, materials like PC have both favorable chemical and physical robustness properties, whilst being cheaper, than typical manufacturing materials such as 316 stainless steel. In the context of microbial biofilm colonisation and clean, materials such as PC could be suitable alternatives to steel in 'clean' manufacturing environments. Additionally, an alternative to using other substratum materials is the use of thin-film coatings that could be used to remodel the substratum boundary environment, reducing the propensity of microbial binding on classically highly colonisable surfaces such as stainless steel. The ultimate aim of the project was to elicit more information about biofilm formation phenomena, from the initial biofilm formation stage, their subsequent growth, and ease of removal, in relation to different substratum materials.

One of the challenges in biofilm research has been the establishment of quick and reliable assay methods that allows for the quantification of the microbes at the initial attachment phase of biofilm formation, ideally to different test substratums, with differing topographies, that is able to accurately and reproducibly quantify all of the microbes upon a surface.

The methods employed by other authors are often limited to the single substratum material they are testing, which are not able to be used generally, across differing materials, or do not capture all of the microbe data upon different substratums. Typical microbe surface attachment assays consist of swabbing a surface under investigation (Wirtanen et al., 2001) and culturing the microbes on selective agar plates or re-suspending them in a recovery medium, with quantification by CFU counting or using dyes such as crystal violet using a spectrophotometer

(Merritt et al., 2005), respectively. Swabbing introduces sampling ambiguity that tends to select for only those microbes at the tops of the topographical features, whilst giving no spatial information on the surface distribution of the microbes (in x and y or z) and the error therein. Direct surface measurements, are all microscopy based and can be carried out using either a SLM (Weiss, 1961), phase contrast microscopy (Marshall et al., 1971), (SEM), AFM (Powell et al, 2017) or epifluorescent microscopy (Flint et al., 1997). Both (SLM) and (SEM) are time consuming, and inaccurate relying on the researcher, to both identify and count the microbes against the background of the surface, with SEM being limited to electrically conducting materials for example stainless steel, or having to decide between micro scale surface features and microbes following gold sputtering. Staining the microbes prior to imaging with fluorescent stains such as Acridine orange (Flint et al., 1997), or Syto®9 and imaging using an epifluorescent microscope does overcome some of the issues observed in SLM and SEM, but does not discriminate from substratum reflected light from light emitted from stained microbes, which when testing novel materials that possess different optical properties or are reflective can render manual or automated counting difficult or impossible. In standard fluorescence microscopy, the microscope detector detects all of the light being emitted, all at once, with spatial resolution in only the X and Y dimensions (2D). This is great, for examining surfaces, where perhaps 2 dimensional data differentiation is required. In such an example all of the z dimension data is lumped together, but cannot be deconvoluted from background reflectance or florescence which can be beneficial, depending on application, but is problematic when examining bacteria on different surfaces.

This thesis has described a new microbe initial attachment assay that is very reproducible, quick to perform, and can be performed across a range of substratum materials, and surface roughness's, and then directly quantitatively compared. The assay was validated, with numerous controls and shown to be able to quantitatively assess microbe numbers on multiple materials. The assay was used to evaluate the initial binding of *Pseudomonas* to different substratums, corroborating binding phenomena observed in the literature as discussed in Chapter 1.20.

Most of the literature published either neglected roughness entirely, or not did not control it. However, one author (Pereni et al., 2006), tested a number of materials (see Figure 1.17) but with a very narrow roughness range R_a=0.08 - 0.25µm). Results presented herein extend the substratums materials that have been examined from a microbe attachment perspective. By possessing both rough and smooth variants (R_a=0.049µm - 3.5µm) of the different substratum

materials the effect of roughness within the scope of the experimental model was shown to be unimportant for attachment and cleaning. This larger range of roughness's tested include dimensions that are much smaller than the size of the bacteria, to dimensions much larger than the bacteria. *Pseudomonas* initial attachment and cleaning was confirmed to be relatively unimportant, with no clear correlations observed with roughness (Figure 6.14 and Figure 9.9 respectively).

Previously published data in the biofilm field includes; microbe initial attachment- γ_S correlations, including works by (Fletcher and Pringle, 1985, Dexter, 1979b, Baier, 1972, Baier, 1973, Hilbert et al., 2003). In this study similar correlations were observed with γ_S, but in addition the importance of γ^p_S has been found to have good correlations with *Pseudomonas* initial attachment, whilst γ^d_S has been shown to correlate well with the increased removal (clean) of mature biofilm in high shear experiments.

A range of industrial and novel surface treatments were evaluated to establish their performance with respect to biofilms attachment and cleaning. Following the modification of 'low energy' substratums for example PTFE and polycarbonate, with a gold 30nm thin film the initial binding of *Pseudomonas* was greatly increased, correlating well with the increase in both γ_S and γ^p_S. Inversely, 'high energy' stainless steel surfaces which were modified with a PTFE-AF thin film, resulted in a drastic decrease in microbe initial binding, which again correlated well with the surface energy metrics γ_S and γ^p_S. Thus, I have shown that the propensity of microbes to attach to a substratum can be inferred from substratum surface energy metrics. Additionally, thin-film modifications can be deployed to reduced or enhanced microbial attachment as required (see Figure 6.15). The longevity of these effects was not evaluated in this work, but will be subject to further investigation in the future.

The only deviation between the surface energy parameters and microbe initial attachment was seen when analysing the Sharklet™ PDMS substratum. However this material which is designed to resist microbial attachment was observed to be poor at this behaviour, relative to the polymers tested in this work, and was similar to smooth stainless steel in its microbial attachment performance. This material possessed very low surface energy, similar to that of both PTFE-AF 316 coated stainless steel and PTFE. As discussed in Chapter 6.6, this deviation maybe due to

the engineered topography being of similar scale to that of the microbes, enabling them to become trapped within the topographical features. This would have the effect of reducing the efficacy of the rinse step, which usually efficiently removes unbound microbes from the different substratums.

In addition to the initial attachment work, it was also shown that given time (four days) not only will mature biofilms form on all of the different substratums tested, including the thin film modified surfaces, but they will appear remarkably similar in many ways (see Chapter 8). For example, they possess approximately the same gross physical thicknesses and biomass regardless of substrate as determined by examining the dried physical data (Figure 8.4 and Figure 8.9) and inferred biomass data (Figure 8.1 and Figure 8.6) using confocal. A related conclusion was reached by Dexter who was conducting mixed species biofilm experiments in the harbors of ports (Dexter et al., 1975), for extended periods of up to 504 hours. But not within a controlled reproduced environment, as with the substratums tested in this work. It was interesting to observe that the relative abundance of the individual biofilm constituents (namely; polysaccharide: protein: microbe) did vary across the different materials, and over the different experiments that were conducted, for example when comparing data from the growth of biofilm on defined thin film modified substratums (Figure D1.4 and Figure D1.6) to data obtained for the negative controls in the high shear cleaning experiments (Figure E1.1 and Figure E1.3). Such differences are likely due to every biofilms essentially being unique, which arises from the fact that the surfaces were non-ideal, and the initial attachment locations and the exacting nature of individual microbes is not identical, all of which give rise to 'chaotic' inter biofilm component expression, that is tempered on a gross scale by the fluid flow conditions about their structures, limiting the net height.

Upon observing the biomass and average thickness of each of the mature *Pseudomonas* colony morphological elements that were evaluated during the course of this work it is evident that of the three microbial components the polysaccharide (ConA) component was typically the most abundant, throughout the most of the biofilm colonies. This observation is evident in biomass and average height datasets from both the TCS SP2 (Figure D1.1 and Figure D1.2 respectively) and TSC SP8 microscope data (Figure D1.4 and Figure D1.6 respectively). The relative abundance and over expression of polysaccharide by *Pseudomonas* has been reported in the literature on both inanimate surfaces by Matsukawa (Matsukawa and Greenberg, 2004), and also within biological environments i.e. the CF lung (Hentzer et al., 2001). Matsukawa also noted that the

abundance of protein in the EPS was less than both the protein and nuclear component, which was also typically observed during this study in both biomass and average height metrics (Figures D1.4, E1.1, E1.6 and Figures D1.6, E1.3 and E1.4 respectively).

The development of an assay that is able to elicit information on the gross structural stability and interfacial adhesion of biofilm was preliminarily developed. The assay tested one representative increased 'high' shear rate (relative to growth conditions) and was able to detect a correlation between decreases in surface energy metrics with increases in percentage biofilm removal. The assay was used to test which surfaces would be easier to 'clean' i.e. when imparting a constant force upon the pre-grown biofilms (grown and subjected to 44N/m^2 and 188N/m^2 shear stress, respectively), this was analogous to scrubbing a dirty Teflon^{TM} nonstick pan, versus a standard steel pan. One author (Mohandas et al., 1974) found a correlation with increases in substratum surface energy with an increase in the amount of shear required to remove in this case RBCs, the materials studied were glass, siliconized glass, polyethylene and Teflon^{TM}; this is similar to the observations made in Chapter 9.1. Another author also reported the removal of some 75 percent of cultured *Pseudomonas fluroscens* biofilm on 316 stainless steel with shear stresses of 75N/m^2 (Lowe., 1988). Here on stainless steel I report a 41 percent biomass removal using a shear rate of 188N/m^2 rate for 30 minutes. I have therefore been able to further add to this picture, whereby the amount of shear required to remove cells or bacteria is related to the surface energy of the substratums under investigation.

As part of this research effort a PTFE-AF thin film coating was applied to 316 stainless steel and was observed to greatly reduce microbial (*Pseudomonas*) attachment by some 88 percent, relative to uncoated stainless steel.

Busscher (Busscher and van Der Mei, 1995), commented that biofilm research should be directed to the removal of mature biofilms from substratums, and not initial attachment. But I would suggest that initial attachment, and mature biofilm removal are intimately related via the surface energy of the substratum, and that by lowering the surface energy of the material both microbe initial attachment is decreased, and high shear cleaning processes would have increased success.

To this end, by simply studying the rates of initial attachment, one could infer their cleanability, as was shown experimentally here, which is a far quicker, and accurate assay method. Hilbert and colleagues (Hilbert et al., 2003), found there was a link between surface energy and initial

attachment and also with the cleaning, this was however a review and summation of three papers, the observation was not likely coincidental.

CHAPTER 12 Conclusions and Future Work

12.1 Conclusions

This work ultimately focused on the interfacial relationship between prokaryotic multicellular communities at 2 stages of their life cycle (early stage adhesion and the mature biofilm) and their attachment/adhesion to inanimate surfaces. The following outcomes were found:

- To conduct these investigations two new biofilm assays were developed based on confocal microscopy; one that quickly quantifies the relative quantity of microbes attached on a given surface, irrespective of roughness, and another that probes mature biofilm removal. Both of these methods are able to provide quantitative measures of biofilm behaviour under real world conditions in solution.

- The confocal analysis allowed for the first time the protein, carbohydrate and microbial content of mature biofilms to the simultaneously determined. This study concluded that bio-film morphology with respect to these three components was, within experimental errors, independent of substrate roughness and composition.

- A relationship was established on the propensity of *Pseudomonas* to attach to a given surface which was principally driven by surface energy descriptors of the substrate.

- Given enough time (four days) all of the tested surfaces were colonised to a similar extent with mature biofilm in-situ as reflected in average film thicknesses.

- The surface energy link to initial attachment was further related to the 'cleanability' or removal of mature biofilm from surfaces. Further suggesting that the interfacial surface thermodynamics are still important for mature biofilm removal.

- Microbe bio-adhesion to stainless steel could be decreased via the use of PTFE-AF thin film coated onto stainless steel, producing a 88% reduction in *Pseudomonas* initial attachment, whilst also enhancing biofilm cleanability/removal. Treating hydrophobic low

energy surfaces (eg PTFE) with metallic coatings increased bio-adhesion. All microbial attachment and adhesion appear to be driven by the surface energy of the substratums.

- Surface roughness was shown to be essentially irrelevant to:

  - o to the initial attachment of Pseudomonas
  - o the resultant biofilm gross physical morphology
  - o the ease at which mature biofilm can be removed with high shear

- The results from the mature biofilm studies suggests that should a substratum have low surface energy, once colonised, the underlying interface between the biofilm superstructure will remain weak such that the biofilm will be more easily removed when physically challenged. This also suggests that *PA* is not able to readily adapt to attaching to low energy surface substrates, certainly within the 4 days of growth evaluated in this thesis.

12.2 Future work

Future work related to this project would include ascertaining whether there are differing growth rates for those microbes attached to the different substratums. This interest arises due to the observation of the structurally (eg thickness) similar biofilms observed after 4 days that did not correlate with the apparent differences in initial attachment behaviour.

Testing the binding, growth and cleanability of other microbes, including gram positive microbes and multispecies biofilms using these methods. This would help confirm and cross reference the reported importance of substrate surface energy. In addition to this work it would also be of benefit to examine the hydrophobicity of the microbes themselves, including their net surface charge, which is likely important in cell-substratum interactions.

Other important area for future work will include the testing of the stability and durability of the PTFE-AF thin film coating on both stainless steel and on other materials, whilst assaying its long term cleaning and anti-microbial efficacy.

It would be interesting to confirm *Pseudomonas* binding to a poly(dimethylsiloxane) surface analogous to the Sharklet™ substratum to aid in the investigation into the validity of the Sharklet™ pattern which allegedly drives a decrease in microbial adhesion, solely based on surface topography.

Finally it would be beneficial to extend the number of substratums tested in the high shear/silica abrasive cleaning experiments.

References

ABU-LAIL, N. I. & CAMESANO, T. A. 2003a. Role of Ionic Strength on the Relationship of Biopolymer Conformation, DLVO Contributions, and Steric Interactions to Bioadhesion of Pseudomonas putida KT2442. *Biomacromolecules,* 4**,** 1000-1012.

ABU-LAIL, N. I. & CAMESANO, T. A. 2003b. Role of Lipopolysaccharides in the Adhesion, Retention, and Transport of Escherichia coli JM109. *Environmental Science & Technology,* 37**,** 2173-2183.

ALBERTS, B., BRAY, D., LEWIS, J., RAFF, M., ROBERTS, K. & WATSON, J. D. 1983. *Molecular Biology of the cell*, Garland Publishing, Inc. New York & Londom.

ALDRICH, S. 2016. Product Information Concanavalin A from Canavalia ensiformis (Jack bean) γ-Irradiated. *In:* ALDRICH, S. (ed.).

ALLESEN-HOLM, M., BARKEN, K. B., YANG, L., KLAUSEN, M., WEBB, J. S., KJELLEBERG, S., MOLIN, S., GIVSKOV, M. & TOLKER-NIELSEN, T. 2006. A characterization of DNA release in PA cultures and biofilms. *Molecular Microbiology,* 59**,** 1114-1128.

ALLION, A., BARON, J.-P. & BOULANGE-PETERMANN, L. 2006. Impact of surface energy and roughness on cell distribution and viability. *Biofouling,* 22**,** 269-278.

AMANO, A., NAKAGAWA, I. & HAMADA, S. 1999. [36] Studying initial phase of biofilm formation: Molecular interaction of host proteins and bacterial surface components. *In:* RON, J. D. (ed.) *Methods in Enzymology.* Academic Press.

AMAZON.COM, I. 2013. *Dawn Ultra Hand Renewal with Olay Beauty Scent Dishwashing Liquid, Pomegranate Splash, 38 Ounce (Pack of 2)* [Online]. Amazon.com, Inc. Available:http://www.amazon.com/Dawn-Renewal-Beauty-Dishwashing-Pomegranate/dp/B004I9BT7M [Accessed 06.11.2013 2013].

AMRO, N. A., KOTRA, L. P., WADU-MESTHRIGE, K., BULYCHEV, A., MOBASHERY, S. & LIU, G.-Y. 2000. High-Resolution Atomic Force Microscopy Studies of the Escherichia coli Outer Membrane: Structural Basis for Permeability. *Langmuir,* 16**,** 2789-2796.

AN, Y. H. & FRIEDMAN, R. J. 1998. Concise review of mechanisms of bacterial adhesion to biomaterial surfaces. *Journal of Biomedical Materials Research,* 43**,** 338-348.

ANDERL, J. N., FRANKLIN, M. J. & STEWART, P. S. 2000. Role of Antibiotic Penetration Limitation in Klebsiella pneumoniae Biofilm Resistance to Ampicillin and Ciprofloxacin. *Antimicrobial Agents and Chemotherapy,* 44**,** 1818-1824.

ANGLES, M. L., MARSHALL, K. C. & GOODMAN, A. E. 1993. Plasmid Transfer between Marine Bacteria in the Aqueous Phase and Biofilms in Reactor Microcosms. *Appl Environ Microbiol,* 59**,** 843-50.

ARNOLD, J. W., BOOTHE, D. H., SUZUKI, O. & BAILEY, G. W. 2004. Multiple imaging techniques demonstrate the manipulation of surfaces to reduce bacterial contamination and corrosion. *Journal of Microscopy,* 216**,** 215-221.

AUERBACH, I. D., SORENSEN, C., HANSMA, H. G. & HOLDEN, P. A. 2000. Physical Morphology and Surface Properties of Unsaturated Pseudomonas putida Biofilms. *Journal of Bacteriology,* 182**,** 3809-3815.

AZADI, G., CHAUHAN, A. & TRIPATHI, A. 2013. Dilution of protein-surfactant complexes: A fluorescence study. *Protein Science : A Publication of the Protein Society,* 22**,** 1258-1265.

BACALLAO, R., KIAI, K. & JESAITIS, L. 1995. Guiding Principles of Specimen Preservation for Confocal Fluorescence Microscopy. *In:* PAWLEY, J. (ed.) *Handbook of Biological Confocal Microscopy.* Springer US.

BAIER, R. E. 1972. The role of surface energy in thrombogenesis. *Bulletin of the New York Academy of Medicine,* 48**,** 257-272.

BAIER, R. E. 1973. Influence of the initial surface condition of materials on bioadhesion. *In: Proc. 3rd Int. Congress on Marine Corrosion and Fouling.***,** 633-639.

BAIER, R. E. 2015. Correlations of Materials Surface Properties with Biological Responses. *Journal of Surface Engineered Materials and Advanced Technology,* 5**,** 42-51.

BAIER, R. E., DEPALMA, V. A., GOUPIL, D. W. & COHEN, E. 1985. Human platelet spreading on substrata of known surface chemistry. *J Biomed Mater Res,* 19**,** 1157-67.

BAKER, B. J., SAW, J. H., LIND, A. E., LAZAR, C. S., HINRICHS, K.-U., TESKE, A. P. & ETTEMA, T. J. G. 2016. Genomic inference of the metabolism of cosmopolitan subsurface Archaea, Hadesarchaea. *Nature Microbiology,* 1**,** 16002.

BARNES, L.-M., LO, M. F., ADAMS, M. R. & CHAMBERLAIN, A. H. L. 1999. Effect of Milk Proteins on Adhesion of Bacteria to Stainless Steel Surfaces. *Applied and Environmental Microbiology,* 65**,** 4543-4548.

BAYER, M. A. 2009. Makrolon 2858 ISO Data Sheet. *In:* SCIENCE, B. M. (ed.) 08.05.2009 ed. Online: Bayer Scientific.

BECKER, W. M., KLEINSMITH, L. J. & HARDIN, J. 2000. *The World of the Cell*, The Benjamin/Cummings Publishing Company.

BEENKEN, K. E., MRAK, L. N., GRIFFIN, L. M., ZIELINSKA, A. K., SHAW, L. N., RICE, K. C., HORSWILL, A. R., BAYLES, K. W. & SMELTZER, M. S. 2010. Epistatic Relationships between sarA and agr in Staphylococcus aureus Biofilm Formation. *PLoS ONE,* 5**,** e10790.

BICO, J., THIELE, U. & QUÉRÉ, D. 2002. Wetting of textured surfaces. *Colloids and Surfaces A: Physicochemical and Engineering Aspects,* 206**,** 41-46.

BIKSON, B. C., DING, Y. C., LE, R. J. E. & NELSON, J. K. C. 2004. *Gas separation using membranes formed from blends of perfluorinated polymers*. EU patent application 03014840.7.

BIOMED, P. 2016a. *RE: Staphylococcus aureus growth on Domino encapsulate in laminar flow (robbins device).* Type to KEVIN, W. & PALMER, J.

BIOMED, P. 2016b. *RE: Staphylococcus aureus growth on NILT in laminar flow (Robbins device).* Type to KEVIN, W. & PALMER, J.

BJERGBÆK, L. A., HAAGENSEN, J. A. J., REISNER, A., MOLIN, S. & ROSLEV, P. 2006. Effect of oxygen and growth medium on in vitro biofilm formation by Escherichia coli. *Biofilms,* 3**,** 1-10.

BLEL, W., LEGENTILHOMME, P., LEGRAND, J., BÉNÉZECH, T. & GENTIL-LELIÈVRE, C. L. 2008. Hygienic design: Effect of hydrodynamics on the cleanability of a food processing line. *AIChE Journal,* 54**,** 2553-2566.

BOLLENL, C. M. L., LAMBRECHTS, P. & QUIRYNEN, M. 1997. Comparison of surface roughness of oral hard materials to the threshold surface roughness for bacterial plaque retention: A review of the literature. *Dental Materials,* 13**,** 258-269.

BOULANGÉ-PETERMANN, L., RAULT, J. & BELLON-FONTAINE, M. N. 1997. Adhesion of streptococcus thermophilus to stainless steel with different surface topography and roughness. *Biofouling,* 11**,** 201-216.

BOYD, R. D., VERRAN, J., JONES, M. V. & BHAKOO, M. 2002. Use of the Atomic Force Microscope To Determine the Effect of Substratum Surface Topography on Bacterial Adhesion. *Langmuir,* 18**,** 2343-2346.

BRAGONZI, A., WIEHLMANN, L., KLOCKGETHER, J., CRAMER, N., WORLITZSCH, D., DORING, G. & TUMMLER, B. 2006. Sequence diversity of the mucABD locus in PA isolates from patients with cystic fibrosis. *Microbiology,* 152**,** 3261-9.

BRIANDET, R., MEYLHEUC, T., MAHER, C. & BELLON-FONTAINE, M. N. 1999. Listeria monocytogenes Scott A: Cell Surface Charge, Hydrophobicity, and Electron Donor and Acceptor Characteristics under Different Environmental Growth Conditions. *Applied and Environmental Microbiology,* 65**,** 5328-5333.

BRIDIER, A., DUBOIS-BRISSONNET, F., GREUB, G., THOMAS, V. & BRIANDET, R. 2011. Dynamics of the Action of Biocides in PA Biofilms. *Antimicrobial Agents and Chemotherapy,* 55**,** 2648-2654.

BRUINSMA, G. M., RUSTEMA-ABBING, M., VAN DER MEI, H. C. & BUSSCHER, H. J. 2001. Effects of cell surface damage on surface properties and adhesion of PA. *Journal of Microbiological Methods,* 45**,** 95-101.

BRYERS, J. D. & RATNER, B. D. 2004. Bioinspired Implant Materials Befuddle Bacteria. *ASM News,* 70**,** 232-237.

BUENO, H. 2005. *The critical surface tension of 316L stainless steel.* Masters of Science, San Jose State University.

BURKS, G. A., VELEGOL, S. B., PARAMONOVA, E., LINDENMUTH, B. E., FEICK, J. D. & LOGAN, B. E. 2003. Macroscopic and Nanoscale Measurements of the Adhesion of Bacteria with Varying Outer Layer Surface Composition. *Langmuir,* 19**,** 2366-2371.

BURMØLLE, M., WEBB, J. S., RAO, D., HANSEN, L. H., SØRENSEN, S. J. & KJELLEBERG, S. 2006. Enhanced Biofilm Formation and Increased Resistance to Antimicrobial Agents and Bacterial Invasion Are Caused by Synergistic Interactions in Multispecies Biofilms. *Applied and Environmental Microbiology,* 72**,** 3916-3923.

BUSSCHER, H. J., NORDE, W. & VAN DER MEI, H. C. 2008. Specific Molecular Recognition and Nonspecific Contributions to Bacterial Interaction Forces. *Applied and Environmental Microbiology,* 74**,** 2559-2564.

BUSSCHER, H. J. & VAN DER MEI, H. C. 2006. Microbial Adhesion in Flow Displacement Systems. *Clinical Microbiology Reviews,* 19**,** 127-141.

BUSSCHER, H. J. & VAN DER MEI, R. B. H. C. 1995. Initial microbial adhesion is a determinant for the strength of biofilm adhesion. *FEMS Microbiology Letters,* 128**,** 229-234.

BYRD, M. S., SADOVSKAYA, I., VINOGRADOV, E., LU, H., SPRINKLE, A. B., RICHARDSON, S. H., MA, L., RALSTON, B., PARSEK, M. R., ANDERSON, E. M., LAM, J. S. & WOZNIAK, D. J. 2009. Genetic and Biochemical Analyses of the PA Psl Exopolysaccharide Reveal Overlapping Roles for Polysaccharide Synthesis Enzymes in Psl and LPS Production. *Molecular microbiology,* 73**,** 622-638.

CALLEJA. G., JOURDAN. A., AMEDURI. B., HABAS. J-P. 2013. Where is the glass transition temperature of poly(tetra uoroethylene)? A new approach by dynamic rheometry and mechanical tests. *European Polymer Journal,* 49**,** 2214-2222.

CARMAN, M. L., ESTES, T. G., FEINBERG, A. W., SCHUMACHER, J. F., WILKERSON, W., WILSON, L. H., CALLOW, M. E., CALLOW, J. A. & BRENNAN, A. B. 2006. Engineered antifouling microtopographies – correlating wettability with cell attachment. *Biofouling,* 22**,** 11-21.

CARNY, O. & GAZIT, E. 2005. A model for the role of short self-assembled peptides in the very early stages of the origin of life. *FASEB J,* 19**,** 1051-5.

CARPENTIER, B. & CERF, O. 1993. Biofilms and their consequences, with particular reference to hygiene in the food industry. *J Appl Bacteriol,* 75**,** 499-511.

CASSIE, A. B. D. & BAXTER, S. 1944. Wettability of porous surfaces. *Transactions of the Faraday Society,* 40**,** 546-551.

CHANG, S. K., HUM, O. S., MOSCARELLO, M. A., NEUMANN, A. W., ZINGG, W., LEUTHEUSSER, M. J. & RUEGSEGGER, B. 1977. Platelet adhesion to solid surfaces. The effects of plasma proteins and substrate wettability. *Med Prog Technol,* 5**,** 57-66.

CHANG, W.-S., VAN DE MORTEL, M., NIELSEN, L., NINO DE GUZMAN, G., LI, X. & HALVERSON, L. J. 2007. Alginate Production by Pseudomonas putida Creates a Hydrated Microenvironment and Contributes to Biofilm Architecture and Stress Tolerance under Water-Limiting Conditions. *Journal of Bacteriology,* 189**,** 8290-8299.

CHANG, Y.-I. & CHANG, P.-K. 2002. The role of hydration force on the stability of the suspension of Saccharomyces cerevisiae–application of the extended DLVO theory. *Colloids and Surfaces A: Physicochemical and Engineering Aspects,* 211**,** 67-77.

CHAPMAN, M. R., ROBINSON, L. S., PINKNER, J. S., ROTH, R., HEUSER, J., HAMMAR, M., NORMARK, S. & HULTGREN, S. J. 2002. Role of Escherichia coli curli operons in directing amyloid fiber formation. *Science,* 295**,** 851-5.

CHARACKLIS, W. G. 1981. Bioengineering report: Fouling biofilm development: A process analysis. *Biotechnology and Bioengineering,* 23**,** 1923-1960.

CHEMOURS-COMPANY 2016a. Teflon™ AF Amorphous Fluoroplastic Resins. *In:* THE-CHEMOURS-COMPANY (ed.).

CHEMOURS-COMPANY 2016b. Teflon™ AF Amorphous Fluoroplastic Resins Preparing Solutions of Teflon™ AF. *In:* COMPANY, T. C. (ed.).

CHEMOURS-COMPANY. 2016c. *Teflon™ AF Applications* [Online]. Chemours. Available: https://chemours.com/Teflon_Industrial/en_US/products/product_by_name/teflon_af/apps.html [Accessed 24.11.16 2016].

CHEMTEX, S. L. 2013. *Biocides and Microbiocides* [Online]. Available: http://www.chemtexlimited.com/biocides-and-microbiocides.html [Accessed 10.05.2013 2013].

CHEN, M.-Y., CHEN, M.-J., LEE, P.-F., CHENG, L.-H., HUANG, L.-J., LAI, C.-H. & HUANG, K.-H. 2010. Towards real-time observation of conditioning film and early biofilm formation under laminar flow conditions using a quartz crystal microbalance. *Biochemical Engineering Journal,* 53**,** 121-130.

CHMIELEWSKI, R. A. N. & FRANK, J. F. 2003. Biofilm Formation and Control in Food Processing Facilities. *Comprehensive Reviews in Food Science and Food Safety,* 2**,** 22-32.

CHRISTENSEN, B. E. 1989. The role of extracellular polysaccharides in biofilms. *Journal of Biotechnology,* 10**,** 181-202.

CHRISTERSSON, C. E., GLANTZ, P.-O. J. & BAIER, R. E. 1988. Role of temperature and shear forces on microbial detachment. *European Journal of Oral Sciences,* 96**,** 91-98.

CHUANG, S. E., BURLAND, V., PLUNKETT, G., 3RD, DANIELS, D. L. & BLATTNER, F. R. 1993. Sequence analysis of four new heat-shock genes constituting the hslTS/ibpAB and hslVU operons in Escherichia coli. *Gene,* 134**,** 1-6.

CHUNG, K. K., SCHUMACHER, J. F., SAMPSON, E. M., BURNE, R. A., ANTONELLI, P. J. & BRENNAN, A. B. 2007. Impact of engineered surface microtopography on biofilm formation of Staphylococcus aureus. *Biointerphases,* 2**,** 89-94.

CLAXTON. N.S., F. J. T., DAVIDSON. M. W. 2005. Laser Scanning Confocal Microscopy. Available: http://www.olympusconfocal.com/theory/LSCMIntro.pdf.

COGNARD, J. 1984. Adhesion to gold: A review. *Gold Bulletin,* 17**,** 131-139.

COLE, S. J., RECORDS, A. R., ORR, M. W., LINDEN, S. B. & LEE, V. T. 2014. Catheter-Associated Urinary Tract Infection by PA Is Mediated by Exopolysaccharide-Independent Biofilms. *Infection and Immunity,* 82**,** 2048-2058.

COLVIN, K. M., GORDON, V. D., MURAKAMI, K., BORLEE, B. R., WOZNIAK, D. J., WONG, G. C. L. & PARSEK, M. R. 2011. The Pel Polysaccharide Can Serve a Structural and Protective Role in the Biofilm Matrix of PA. *PLoS Pathog,* 7**,** e1001264.

COLVIN, K. M., IRIE, Y., TART, C. S., URBANO, R., WHITNEY, J. C., RYDER, C., HOWELL, P. L., WOZNIAK, D. J. & PARSEK, M. R. 2012. The Pel and Psl polysaccharides provide PA structural redundancy within the biofilm matrix. *Environ Microbiol,* 14**,** 1913-28.

COMPÈRE, C., BELLON-FONTAINE, M. N., BERTRAND, P., COSTA, D., MARCUS, P., POLEUNIS, C., PRADIER, C. M., RONDOT, B. & WALLS, M. G. 2001. Kinetics of conditioning layer formation on stainless steel immersed in seawater. *Biofouling,* 17**,** 129-145.

COSTERTON, J. W., LEWANDOWSKI, Z., CALDWELL, D. E., KORBER, D. R. & LAPPIN-SCOTT, H. M. 1995. Microbial Biofilms. *Annual Review of Microbiology,* 49**,** 711-745.

COSTERTON. W. J., C. K. J., GEESEY. G. G., LADD. T. I., NICKLE. J. C., DASGUPTA. M., MARRIE. T. J. 1987. Bacterial Biofilms in nature and disease. *Annual Review Microbiology,* 41**,** 435-464.

CROSS, S. E., KRETH, J., WALI, R. P., SULLIVAN, R., SHI, W. & GIMZEWSKI, J. K. 2009. Evaluation of bacteria-induced enamel demineralization using optical profilometry. *Dental materials : official publication of the Academy of Dental Materials,* 25**,** 1517-1526.

CUCARELLA, C., SOLANO, C., VALLE, J., AMORENA, B., LASA, Í. & PENADÉS, J. R. 2001. Bap, a Staphylococcus aureus Surface Protein Involved in Biofilm Formation. *Journal of Bacteriology,* 183**,** 2888-2896.

DALBY, M. J., RIEHLE, M. O., YARWOOD, S. J., WILKINSON, C. D. & CURTIS, A. S. 2003. Nucleus alignment and cell signaling in fibroblasts: response to a micro-grooved topography. *Exp Cell Res,* 284**,** 274-82.

DALTON, H. M., POULSEN, L. K., HALASZ, P., ANGLES, M. L., GOODMAN, A. E. & MARSHALL, K. C. 1994. Substratum-induced morphological changes in a marine bacterium and their relevance to biofilm structure. *Journal of bacteriology,* 176,**,** 6900±6906.

DANIEL J. WOZNIAK, T. J. O. W., MELISSA STARKEY, REBECCA KEYSER, PARASTOO AZADI, GEORGE A. O'TOOLE, MATTHEW R. PARSEK 2003. Alginate is not a significant component of the extracellular polysaccharide matrix of PA14 and PAO1 PA biofilms. *PNAS,* 100 7907-7912.

DANKERT, J., HOGT, A.H. AND FEIJEN, J. 1986. Biomedical polymers: Bacterial adhesion, colonization and infection. *CRC Critical Reviews in Biocompatibility,* 2**,** 219-301.

DARREN R. KORBER, J. R. L., HILARY M. LAPPIN-SCOTT, COSTERTON, J. W., KORBER, D. R., . & ET AL. 1995. *Growth of Microorganisms on Surfaces*

Microbial Biofilms, Cambridge University Press.

DARZINS, A. & RUSSELL, M. A. 1997. Molecular genetic analysis of type-4 pilus biogenesis and twitching motility using PA as a model system – a review1. *Gene,* 192**,** 109-115.

DARZINS A., C. A. 1984. Cloning of genes controlling alginate biosynthesis from a mucoid cystic fibrosis isolate of PA. *Journal of Bacteriology,* 159**,** 9-18.

DAS, T., SHARMA, P. K., BUSSCHER, H. J., VAN DER MEI, H. C. & KROM, B. P. 2010. Role of Extracellular DNA in Initial Bacterial Adhesion and Surface Aggregation. *Applied and Environmental Microbiology,* 76**,** 3405-3408.

DAVID, Q., AURÉLIE, L. & JOSÉ, B. 2003. Slippy and sticky microtextured solids. *Nanotechnology,* 14**,** 1109.

DAVIES, D. G. 2000. *Physiological events in biofilm formation, Community structure and co-operation in biofilms*, Society for General Microbiology.

DE BEER, D., STOODLEY, P. & LEWANDOWSKI, Z. 1994a. Liquid flow in heterogeneous biofilms. *Biotechnology and Bioengineering,* 44**,** 636-641.

DE BEER, D., STOODLEY, P., ROE, F. & LEWANDOWSKI, Z. 1994b. Effects of biofilm structures on oxygen distribution and mass transport. *Biotechnology and Bioengineering,* 43**,** 1131-1138.

DE KERCHOVE, A. J. & ELIMELECH, M. 2008. Calcium and Magnesium Cations Enhance the Adhesion of Motile and Nonmotile PA on Alginate Films. *Langmuir,* 24**,** 3392-3399.

DE KIEVIT, T. 2011. 1.41 - Biofilms. *In:* EDITOR-IN-CHIEF: MURRAY, M.-Y. (ed.) *Comprehensive Biotechnology (Second Edition).* Burlington: Academic Press.

DE PRIJCK, K., NELIS, H. & COENYE, T. 2007. Efficacy of silver-releasing rubber for the prevention of PA biofilm formation in water. *Biofouling,* 23**,** 405-411.

DE. SANGOSSE, L. 2004. Spray Enhancers - Silwet L-77. *In:* LTD, D. S. (ed.).

DELL'ANNO, A., STEFANO, B. & DANOVARO, R. 2002. Quantification, base composition, and fate of extracellular DNA in marine sediments. *Limnology and Oceanography,* 47**,** 899-905.

DEPAS, W. H. & CHAPMAN, M. R. 2012. Microbial manipulation of the amyloid fold. *Research in Microbiology,* 163**,** 592-606.

DEPAS, W. H., SYED, A. K., SIFUENTES, M., LEE, J. S., WARSHAW, D., SAGGAR, V., CSANKOVSZKI, G., BOLES, B. R. & CHAPMAN, M. R. 2014. Biofilm Formation Protects Escherichia coli against Killing by Caenorhabditis elegans and Myxococcus xanthus. *Applied and Environmental Microbiology,* 80**,** 7079-7087.

DEVELOPMENT, O. F. E. C.-O. A. 2006. Safety Assessment of Transgenic Organisms. *In:* BIOTECHNOLOGY, W. G. O. H. O. R. O. I. (ed.). OECD.

DEXTER, S. C. 1979a. Human platelet spreading on substrata of known surface chemistry. *J Colloid Interface Sci,* 70**,** 346.

DEXTER, S. C. 1979b. Influence of substratum critical surface tension on bacterial adhesion—in Situ studies. *Journal of Colloid and Interface Science,* 70**,** 346-354.

DEXTER, S. C., SULLIVAN, J. D., WILLIAMS, J. & WATSON, S. W. 1975. Influence of Substrate Wettability on the Attachment of Marine Bacteria to Various Surfaces. *Applied Microbiology,* 30**,** 298-308.

DÍAZ, C., SCHILARDI, P. L., DOS SANTOS CLARO, P. C., SALVAREZZA, R. C. & FERNÁNDEZ LORENZO DE MELE, M. A. 2009. Submicron Trenches Reduce the Pseudomonas fluorescens Colonization Rate on Solid Surfaces. *ACS Applied Materials & Interfaces,* 1**,** 136-143.

DICKSON, J. S. 1991. Attachment ofSalmonella typhimurium andListeria monocytogenes to beef tissue: effects of inoculum level, growth temperature and bacterial culture age. *Food Microbiology,* 8**,** 143-151.

DICKSON, J. S. & KOOHMARAIE, M. 1989. Cell surface charge characteristics and their relationship to bacterial attachment to meat surfaces. *Applied and Environmental Microbiology,* 55**,** 832-836.

DIXON, M. C. 2008. Quartz Crystal Microbalance with Dissipation Monitoring: Enabling Real-Time Characterization of Biological Materials and Their Interactions. *Journal of Biomolecular Technology,* 19**,** 151-158.

DONLAN, R. M. 2002. Biofilms: Microbial Life on Surfaces. *Centers for Disease Control and Prevention,* 8**,** 881-890.

DONLAN, R. M. & COSTERTON, J. W. 2002. Biofilms: Survival Mechanisms of Clinically Relevant Microorganisms. *Clinical Microbiology Reviews,* 15**,** 167-193.

DOWHAN, W., M, B., E, M. & O., R. C. 2008. *Biochemistry of Lipids, Lipoproteins and Membranes, 5th Edition*.

DUEHOLM, M. S., PETERSEN, S. V., SONDERKAER, M., LARSEN, P., CHRISTIANSEN, G., HEIN, K. L., ENGHILD, J. J., NIELSEN, J. L., NIELSEN, K. L., NIELSEN, P. H. & OTZEN, D. E. 2010. Functional amyloid in Pseudomonas. *Mol Microbiol,* 77**,** 1009-20.

DUNNE, W. M. 2002. Bacterial Adhesion: Seen Any Good Biofilms Lately? *Clinical Microbiology Reviews,* 15**,** 155-166.

EHEDG, E. H. E. A. D. G. 2009. EHEDG Type EL - CLASS I Certification. European Hygienic Engineering and Design Group.

EMITECH, Q. 2007. K550X Sputter Coater Instruction Manual. *In:* EMITECH, Q. (ed.) 5th Issue ed.

ENGELHART, S., KRIZEK, L., GLASMACHER, A., FISCHNALLER, E., MARKLEIN, G. & EXNER, M. 2002. PA outbreak in a haematology–oncology unit associated with contaminated surface cleaning equipment. *Journal of Hospital Infection,* 52**,** 93-98.

ETZLER, F. M. 2003. Characterization of surface free energies and surface chemistry of solids. *In:* MITTAL, K. L. (ed.) *Contact Angle, Wettability and Adhesion.* Boston and Utrecht: VSP.

EVANS, L. R. & LINKER, A. 1973. Production and Characterization of the Slime Polysaccharide of PA. *Journal of Bacteriology,* 116**,** 915-924.

FAVERO, M. S., CARSON, L. A., BOND, W. W. & PETERSEN, N. J. 1971. PA: growth in distilled water from hospitals. *Science,* 173**,** 836-8.

FAZLI, M., BJARNSHOLT, T., KIRKETERP-MØLLER, K., JØRGENSEN, B., ANDERSEN, A. S., KROGFELT, K. A., GIVSKOV, M. & TOLKER-NIELSEN, T. 2009. Nonrandom Distribution of PA and Staphylococcus aureus in Chronic Wounds. *Journal of Clinical Microbiology,* 47**,** 4084-4089.

FISHBANE, P. M., GASIOROWICZ, S. & THORNTON, S. T. 1996. *Physics for Scientists and Engineers,* New Jersey, Prentice-Hall Inc.

FISHER SCIENTIFIC, M. P. 2003. SYPRO® Orange and SYPRO® Red Protein Gel Stains. *In:* FISHER SCIENTIFIC, M. P. (ed.).

FISHER SCIENTIFIC, M. P. 2004. LIVE/DEAD BacLight Bacterial Viability Kits. *In:* FISHER SCIENTIFIC, M. P. (ed.).

FLEMMING, H.-C. & WINGENDER, J. 2010. The biofilm matrix. *Nat Rev Micro,* 8**,** 623-633.

FLETCHER, M. 1976. The Effects of Proteins on Bacterial Attachment to Polystyrene. *Journal of General Microbiology,* 94**,** 400-404.

FLETCHER, M. & PRINGLE, J. H. 1985. The effect of surface free energy and medium surface tension on bacterial attachment to solid surfaces. *Journal of Colloid and Interface Science,* 104**,** 5-14.

FLINT, S. H., BROOKS, J. D. & BREMER, P. J. 1997. The influence of cell surface properties of thermophilic streptococci on attachment to stainless steel. *J Appl Microbiol,* 83**,** 508-17.

FLINT, S. H., BROOKS, J. D. & BREMER, P. J. 2000. Properties of the stainless steel substrate, influencing the adhesion of thermo-resistant streptococci. *Journal of Food Engineering,* 43**,** 235-242.

FOWKES, F. M. 1962. DETERMINATION OF INTERFACIAL TENSIONS, CONTACT ANGLES, AND DISPERSION FORCES IN SURFACES BY ASSUMING ADDITIVITY OF INTERMOLECULAR INTERACTIONS IN SURFACES. *The Journal of Physical Chemistry,* 66**,** 382-382.

FOWKES, F. M. 1964. ATTRACTIVE FORCES AT INTERFACES. *Industrial & Engineering Chemistry,* 56**,** 40-52.

FRANK, J. F. & CHMIELEWSKI, R. 2001. Influence of surface finish on the cleanability of stainless steel. *J Food Prot,* 64**,** 1178-82.

FRANKLIN, M. J., NIVENS, D. E., WEADGE, J. T. & HOWELL, P. L. 2011. Biosynthesis of the PA Extracellular Polysaccharides, Alginate, Pel, and Psl. *Frontiers in Microbiology,* 2.

FRIEDMAN, L. & KOLTER, R. 2004. Genes involved in matrix formation in PA PA14 biofilms. *Mol Microbiol,* 51**,** 675-90.

GADELMAWLA, E. S., KOURA, M. M., MAKSOUD, T. M. A., ELEWA, I. M. & SOLIMAN, H. H. 2002. Roughness parameters. *Journal of Materials Processing Technology,* 123**,** 133-145.

GALLI MARXER, C., COLLAUD COEN, M., GREBER, T., GREBER, U. & SCHLAPBACH, L. 2003. Cell spreading on quartz crystal microbalance elicits positive frequency shifts indicative of viscosity changes. *Analytical and Bioanalytical Chemistry,* 377**,** 578-586.

GAMBLIN, T. C., CHEN, F., ZAMBRANO, A., ABRAHA, A., LAGALWAR, S., GUILLOZET, A. L., LU, M., FU, Y., GARCIA-SIERRA, F., LAPOINTE, N., MILLER, R., BERRY, R. W., BINDER, L. I. & CRYNS, V. L. 2003. Caspase cleavage of tau: Linking amyloid and neurofibrillary tangles in Alzheimer's disease. *Proceedings of the National Academy of Sciences,* 100**,** 10032-10037.

GARRETT, T. R., BHAKOO, M. & ZHANG, Z. 2008. Bacterial adhesion and biofilms on surfaces. *Progress in Natural Science,* 18**,** 1049-1056.

GEESEY, G. G., JANG, L., JOLLEY, J. G., HANKINK, M. R., IWAOKA, T. & GRIFFITHS, P. R. 1988. Binding of Metal Ions by Extracellular Polymers of Biofilm Bacteria. *Water Science & Technology,* 20**,** 161-165.

GLEICK, J. 1998. *Chaos*, Vintage.

GLOAG, E. S., TURNBULL, L., HUANG, A., VALLOTTON, P., WANG, H., NOLAN, L. M., MILILLI, L., HUNT, C., LU, J., OSVATH, S. R., MONAHAN, L. G., CAVALIERE, R., CHARLES, I. G., WAND, M. P., GEE, M. L., PRABHAKAR, R. & WHITCHURCH, C. B. 2013. Self-organization of bacterial biofilms is facilitated by extracellular DNA. *Proceedings of the National Academy of Sciences,* 110**,** 11541-11546.

GOLDSTEIN, I. J., HOLLERMAN, C. E. & SMITH, E. E. 1965. Protein-Carbohydrate Interaction. II. Inhibition Studies on the Interaction of Concanavalin A with Polysaccharides*. *Biochemistry,* 4**,** 876-883.

GORB, S. N. K., K. 2014. *Beilstein J. Nanotechnol.,* 5**,** 1450–1451.

GORDON, C. A., HODGES, N. A. & MARRIOTT, C. 1988. Antibiotic interaction and diffusion through alginate and exopolysaccharide of cystic fibrosis-derived PA. *Journal of Antimicrobial Chemotherapy,* 22**,** 667-674.

GOTTENBOS, B., VAN DER MEI, H., C. & BUSSCHER, H., J 2000. Initial adhesion and surface growth of Staphylococcus epidermidis and PA on biomedical polymers. *Journal of Biomedical Materials Research,* 50**,** 208-214.

GOTTENBOS, B., VAN DER MEI, H. C., BUSSCHER, H. J., GRIJPMA, D. W. & FEIJEN, J. 1999. Initial adhesion and surface growth of PA on negatively and positively charged poly(methacrylates). *Journal of Materials Science: Materials in Medicine,* 10**,** 853-855.

GOVAN, J. R. 1975. Mucoid strains of PA: the influence of culture medium on the stability of mucus production. *J Med Microbiol,* 8**,** 513-22.

GOVAN, J. R. & DERETIC, V. 1996. Microbial pathogenesis in cystic fibrosis: mucoid PA and Burkholderia cepacia. *Microbiological Reviews,* 60**,** 539-74.

GUÐBJÖRNSDÓTTIR, B., EINARSSON, H., THORKELSSON, G. 2005. Microbial Adhesion to Processing Lines for Fish Fillets and Cooked Shrimp: Influence of Stainless Steel Surface Finish and Presence of Gram-Negative Bacteria on the Attachment of Listeria monocytogenes. *Food Technology and Biotechnology,* 43**,** 55-61.

GUNASEKARAN, G., CHONGDAR, S., GAONKAR, S. N. & KUMAR, P. 2004. Influence of bacteria on film formation inhibiting corrosion. *Corrosion Science,* 46**,** 1953-1967.

HAMZA, A., PHAM, V. A., MATSUURA, T. & SANTERRE, J. P. 1997. Development of membranes with low surface energy to reduce the fouling in ultrafiltration applications. *Journal of Membrane Science,* 131**,** 217-227.

HAO, L., LAWRENCE, J. & LI, L. 2005. The wettability modification of bio-grade stainless steel in contact with simulated physiological liquids by the means of laser irradiation. *Applied Surface Science,* 247**,** 453-457.

HARA, T., SEINOSUKE. UEDA 1981. A Study on the Mechanism of DNA Excretion from P. aeruginosa KYU-1 — Effect of Mitomycin C on Extracellular DNA Production. *Agricultural and Biological Chemistry,* 45**,** 2457-2461.

HARDALO, C. & EDBERG, S. C. 1997. PA: assessment of risk from drinking water. *Crit Rev Microbiol,* 23**,** 47-75.

HAWE, A., SUTTER, M. & JISKOOT, W. 2008. Extrinsic Fluorescent Dyes as Tools for Protein Characterization. *Pharmaceutical Research,* 25**,** 1487-1499.

HAY, I. D., REHMAN, Z. U., MORADALI, M. F., WANG, Y. & REHM, B. H. A. 2013. Microbial alginate production, modification and its applications. *Microbial Biotechnology,* 6**,** 637-650.

HEDBERG, Y., KARLSSON, M.-E., BLOMBERG, E., ODNEVALL WALLINDER, I. & HEDBERG, J. 2014. Correlation between surface physicochemical properties and the release of iron from stainless steel AISI 304 in biological media. *Colloids and Surfaces B: Biointerfaces,* 122**,** 216-222.

HEJDA, F. 2010. *Surface Free Energy Determination by Contact Angle Measurements - A Comparison of Various Approaches*.

HENTZER, M., TEITZEL, G. M., BALZER, G. J., HEYDORN, A., MOLIN, S., GIVSKOV, M. & PARSEK, M. R. 2001. Alginate overproduction affects PA biofilm structure and function. *J Bacteriol,* 183**,** 5395-401.

HERALD, P. J. & ZOTTOLA, E. A. 1988. Attachment of Listeria monocytogenes to Stainless Steel Surfaces at Various Temperatures and pH Values. *Journal of Food Science,* 53**,** 1549-1562.

HERMANSSON, M. 1999. The DLVO theory in microbial adhesion. *Colloids and Surfaces B: Biointerfaces,* 14**,** 105-119.

HEYDORN, A., NIELSEN, A. T., HENTZER, M., STERNBERG, C., GIVSKOV, M., ERSBOLL, B. K. & MOLIN, S. 2000. Quantification of biofilm structures by the novel computer program COMSTAT. *Microbiology,* 146 (Pt 10)**,** 2395-407.

HILBERT, L. R., BAGGE-RAVN, D., KOLD, J. & GRAM, L. 2003. Influence of surface roughness of stainless steel on microbial adhesion and corrosion resistance. *International Biodeterioration & Biodegradation,* 52**,** 175-185.

HOGARDT, M., TREBESIUS, K., GEIGER, A. M., HORNEF, M., ROSENECKER, J. & HEESEMANN, J. 2000. Specific and Rapid Detection by Fluorescent In Situ Hybridization of Bacteria in Clinical Samples Obtained from Cystic Fibrosis Patients. *Journal of Clinical Microbiology,* 38**,** 818-825.

HOGT, A. H., DANKERT, J. & FEIGEN, J. 1985. Adhesion of Staphylococcus epidermidis and Staphylococcus saprophyticus to a Hydrophobic Biomaterial. *Journal of General Microbiology,* 131**,** 2485-2491.

HØIBY, N., KROGH JOHANSEN, H., MOSER, C., SONG, Z., CIOFU, O. & KHARAZMI, A. 2001. PA and the in vitroand in vivo biofilm mode of growth. *Microbes and Infection,* 3**,** 23-35.

HOOD, S. K. & ZOTTOLA, E. A. 1997. Adherence to stainless steel by foodborne microorganisms during growth in model food systems. *International Journal of Food Microbiology,* 37**,** 145-153.

HORI, K. & MATSUMOTO, S. 2010. Bacterial adhesion: From mechanism to control. *Biochemical Engineering Journal,* 48**,** 424-434.

HSU, L. C., FANG, J., BORCA-TASCIUC, D. A., WOROBO, R. W. & MORARU, C. I. 2013. Effect of Micro- and Nanoscale Topography on the Adhesion of Bacterial Cells to Solid Surfaces. *Applied and Environmental Microbiology,* 79**,** 2703-2712.

HUBER. ENGINEERED. MATERIALS. CORP 2015. MATERIAL SAFETY DATA SHEET Zeodent® 119. *In:* HUBER (ed.) 1.2 ed.

IQBAL, K., DEL C. ALONSO, A., CHEN, S., CHOHAN, M. O., EL-AKKAD, E., GONG, C.-X., KHATOON, S., LI, B., LIU, F., RAHMAN, A., TANIMUKAI, H. & GRUNDKE-IQBAL, I. 2005. Tau pathology in Alzheimer disease and other tauopathies. *Biochimica et Biophysica Acta (BBA) - Molecular Basis of Disease,* 1739**,** 198-210.

IRIE, Y., ROBERTS, A., KRAGH, K., GORDON, V., HUTCHISON, J., ALLEN, R., MELAUGH, G., BJARNSHOLT, T., WEST, S. & DIGGLE, S. 2016. The PA polysaccharide PSL is a social but non-cheatable trait in biofilms. *bioRxiv*.

IVANOVA, N. A., STAROV, V., RUBIO, R., RITACCO, H., HILAL, N. & JOHNSON, D. 2010. Critical wetting concentrations of trisiloxane surfactants. *Colloids and Surfaces A: Physicochemical and Engineering Aspects,* 354**,** 143-148.

JACK, R. F., RINGELBERG, D. B. & WHITE, D. C. 1992. Differential corrosion rates of carbon steel by combinations of Bacillus sp., Hafnia alvei and Desulfovibrio gigas established by phospholipid analysis of electrode biofilm. *Corrosion Science,* 33**,** 1843-1853.

JAYARAMAN, A., MANSFELD, F. B. & WOOD, T. K. 1999. Inhibiting sulfate-reducing bacteria in biofilms by expressing the antimicrobial peptides indolicidin and bactenecin. *Journal of Industrial Microbiology and Biotechnology,* 22**,** 167-175.

JOHANNSMANN, D. 2007. Studies of Viscoelasticity with the QCM. *In:* STEINEM, C. & JANSHOFF, A. (eds.) *Piezoelectric Sensors.* Springer Berlin Heidelberg.

JONES, C. J., RYDER, C. R., MANN, E. E. & WOZNIAK, D. J. 2013. AmrZ modulates PA biofilm architecture by directly repressing transcription of the psl operon. *J Bacteriol,* 195**,** 1637-44.

JONES, J. F., FEICK, J. D., IMOUDU, D., CHUKWUMAH, N., VIGEANT, M. & VELEGOL, D. 2003. Oriented Adhesion of Escherichia coli to Polystyrene Particles. *Applied and Environmental Microbiology,* 69**,** 6515-6519.

K P SCHMID, R. S., G PALMISANO, S DOPPLER, M. WINKLER 2011. Efficacy of microscopic surface patterning for reducing hospital environmental contamination. *ThGOT Zeulenroda.* Germany.

KAPER, H. J., BUSSCHER, H. J. & NORDE, W. 2003. Characterization of poly(ethylene oxide) brushes on glass surfaces and adhesion of Staphylococcus epidermidis. *J Biomater Sci Polym Ed,* 14**,** 313-24.

KIM, H., RYU, J.-H. & BEUCHAT, L. R. 2006. Attachment of and Biofilm Formation by Enterobacter sakazakii on Stainless Steel and Enteral Feeding Tubes. *Applied and Environmental Microbiology,* 72**,** 5846-5856.

KIM, J., PARK, H.-D. & CHUNG, S. 2012. Microfluidic Approaches to Bacterial Biofilm Formation. *Molecules,* 17**,** 9818-9834.

KIM, W., TENGRA, F. K., YOUNG, Z., SHONG, J., MARCHAND, N., CHAN, H. K., PANGULE, R. C., PARRA, M., DORDICK, J. S., PLAWSKY, J. L. & COLLINS, C. H. 2013. Spaceflight Promotes Biofilm Formation by PA. *PLoS ONE,* 8**,** e62437.

KLAUSEN, M., AAES-JØRGENSEN, A., MOLIN, S. & TOLKER-NIELSEN, T. 2003. Involvement of bacterial migration in the development of complex multicellular structures in PA biofilms. *Molecular Microbiology,* 50**,** 61-68.

KLEMM, P. & SCHEMBRI, M. A. 2000. Bacterial adhesins: function and structure. *International Journal of Medical Microbiology,* 290**,** 27-35.

KOCHAROVA, N. A., KNIREL, Y. A., SHASHKOV, A. S., KOCHETKOV, N. K. & PIER, G. B. 1988. Structure of an extracellular cross-reactive polysaccharide from PA immunotype 4. *J Biol Chem,* 263**,** 11291-5.

KOLARI, M., NUUTINEN, J., RAINEY, F. A. & SALKINOJA-SALONEN, M. S. 2003. Colored moderately thermophilic bacteria in paper-machine biofilms. *Journal of Industrial Microbiology and Biotechnology,* 30**,** 225-238.

KORBER, D. R., CHOI, A., WOLFAARDT, G. M., INGHAM, S. C. & CALDWELL, D. E. 1997. Substratum topography influences susceptibility of Salmonella enteritidis biofilms to trisodium phosphate. *Applied and Environmental Microbiology,* 63**,** 3352-3358.

KORBER, D. R., LAWRENCE, J. R. & CALDWELL, D. E. 1994. Effect of Motility on Surface Colonization and Reproductive Success of Pseudomonas fluorescens in Dual-Dilution Continuous Culture and Batch Culture Systems. *Appl Environ Microbiol,* 60**,** 1421-9.

KORBER, D. R., LAWRENCE, J. R., HENDRY, M. J. & CALDWELL, D. E. 1993. Analysis of spatial variability within mot+ and mot− pseudomonas fluorescens biofilms using representative elements. *Biofouling,* 7**,** 339-358.

KORBER, D. R., LAWRENCE, J. R., SUTTON, B. & CALDWELL, D. E. 1989. Effect of laminar flow velocity on the kinetics of surface recolonization by Mot+ and Mot− Pseudomonas fluorescens. *Microbial Ecology,* 18**,** 1-19.

KORSTGENS, V., FLEMMING, H. C., WINGENDER, J. & BORCHARD, W. 2001. Influence of calcium ions on the mechanical properties of a model biofilm of mucoid PA. *Water Sci Technol,* 43**,** 49-57.

KUCZYNSKA-WISNIK, D., MATUSZEWSKA, E. & LASKOWSKA, E. 2010. Escherichia coli heat-shock proteins IbpA and IbpB affect biofilm formation by influencing the level of extracellular indole. *Microbiology,* 156**,** 148-57.

KUMAR, C. G. & ANAND, S. K. 1998. Significance of microbial biofilms in food industry: a review. *International Journal of Food Microbiology,* 42**,** 9-27.

KUSUMAATMAJA, H., BLOW, M. L., DUPUIS, A. & YEOMANS, J. M. 2008. The collapse transition on superhydrophobic surfaces. *EPL (Europhysics Letters),* 81**,** 36003.

KUZNAR, Z. A. & ELIMELECH, M. 2004. Adhesion Kinetics of Viable Cryptosporidium parvum Oocysts to Quartz Surfaces. *Environmental Science & Technology,* 38**,** 6839-6845.

LANDROCK. A, H. 2015. *Handbook of Adhesive Technology* Elsevier.

LATASA, C., SOLANO, C., PENADÉS, J. R. & LASA, I. 2006. Biofilm-associated proteins. *Comptes Rendus Biologies,* 329**,** 849-857.

LAWRENCE, J. & LI, L. 1999. Carbon steel wettability characteristics enhancement for improved enamelling using a 1.2 kW high power diode laser. *Optics and Lasers in Engineering,* 32**,** 353-365.

LAWRENCE, J. R., DELAQUIS, P. J., KORBER, D. R. & CALDWELL, D. E. 1987. Behavior ofPseudomonas fluorescens within the hydrodynamic boundary layers of surface microenvironments. *Microbial Ecology,* 14**,** 1-14.

LAWRENCE, J. R., KORBER, D. R., HOYLE, B. D., COSTERTON, J. W. & CALDWELL, D. E. 1991. Optical sectioning of microbial biofilms. *Journal of Bacteriology,* 173**,** 6558-6567.

LEE, D. G., URBACH, J. M., WU, G., LIBERATI, N. T., FEINBAUM, R. L., MIYATA, S., DIGGINS, L. T., HE, J., SAUCIER, M., DÉZIEL, E., FRIEDMAN, L., LI, L., GRILLS, G., MONTGOMERY, K., KUCHERLAPATI, R., RAHME, L. G. & AUSUBEL, F. M. 2006a. Genomic analysis reveals that PA virulence is combinatorial. *Genome Biology,* 7**,** 1-14.

LEE, S.-M., LEE, H. S., KIM, D. S. & KWON, T. H. 2006b. Fabrication of hydrophobic films replicated from plant leaves in nature. *Surface and Coatings Technology,* 201**,** 553-559.

LEREBOUR, G., CUPFERMAN, S. & BELLON-FONTAINE, M. N. 2004. Adhesion of Staphylococcus aureus and Staphylococcus epidermidis to the Episkin reconstructed epidermis model and to an inert 304 stainless steel substrate. *J Appl Microbiol,* 97**,** 7-16.

LEVY, S. B. & MARSHALL, B. 2004. Antibacterial resistance worldwide: causes, challenges and responses. *Nature Medicine,* 10**,** 122-129.

LEWANDOWSKI, Z. 2005. Structure and Function of Biofilms. *In:* EVANS, L. V. (ed.) *Biofilms: recent advances in their study and control.* Harwood Academic Publishers.

LEWIS, K. & KLIBANOV, A. M. 2005. Surpassing nature: rational design of sterile-surface materials. *Trends in Biotechnology,* 23**,** 343-348.

LI, B. & LOGAN, B. E. 2004. Bacterial adhesion to glass and metal-oxide surfaces. *Colloids and Surfaces B: Biointerfaces,* 36**,** 81-90.

LI, L., MOLIN, S., YANG, L. & NDONI, S. 2013. Sodium Dodecyl Sulfate (SDS)-Loaded Nanoporous Polymer as Anti-Biofilm Surface Coating Material. *International Journal of Molecular Sciences,* 14**,** 3050-3064.

LIU, X., SUN, X., WU, Y., XIE, C., ZHANG, W., WANG, D., CHEN, X., QU, D., GAN, J., CHEN, H., JIANG, H., LAN, L. & YANG, C. G. 2013. Oxidation-sensing regulator AbfR regulates oxidative stress responses, bacterial aggregation, and biofilm formation in Staphylococcus epidermidis. *J Biol Chem,* 288**,** 3739-52.

LIU, Y. & TAY, J.-H. 2002. The essential role of hydrodynamic shear force in the formation of biofilm and granular sludge. *Water Research,* 36**,** 1653-1665.

LIU, Y. & ZHAO, Q. 2005. Influence of surface energy of modified surfaces on bacterial adhesion. *Biophysical Chemistry,* 117**,** 39-45.

LOOSDRECHT, M. M., NORDE, W., LYKLEMA, J. & ZEHNDER, A. B. 1990. Hydrophobic and electrostatic parameters in bacterial adhesion. *Aquatic Sciences,* 52**,** 103-114.

LORENZ, E. D. 1963. Deritministic Nonperiodic Flow. *Journal of the Atmospheric Sciences,* 20**,** 130-141.

LOWE., M. J. 1988. *The effect of inorganic particulate materials on the development of biological fouling films.* PhD, Birmingham University.

LUCKLUM, R., BEHLING, C. & HAUPTMANN, P. 1999. Role of Mass Accumulation and Viscoelastic Film Properties for the Response of Acoustic-Wave-Based Chemical Sensors. *Analytical Chemistry,* 71**,** 2488-2496.

LYMAN, D. J., BRASH, J. L., CHAIKIN, S. W., KLEIN, K. G. & CARINI, M. 1968. THE EFFECT OF CHEMICAL STRUCTURE AND SURFACE PROPERTIES OF SYNTHETIC POLYMERS ON THE COAGULATION OF BLOOD. II. PROTEIN AND PLATELET INTERACTION WITH POLYMER SURFACE. *ASAIO Journal,* 14**,** 250-255.

MA, L., CONOVER, M., LU, H., PARSEK, M. R., BAYLES, K. & WOZNIAK, D. J. 2009. Assembly and Development of the PA Biofilm Matrix. *PLoS Pathog,* 5**,** e1000354.

MA, L., JACKSON, K. D., LANDRY, R. M., PARSEK, M. R. & WOZNIAK, D. J. 2006. Analysis of PA Conditional Psl Variants Reveals Roles for the Psl Polysaccharide in Adhesion and Maintaining Biofilm Structure Postattachment. *Journal of Bacteriology,* 188**,** 8213-8221.

MADSEN, J. S., BURMØLLE, M., HANSEN, L. H. & SØRENSEN, S. J. 2012. The interconnection between biofilm formation and horizontal gene transfer. *FEMS Immunology &amp; Medical Microbiology,* 65**,** 183.

MAI-PROCHNOW, A., BRADBURY, M. & MURPHY, A. B. 2015. Draft Genome Sequence of PA ATCC 9027 (DSM 1128), an Important Rhamnolipid Surfactant Producer and Sterility Testing Strain. *Genome Announcements,* 3**,** e01259-15.

MAI, G. T., SEOW, W. K., PIER, G. B., MCCORMACK, J. G. & THONG, Y. H. 1993. Suppression of lymphocyte and neutrophil functions by PA mucoid exopolysaccharide (alginate): reversal by physicochemical, alginase, and specific monoclonal antibody treatments. *Infection and Immunity,* 61**,** 559-564.

MAJUMDAR, P., LEE, E., PATEL, N., WARD, K., STAFSLIEN, S. J., DANIELS, J., CHISHOLM, B. J., BOUDJOUK, P., CALLOW, M. E., CALLOW, J. A. & THOMPSON, S. E. 2008. Combinatorial materials research applied to the development of new surface coatings IX: an investigation of novel antifouling/fouling-release coatings containing quaternary ammonium salt groups. *Biofouling,* 24**,** 185-200.

MANGOLINI., F. 2010. Non-Contact (Optical) Profilometry. *SEACOAT −Developments in Surface Analysis: in situ to in vacuo* [Online], Department of Materials. Available: http://www.birmingham.ac.uk/generic/seacoat/documents/ATC2-talks/Mangoliniinterferometry.pdf.

MANN, E. E., MANNA, D., METTETAL, M. R., MAY, R. M., DANNEMILLER, E. M., CHUNG, K. K., BRENNAN, A. B. & REDDY, S. T. 2014. Surface micropattern limits bacterial contamination. *Antimicrobial Resistance and Infection Control,* 3**,** 28.

MANSFELD, F., HSU, H., ÖRNEK, D., WOOD, T. K. & SYRETT, B. C. 2002. Corrosion control using regenerative biofilms on aluminum 2024 and brass in different media. *Journal of the Electrochemical Society,* 149**,** B130-B138.

MARCUS, I. M., HERZBERG, M., WALKER, S. L. & FREGER, V. 2012. PA Attachment on QCM-D Sensors: The Role of Cell and Surface Hydrophobicities. *Langmuir,* 28**,** 6396-6402.

MARION-FEREY, K., PASMORE, M., STOODLEY, P., WILSON, S., HUSSON, G. P. & COSTERTON, J. W. 2003. Biofilm removal from silicone tubing: an assessment of the efficacy of dialysis machine decontamination procedures using an in vitro model. *Journal of Hospital Infection,* 53**,** 64-71.

MARSHALL, K. C., STOUT, R. & MITCHELL, R. 1971. Mechanism of the Initial Events in the Sorption of Marine Bacteria to Surfaces. *Microbiology,* 68**,** 337-348.

MARTIN, D. W., SCHURR, M. J., MUDD, M. H. & DERETIC, V. 1993. Differentiation of PA into the alginate-producing form: inactivation of mucB causes conversion to mucoidy. *Mol Microbiol,* 9**,** 497-506.

MARX, K. A. 2003. Quartz Crystal Microbalance: A Useful Tool for Studying Thin Polymer Films and Complex Biomolecular Systems at the Solution–Surface Interface. *Biomacromolecules,* 4**,** 1099-1120.

MARX, K. A. 2006. The Quartz Crystal Microbalance and Electrochemical QCM: Applications to Studies of Thin Polymer Films, Electron Transfer Systems, Biologicalmolecules, Biosensors, and Cells. *Piezoelectric Sensors.* Berlin, Heidelberg< New York: Springer.

MARX, K. A., ZHOU, T., MONTRONE, A., SCHULZE, H. & BRAUNHUT, S. J. 2001. A quartz crystal microbalance cell biosensor: detection of microtubule alterations in living cells at nM nocodazole concentrations. *Biosensors and Bioelectronics,* 16**,** 773-782.

MARX, K. A., ZHOU, T. & SARMA, R. 1999. Quartz Crystal Microbalance Measurement of Self-Assembled Micellar Tubules of the Amphiphilic Decyl Ester of d-Tyrosine and Their Enzymatic Polymerization. *Biotechnology Progress,* 15**,** 522-528.

MATJIE, R., ZHANG, S., ZHAO, Q., MABUZA, N. & BUNT, J. R. 2016. Tailored surface energy of stainless steel plate coupons to reduce the adhesion of aluminium silicate deposit. *Fuel,* 181**,** 573-578.

MATSUKAWA, M. & GREENBERG, E. P. 2004. Putative Exopolysaccharide Synthesis Genes Influence PA Biofilm Development. *Journal of Bacteriology,* 186**,** 4449-4456.

MAUKONEN, J., MÄTTÖ, J., WIRTANEN, G., RAASKA, L., MATTILA-SANDHOLM, T. & SAARELA, M. 2003. Methodologies for the characterization of microbes in industrial environments: a review. *Journal of Industrial Microbiology and Biotechnology,* 30**,** 327-356.

MAY, R. M., HOFFMAN, M. G., SOGO, M. J., PARKER, A. E., O'TOOLE, G. A., BRENNAN, A. B. & REDDY, S. T. 2014. Micro-patterned surfaces reduce bacterial colonization and biofilm formation in vitro: Potential for enhancing endotracheal tube designs. *Clinical and Translational Medicine,* 3**,** 8.

MCHALE, G., SHIRTCLIFFE, N. J. & NEWTON, M. I. 2004. Super-hydrophobic and super-wetting surfaces: Analytical potential? *Analyst,* 129**,** 284-287.

MEADOWS, P. S. 1971. The attachment of bacteria to solid surfaces. *Archiv für Mikrobiologie,* 75**,** 374-381.

MÉCHIN, L., DUBOIS-BRISSONNET, F., HEYD, B. & LEVEAU, J. Y. 1999. Adaptation of PA ATCC 15442 to didecyldimethylammonium bromide induces changes in membrane fatty acid composition and in resistance of cells. *Journal of Applied Microbiology,* 86**,** 859-866.

MEDILANSKI, E., KAUFMANN, K., WICK, L. Y., WANNER, O. & HARMS, H. 2002. Influence of the Surface Topography of Stainless Steel on Bacterial Adhesion. *Biofouling,* 18**,** 193-203.

MEINDERS, J. M., VAN DER MEI, H. C. & BUSSCHER, H. J. 1995. Deposition Efficiency and Reversibility of Bacterial Adhesion under Flow. *Journal of Colloid and Interface Science,* 176**,** 329-341.

MELO, L. F. & BOTT, T. R. 1997. Biofouling in water systems. *Experimental Thermal and Fluid Science,* 14**,** 375-381.

MERRITT, J. H., KADOURI, D. E. & O'TOOLE, G. A. 2005. Growing and Analyzing Static Biofilms. *Current Protocols in Microbiology.* John Wiley & Sons, Inc.

MERZ, A. J., SO, M. & SHEETZ, M. P. 2000. Pilus retraction powers bacterial twitching motility. *Nature,* 407**,** 98-102.

MESNAGE, S., TOSI-COUTURE, E., GOUNON, P., MOCK, M. & FOUET, A. 1998. The Capsule and S-Layer: Two Independent and Yet Compatible Macromolecular Structures in Bacillus anthracis. *Journal of Bacteriology,* 180**,** 52-58.

METTLER, E. A. C., B 1998. Variations over time of microbial load and physicochemical properties of floor materials after cleaning in food industry premises. *Journal of Food Protection,* 61**,** 57-65.

MIKE, C. & JOE, A. 2005. A comparison of surface metrology techniques. *Journal of Physics: Conference Series,* 13**,** 458.

MIKKELSEN, H., HUI, K., BARRAUD, N. & FILLOUX, A. 2013. The pathogenicity island encoded PvrSR/RcsCB regulatory network controls biofilm formation and dispersal in PA PA14. *Molecular Microbiology,* 89**,** 450-463.

MILLEDGE, J. J. 2010. The cleanability of stainless steel used as a food contact surface: an updated short review. *The journal of the Institute of Food Science and Technology,* 24.

MINSKY, M. 1961. *Microscopy Apparatus*. US patent application.

MISHRA, M., BYRD, M. S., SERGEANT, S., AZAD, A. K., PARSEK, M. R., MCPHAIL, L., SCHLESINGER, L. S. & WOZNIAK, D. J. 2012. PA Psl polysaccharide reduces neutrophil phagocytosis and the oxidative response by limiting complement-mediated opsonization. *Cell Microbiol,* 14**,** 95-106.

MITIK-DINEVA, N., WANG, J., STODDART, P. R., CRAWFORD, R. J. & IVANOVA, E. P. Nano-structured surfaces control bacterial attachment. 2008 International Conference on Nanoscience and Nanotechnology, 25-29 Feb. 2008 2008. 113-116.

MITIK-DINEVA, N., WANG, J., TRUONG, V. K., STODDART, P. R., MALHERBE, F., CRAWFORD, R. J. & IVANOVA, E. P. 2009. Differences in colonisation of five marine bacteria on two types of glass surfaces. *Biofouling,* 25**,** 621-631.

MOHAMED, N., RAINIER, T. R. & ROSS, J. M. 2000. Novel experimental study of receptor-mediated bacterial adhesion under the influence of fluid shear. *Biotechnology and Bioengineering,* 68**,** 628-636.

MOHANDAS, N., HOCHMUTH, R. M. & SPAETH, E. E. 1974. Adhesion of red cells to foreign surfaces in the presence of flow. *Journal of Biomedical Materials Research,* 8**,** 119-136.

MOLECULAR PROBES, I. 2006. Concanavalin A Conjugates. *In:* INVITROGEN, L. (ed.). Molecular Probes, Inc.

MOLIN, S. & TOLKER-NIELSEN, T. 2003. Gene transfer occurs with enhanced efficiency in biofilms and induces enhanced stabilisation of the biofilm structure. *Current Opinion in Biotechnology,* 14**,** 255-261.

MOLINA., D. D., COLON., M, BERMUDEZ., R.H., RAMIREX-RONDA, C. H. 1991. Unusual presentation of PA infections: A review. *Bol Asoc Med P R,* 83**,** 160-163.

MOREAU-MARQUIS, S., STANTON, B. A. & O'TOOLE, G. A. 2008. PA biofilm formation in the cystic fibrosis airway. *Pulmonary Pharmacology & Therapeutics,* 21**,** 595-599.

MORI, K., TSURUMARU, H. & HARAYAMA, S. 2010. Iron corrosion activity of anaerobic hydrogen-consuming microorganisms isolated from oil facilities. *Journal of Bioscience and Bioengineering,* 110**,** 426-430.

MUELLER, R. F., CHARACKLIS, W. G., JONES, W. L. & SEARS, J. T. 1992. Characterization of initial events in bacterial surface colonization by two Pseudomonas species using image analysis. *Biotechnology and Bioengineering,* 39**,** 1161-1170.

MURAMATSU, H., EGAWA, A. & ATAKA, T. 1995. Reliability of correlation between mass change and resonant frequency change for a viscoelastic-film-coated quartz crystal. *Journal of Electroanalytical Chemistry,* 388**,** 89-92.

MURGA, R., MILLER, J. M. & DONLAN, R. M. 2001. Biofilm Formation by Gram-Negative Bacteria on Central Venous Catheter Connectors: Effect of Conditioning Films in a Laboratory Model. *Journal of Clinical Microbiology,* 39**,** 2294-2297.

NEU, T. R., DENGLER, T., JANN, B. & PORALLA, K. 1992. Structural studies of an emulsion-stabilizing exopolysaccharide produced by an adhesive, hydrophobic Rhodococcus strain. *Journal of General Microbiology,* 138**,** 2531-2537.

NEUMANN, A. W., MOSCARELLO, M. A., ZINGG, W., HUM, O. S. & CHANG, S. K. 1979. Platelet adhesion from human blood to bare and protein-coated polymer surfaces. *Journal of Polymer Science: Polymer Symposia,* 66**,** 391-398.

NIEMEYER, J. & GESSLER, F. 2002. Determination of free DNA in soils. *Journal of Plant Nutrition and Soil Science,* 165**,** 121-124.

NIL. TECHNOLOGY. CORP. 2016. *RE: Polypropylene Samples with Microlens Array and Nana-Grass.* Type to KEVIN, W. & JONATHAN PALMER, D. R. W.

NOBUYUKI., O. 1979. A Tlreshold Selection Method from Gray-Level Histograms. *TRANSACTIONS ON SYSTREMS, MAN, AND CYBERNETICS,,* 9.

NOVAK, M., KABAT, J. & WISCHIK, C. M. 1993. Molecular characterization of the minimal protease resistant tau unit of the Alzheimer's disease paired helical filament. *EMBO J,* 12**,** 365-70.

NUTMAN, A. P., BENNETT, V. C., FRIEND, C. R. L., VAN KRANENDONK, M. J. & CHIVAS, A. R. 2016. Rapid emergence of life shown by discovery of 3,700-million-year-old microbial structures. *Nature,* advance online publication.

O'TOOLE, G. A. & KOLTER, R. 1998a. Flagellar and twitching motility are necessary for PA biofilm development. *Mol Microbiol,* 30**,** 295-304.

O'TOOLE, G. A. & KOLTER, R. 1998b. Initiation of biofilm formation in Pseudomonas fluorescens WCS365 proceeds via multiple, convergent signalling pathways: a genetic analysis. *Mol Microbiol,* 28**,** 449-61.

OBUEKWE, C. O., WESTLAKE, D. W. S. & PLAMBECK, J. A. 1987. Evidence that available energy is a limiting factor in the bacterial corrosion of mild steel by a Pseudomonas sp. *Canadian Journal of Microbiology,* 33**,** 272-275.

OLOFSSON, A.-C., HERMANSSON, M. & ELWING, H. 2003. N-Acetyl-l-Cysteine Affects Growth, Extracellular Polysaccharide Production, and Bacterial Biofilm Formation on Solid Surfaces. *Applied and Environmental Microbiology,* 69**,** 4814-4822.

OLSSON, A. L. J., VAN DER MEI, H. C., BUSSCHER, H. J. & SHARMA, P. K. 2011. Acoustic sensing of the bacterium–substratum interface using QCM-D and the influence of extracellular polymeric substances. *Journal of Colloid and Interface Science,* 357**,** 135-138.

OLYMPUS, C. 2016. *Knowledge Roughness (2D) parameter* [Online]. Olympus Corporation. Available:http://www.olympusims.com/en/knowledge/metrology/roughness/2d_parameter/ [Accessed 12.09.2016.

ORGAD, O., OREN, Y., WALKER, S. L. & HERZBERG, M. 2011. The role of alginate in PA EPS adherence, viscoelastic properties and cell attachment. *Biofouling,* 27**,** 787-798.

ÖRNEK, D., WOOD, T. K., HSU, C. H., SUN, Z. & MANSFELD, F. 2002. Pitting corrosion control of aluminum 2024 using protective biofilms that secrete corrosion inhibitors. *Corrosion,* 58**,** 761-767.

ORTEGA, M. P., HAGIWARA, T., WATANABE, H. & SAKIYAMA, T. 2010. Adhesion behavior and removability of Escherichia coli on stainless steel surface. *Food Control,* 21**,** 573-578.

OTTO, K. 2008. Biophysical approaches to study the dynamic process of bacterial adhesion. *Research in Microbiology,* 159**,** 415-422.

OTTO, K., ELWING, H. & HERMANSSON, M. 1999a. Effect of ionic strength on initial interactions of Escherichia coli with surfaces, studied on-line by a novel quartz crystal microbalance technique. *Journal of bacteriology,* 181**,** 5210-5218.

OTTO, K., ELWING, H. & HERMANSSON, M. 1999b. The role of type 1 fimbriae in adhesion of Escherichia coli to hydrophilic and hydrophobic surfaces. *Colloids and Surfaces B: Biointerfaces,* 15**,** 99-111.

OXFORD UNIVERSITY PRESS, I. 1999. *Polymer Data Handbook*.

PALMER, J., FLINT, S. & BROOKS, J. 2007. Bacterial cell attachment, the beginning of a biofilm. *Journal of Industrial Microbiology & Biotechnology,* 34**,** 577-588.

PAMP, S. J. & TOLKER-NIELSEN, T. 2007. Multiple Roles of Biosurfactants in Structural Biofilm Development by PA. *Journal of Bacteriology,* 189**,** 2531-2539.

PARK, M. R., BANKS, M. K., APPLEGATE, B. & WEBSTER, T. J. 2008. Influence of nanophase titania topography on bacterial attachment and metabolism. *International Journal of Nanomedicine,* 3**,** 497-504.

PARKAR, S. G., FLINT, S. H., PALMER, J. S. & BROOKS, J. D. 2001. Factors influencing attachment of thermophilic bacilli to stainless steel. *Journal of Applied Microbiology,* 90**,** 901-908.

PATANKAR, N. A. 2004. Transition between Superhydrophobic States on Rough Surfaces. *Langmuir,* 20**,** 7097-7102.

PENG, J.-S., TSAI, W.-C. & CHOU, C.-C. 2002. Inactivation and removal of Bacillus cereus by sanitizer and detergent. *International Journal of Food Microbiology,* 77**,** 11-18.

PEREIRA, M. O., KUEHN, M., WUERTZ, S., NEU, T. & MELO, L. F. 2002. Effect of flow regime on the architecture of a Pseudomonas fluorescens biofilm. *Biotechnology and Bioengineering,* 78**,** 164-171.

PERENI, C. I., ZHAO, Q., LIU, Y. & ABEL, E. 2006. Surface free energy effect on bacterial retention. *Colloids and Surfaces B: Biointerfaces,* 48**,** 143-147.

PETERSEN, F. C., ASSEV, S., VAN DER MEI, H. C., BUSSCHER, H. J. & SCHEIE, A. A. 2002. Functional variation of the antigen I/II surface protein in Streptococcus mutans and Streptococcus intermedius. *Infect Immun,* 70**,** 249-56.

POLLACK., M. 1995. *PA,* New York, Churchill Livingstone.

POORTINGA, A. T., BOS, R. & BUSSCHER, H. J. 2001. Lack of effect of an externally applied electric field on bacterial adhesion to glass. *Colloids and Surfaces B: Biointerfaces,* 20**,** 189-194.

POPAT, K. C., CHATVANICHKUL, K. I., BARNES, G. L., LATEMPA, T. J., JR., GRIMES, C. A. & DESAI, T. A. 2007. Osteogenic differentiation of marrow stromal cells cultured on nanoporous alumina surfaces. *J Biomed Mater Res A,* 80**,** 955-64.

POWELL, L. C., HILAL, N. & WRIGHT, C. J. 2017. Atomic force microscopy study of the biofouling and mechanical properties of virgin and industrially fouled reverse osmosis membranes. *Desalination,* 404**,** 313-321.

PRATT, L. A. & KOLTER, R. 1998. Genetic analysis of Escherichia coli biofilm formation: roles of flagella, motility, chemotaxis and type I pili. *Mol Microbiol,* 30**,** 285-93.

PROUTY, A. M., SCHWESINGER, W. H. & GUNN, J. S. 2002. Biofilm Formation and Interaction with the Surfaces of Gallstones by Salmonella spp. *Infection and Immunity,* 70**,** 2640-2649.

PUCKETT, S. D., TAYLOR, E., RAIMONDO, T. & WEBSTER, T. J. 2010. The relationship between the nanostructure of titanium surfaces and bacterial attachment. *Biomaterials,* 31**,** 706-713.

PUREVDORJ, B., COSTERTON, J. W. & STOODLEY, P. 2002. Influence of Hydrodynamics and Cell Signaling on the Structure and Behavior of PA Biofilms. *Applied and Environmental Microbiology,* 68**,** 4457-4464.

QIN, Z., OU, Y., YANG, L., ZHU, Y., TOLKER-NIELSEN, T., MOLIN, S. & QU, D. 2007. Role of autolysin-mediated DNA release in biofilm formation of Staphylococcus epidermidis. *Microbiology,* 153**,** 2083-2092.

QUIRYNEN, M., BOLLEN, C. M., PAPAIOANNOU, W., VAN ELDERE, J. & VAN STEENBERGHE, D. 1996. The influence of titanium abutment surface roughness on plaque accumulation and gingivitis: short-term observations. *Int J Oral Maxillofac Implants,* 11**,** 169-78.

QUIRYNEN, M., MARECHAL, M., BUSSCHER, H. J., WEERKAMP, A. H., DARIUS, P. L. & VAN STEENBERGHE, D. 1990. The influence of surface free energy and surface roughness on early plaque formation. An in vivo study in man. *J Clin Periodontol,* 17**,** 138-44.

R M MAY, M. G. H., K K CHUNG, S T REDDY 2011. Evaluating the Feasibility of Reducing Surface Contamination in Healthcare Facilities with Micro-Pattern Films. *51st ICACC Conference.* North America.

RAMAGE, G., CULSHAW, S., JONES, B. & WILLIAMS, C. 2010. Are we any closer to beating the biofilm: novel methods of biofilm control. *Current Opinion in Infectious Diseases,* 23**,** 560-566 10.1097/QCO.0b013e32833e5850.

REDDY, S. T., CHUNG, K. K., MCDANIEL, C. J., DAROUICHE, R. O., LANDMAN, J. & BRENNAN, A. B. 2011. Micropatterned Surfaces for Reducing the Risk of Catheter-Associated Urinary Tract Infection: An In Vitro Study on the Effect of Sharklet Micropatterned Surfaces to Inhibit Bacterial Colonization and Migration of Uropathogenic Escherichia coli. *Journal of Endourology,* 25**,** 1547-1552.

RIJNAARTS, H. H. M., NORDE, W., BOUWER, E. J., LYKLEMA, J. & ZEHNDER, A. J. B. 1993. Bacterial Adhesion under Static and Dynamic Conditions. *Applied and Environmental Microbiology,* 59**,** 3255-3265.

RUPP, C. J., FUX, C. A. & STOODLEY, P. 2005. Viscoelasticity of Staphylococcus aureus Biofilms in Response to Fluid Shear Allows Resistance to Detachment and Facilitates Rolling Migration. *Applied and Environmental Microbiology,* 71**,** 2175-2178.

S T REDDY, M. G. H., K K CHUNG, R O DAROUICHE,; J LANDMAN, A B BRENNAN 2011. Micro-patterned surfaces for reducing bacterial migration associated with catheter-associated urinary tract infection. *Annual APIC 2011 Educational Conference & International Meeting.* North America.

SÁRA, M. & SLEYTR, U. B. 2000. S-Layer Proteins. *Journal of bacteriology,* 182**,** 859-868.

SAUERBREY, G. 1959. Verwendung von Schwingquarzen zur Wägung dünner Schichten und zur Mikrowägung. *Zeitschrift für Physik,* 155**,** 206-222.

SCHWARTZ, K., GANESAN, M., PAYNE, D. E., SOLOMON, M. J. & BOLES, B. R. 2016. Extracellular DNA facilitates the formation of functional amyloids in Staphylococcus aureus biofilms. *Mol Microbiol,* 99**,** 123-34.

SCOTT, J. K., LOGANATHAN, D., EASLEY, R. B., GONG, X. & GOLDSTEIN, I. J. 1992. A family of concanavalin A-binding peptides from a hexapeptide epitope library. *Proceedings of the National Academy of Sciences,* 89**,** 5398-5402.

SEDLAČEK, M., PODGORNIK, B. & VIŽINTIN, J. 2009. Influence of surface preparation on roughness parameters, friction and wear. *Wear,* 266**,** 482-487.

SHARE, J. 2014. Global Demand For Polyethylene To Reach 99.6 Million Tons In 2018. *Pipeline & Gas Journal,* 241.

SHENG, X., TING, Y.-P. & PEHKONEN, S. O. 2007. The influence of sulphate-reducing bacteria biofilm on the corrosion of stainless steel AISI 316. *Corrosion Science,* 49**,** 2159-2176.

SHEWMAKER, F., MCGLINCHEY, R. P. & WICKNER, R. B. 2011. Structural Insights into Functional and Pathological Amyloid. *Journal of Biological Chemistry*.

SHIRTCLIFFE, N. J., MCHALE, G., ATHERTON, S. & NEWTON, M. I. 2010. An introduction to superhydrophobicity. *Advances in Colloid and Interface Science,* 161**,** 124-138.

SHIRTLIFF, M. E., MADER, J. T. & CAMPER, A. K. 2002. Molecular Interactions in Biofilms. *Chemistry & Biology,* 9**,** 859-871.

SIMÕES, M., PEREIRA, M. O. & VIEIRA, M. J. 2003. Effect of Different Concentrations of Ortho-phthalaldehyde on Biofilms Formed by Pseudomonas fluorescens Under Different Flow Conditions. *Biofouling,* 19**,** 287-295.

SINGLETON, P. 1999. *Bacteria in Biology, Biotechnology and Medicine,* New York, John Wiley & sons, LTD.

SJOLLEMA, J., BUSSCHER, H. J. & WEERKAMP, A. H. 1988. Deposition of oral streptococci and polystyrene latices onto glass in a parallel plate flow cell. *Biofouling,* 1**,** 101-112.

SLEYTR, U. B., MESSNER, P., PUM, D., SARA, M. 1996. *Biological Intelligence Unit, Crystalline Bacterial Cell Layer Proteins*, Academic Press, Inc.

SLONCZEWSKI, J., L & FOSTER, J., W 2011. *Microbiology, An Evolving Science,* Canada, W.W. Norton & Company, Inc.

SOLOMON, E., P, BERH, L., R & MARTIN, D., W. 1999. Biology, Fifth Edition. Emily Barrosse.

STADLER, H., MONDON, M. & ZIEGLER, C. 2003. Protein adsorption on surfaces: dynamic contact-angle (DCA) and quartz-crystal microbalance (QCM) measurements. *Analytical and Bioanalytical Chemistry,* 375**,** 53-61.

STEEL, A. 2007. 316/316L Product Data Sheet UNS S31600 AND UNS S31603. *In:* STEEL, A. (ed.).

STEINBERG, T. H., HAUGLAND, R. P. & SINGER, V. L. 1996a. Applications of SYPRO orange and SYPRO red protein gel stains. *Anal Biochem,* 239**,** 238-45.

STEINBERG, T. H., JONES, L. J., HAUGLAND, R. P. & SINGER, V. L. 1996b. SYPRO orange and SYPRO red protein gel stains: one-step fluorescent staining of denaturing gels for detection of nanogram levels of protein. *Anal Biochem,* 239**,** 223-37.

STEINBERGER, R. E. & HOLDEN, P. A. 2004. Macromolecular composition of unsaturated PA biofilms with time and carbon source. *Biofilms,* 1**,** 37-47.

STEINBERGER, R. E. & HOLDEN, P. A. 2005. Extracellular DNA in Single- and Multiple-Species Unsaturated Biofilms. *Applied and Environmental Microbiology,* 71**,** 5404-5410.

STEWART, P. S. & WILLIAM COSTERTON, J. 2001. Antibiotic resistance of bacteria in biofilms. *The Lancet,* 358**,** 135-138.

STOCKS, S. M. 2004. Mechanism and use of the commercially available viability stain, BacLight. *Cytometry A,* 61**,** 189-95.

STOODLEY, P., CARGO, R., RUPP, C. J., WILSON, S. & KLAPPER, I. 2002a. Biofilm material properties as related to shear-induced deformation and detachment phenomena. *Journal of Industrial Microbiology and Biotechnology,* 29**,** 361-367.

STOODLEY, P., SAUER, K., DAVIES, D. G. & COSTERTON, J. W. 2002b. Biofilms as complex differentiated communities. *Annual Review of Microbiology,* 56**,** 187-209.

STOODLEY, P., SIDHU, S., NISTICO, L., MATHER, M., BOUCEK, A., HALL-STOODLEY, L. & KATHJU, S. 2012. Kinetics and morphology of polymicrobial biofilm formation on polypropylene mesh. *FEMS Immunology & Medical Microbiology,* 65**,** 283-290.

STOVER, C. K., PHAM, X. Q., ERWIN, A. L., MIZOGUCHI, S. D., WARRENER, P., HICKEY, M. J., BRINKMAN, F. S., HUFNAGLE, W. O., KOWALIK, D. J. & LAGROU, M. 2000. Complete genome sequence of PAPA01, an opportunistic pathogen. *Nature,* 406.

STRATHMANN, M., WINGENDER, J. & FLEMMING, H. C. 2002. Application of fluorescently labelled lectins for the visualization and biochemical characterization of polysaccharides in biofilms of PA. *J Microbiol Methods,* 50**,** 237-48.

SU, X.-L. & LI, Y. 2005. A QCM immunosensor for Salmonella detection with simultaneous measurements of resonant frequency and motional resistance. *Biosensors and Bioelectronics,* 21**,** 840-848.

SUTAR., S. S. 2014. Analysis of Ductile-to-Brittle Transition Temperature of Stainless steel of 304 grades *INTERNATIONAL JOURNAL OF INNOVATIONS IN ENGINEERING RESEARCH AND TECHNOLOGY* 1**,** 1-10.

SUTHERLAND, I. W. 2001. The biofilm matrix – an immobilized but dynamic microbial environment. *Trends in Microbiology,* 9**,** 222-227.

SWEITY, A., YING, W., ALI-SHTAYEH, M. S., YANG, F., BICK, A., ORON, G. & HERZBERG, M. 2011. Relation between EPS adherence, viscoelastic properties, and MBR operation: Biofouling study with QCM-D. *Water Research,* 45**,** 6430-6440.

SYSTEMS, S. 2015. Polycarbonate (PC) FDM Material Properties *In:* SYSTEMS, S. (ed.).

SYSTEMS, S. R. 2010a. QCM100 - Quartz Crystal Microbalance Theory and Calibration. *In:* SYSTEMS, S. R. (ed.) Revision 2.3 (5/2010) ed. USA.

SYSTEMS, S. R. 2010b. QCM 200 Quartz Crystal Microbalance, QCM25 5MHz Crystal Oscillator. *In:* SYSTEMS, S. R. (ed.) Revision 2.3 (5/2010) ed. USA.

TEBBS, S. E., SAWYER, A. & ELLIOTT, T. S. 1994. Influence of surface morphology on in vitro bacterial adherence to central venous catheters. *Br J Anaesth,* 72**,** 587-91.

TESCO.COM. 2013. *Viakal Limescale Spray 500Ml* [Online]. Tesco.com. Available: http://www.tesco.com/groceries/Product/Details/?id=252675391 [Accessed 06.11.2013 2013].

THERMOFISHER SCIENTIFIC, M. P. 2010. The Alexa Fluor Dye Series—Note 1.1. *The Molecular Probes™ Handbook: A Guide to Fluorescent Probes and Labeling Technologies.* Internet: ThermoFisher Scientific.

THERMOFISHER SCIENTIFIC, M. P. 2014. Syto Green Fluorescent Nuclear Acid Stains. *In:* THERMOFISHER SCIENTIFIC, M. P. (ed.).

THERMOFISHER SCIENTIFIC, M. P. 2015. *Fluorescence SpectraViewer* [Online]. ThermoFisher Scientific Inc. Available: https://www.thermofisher.com/be/en/home/life-science/cell-analysis/labeling-chemistry/fluorescence-spectraviewer.html [Accessed 24.09.2015 2015].

THERMOFISHER SCIENTIFIC, M. P. 2016. *SYTO® 9 Green Fluorescent Nucleic Acid Stain, Frequently asked questions* [Online]. Available: https://www.thermofisher.com/order/catalog/product/S34854 [Accessed 30.08.2016.

THEVENOT, P., HU, W. & TANG, L. 2008. SURFACE CHEMISTRY INFLUENCE IMPLANT BIOCOMPATIBILITY. *Current topics in medicinal chemistry,* 8**,** 270-280.

THOMSON N.R. 2008. PA LESB58 complete genome sequence. Pathogen Sequencing Unit, The Wellcome Trust Sanger Institute,.

TIDE, C., HARKIN, S. R., GEESEY, G. G., BREMER, P. J. & SCHOLZ, W. 1999. The influence of welding procedures on bacterial colonization of stainless steel weldments. *Journal of Food Engineering,* 42**,** 85-96.

TODAR, K. 2013a. *Online Text book of Bacteriology, PA* [Online]. Available: http://textbookofbacteriology.net/pseudomonas.html [Accessed 07.02.2017 2016].

TODAR, K. 2013b. *Online Text book of Bacteriology, Structure and Function of Bacterial Cells, The Cell Envelope: capsules, cell walls and cell membranes* [Online]. Available: http://www.textbookofbacteriology.net/structure_4.html [Accessed 20.10.2013 2013].

VADILLO-RODRíGUEZ, V., BUSSCHER, H. J., NORDE, W., DE VRIES, J. & VAN DER MEI, H. C. 2004. Atomic force microscopic corroboration of bond aging for adhesion of Streptococcus thermophilus to solid substrata. *Journal of Colloid and Interface Science,* 278**,** 251-254.

VAN DER MEI, H. C. & BUSSCHER, H. J. 2001. Electrophoretic Mobility Distributions of Single-Strain Microbial Populations. *Applied and Environmental Microbiology,* 67**,** 491-494.

VAN LOOSDRECHT, M. C., LYKLEMA, J., NORDE, W., SCHRAA, G. & ZEHNDER, A. J. 1987. The role of bacterial cell wall hydrophobicity in adhesion. *Applied and Environmental Microbiology,* 53**,** 1893-1897.

VASSEUR, P., VALLET-GELY, I., SOSCIA, C., GENIN, S. & FILLOUX, A. 2005. The pel genes of the PA PAK strain are involved at early and late stages of biofilm formation. *Microbiology,* 151**,** 985-97.

VATANYOOPAISARN, S., NAZLI, A., DODD, C. E. R., REES, C. E. D. & WAITES, W. M. 2000. Effect of Flagella on Initial Attachment of Listeria monocytogenes to Stainless Steel. *Applied and Environmental Microbiology,* 66**,** 860-863.

VEECO, I. I. 2007. WYKO NT9100 SURFACE PROFILER, SETUP AND OPERATION GUIDE. *In:* INC., V. I. (ed.) Revision 0 ed. Tucson, Arizona, US.

VERRAN, J. & WHITEHEAD, K. A. 2006. Assessment of Organic Materials and Microbial Components on Hygienic Surfaces. *Food and Bioproducts Processing,* 84**,** 260-264.

VIEIRA, M. J., MELO, L. F. & PINHEIRO, M. M. 1993. Biofilm formation: Hydrodynamic effects on internal diffusion and structure. *Biofouling,* 7**,** 67-80.

VILLA, F., REMELLI, W., FORLANI, F., GAMBINO, M., LANDINI, P. & CAPPITELLI, F. 2012. Effects of chronic sub-lethal oxidative stress on biofilm formation by Azotobacter vinelandii. *Biofouling,* 28**,** 823-33.

VORREGAARD, M. 2008. Comstat2 - a modern 3D image analysis environment for biofilms, in Informatics and Mathematical Modelling. Technical University of Denmark: Kongens Lyngby, Denmark

W.S. HAMPSHIRE, I. 2016. POLYETHYLENE. *In:* W.S. HAMPSHIRE, I. (ed.) *Information Leaflet.*

WAAR, K., VAN DER MEI, H. C., HARMSEN, H. J., DEGENER, J. E. & BUSSCHER, H. J. 2002. Enterococcus faecalis surface proteins determine its adhesion mechanism to bile drain materials. *Microbiology,* 148**,** 1863-70.

WALKER, S. L., HILL, J. E., REDMAN, J. A. & ELIMELECH, M. 2005. Influence of Growth Phase on Adhesion Kinetics of Escherichia coli D21g. *Applied and Environmental Microbiology,* 71**,** 3093-3099.

WALKER, S. L., REDMAN, J. A. & ELIMELECH, M. 2004. Role of Cell Surface Lipopolysaccharides in Escherichia coli K12 Adhesion and Transport. *Langmuir,* 20**,** 7736-7746.

WANG, S., PARSEK, M. R., WOZNIAK, D. J. & MA, L. Z. 2013. A spider web strategy of type IV pili-mediated migration to build a fibre-like Psl polysaccharide matrix in PA biofilms. *Environ Microbiol,* 15**,** 2238-53.

WEISS, L. 1961. The measurement of cell adhesion. *Experimental Cell Research,* 8**,** 141-153.

WENZEL, R. N. 1936. RESISTANCE OF SOLID SURFACES TO WETTING BY WATER. *Industrial & Engineering Chemistry,* 28**,** 988-994.

WENZEL, R. N. 1949. Surface Roughness and Contact Angle*. The Journal of Physical and Colloid Chemistry,* 53**,** 1466-1467.

WHITCHURCH, C. B., HOBBS, M., LIVINGSTON, S. P., KRISHNAPILLAI, V. & MATTICK, J. S. 1991. Characterisation of a PA twitching motility gene and evidence for a specialised protein export system widespread in eubacteria. *Gene,* 101**,** 33-44.

WHITCHURCH, C. B., TOLKER-NIELSEN, T., RAGAS, P. C. & MATTICK, J. S. 2002. Extracellular DNA Required for Bacterial Biofilm Formation. *Science,* 295**,** 1487.

WHITE., D. J., M., K. K., V, B. & FRANC. R. 2004. *Oral Compositions*. US patent application.

WHITE., J. G. 1987. An evaluation of confocal versus conventional imaging of biological structures by fluorescence light microscopy. *The Journal of Cell Biology,* 105**,** 41-48.

WHITEHEAD, K. A., COLLIGON, J. & VERRAN, J. 2005. Retention of microbial cells in substratum surface features of micrometer and sub-micrometer dimensions. *Colloids and Surfaces B: Biointerfaces,* 41**,** 129-138.

WHITEHEAD, K. A. & VERRAN, J. 2006. The Effect of Surface Topography on the Retention of Microorganisms. *Food and Bioproducts Processing,* 84**,** 253-259.

WIENER, M. C. & HORANYI, P. S. 2011. How hydrophobic molecules traverse the outer membranes of Gram-negative bacteria. *Proceedings of the National Academy of Sciences,* 108**,** 10929-10930.

WILLIAMS, D. 22.10.2013 2013. *RE: Contact angle calculations discussion.* Type to PALMER, J.

WILLIAMS, V. & FLETCHER, M. 1996. Pseudomonas fluorescens adhesion and transport through porous media are affected by lipopolysaccharide composition. *Applied and Environmental Microbiology,* 62**,** 100-4.

WILTON, M., CHARRON-MAZENOD, L., MOORE, R. & LEWENZA, S. 2016. Extracellular DNA Acidifies Biofilms and Induces Aminoglycoside Resistance in PA. *Antimicrobial Agents and Chemotherapy,* 60**,** 544-553.

WIRTANEN, G., SALO, S., HELANDER, I. M. & MATTILA-SANDHOLM, T. 2001. Microbiological methods for testing disinfectant efficiency on Pseudomonas biofilm. *Colloids and Surfaces B: Biointerfaces,* 20**,** 37-50.

WRIGHT, K., PRENDERGAST, M. & ALUM, Z. 2013. *RE: Meeting with P&G held 03.07.2013.* Type to JONATHAN PALMER, D. R. W.

XU, C. P., VAN DE BELT-GRITTER, B., DIJKSTRA, R. J., NORDE, W., VAN DER MEI, H. C. & BUSSCHER, H. J. 2007. Interaction forces between salivary proteins and Streptococcus mutans with and without antigen I/II. *Langmuir,* 23**,** 9423-8.

YANEFF, P. V. 2003. *Coatings of Polymers and Plastics,* New York, Marcel Dekker, Ink.

YANG, Z., WANG, J., LUO, R., MAITZ, M. F., JING, F., SUN, H. & HUANG, N. 2010. The covalent immobilization of heparin to pulsed-plasma polymeric allylamine films on 316L stainless steel and the resulting effects on hemocompatibility. *Biomaterials,* 31**,** 2072-83.

YOON, S. S., HENNIGAN, R. F., HILLIARD, G. M., OCHSNER, U. A., PARVATIYAR, K., KAMANI, M. C., ALLEN, H. L., DEKIEVIT, T. R., GARDNER, P. R., SCHWAB, U., ROWE, J. J., IGLEWSKI, B. H., MCDERMOTT, T. R., MASON, R. P., WOZNIAK, D. J., HANCOCK, R. E. W., PARSEK, M. R., NOAH, T. L., BOUCHER, R. C. & HASSETT, D. J. 2002. PA Anaerobic Respiration in Biofilms: Relationships to Cystic Fibrosis Pathogenesis. *Developmental Cell,* 3**,** 593-603.

YOSHIDA, S., HIRAGA, K., TAKEHANA, T., TANIGUCHI, I., YAMAJI, H., MAEDA, Y., TOYOHARA, K., MIYAMOTO, K., KIMURA, Y. & ODA, K. 2016. A bacterium that degrades and assimilates poly(ethylene terephthalate). *Science,* 351**,** 1196.

YOUNG, T. 1805. An Essay on the Cohesion of Fluids. *Philosophical Transactions of the Royal Society of London,* 95**,** 65-87.

ZHANG, K., HU, R., FAN, G. & LI, G. 2017. Graphene oxide/chitosan nanocomposite coated quartz crystal microbalance sensor for detection of amine vapors. *Sensors and Actuators B: Chemical,* 243**,** 721-730.

ZHANG, T. C. & BISHOP, P. L. 1996. Evaluation of substrate and pH effects in a nitrifying biofilm. *Water Environment Research,* 68**,** 1107-1115.

ZHANG, W., DAI, W., TSAI, S. M., ZEHNDER, S. M., SARNTINORANONT, M. & ANGELINI, T. E. 2015. Surface indentation and fluid intake generated by the polymer matrix of Bacillus subtilis biofilms. *Soft Matter,* 11**,** 3612-7.

ZHANG, Y., DU, B., CHEN, X. & MA, H. 2009. Convergence of Dissipation and Impedance Analysis of Quartz Crystal Microbalance Studies. *Analytical Chemistry,* 81**,** 642-648.

ZHANG, Y. & MILLER, R. M. 1992. Enhanced octadecane dispersion and biodegradation by a Pseudomonas rhamnolipid surfactant (biosurfactant). *Applied and Environmental Microbiology,* 58**,** 3276-3282.

ZHAO, K., TSENG, B. S., BECKERMAN, B., JIN, F., GIBIANSKY, M. L., HARRISON, J. J., LUIJTEN, E., PARSEK, M. R. & WONG, G. C. L. 2013. Psl trails guide exploration and microcolony formation in PA biofilms. *Nature,* 497**,** 388-391.

ZHAO, Q., WANG, S. & MÜLLER-STEINHAGEN, H. 2004. Tailored surface free energy of membrane diffusers to minimize microbial adhesion. *Applied Surface Science,* 230**,** 371-378.

ZHENG, D., TAYLOR, G. T. & GYANANATH, G. 1994. Influence of laminar flow velocity and nutrient concentration on attachment of marine bacterioplankton. *Biofouling,* 8**,** 107-120.

ZHOU, T., MARX, K. A., WARREN, M., SCHULZE, H. & BRAUNHUT, S. J. 2000. The quartz crystal microbalance as a continuous monitoring tool for the study of endothelial cell surface attachment and growth. *Biotechnol Prog,* 16**,** 268-77.

ZIPFEL, W. R., WILLIAMS, R. M., CHRISTIE, R., NIKITIN, A. Y., HYMAN, B. T. & WEBB, W. W. 2003. Live tissue intrinsic emission microscopy using multiphoton-excited native fluorescence and second harmonic generation. *Proceedings of the National Academy of Sciences of the United States of America,* 100**,** 7075-7080.

ZODROW, K. R., SCHIFFMAN, J. D. & ELIMELECH, M. 2012. Biodegradable Polymer (PLGA) Coatings Featuring Cinnamaldehyde and Carvacrol Mitigate Biofilm Formation. *Langmuir,* 28**,** 13993-13999.

ZUO, R., ÖRNEK, D., SYRETT, B. C., GREEN, R. M., HSU, C. H., MANSFELD, F. B. & WOOD, T. K. 2004. Inhibiting mild steel corrosion from sulfate-reducing bacteria using antimicrobial-producing biofilms in Three-Mile-Island process water. *Applied Microbiology and Biotechnology,* 64**,** 275-283.

Appendix A - Reynolds and Shear Calculation For CDC Reactor Coupons at Different Impeller Speeds, and Error Propagation

Reynolds Number Calculation for CDC reactor

$$Re_i = \frac{D^2 n \rho \alpha}{\mu}$$

Eqn. 21

D^2 = Impeller Diameter (0.025m^2), μ = Dynamic Viscosity (0.001005 Kg/(m.s), ρ = Density of fluid (998.23 kg/m^3), n = Number of revolution per minute at the inner baffle (rpm), α = Ratio of inner to outer rotating cylinder.

Darcy Friction Factor as calculated using Blasius Calculation (assumed Smooth) (f)

$$f = \frac{0.0791}{Re_i^{0.25}}$$

Eqn. 22

Re$_i$ = Reynolds Number

Velocity of Fluid Calculation

$$V = \frac{(n^2 R_i R_o)}{2}$$

Eqn. 23

n = Number of revolution per minute at the inner baffle (rpm), R$_i$= Radius of inner cylinder (2.5cm), R$_o$ Radius of outer cylinder (3cm).

Shear Stress Calculation (τ)

$$\tau = \frac{f \rho \, (n^2) R_i R_o}{2}$$

Eqn. 24

f=Darcy Friction Factor, ρ = Density of Fluid, n = Number of revolution per minute at the inner baffle (rpm), R$_i$= Radius of inner cylinder (2.5cm), R$_o$= Radius of outer cylinder (3cm).

Impeller RPM (n)	Reynolds Number (Re_i) @32.5ºC	Shear Stress (τ) (N/m^2) @ 32.5ºC
100	97,653	16.7

150	146,479	33.9
174	169,916	44.00
200	195,306	56.1
250	244,132	83.0
440	514,280	223.1

Table A1. Examples of Reynolds and shear stress metrics for CDC reactor at different impeller speeds.

Error Propagation Equations

Error Propagation when Subtracting Quantities that Both Carry an Error

$$\delta Q = \sqrt{(\delta a)^2 + (\delta b)^2}\ldots\ldots \qquad \text{Eqn. 25}$$

Q = Uncertainty. This was used in the high shear cleaning experiments. δ = Standard Deviation or Standard Error.

Error Propagation for Division of Quantities that Both Carry an Error.

$$\frac{\delta Q}{Q} = \sqrt{\left(\frac{\delta^1}{A^1}\right)^2 + \left(\frac{\delta^2}{A^2}\right)^2 + \left(\frac{\delta^3}{A^3}\right)^2 \ldots\ldots} \qquad \text{Eqn. 26}$$

Q = Uncertainty. This was used in the high shear cleaning experiments. δ = Standard Deviation or Standard Error. A = Average.

Appendix B – Confocal Microscopy Optical Thickness Table.

Lens Used	AU	Emission Wave Length (λ)	Optical Slice Thickness (dZ) (µm)
10x	1.0	580	17.077
10x	1.0	633	18.65
10x	0.5	580	11.328
10x	0.5	633	12.331

25x	1.0	580	1.702
25x	1.0	633	1.864
25x	0.5	580	1.124
25x	0.5	633	1.23
25x	0.36	580	1.005
25x	10.16	580	15.00
63x	1.0	580	1.90
63x	1.0	633	2.073
63x	0.5	580	1.261
63x	0.5	633	1.373

Table B1. Examples of different dz values for alternate opjective lenses, and AU settings.

Appendix C – Confocal Microscopes TCS SP2 and SP8 Negative Control Data

This data is relevant to Chapter 7, and details the results obtained when imaging the different coupon materials using the TCS SP2 following staining, with probes as per Figure 2.5, but in the absence of *Pseudomonas* biofilms.

Negative Controls for the TCS SP2 Microscope
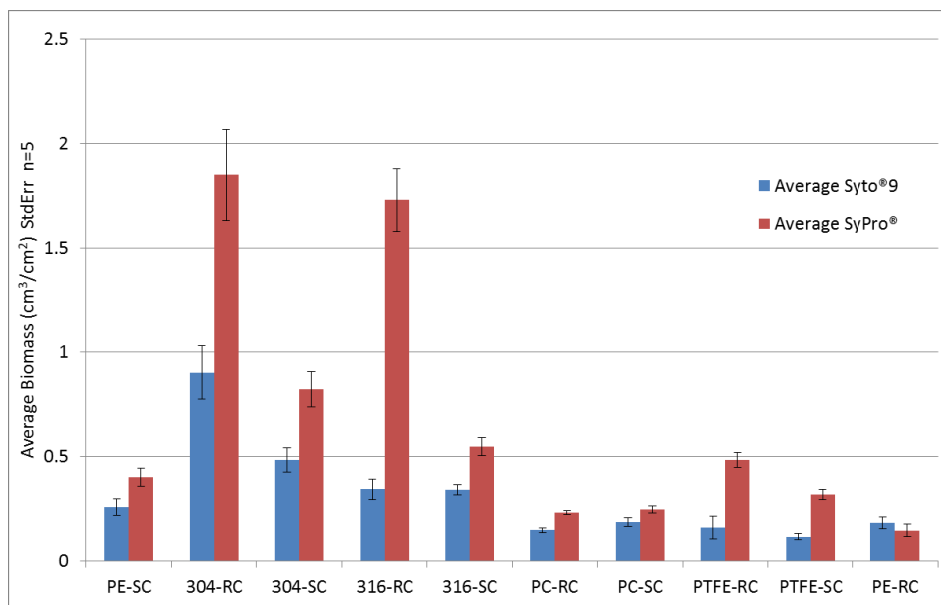
Figure C1.1. Negative control for the SP2 TCS microscope for reference. Syto®9/Sypro® probe combination for biomass metric. Substratums were treated with probes as per Figure 2.5.
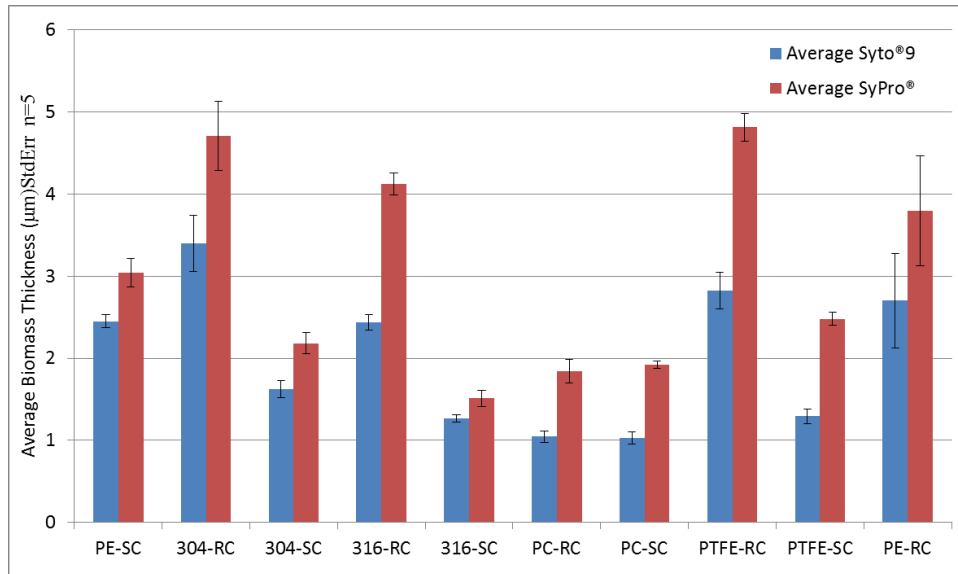
Figure C1.2. Negative control for the SP2 TCS microscope for reference. Syto®9/Sypro® probe combination for average biomass thickness metric. Substratums were treated with probes as per Figure 2.5.
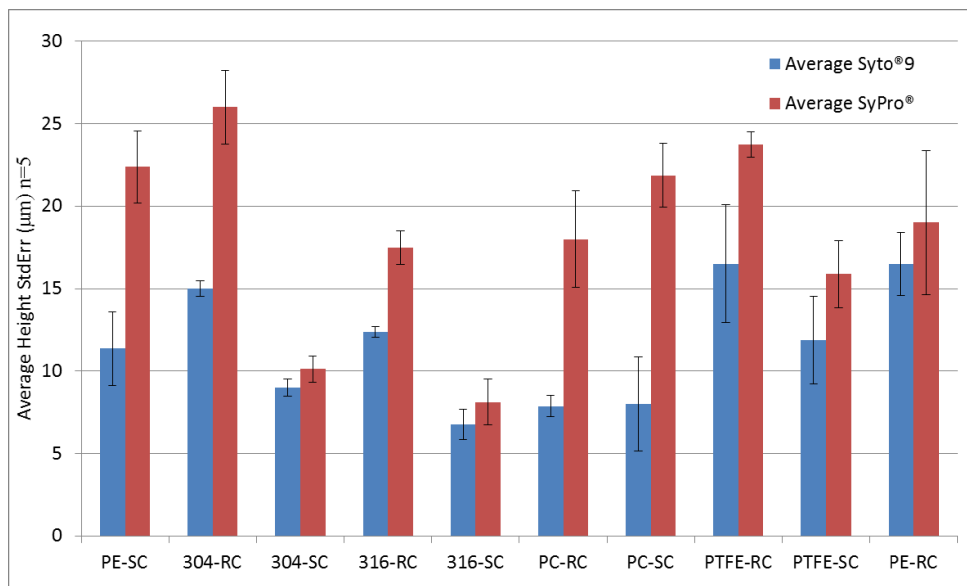
Figure C1.3. Negative control for the SP2 TCS microscope for reference. Syto®9/Sypro® probe combination for maximum biomass thickness metric. Substratums were treated with probes as per Figure 2.5.
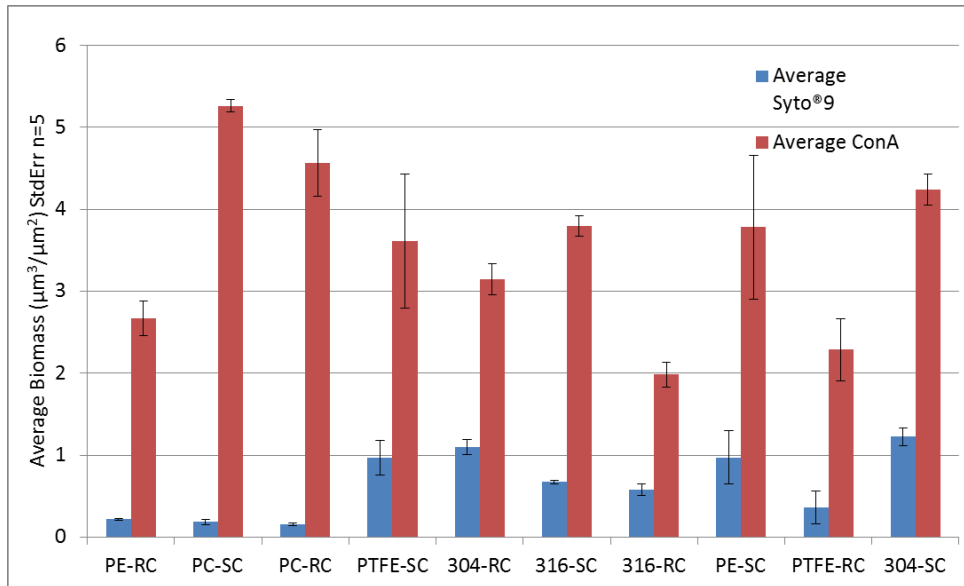
Figure C1.4. Negative control for the SP2 TCS microscope for reference. Syto®9/ConA probe combination for biomass metric. Substratums were treated with probes as per Figure 2.5.
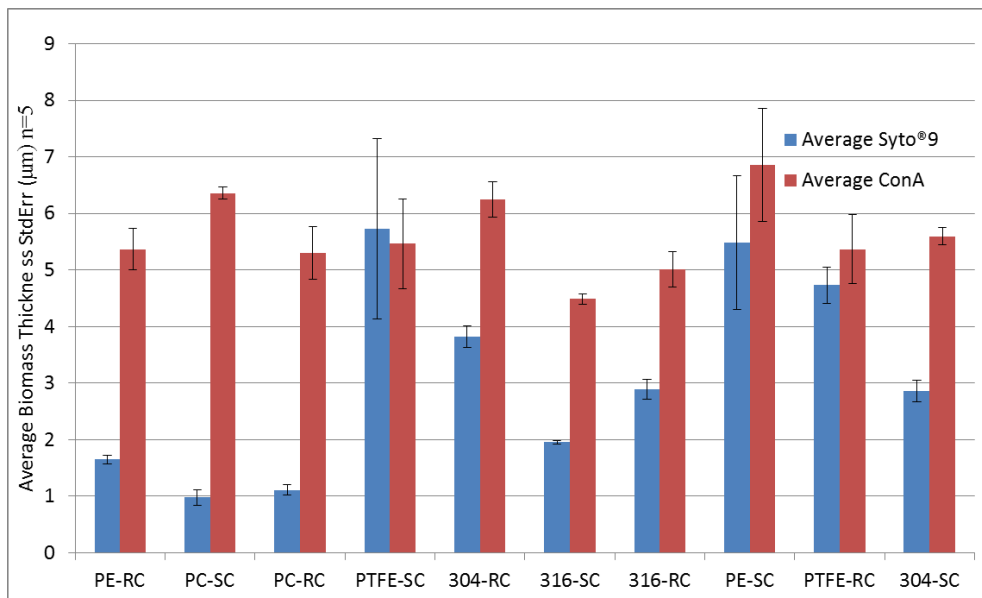
Figure C1.5. Negative control for the SP2 TCS microscope for reference. Syto®9/ConA probe combination for average biomass thickness metric. Substratums were treated with probes as per Figure 2.5.
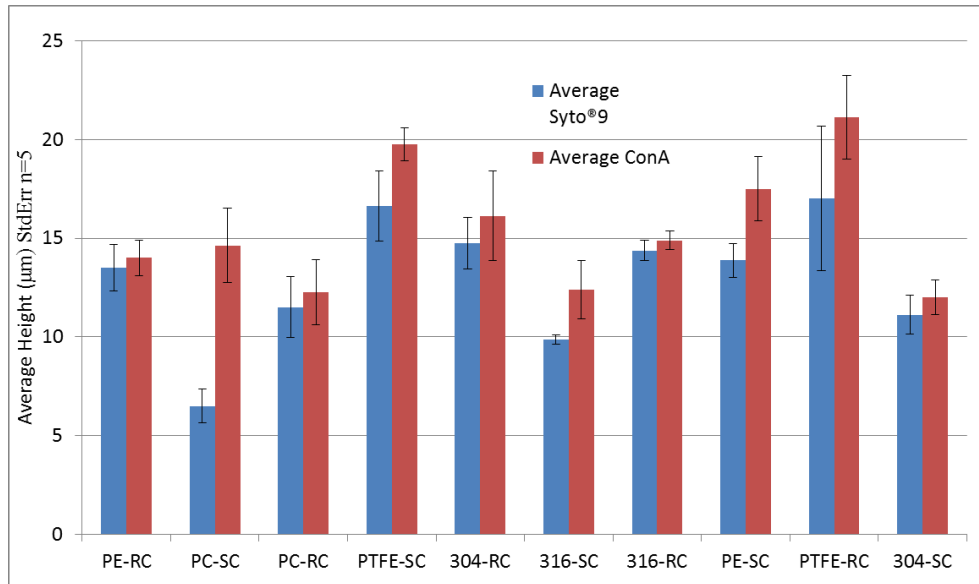
Figure C1.6. Negative control for the SP2 TCS microscope for reference. Syto®9/ConA probe combination for maximum biomass thickness metric. Substratums were treated with probes as per Figure 2.5.

Negative Controls for the TCS SP8 Microscope
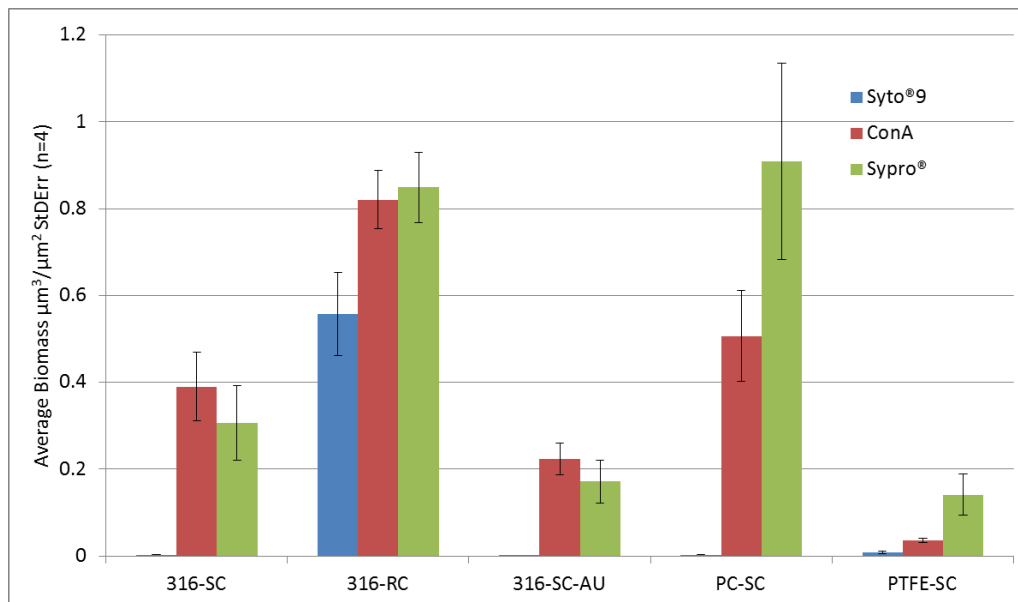
Figure C1.7. Biomass negative control for the SP8 TCS microscope. Substratums were treated with

probes as per Figure 2.5.
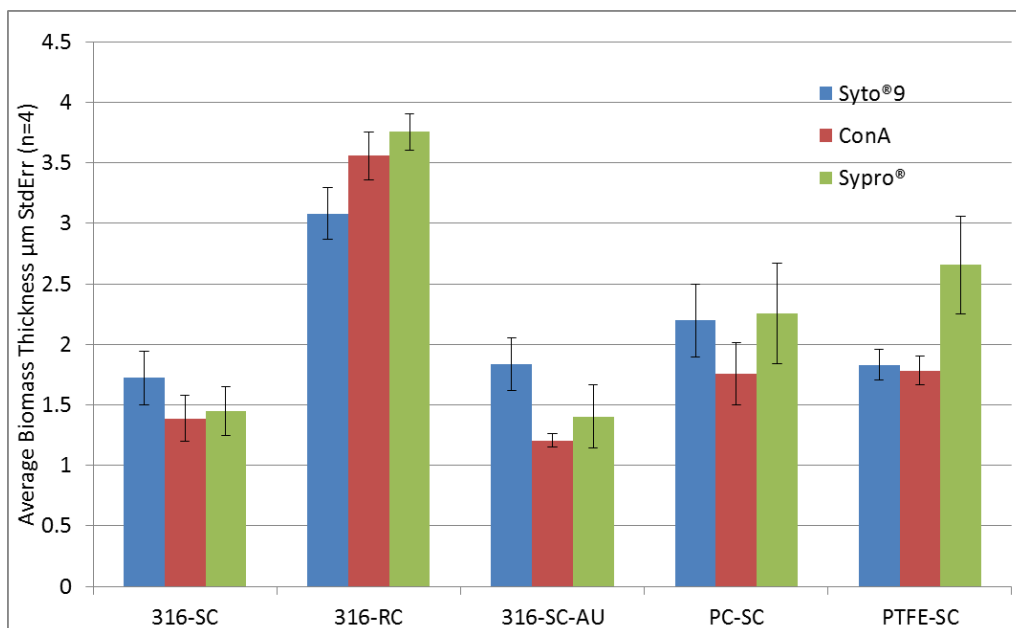
Figure C1.8. Average biomass thickness negative control for the SP8 TCS microscope. Substratums were treated with probes as per Figure 2.5.
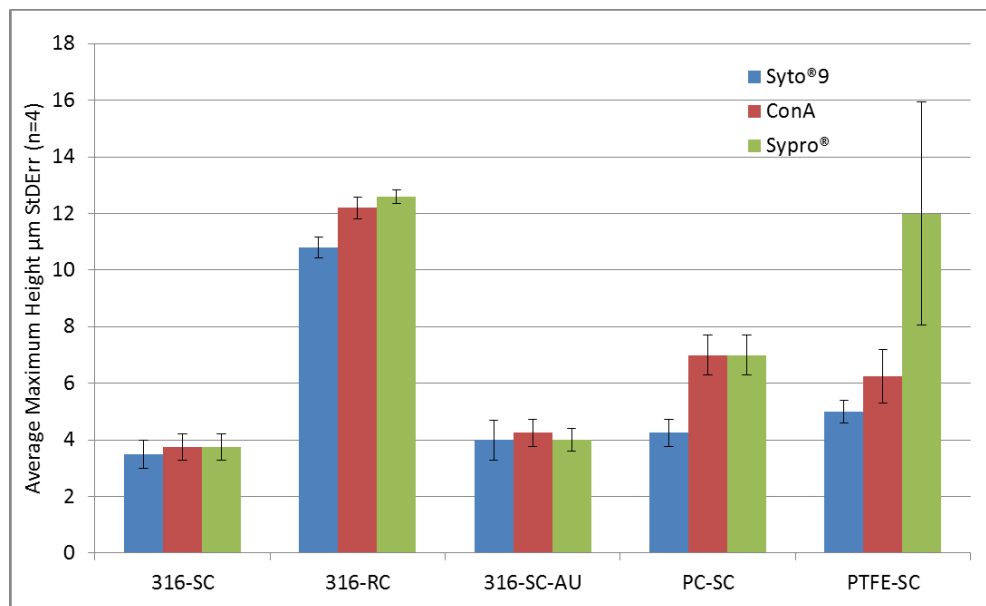
Figure C1.9. Average maximum height negative control for the SP8 TCS microscope. Substratums were treated with probes as per Figure 2.5.

Appendix D – Growth of Mature *Pseudomonas* Biofilm on Different and Thin Film modified Substratums – Individual Confocal Metric Breakdown
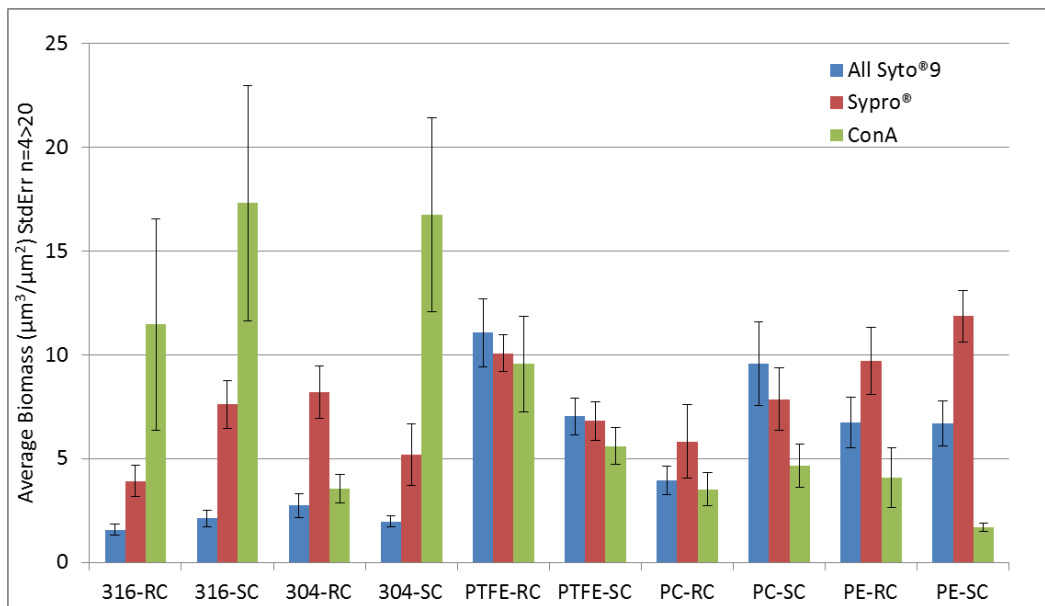
Figure D1.1. *PA* biofilm biomass data.
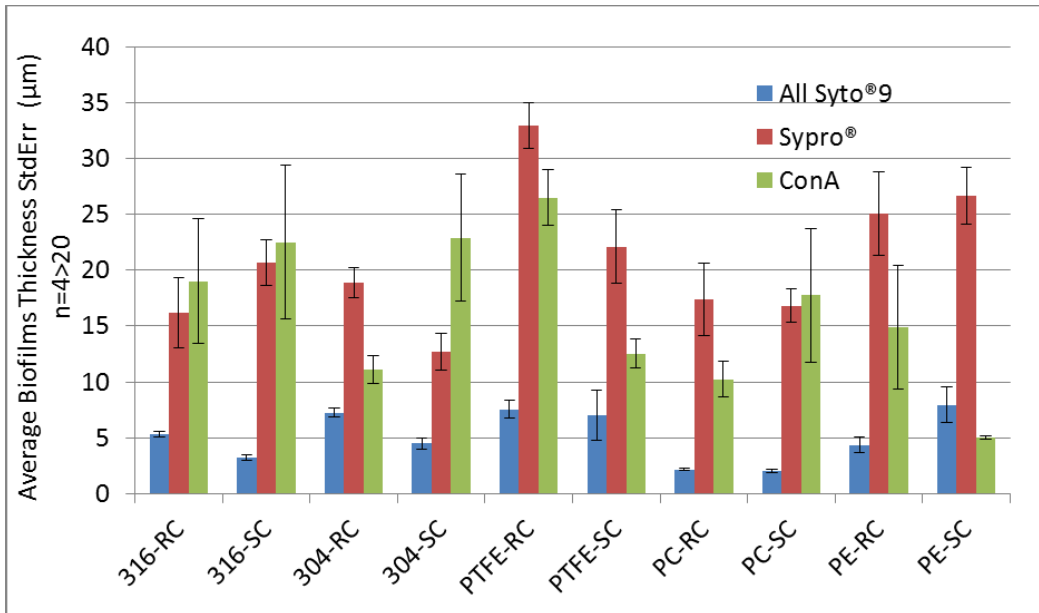
Figure D1.2. *PA* biofilm biomass average thickness data.
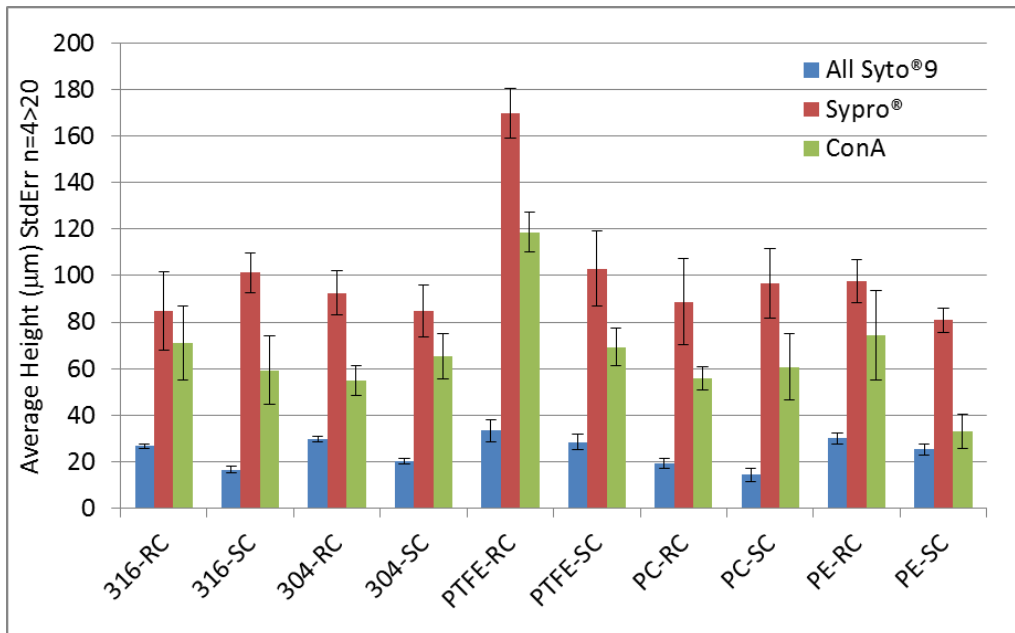
Figure D1.3. *PA* biofilm maximum height data.
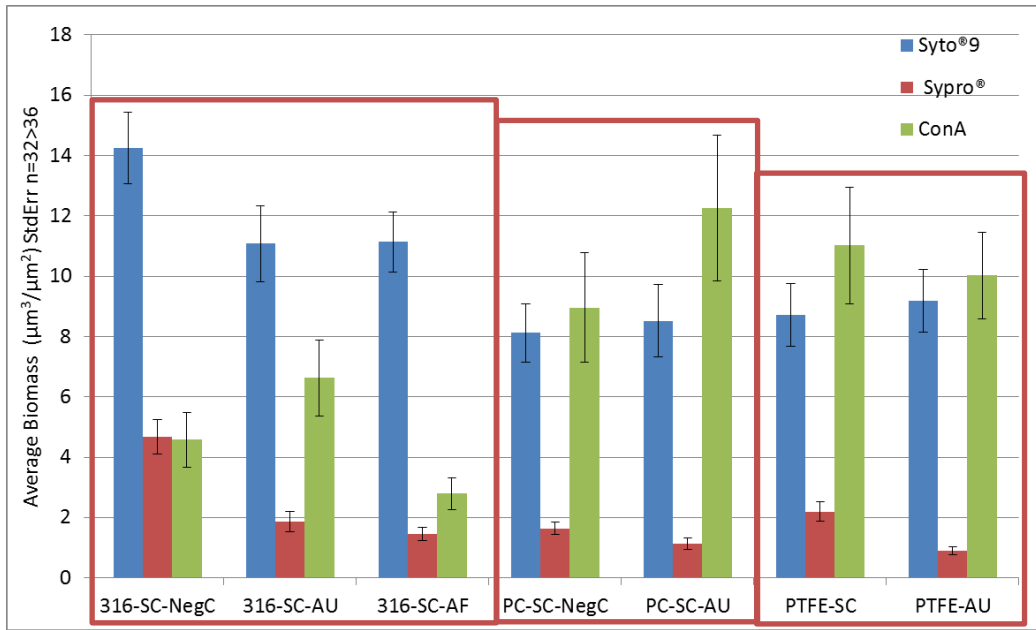
Figure D1.4. *PA* biofilm biomass, following growth on modified substratum.
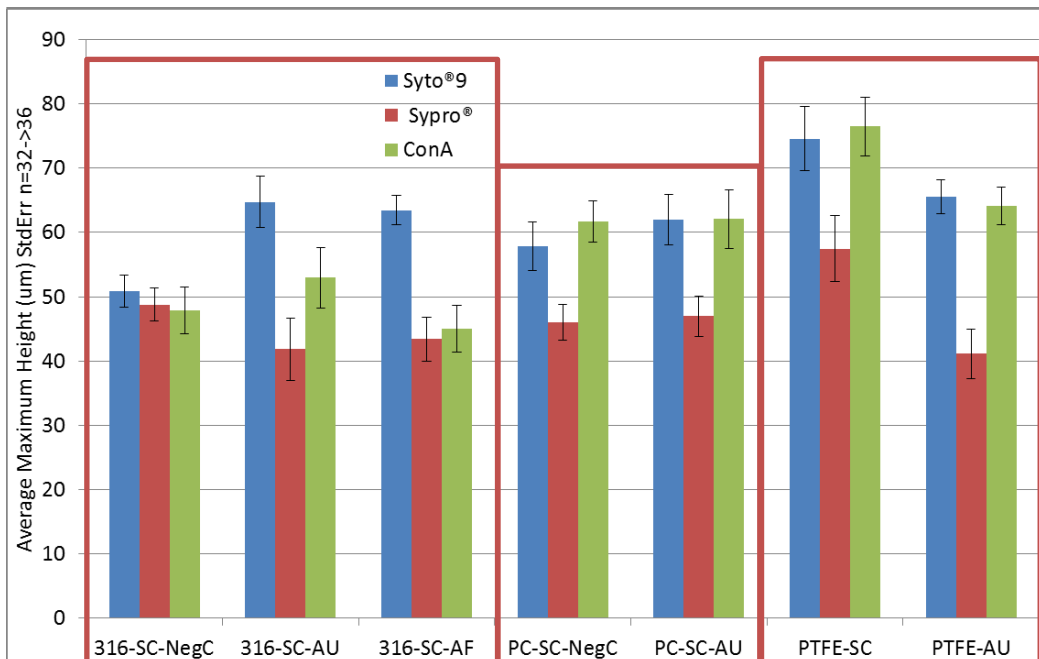
Figure D1.5. *PA* biofilm maximum height, following growth on modified substratums.
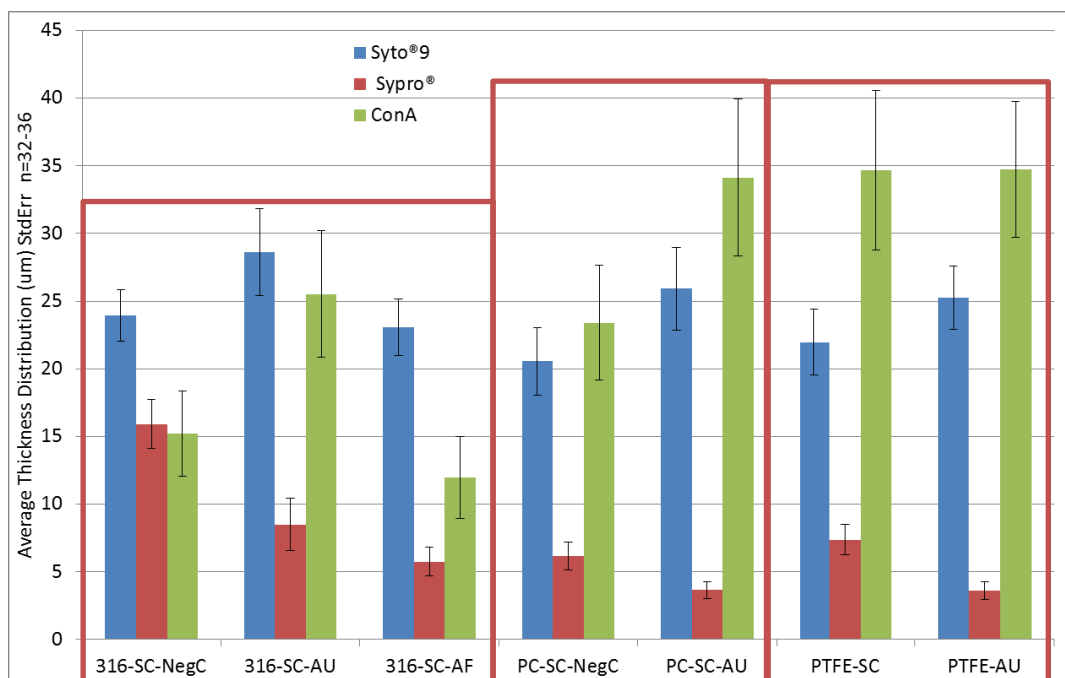
Figure D1.6. *PA* biofilm average biofilm thickness, following growth on modified substratums, i.e. gold coated polycarbonate, gold coated PTFE, PTFE-AF coated 316 smooth stainless steel. Boxes control substratum relevant control and modified surfaces.

Appendix E – High Shear Cleaning With/Out Abrasive Study on Mature *Pseudomonas* Biofilms – Individual Confocal Metric Breakdown
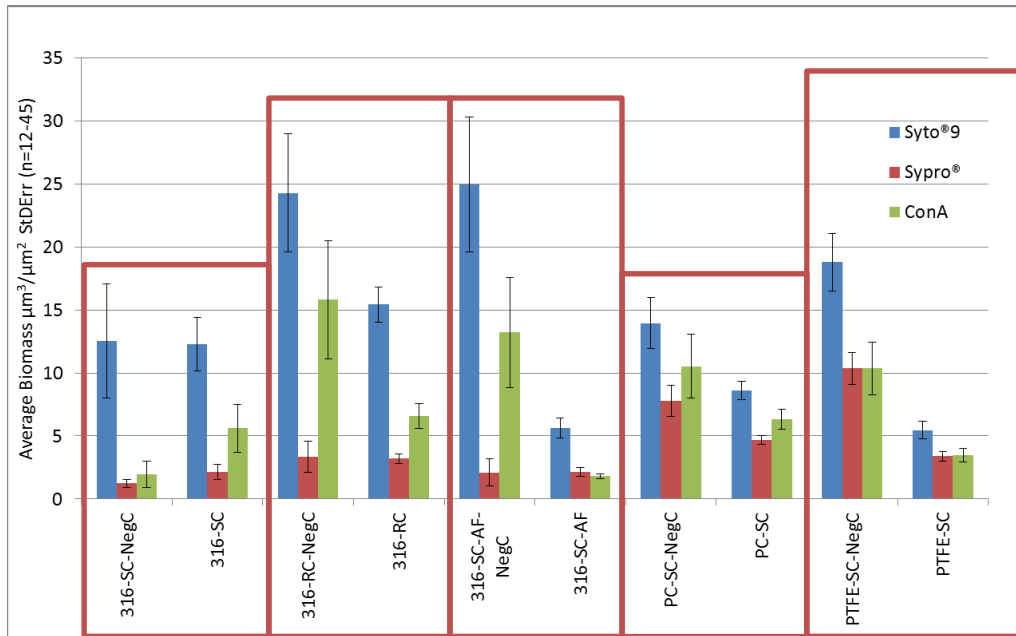
Figure E1.1. High shear cleaning experiment result showing biomass metric and individual biofilm components. Boxes control substratum relevant control and modified surfaces.
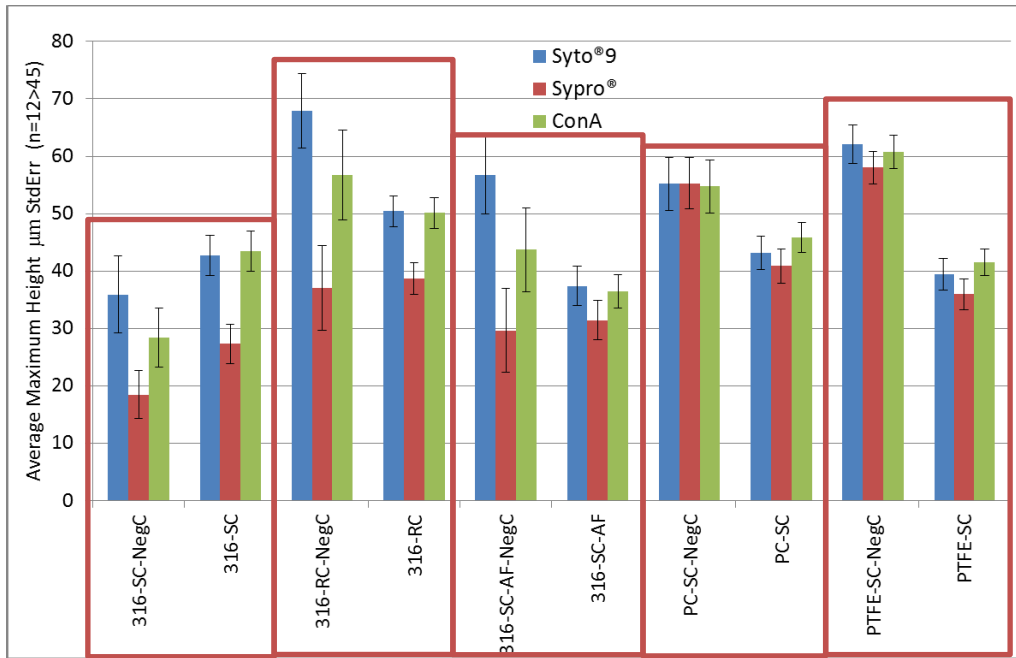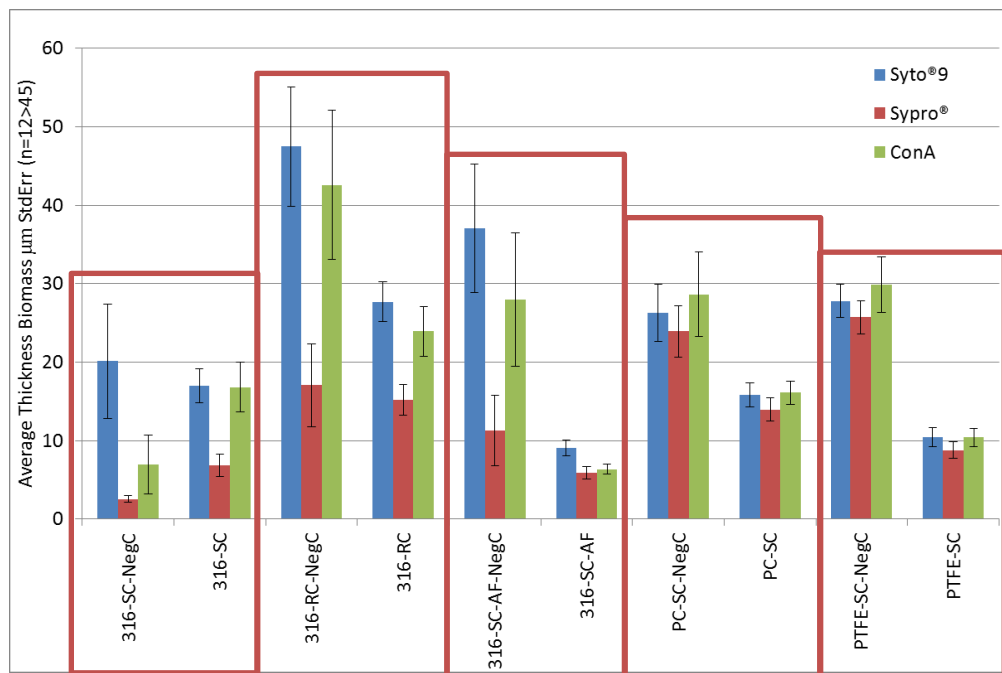
Figure E1.2. High shear cleaning experiment result showing maximum height metric and individual biofilm components. Boxes control substratum relevant control and modified surfaces.

Figure E1.3. High shear cleaning experiment result showing average biomass thickness metric and individual biofilm components. Boxes control substratum relevant control and modified surfaces.
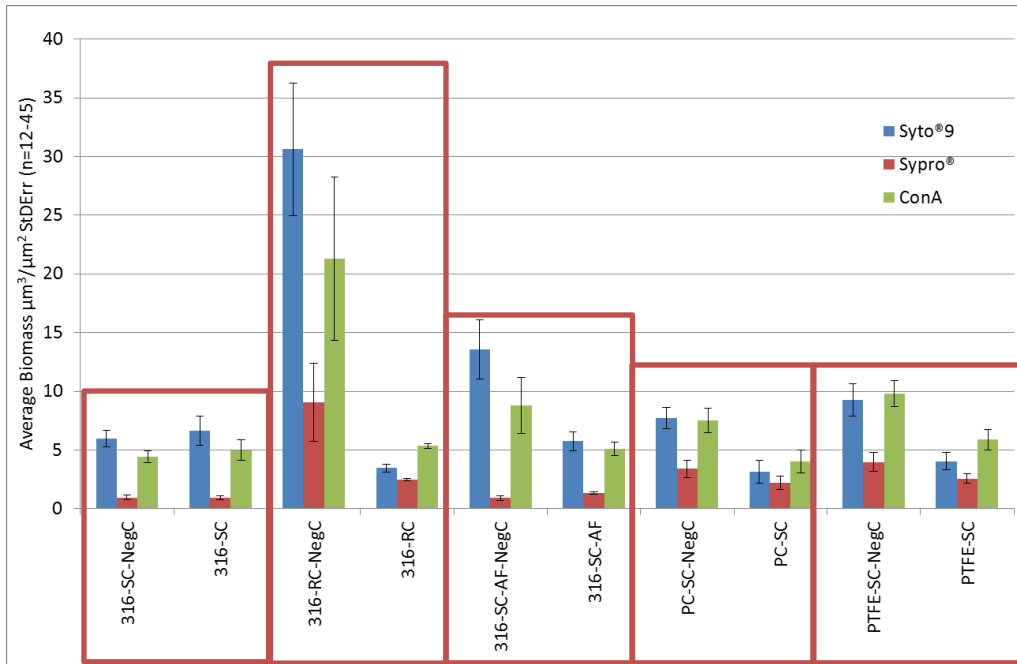
Figure E1.4. High shear cleaning experiment with Silica powderresult showing biomass metric and individual biofilm components. Boxes control substratum relevant control and modified surfaces.
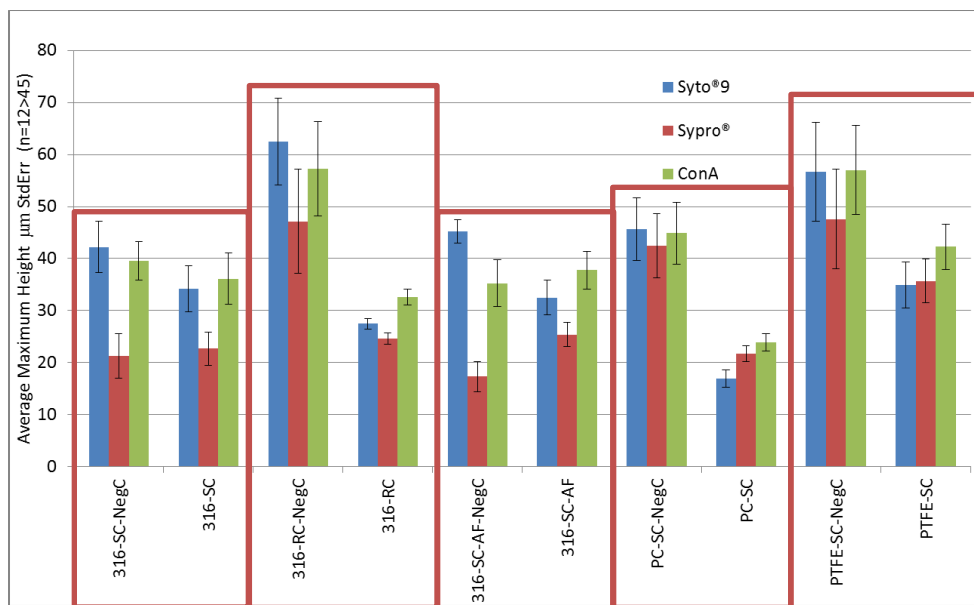

Figure E1.5. High shear cleaning experiment with Silica powder result showing maximum thickness metric and individual biofilm components. Boxes control substratum relevant control and modified surfaces.
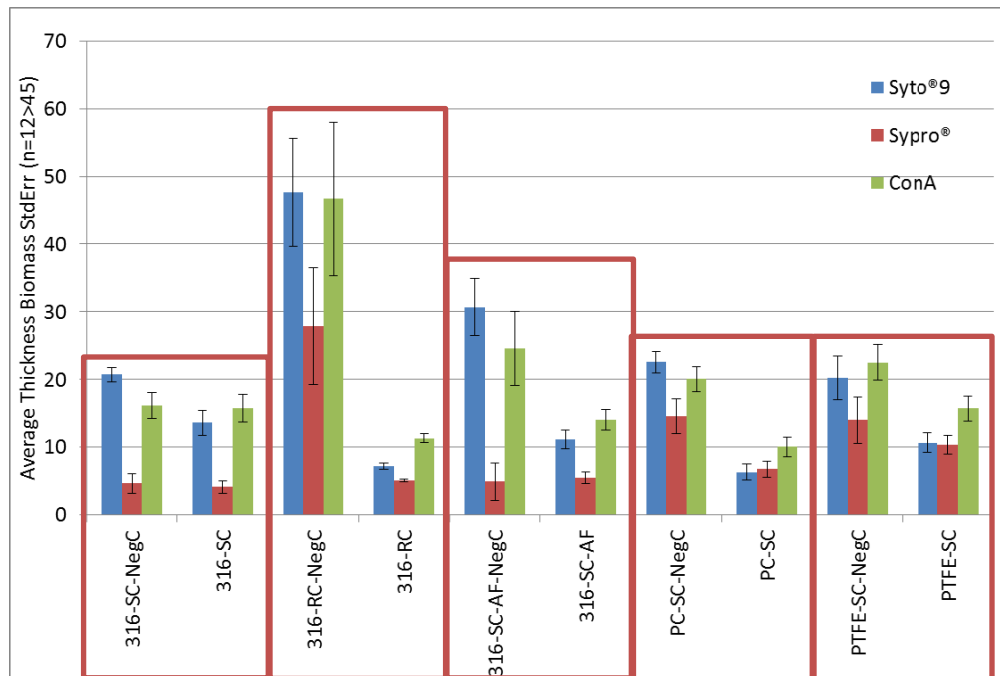
Figure E1.6. High shear cleaning experiment result with Silica powder showing average biomass thickness metric and individual biofilm components. Boxes control substratum relevant control and modified surfaces.

End of report